THE UNIVERSITY OF
SYDNEY

The effect of climate variables on sapwood anatomy of *Eucalyptus*

A dissertation submitted in partial fulfilment of the requirements for the degree of Doctor of Philosophy

Marco Harbusch

Faculty of Agriculture and Environment

New South Wales, Australia

“Die Natur schlägt im Menschen die Augen auf und bemerkt, dass sie da ist.”

Friedrich Wilhelm Joseph Schelling (1775 –1854)

DECLARATION

The work described in this Thesis was performed between March 2010 and April 2014 in the Faculty of Agriculture and Environment at the University of Sydney. The author hereby declares that this thesis contains no material previously published or written by another person unless stated otherwise. This work has not been submitted, in part or full, for the purpose of obtaining any other degree.

Marco Harbusch
Sydney, April 2014

ABSTRACT

This thesis considerably expands our understanding of hydraulic architecture in the genus Eucalyptus.

The major finding is that xylem vessels in eucalypts taper at variable rates from the base of the stem to the top of the tree, depending on species and environment. The systematic assessment of changes in the structure of vessel tapering (reduction in xylem vessel diameter per unit length of stem, from the base to the apex) across a gradient of increasing aridity uncovers that the degree of taper is not a function of plant height but for coping with prevalent limitations like water or light. In some tall species from mesic climates (e.g. Eucalyptus regnans F. Muell.) vessel taper may be close to zero for the great majority of the stem, before increasing rapidly within the apical region of the canopy. For other species, such as those from semi-arid environments (e.g. Eucalyptus gracilis F. Muell.), tapering begins much further towards the base of the stem. These findings are highly novel and contradict some major theories (e.g. Metabolic Scaling Theory, MST). Yet, they are entirely in keeping with the general thrust of the 'cohesion-tension' theory of water movement in trees.

This thesis includes several supporting studies for the above. A glasshouse study suggested thateven at seedling stage, environmental conditions such as temperature and moisture and nutrient availability, play roles in xylem formation (xylogenesis). Despite these suggestions, research in the glasshouse was inconclusive. This was most likely due to the relatively slow response of major biophysical processes, such as the development of structural entities like xylem vessels, when compared to faster responses to environmental conditions of biochemical processes such as those involved in photosynthesis and respiration. A field study of the potential role of water storage in heartwood (i.e. capacitance) in water transport, was hampered by prevailing environmental conditions and uncertainty around the sources of water being used by the study tree. Nonetheless, the data and the knowledge gained by both experiments add to current understanding how functionality of xylem tissues can be maintained under different environmental conditions, including elevated temperatures and water shortage.

However, the major body of work in this thesis rests with analysis of xylem vessels at a microscopic scale. This work required significant development of techniques suitable for use with eucalypts that contain some of the hardest wood of all trees. The research also required development of software scripts capable of quantification of properties in large numbers (>150,000) of vessels across a dozen or so species, and multiple field sites. Additionally, the work reported here includes a rigorous assessment of climate across field sites and then use of that to interpret xylem structure. The resultant phase analysis of rates of tapering within trees, is both an Australian and world first. Adopting methodology widely used in other fields of biology, this thesis employs a phase analysis of tapering of xylem vessels to highlight:

1. That the insertion point of vessel taper towards the top of trees differs largely among eucalypt species.

2. That regardless of species and location, vessel diameter at the apex does not differ widely among species – this, at least, accords with *MST*.

3. That rates of taper within the apical region of canopies where the risk of cavitation is greatest are closely related to environmental conditions, particularly the availability of water and competition for light.

ACKNOWLEDGEMENTS

I want to thank a number of people for their indispensable support in the creation process of this thesis.
First of all I would like to thank the University of Sydney, the Faculty of Agriculture and Environment and especially Prof Mark Adams for his supervision and the financial support that made my stay and study possible.

I would like to thank Dr Sebastian Pfautsch for his outstanding supervision. No matter how trivial the question or how small the matter, his door was always open for me. I thank him for the much appreciated ideas, fruitful discussions and valuable advice he gave me throughout the entire four years.

I thank Dr Tina Bell for her very helpful conversations and hints concerning general research and writing skills. Furthermore I was very thankful for the delicious and nutritious food which helped my brain working better.

Many thanks to Dr Floris Van Ogtrop for his help writing the software necessary to manage and analyze my huge set of data. He also taught me valuable statistical skills, while he was assisting in statistical analyses.

I want to thank everyone in the Faculty of Agriculture and Environment. It has been a pleasure to work with you, to meet and chat with you all, in the hallways and tea rooms and at all kinds of other occasions.

My special thanks go to all DSE "Department of Sustainability and Environment, Victoria" Staff members who generously helped me during all undertaken field trips. Offices enrolled were namely the ones in Alexandra, Ballarat, Bendigo, Horsham, Mildura and St. Arnaud. They all helped me identifying, from a European point of view, very similar looking *Eucalyptus* species. They gave me allowance to fell and sample them. They helped me with the sampling and they pulled my car out of the mud when it was stuck.

Further I would like to express my special thanks to the research staff of the Institute for Environmental Research (IER) at the Australian Nuclear Science and Technology Organisation (ANSTO) , namely, Dr Suzanne Hollins, Mr Chris Dimovski and Ms Barbora Neklapilova who helped me out with necessary equipment and personal help and advice.

I thank the friendly staff members of the histopathology laboratory, namely Ms Sanaz Maleki and team for giving me the opportunity to use some of their machines. Further I want to thank the Australian Centre for Microscopy and Microanalysis, especially Dr Matthew Foley for introduction into- and continuous help with the scanning electron mircroscope.

Last but not least I thank Ms Fiona Lawrence for her outstanding performance in helping me finalise the paperwork needed to include me in the graduation ceremony.

TABLE OF CONTENTS

LIST OF FIGURES

LIST OF TABLES

ABBRVIATIONS

AI	Aridity Index
ANSTO	Australian Nuclear Science and Technology Organisation
CLIMARC	Australian climate archive
C-T Theory	Cohesion-Tension Theory
d	equivalent circular diameter (µm)
DBH	diameter at breast height (cm)
D*h*	hydraulically weighted vessel diameter (µm)
Dh_{max}	maximum hydraulically weighted vessel diameter (µm)
Dh_{min}	minimum hydraulically weighted vessel diameter (µm)
d_{max}	maximum equivalent circular vessel diameter (µm)
d_{min}	minimum equivalent circular vessel diameter (µm)
Dh_b	hydraulically weighted vessel diameter at stem base (µm)
DW	sapwood dry weight (g)
EG	*Eucalyptus grandis*
EM	*Eucalyptus melliodora*
ENSO	El Niño–Southern Oscillation
Eq.	Equation
FAO56	potential evapotranspiration (mm)
Fig.	Figure
MST	Hydraulic Limitation Hypothesis
HRM	Heat Ratio Method
*J*s	Flux density of sap (ml $cm^{-2}h^{-1}$)
l	vessel-/ path length
L	Litres
(m) a.s.l.	(meters) above sea level

MST	Metabolic Scaling Theory
N	normal nitrogen treatment
N+	increased nitrogen treatment
NSW	New South Wales, Australia
P	precipitation (mm)
PAR	photosynthetically active radiation (µmol m^{-2} s^{-1})
R	hydraulic resistance (cm^{-3} MPa s^{-1})
R_{rel}	relative hydraulic resistance (%)
R_{sec}	resistance for an idealized conduit section (cm^{-3} MPa^{-1} s^{-1})
R_{tot}	total hydraulic resistance (cm^{-3} MPa^{-1} s^{-1})
T	air temperature (°C)
TIP	tapering initiation point
T_{max}	daily maximum air temperature (°C)
TPTA	Three Phase Taper Analyses
UNEP	United Nations Environment Program
VC	vessel count
VD	vessel density (n cm^{-2})
VD_b	vessel density at stem base (n cm^{-2})
VD_{min}	minimum vessel density (n cm^{-2})
VIC	Victoria, Australia
VPD	vapour pressure deficit (kPa)
V_h	heat velocity (cm h^{-1})
V_s	sap velocity (cm h^{-1})
VSMOW	Vienna Standard Mean Ocean Water
VtW	void to wood fraction (%)
WBE	West, Brown and Enquist (West *et al.*, 1999)
WD	density of sapwood (g cm^{-3})

W	normal water treatment
-W	limited water treatment
Q	sap flow ($cm^3\ s^{-1}$)
QLD	Queensland, Australia

Chapter 1 – Literature review and general introduction

1.1 Background

The genus *Eucalyptus* dominates many of Australia's ecosystems. This genus includes over 800 species, and forms the dominant canopy in many forests and woodlands across the Australian continent (Boland *et al.*, 1984; Merchant *et al.*, 2007). Apart from their ecological significance in native forests, woodlands and savannas, eucalypts are worldwide the most common plantation tree in the tropics, with >10 million hectares planted (Brown and Ball, 2000). Plant species of economic significance are often the subject of research into effects on plant structure and function of major environmental events, like droughts (Clark *et al.*, 2002; Guarnaschelli *et al.*, 2003; Tausz *et al.*, 2008; Ryan *et al.*, 2010) and heatwaves and freezing conditions (IPCC, 2007; Woldendorp *et al.*, 2008). Similarly, effects of long-term changes in atmospheric CO_2 concentrations on structure of economically important plant species have been well studied (Atwell *et al.*, 2009; Ghannoum, 2009; Luo and Polle, 2009). Despite their ecological and economic significance, there have been few studies of environmental effects on the hydraulic architecture of either plantation or non-plantation *Eucalyptus* species. Recent global analyses (e.g. Choat *et al.* 2012) include relatively few members of the genus.

The climate of south-eastern Australia is predicted to become warmer and mostly drier (IPCC, 2007). Changes in precipitation, surface runoff, solar UV radiation, temperature, and evaporation are some of the predicted outcomes of climate change and ozone depletion. A combination of decreased rainfall, increased solar radiation and decreased cloud cover will likely increase evaporation and decrease plant water availability (Soh *et al.*, 2008). As regional and continental changes in climatic conditions are predicted to clearly modify plant growth and survival (IPCC, 2007) it becomes increasingly important to understand the 'plasticity' of the hydraulic architecture of eucalypt species. This knowledge is required to form the foundation for decision-making by land managers in relation to identify tree species for future plantation, rehabilitation and urban panning projects. Overall, the lack of quantitative analysis of wood structure and architecture in relation to environmental and climatic variables for *Eucalyptus* spp. severely limit our ability to predict structural and functional outcomes of growth under any given set of conditions (Bleby *et al.*, 2009).

The field of hydraulic architecture of plants, and trees in particular, is receiving increased scientific attention. This is in part due to effects of climate change (e.g. Williams *et al.*, 2010). Tree express not only wide inter-, but also substantial intra-species specific variation in features and mechanisms influencing their water use strategy, xylem anatomy and drought tolerance (e.g. Roderick and Berry, 2001; Thomas *et al.*, 2004, Choat *et al.* 2102).

Plant scientists have studied the transport of water in plants for more than a century, shaping current theories of plant hydraulics (e.g. Dixon and Joly, 1895; Huber, 1928; van den Honert, 1948; Huber, 1956; Scholander, 1972). Reviews by Zimmermann (1983) and Boyer (1985) provided a comprehensive platform for research in the past 25 or so years. Today, the basic mechanisms that govern water transport are widely accepted and descriptive theories and mathematical models have been proposed (Chapter 1.4). As just one example of this acceptance and its development, researchers have more recently been investigating mechanistic and structural features of trees that might explain variation in maximum height. As another, linking plant water transport to biomass accumulation is important to increase our ability to accurately calculate the carbon storage capacity of natural and managed forest ecosystems (Woodruff *et al.*, 2008). Broadly speaking, we now know that structural features of xylem are closely related to site-specific conditions such as seasonal climate, soil water and nutrient availability, landscape geomorphology and even species competitiveness for available resources (e.g. Thomas *et al.*, 2007; Sperry, 2008; Petit *et al.*, 2010). While the functional significance of changes in xylem structure for water transport are obvious, they are also important to the properties of wood as a commercial product – for example, properties related to wood strength. As a consequence there is a separate body of knowledge that comes from investigations of the microscopic structure of wood as an engineering material.

Taken together, there is now a considerable body of knowledge of relations between climate and wood anatomy. Even so, we lack models (of any description – conceptual, mechanistic and empirical) that properly describe the development of wood anatomy under changing climates (Aber *et al.*, 2001; Swenson and Enquist, 2007).

Changes in hydraulic architecture, maximum tree height and, arguably, maximum tree biomass, can have a very significant impact on local, regional and global water and carbon cycles, as well as species composition (Gitlin *et al.*, 2006). Despite our currently limited understanding of the structure of xylem in eucalypts, it is feasible to study tree hydraulic architecture across different ecosystems. Such an approach is required to elucidate how sapwood features like its density and vessel anatomy relate to environmental conditions, and ultimately to allow us to predict how these changes may affect ecosystems at a range of scales (Zanne *et al.*, 2010).

1.2 Transporting water in trees

As fundamental elements of our ecosystems, trees have long been of scientific interest. A broad range of specific knowledge about principles of hydraulic operation has therefore been accumulated over the last centuries. Even though some of the following underlying principles might not be of necessary importance to understand the central subject of the present thesis, Chapters 1.2.1 to 1.2.4 intend to provide a comprehensive overview of hydraulic design of trees as well as basic physical, chemical and anatomical factors influencing the ascent of water in trees.

1.2.1 The root

Plant roots are a logical starting point for consideration of the hydraulic system of plants. Roots facilitate uptake of water from the soil before it enters the xylem tissue from where it is distributed throughout the plant. The movement of water from soil to the xylem - and subsequently to leaves - is driven by negative hydrostatic pressure in the root (water potential) generated by plant transpiration. A model structure of a root formed by dicotyledonous plants is shown in Figure 1.1.

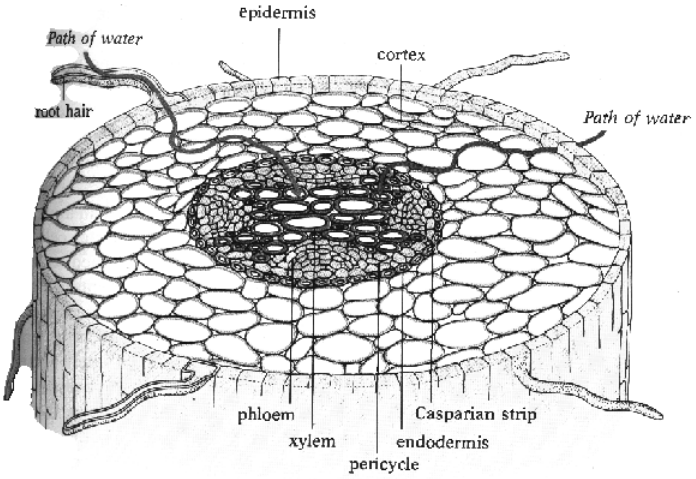

Figure 1.1: Anatomical structure of a dicotyledonous root (www.http://mandevillehigh .stpsb.org/teachersites/laura_decker/ap_roots_stems_and_leaves_diagrams.htm;accessed: 10.03.2014)

The outer layer or epidermis of roots characteristically feature microscopic extensions of epidermal cells known as hair roots, which expand the root surface and enlarge the soil area accessible for resource extraction by the plant. The driving force for water into the root/hair root is the difference in water (Ψ_w) and solute (Ψ_π) potential between root and soil. After passing the epidermis, water crosses the root cortex. The cortex consists of layers of starch-grain-rich parenchyma cells surrounding the vascular cylinder. Water can pass these tissue layers either via a symplastic (within cells) or apoplastic (water filled space outside of cells) pathway. A combination of pathways is common and termed 'transmembrane'. The diffusion of water through membranes is effectively provided through aquaporins. These membrane proteins facilitate and regulate water movement in response to cell internal physiological parameters such as pH, [Ca^{2+}] and osmotic gradients (Tyerman *et al.*, 2002; Shao *et al.*, 2008). After passing the cortex, water reaches the endodermis that bounds the vascular cylinder. Endodermis cells, like cortex cells, contain starch granules as well as mineral ions. These ions form part of the osmoregulatory capacity of plants. For example, they can be actively loaded into xylem vessels to maintain turgor and root pressure. Furthermore, the radial walls of endodermis cells contain high concentrations of suberin that acts as a barrier against apoplastic flow of water and solutes into the vascular cylinder. This safety feature is termed the 'Casparian strip', and its primary function is now thought to be forcing of water to enter the vascular cylinder via the symplast pathway, thus providing the

plant with greater control of water (and nutrient) influx. After water has passed the symplast of endodermis cells, it again moves towards the xylem, passing the pericycle. The pericycle consists of one or more layers of thin-walled parenchyma cells. In the primary body of the root, the pericycle directly borders phloem and xylem strands. In some plants the xylem strands may be in separate units in the periphery of the vascular cylinder or they may extend into the centre. Once water reaches the xylem, negative hydrostatic pressure forces water into xylem vessels from where it is transported towards the transpiring surfaces of the plant.

1.2.2 The stem

Within a tree stem, different types of tissues can be distinguished. The outer bark, or periderm, protects the trunk from biotic and abiotic stresses. The meristem responsible for radial growth is termed 'cambium'. In the initial stages of tree growth, the pro-cambium is responsible for the production of primary xylem and primary phloem. At more advanced stages of development, a vascular cambium arises between these two primary tissues, producing secondary xylem and secondary phloem. The vascular cambium is responsible for secondary growth as it continuously produces (during the growing period) secondary phloem cells towards the bark and secondary xylem cells towards the heartwood of the trunk. Phloem is predominantly a transport system for assimilates from photosynthesis (source) to places of consumption or storage (sink). Phloem cells are short-lived and transform into cork, becoming part of the protective and insulating outer bark (Fig. 1.2). Secondary xylem is a complex axial system of capillary tubes. They are responsible for water and solute transport from roots towards leaves. Heartwood in the centre of a stem primarily provides mechanical support. It consists of inactive cells that are chemically and physically different from sapwood (xylem) cells as they contain greater amounts of cellulose, lignin and polyphenols. Heartwood formation begins with increased cellulose deposition in water transporting pipes. This process is known as 'tylosis'. Increasing amounts of secondary compounds, including tannins and resins, will further increase wood strength and resistance against abiotic (e.g. wind) and biotic stresses (e.g. insect attack) and block any upward movement of water.

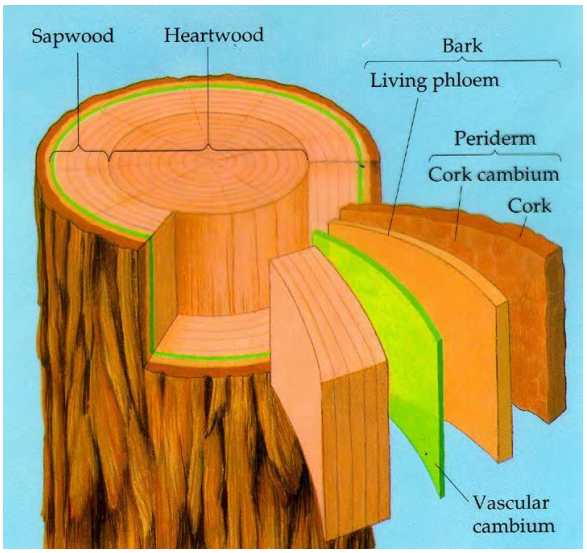

Figure 1.2: Schematic view of tissue structures commonly found in a tree trunk (Wesolowski, 2010).

1.2.3 The crown

The appearance of a mature tree crown depends on genetic code and environmental circumstances (Barthelemy *et al.*, 1989). The latter is easily recognised in the obvious plasticity in crown architecture of most tree species (i.e. narrow crown shape when growing in stands, wide crown shape when growing alone). The distribution of leaves as photosynthetic surfaces within tree crowns is one of the most important functional characteristic of trees inasmuch that their orientation determines the light capturing capacity of a tree and its intra-specific competitiveness (Goulet, 2000; Nikinmaa *et al.*, 2003). Leaves also play a key role in maintaining the balance between transpiration and carbon uptake (Outlaw, 1983; Talbott and Zeiger, 1998; Stern, 2000; Shimazaki *et al.*, 2007). This balancing act represents a driving force for hydraulic conductance within the vessel network of trees and determines water use efficiency at the tree scale (Koch *et al.*, 2004; Johnson *et al.*, 2009). Given the laws of thermodynamics that govern the movement of water, the large gradient in water potential between the mostly dry atmosphere (relatively low Ψ_a), and more moist conditions inside leaves (higher Ψ_l), water moves from the air spaces inside leaves to the atmosphere via stomata. In similar fashion, water moves along the gradient from higher water potential within leaf xylem cells to the lower water potential of the cell walls of the mesophyll (Fitter and Hay, 1987). In addition to the continuous gradient in water potential from the leaf xylem to the atmosphere, water in leaves undergoes a phase-change - from liquid to gaseous – as it moves from cell walls into intercellular

spaces and the sub-stomatal cavity. The amount of water lost via stomata (transpired) can be described according to the difference in vapour pressure between the intercellular spaces and the atmosphere surrounding the leaf (Buckley and Mott, 2013). Small amounts of water (generally <5%) can also be lost through the waxy cuticle (Taiz and Zeiger, 2002). Each stomata is bordered by guard cells that can increase or decrease the stomatal aperture. Asymmetric positioning of microfibrils in guard cell walls provide capacity for plants to quickly respond to changes in turgor pressure. Guard cells function as multisensory valves and react to environmental factors such as light, temperature, relative humidity and intracellular CO_2 concentrations (Taiz and Zeiger, 2002). During photosynthesis, guard cells use energy to acquire K^+ ions from neighbouring epidermal cells. Increased K^+ and/or sugar content reduce water potential in the vacuoles of guard cells and increases turgor pressure (via osmosis). This leads to swelling of vacuoles and widening of stomatal aperture. As guard cells shrink and apertures close, triggered by decreasing Ψ_l, intakes of K^+ and/or sugars decline as a result of reduced rates of carbon fixation. A key safety mechanism of plants is that stomata remain closed under conditions of a dry atmosphere and low soil water potential (Ψ_s), as leaves cannot provide sufficient amounts of water for building turgor pressure in guard cell vacuoles. This effectively decouples plants from the atmosphere and prevents large negative water potentials in the xylem, that could potentially lead to xylem failure via cavitation (Chapter 1.3.3) (Blackman *et al.*, 2010). A consequence is that CO_2 cannot be taken up by leaves, reducing production of photosynthates and ultimately leading to leaf abscission. Beside stomatal resistance (r_s), which is proportional to stomatal frequency and inversely proportional to the diameter of stomatal aperture, the resistance of the 'boundary layer' (r_b) also limits water diffusion from the leaf to the atmosphere (Fitter and Hay, 1987; Taiz and Zeiger, 2002). Boundary layers are defined as the space immediately adjacent to leaf surfaces, and are enriched in water vapour compared to turbulent air. The extent of any given boundary layer is determined by wind speed and the shape of leaves and canopy roughness (Fitter and Hay, 1987). A principal function of boundary layers is that of buffering vapour pressure deficits (VPD) between stomata and the atmosphere (Daudet *et al.*, 1999; Taiz and Zeiger, 2002). Boundary layers can indirectly reduce stomatal conductance (Aphalo and Jarvis, 1993). In agreement with the hydraulic limitation hypothesis (Chapter 1.4.1), there is good evidence that stomatal conductance is usually coordinated with overall

hydraulic conductance of the pathway from roots to canopy (Meinzer and Grantz, 1990; Bond and Kavanagh, 1999; Rust *et al.*, 2002). A net result is that photosynthetic activity is often inversely related to tree height, regardless of soil water status or VPD.

Branch junctions also serve to reduce the hydraulic conductivity of a tree crown. Depending on branch position, additional resistance may be introduced by the branch collar (Aloni *et al.*, 1997; Eisner *et al.*, 2002). Vessels or tracheids in branch junctions may be shorter and narrower compared to their counterparts in stems (Eisner *et al.*, 2002). Since conduit end walls provide significant resistance to flow, shorter vessels/tracheids generally reduce hydraulic conductance (Zimmermann, 1983). Vessel orientation and changes therein further affect conductance (Tyree and Ewers, 1991; Rust *et al.*, 2002). Axially orientated branches may have less resistance to water movement than those oriented perpendicularly, and it is worthwhile noting that each junction from the main axis may introduce a change in vessel structure and orientation (Rust *et al.*, 2002).

1.2.4 Differences between gymnosperms and angiosperms

Sapwood anatomy in gymnosperms differs strongly from that in angiosperms, while the two groups share similar features in their xylem networks. Gymnosperm wood is composed mostly of single-celled tracheids that function both as a conduit for water flow and mechanical stabilizer (Hacke *et al.*, 2004). Tracheids vary in length (0.5 to11 mm) and diameter (10 to 40 μm) within and between species (Zimmermann, 1983; Pittermann and Sperry, 2003). According to the Hagen-Poiseuille formula (Equation 1.6) the increase of specific conductivity of water flow in a xylem conduit increases by the fourth power of the conduit diameter (Zimmermann, 1983; McCulloh *et al.*, 2003; Sperry *et al.*, 2006). As tracheids are usually smaller in diameter compared to vessel elements of angiosperms, their hydraulic resistance is generally greater. Tracheids are slender tapered cells with multiple pits (Zimmermann, 1983; Amritphale and Sharma, 2010). They are organized in bundles and water passes from cell to cell via pits. Pairs of pits are usually separated by a torus-margo pit membrane (Fig. 1.3) (Bauch *et al.*, 1972; Zimmermann, 1983). Inter-vessel pits act as valves, allowing water to pass under a given tensile strength. If a vessel is embolized due to formation of an air bubble, the pit membrane will be

pushed against the torus of the neighbouring cell, effectively sealing off the air-filled tracheid and preventing spread of embolism. Overall resistance to water flow in conifers would increase if pit structures were not present (Pittermann *et al.*, 2005).

Compared to gymnosperms, organisation of sapwood in angiosperms is more complex. Angiosperm sapwood is divided into vessels for water transport and lignified fibre cells for mechanical strength. Conducting vessels are constructed from numerous consecutive vessel elements, forming a continuous pipe-like structure. Perforated end walls, so called sieve plates, separate vessel elements (Dickison, 2000) and can differ between species. Plates can be simple or multiple, they can be scalariform (ladder like arrangement), forminate (circular in shape and grouped together) or reticulate (numerous and small, separated by a network of secondary wall thickening) (Cutter, 1978). Vessels are surrounded by living parenchyma cells for storage purposes and fibre cells for mechanical strength. Single vessel elements are usually shorter than tracheids but their greater diameter (10 to 500 μm) permitting greater rates of water to pass (Zimmermann, 1983; Amritphale and Sharma, 2010). Conduit pipes can vary in length from a few mm to more than 10 meters in vines and ring porous trees (Hacke and Sperry, 2001; Amritphale and Sharma, 2010).

The lateral walls of vessel elements can have pits. Inter-vessel pits of angiosperms are mostly less efficient in water transport and less complex in structure when compared to the inter-tracheid pits of gymnosperms (Fig. 1.3). Inter-vessel pits are uniformly microporous, homogenous in thickness and porosity and pose greater resistance to flow of water than intertracheid pits (Hacke *et al.*, 2004; Pittermann *et al.*, 2005). Some investigations have shown that angiosperm pit membranes can be responsible for 50% or more of the hydraulic resistance in the xylem (Wheeler *et al.*, 2005; Choat *et al.*, 2006; Hacke *et al.*, 2006; Jansen *et al.*, 2009) and architectural features of pit membranes such as thickness and porosity have significant influence on total hydraulic resistance in trees (Jansen *et al.*, 2009). Nevertheless, the smaller the pit, the better the protection against cavitation (Choat and Pittermann, 2009). Despite differences in the water transporting system of angiosperms and gymnosperms, their hydraulic efficiency to transport water appears roughly similar for a given vessel diameter, including branches and leaves (Becker *et al.*, 1999; Pittermann *et al.*, 2005).

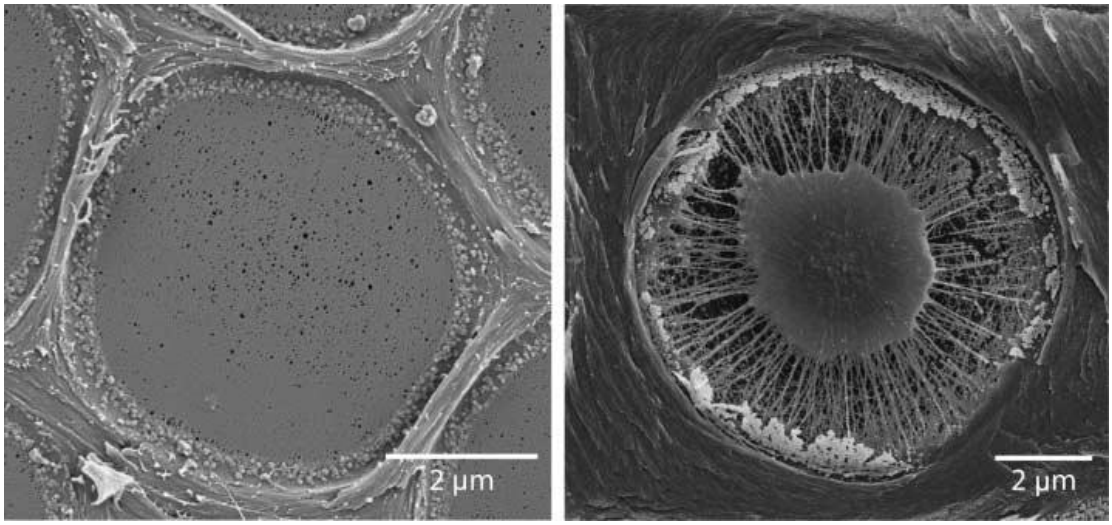

Figure 1. 3: Pit structures in angiosperms and conifers.Left: a homogeneous pit membrane of an angiosperm species, *Acer negundo*. Right: a torus-margo type pit membrane of a conifer, *Calocedrus decurrens* (Choat and Pittermann, 2009).

1.3 Hydraulic architecture

1.3.1 Parameters and matrices to describe hydraulic architecture

Water potential (Ψ)

The ascent of water is a passive process within the xylem driven by different chemical potentials of water (μ) within different systems (e.g. atmosphere and leaf). μ describes the energy state of water, and is often expressed in J mol^{-1} (Tyree and Zimmermann, 2002). The water potential (Ψ) of a system can be determined by comparing its potential for chemical work with a reference potential. For liquid water, the reference is pure water at atmospheric pressure : Ψ = 0 Pascal (Pa) (Boyer, 1995; Tyree and Zimmermann, 2002). Mathematically, this is expressed as (μ_w-μ_0) where μ_w is the measured chemical potential and μ_0 is the chemical potential of pure water. Converting J mol^{-1} to the equivalent units of pressure (Pa), requires that μ be divided by the partial molar volume of water at atmospheric pressure (V_w), as first proposed by Slayter and Taylor (1960):

$$\Psi = \frac{\mu w - \mu 0}{Vw} \qquad \text{(Equation 1.1)}$$

Ψ can also be expressed as the sum of pressure (P) and the osmotic potential (π):

$$\Psi = P + \pi \qquad \text{(Equation 1.2)}$$

The Cohesion-Tension Theory

The Cohesion-Tension (C-T) theory was first proposed by Dixon and Joly (1894) and describes the biophysics of the ascent of sap. The low water potential of the atmosphere drives evaporation of water from cell walls in substomatal chambers, leading to curvature in the menisci of apoplastic water within cellulosic microfibril pores of cell walls. This in turn increases xylem pressure and lowers the water potential of adjacent tissues (protoplasts and cell walls). Due to the tensile strength of water (created by hydrogen bonding), a continuous column of water is 'pulled' towards substomatal chambers. Negative tension is thus transferred through the entire length of xylem. As a consequence, the water potential of roots is generally lower than that of soil and water uptake by roots is literally driven by transpiration of water from leaves (Tyree, 1997; Tyree and Zimmermann, 2002). The rising water column can withstand tensile stress without rupturing due to inherent stability of a liquid when mechanically stretched, and the additional stability conferred by the minutely subdivided structure of conducting tissue, which renders the stressed liquid stable even in the presence of free gas (Dixon and Joly, 1894). The C-T theory was transferred to a quantitative basis by van den Honert (1948) who used an analogue of Ohm's law.

Ohm's Law

According to van den Honert (1948), water flow through plants can be regarded as a catenary process, as formulated for the flow of electrons by Ohm. Van den Honert suggested each element in this catenary process has its own hydraulic conductance, with the total conductance being calculable via considering the series and parallel conductances of roots, stems, and leaves (van den Honert, 1948; Tyree, 1997; Tyree and Zimmermann, 2002). Water potential gradients as the driving force for sap flow must therefore decline along the segments of conducting tissue arranged in series. If the endodermis of the root, for example, represents the greatest resistance, the decline in water potential must also be greatest at this point (Steudle and Peterson, 1998).

The pressure gradient of any point of the tree can thus be calculated as:

$$-\frac{\Delta p}{\Delta x} = \frac{F}{k} + \rho g \frac{dh}{dx} \qquad \text{(Equation 1.3)}$$

Where $-\frac{\Delta p}{\Delta x}$ is the pressure gradient, F is the rate of water flow in the considered stem segment with the hydraulic conductivity (k) and $\rho g \frac{dh}{dx}$ is the gravitational potential gradient and represents the gravitational influence at a chosen height; ρ is the density of water, *g* is the acceleration due to gravity and *dh*/*dx* the height achieved per unit of distance (*dh*) and travelled by water in the stem segment (*dx*).
This analogue of Ohm's law leads to two major assumptions for water flow in trees (Tyree and Zimmermann 2002):

1. Driving force of sap is a continuous decrease in xylem pressure in the direction of sap flow.
2. Evaporative flux density from leaves is proportional to the pressure gradient at any given point (cross section) along the transpiration stream (Tyree and Zimmermann, 2002).

Darcy's Law

Originally, Darcy (1856) investigated the infiltration of water through saturated sand and formulated a general law:
Conductivity = Flux/Pressure Gradient (Siau, 1984).
Principal assumptions for Darcy's law, as formulated by Siau (1984), are:

1. Flow is viscous and linear. Linear velocity and volumetric rates of flow are then directly proportional to the applied pressure differential.
2. The fluid is homogeneous and incompressible.
3. The porous medium is homogeneous.
4. Permeability is independent of the length of the specimen in the direction of flow.

Assumptions three and four clearly fail for water transport through wood. Even so, Darcy's law has been widely applied to the relationship between the rate of flow and the pressure gradient for porous media (Siau, 1984; Reid *et al.*, 2005).

$$k = \frac{Q/A}{\Delta\Psi/L} = \frac{QL}{A\Delta\Psi} \qquad \text{(Equation 1.4)}$$

where k is conductivity, Q is flow per unit time (cm^3s^{-1}) through a column of porous material of cross sectional area A (cm^2) and length L (cm); $\Delta\Psi$ is the water potential gradient.

The Hagen-Poiseuille Equation and its implications

In the 19th century, Hagen and Poiseuille developed an equation describing the rate and velocity of flow of a fluid through a circular tube. They showed that velocity of water increases towards the centre of a tube and that water remains nearly stationary at side walls (Roderick and Berry, 2001; Tyree and Zimmermann, 2002). The mathematical equation describing the water flow in a conduit with certain diameter can be expressed as:

$$k = \frac{r^4\pi}{8\eta} \qquad \text{(Equation 1.5)}$$

where k is the hydraulic conductivity of a tube, r is the radius and η is the dynamic fluid viscosity.

By using diameter instead of radius and adding a pressure gradient for a certain tree height we have:

$$k = -\frac{\pi D^4}{128\eta}\frac{\Delta p}{\Delta x} \qquad \text{(Equation 1.6)}$$

where D is the diameter of a circular conduit, η is the viscosity of water, and $\Delta p/\Delta x$ is the pressure gradient. The negative sign indicates the direction of flow from high to low pressure (Lewis and Boose, 1995).

1.3.2 Radial and tangential transport

Two architectural features influence the transport of water in radial directions. These are the generic inter-vessel- or inter-tracheid pit structures in the conduit network, and wood rays. Wood rays are aggregations of parenchyma cells that extend radially between the vertical tracheary elements from the center of the stem outward to the cambium. They are the only living cells in the xylem of woody plants and are connected to adjacent water-conducting tracheary elements by means of pit pairs in their side walls (Salisbury and Ross, 1992; Dickison, 2000). Normally, those pits are half bordered involving a simple pit on the ray parenchyma side while the pit on the tracheary element side is bordered. However in dicotyledonous trees, rays are scarce and ray transport of water and conduction through rays is usually slow, owing to the high density of parenchyma cells that hinders water transport (Dickison, 2000 ; Tyree and Zimmermann, 2002). Consequently, inter-vessel or inter-tracheid pits arguably provide a quicker and more direct means of radial water transport. Unfortunately, such transport is difficult to quantify and most investigations ignore radial/tangential deviation of sap from the axial path (Kitin *et al.*, 2004; Domec *et al.*, 2006).

Three-dimensional scanning of the vessel structure of *Fraxinus lanuginosa* and *Machilus thunbergii* illustrated interconnections between vessels in radial and tangential directions, even across the borders of annuli (Fujii *et al.*, 2001; Kitin *et al.*, 2004). Many studies have described radial sap flow in ring-porous and conifer species

The majority of studies of conifers, ring- and diffuse-porous species detect the greatest sap flow in outer xylem, close to the cambium, and decreasing sap flow towards heartwood (Granier *et al.*, 1994; James *et al.*, 2003; Delzon *et al.*, 2004; Domec *et al.*, 2005; Domec *et al.*, 2006; Gebauer *et al.*, 2008). While fewer in number, studies have also described relatively even distribution of sap flow over the entire cross-sectional area of sapwood in diffuse-porous species (Jiménez *et al.*, 2000; Cermák *et al.*, 2002).

Decreasing efficiency of xylem elements closer to the heartwood may be genetically programmed (earlywood- and latewood formation) or induced by formation of

incipient tyloses in conducting conduits (McElrone *et al.*, 2010). Reducing pit density per conduit and thicker pit chambers (e.g. Panshin and de Zeeuw 1980) theoretically increases resistance to water transport in radial direction (Calkin *et al.*, 1986; Domec *et al.*, 2005). Acting in the opposite direction (increasing radial transport) are smaller conduits with more inter-vessel / inter-tracheid connections and greater pressure gradients (Canny, 1991; Larson *et al.*, 1994) . Domec (2006) calculated for a small *Pseudotsuga menziesii* that radial sap flow was about 100 times smaller than axial sap flow at breast height, but increased to about 10% of axial sap flow at a height of 10 m. This finding suggests water may move more freely in radial directions in the canopy of trees.

Similar to radial transport, tangential transport is facilitated by greater densities of vessels (Zimmermann and Tomlinson, 1966). Given that wood rays are radially orientated, water that is transported tangentially may have to pass through ray tissue. Such transport could be facilitated by inter-vessel / inter-tracheid pits.

There would appear to be several advantages of tangential transport. Most notable would be improved capacity of trees to take up water from localized sources and then distribute it to the whole canopy. Furthermore, if sections of conducting xylem in roots or trunks are damaged or embolized, water supply for the crown might still be guaranteed (Tyree and Zimmermann, 2002).

In partial support, dye-flow experiments have shown that sap usually ascends following a helical pathway within a growth ring and along a tree stem, indicating well-developed conduit connections in tangential direction (Chaney and Kozlowski, 1977; Kitin *et al.*, 2004; Tyree and Zimmermann, 2002). Even so, in conifers the total number of inter-tracheid pits responsible for tangential flow was found to be 10^3 times less than the number involved in axial flow (Petty, 1970; Flynn, 1995; Fujii *et al.*, 2001).

It is clear that based on present knowledge, assumptions of uniform transport of water over the entire cross-sectional area of xylem can lead to biased estimations of total tree water use. Far more data about radial and tangential water transport are required to fully understand the hydraulic architecture of trees (Delzon *et al.*, 2004).

1.3.3 Cavitation and refilling of conduit embolism

The underlying principle for the C-T theory is the chemical composition of water which is characterised by intermolecular hydrogen bonds. Fundamental dynamical process of liquid water is the making and breaking of these hydrogen bonds (Slayter, 1967; Zimmermann, 1983; Luzar and Chandler, 1996). Vapour pressure of water is 2.3 kPa at 20 °C, below this point xylem sap is in a metastable state (Zimmermann, 1983; Linton *et al.*, 1998). However, water in xylem conduits is exposed to immense negative pressure, usually of -1 to -2 and sometimes as low as -10 MPa (Tyree and Sperry, 1989). Exposed to such negative pressures, hydrogen bonds in the uprising water column can break and gas filled voids develop. Vaporisation of water induced by the release of energy too high to dissipate otherwise is commonly called "cavitation". Under tension, these gas bubbles expand and may finally embolise the entire vessel. Embolised vessels are dysfunctional. As a result hydraulic conductance declines and negative pressure within the remaining functional vessels may increase. In severe cases this might lead to an uncontrollable chain reaction (termed 'runaway embolism') which can potentially kill plants (Zimmermann, 1983; Tyree and Sperry, 1988; Tyree and Ewers, 1991).

Spreading of embolism can be triggered by two major processes. 'Air seeding' is defined as the spread of air through the pit membrane between an embolised and adjacent functional vessel. A higher negative pressure within the functional vessel forces the pit membrane to stretch and the adjacent air-water meniscus is pulled through the widened membrane pores (Fig. 1.4) (Zimmermann, 1983). 'Freezing-induced cavitation' is caused by gas bubbles, which are formed when gas dissolves within freezing sap (Fig. 1.4).

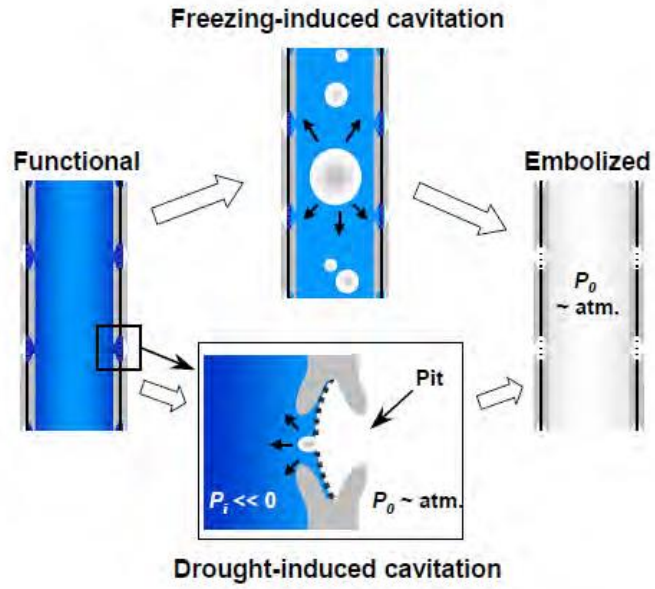

Figure 1.4: Mechanism of freezing-induced and drought-induced cavitation in Angiosperms as consequence of air seeding (Hacke and Sperry 2001)

How plants refill embolised vessels is not fully understood yet. Since water in plants is saturated with air at atmospheric pressure, dissolving air bubbles the in embolised vessels will require plant internal pressure to be greater than atmospheric pressure (Tyree *et al.*, 1999). Surface tension at the air/water interface of voids allows the gas to be at a higher pressure than the liquid (Tyree *et al.*, 1999; Hacke and Sperry, 2003). To calculate the pressure of gas within an embolised conduit (P_g) Tyree *et al.* (1999) suggested the 'capillary equation':

$$P_g = P_x + \frac{2T}{r} \qquad \text{(Equation 1.7)}$$

where P_x is the threshold xylem pressure, T is the surface tension of water in the vessel and r is the radius of curvature of the air/water interface. Positive xylem pressure must therefore at least exceed $-2T/r_v$ (where r_v is the radius of the vessel lumen containing the gas bubble) to overcome atmospheric pressure and collapse the bubble (Tyree *et al.*, 1999; Hacke and Sperry, 2003). Several authors suggested that short plants could develop the required positive pressure in roots during nighttime (Ewers *et al.*, 1991; Fisher *et al.*, 1997) . However, for tall plants like trees a nightime refill via positive root pressure appears very unlikely as the necessary pressure would have to be maintained against gravity over a long distance (Tyree *et*

al., 1999). Consequently, the ability of larger trees to refill embolized vessels requires different mechanisms. Several theories address this problem. Grace (1993) suggested that embolism could be reversed by export of solutes or salt from adjacent living parenchyma cells into vessels (Grace, 1993). Salleo *et al.* (1996) suggested a similar movement of solutes from the phloem. Movement of water due to osmotic differences may be sufficient to increase positive pressure above the $-2T/r_v$ threshold (Clearwater and Goldstein, 2005). Yang and Tyree (1992) suggested that time necessary for dissolution of voids will increase with increasing vessel cross-sectional area, increasing stem diameter, decreasing xylem pressure potential and increasing conduit diameter (Yang and Tyree, 1992). Species with small vessel diameters are therefore not only able to cope with greater negative xylem pressure, but they also might refill the embolised vessels quicker and more efficiently.

1.4 Descriptive models and theories

1.4.1 The Hydraulic Limitation Hypothesis

The Hydraulic Limitation Hypothesis (*HLH*) aims to explain physical limitations within hydraulic architecture and possible impacts on maximum tree height (Ryan and Yoder, 1997; McDowell *et al.*, 2002). It provides a theoretical framework which describes a decline in height growth with age of any tree species. In their original hypothesis Ryan and Yoder (1997) stated that total resistance to water flow in trees varies with both path length (l) and conductivity, resulting in increasing hydraulic resistance (R) with increasing tree height. A result is that the rate of water flow is assumed to be analogue to Ohm's law and equal to the potential difference between the roots and the leaf divided by the total hydraulic resistance (R_{tot}) along the hydraulic pathway (Ryan and Yoder, 1997). With increasing negative pressure towards the apical region of trees, the likelihood of cavitation events increases simultaneously. As pointed out earlier, trees have a certain capacity to regulate negative tension in xylem vessels as stomata react on reduced leaf water potentials with passive closing of guard cells. This mechanism effectively reduces water loss to the atmosphere but restricts the uptake of CO_2. Therefore photosynthetic activity decreases. The closure of stomata with increasing tension in the xylem is nowadays widely accepted as a common safety feature of trees against increasingly negative

water potentials and possible hydraulic failure. This mechanism was observed in many species (Bond and Kavanagh, 1999; Koch *et al.*, 2004; Ambrose *et al.*, 2009). Even though several studies provided evidence for reduced wood growth under limited carbon supply (Waring and Pitman, 1985; Ryan and Waring, 1992; Mencuccini and Grace, 1996; Ryan and Yoder, 1997), the line of argument as provided in the original *HLH* appears incomplete. However, other compensatory mechanisms improve the prediction power of the original hypothesis (Burgess *et al.*, 2006). For example the ratio between leaf- and sapwood-area (Huber Value) was identified as being another important driver for hydraulic efficiency of trees (Meinzer and Grantz, 1990; Pataki *et al.*, 1998; Becker *et al.*, 2000). *HLH* completely ignores vessel network structure, possibly the most powerful 'tool' of trees to adapt to environmental conditions. Vessel sizes on different sites are taken into account when Ryan and Yoder (1997) speculate about maximum achievable tree height on different sites. On nutrient-poor sites for example they expect low rates of stomatal conductance, slower wood growth, smaller vessels and as a result higher resistance to conducting water and shorter trees (Ryan and Yoder, 1997). Overall, *HLH* cleverly combines multiple cross-species observations and it creates a rudimentary framework of driving forces and physical restrictions on uprising sap. Even if *HLH* represents a simplistic approximation to a far more complex phenomenon (Mencuccini and Magnani, 2000), its combination of a range of simultaneous processes makes it a valuable starting point in order to explain limits of tree height growth.

1.4.2 The Metabolic Scaling Theory – original and modified

The original Metabolic Scaling Theory (*MST*) first developed by West *et al.* (1999) is a comprehensive model approach describing optimal plant architecture including hydrodynamics, biomechanics and branching geometry based on the application of a universal theory of resource distribution through hierarchical branching networks of vascular plants. Assumed is an average idealized plant that may not reference to reality (Anfodillo *et al.*, 2006). Individual habitus features such as site-specific branching architecture or compression- and tension wood are not taken into account. For simplification purposes whole tree is hypothetically subdivided into segments, which are connected in series. Both, branch diameters and conduit diameters are assumed to follow a continuous hierarchical network. In-between internal and

external network segments (*k*), conduit ($\bar{r}$) and branch (*r*) radii should scale according to:

$$\overline{\beta}_k(\beta_k) = \frac{\bar{r}(r)_{k+1}}{\bar{r}(r)_k} = n^{-a/2} \qquad \text{(Equation 1.8)}$$

where $\overline{\beta}_k$ is scaling of xylem conduits among adjacent segments, β_k is the scaling of branch to daughter branch segments, and *n* is the number of branches/conduits (West *et al.*, 1999; Anfodillo *et al.*, 2006). *MST* for average idealised plant suggests, a = 1 (the branching architecture is area-preserving, as suggested by Leonardo da Vinci); a = 1/6 (hydrodynamic resistance is minimized); and n = 2 (plant is bifurcated). In this case β_κ = 0.70 (the daughter segment is 70% the diameter of the parent one) and, $\overline{\beta}_k$ = 0.94 (the daughter xylem conduit is 94 % the diameter of the parent one) (West *et al.*, 1999; Anfodillo *et al.*, 2006).

Approximation assumes a universal scaling of sap flow and all other metabolic processes with tree mass and biomass growth rate. The underlying power function to explain most tree size-related variations is minimalised and follows allometric scaling laws:

$$Y = Y_0 M^b \qquad \text{(Equation 1.9)}$$

where *Y* is the variable of interest (conductivity, flow rate, rates of metabolism or growth), Y_0 is a normalization constant, *M* is biomass and *b* is the scaling exponent (West *et al.*, 1999; Sperry *et al.*, 2012). Focusing on the structure of xylem networks, *MST* suggests that plant evolution favoured individuals with a hydraulic system capable to fully compensate for increasing *R* with increasing *l* (West *et al.*, 1999; Anfodillo *et al.*, 2006). Conduits within sapwood are assumed to run parallel from roots to leaf; the vessel diameter is taken to be constant within a single branch segment (*k*); R_{tot} of whole path length can therefore be calculated as

$$R_{tot} = \sum_{k=0}^{N} R_k = \left[\frac{1 - \left[\left(n^{1/3} - 1 \right) l / l_n \right]^{(1-6a)}}{1 - n^{(1/3-2a)}} \right] R_N \qquad \text{(Equation 1.10)}$$

where l is total path length, l_N and R_N are the length and hydraulic resistance of the terminal elements, a and n are parameters characterizing the plant architecture (West *et al.*, 1999; Petit and Anfodillo, 2009). Full compensation for increasing resistance with increasing tree height is theoretically achieved when $\bar{a}$ equals $1/6 \approx 0.17$ (West *et al.*, 1999; Savage *et al.*, 2010). The value of R of each segment, calculated by the Hagen-Poiseuille equation for laminar flow should be conserved and independent from k. However, a perfect conduit tapering structure to fully compensate path length resistance can be approximated as

$$Dh = Y_0 \times L^b \qquad \text{(Equation 1.11)}$$

where Dh is the hydraulically weighted diameter, Y_0 is a allometric constant, L is the distance from the apex and b is the tapering exponent which for *MST* is estimated as $\bar{a}/0.84$ (≈ 0.2) (Anfodillo *et al.*, 2006; Petit and Anfodillo, 2009; Petit *et al.*, 2010). Recent investigations aiming to identify a taper exponent that is able to compensate optimally for increasing R resulted in inconsistent findings. For tall angiosperms such values for b ranged between 0.199 and 0.31(Anfodillo *et al.*, 2006; Weitz *et al.*, 2006; Mencuccini *et al.*, 2007; Petit *et al.*, 2010). The change of Dh in an ideal plant is assumed to be size invariant within single segments. Tapering only occurs between segments while vessel numbers remain constant. Complexity of conductance/resistance within realistic vessel networks, for example by incorporating inter-vessel pit resistance (Becker *et al.*, 2003) or dynamic tapering independent from segmental fragmentation is not yet included in these calculations. However, even though *MST* simplifies and/or ignores a variety of wood-/tree structural features, the revolutionary idea of replacing conductivity as the focus point of former hydraulic models with an optimised allometrical scaling approach sparked numerous scientific discussions (Kozlowski and Konarzewski, 2004; Brown *et al.*, 2005; Kozlowski and Konarzewski, 2005; Zaehle, 2005; Anfodillo *et al.*, 2006; Mäkelä and Valentine, 2006; Petit and Anfodillo, 2009). Recently, Savage *et al.* (2010) introduced a 'packing function' (Savage *et al.*, 2010) to the *MST*, allowing to account for increasing conduit numbers with decreasing conduit diameters. The packing function

used follows the allometric scaling approach, where vessel density (*VD*, mm^{-2}) is calculated from conduit diameter (D_C; µm) (Sperry et al., 2008):

$$VD = k_4 D_C^b \qquad \text{(Equation 1.12)}$$

where *b* is the packing exponent and k_4 (mm^{-2} μm^{-b}) is the multiplier which expresses the fraction of the total wood area occupied by xylem conduits (Savage *et al.*, 2010; Sperry *et al.*, 2012). Especially with these more recent refinements, *MST* provides an effective conceptual basis for modelling biomass accumulation, optimal resource distribution and design of hydraulic networks by assuming optimal allometric scaling. *MST* provides a framework for mathematical interpretation of the architectural complexity of trees.

1.5 Importance of study – aims and research questions

Considering the dominance of the genus *Eucalyptus* within Australian ecosystems, far too little is yet known about the majority of the 800 or so *Eucalyptus* spp.. Species-specific adaptation to the environment and the resilience of Australian plant communities against changing climatic conditions are not yet understood.

To date, there have been few investigations of how changes in climate might affect hydraulic architecture of the genus Eucalyptus, its water use and rates of mortality (O'Grady *et al.*, 2009). There is consensus that investigated species align with global inter-species comparisons of environmental adaptation, so that wood structure such as wood density and the relation of wood area to conduit area, is positively related to temperature and negatively related to elevation and precipitation (Wiemann and Williamson, 2002 ; Searson *et al.*, 2004; Thomas *et al.*, 2004; Swenson and Enquist, 2007).

However, little is known about the structure of the conduit network in eucalypts or other angiosperm and gymnosperm species and genera worldwide. Nowadays approaches mainly lack the necessary amount of empirical data to achieve high-resolution information of vessel tapering within species and the existing models appear incomplete (Chapter 1.4).

This thesis will investigate a range of anatomical features of eucalypt species growing under a wide range of environmental conditions. It addresses several

important and unresolved questions: Is the hydraulic architecture in *Eucalyptus* spp. the key to the species' successful domination of most Australian ecosystems? And if so, will species ranges shift with climate change due to alteration of water availability? More specifically, the current thesis will address the following research questions:

1. How do temperature and water availability alter wood structure and conduit tapering in *Eucalyptus* species?
2. Does a universal conduit tapering strategy exist in the genus Eucalyptus?
3. Is the water transporting vessel system a result of environmental conditions or tree height?
4. How variable is the construction of vessel networks when the same species is grown under variable environmental conditions?
5. Can isotopic markers be used successfully to study the pathway of water in tall trees, particularly highlighting the location of water stores that are used to reduce the risk of embolism within the vessel network?

Following four chapters should be read by keeping in mind that emphases of chapters differed. Chapter two constitutes the most important, by far most work intensive and from a research perspective most powerful part of this thesis. The remaining three chapters were designed to support findings with additional information. Figure 1.5 provides a visual impression of varying importance of subsequent research chapters.

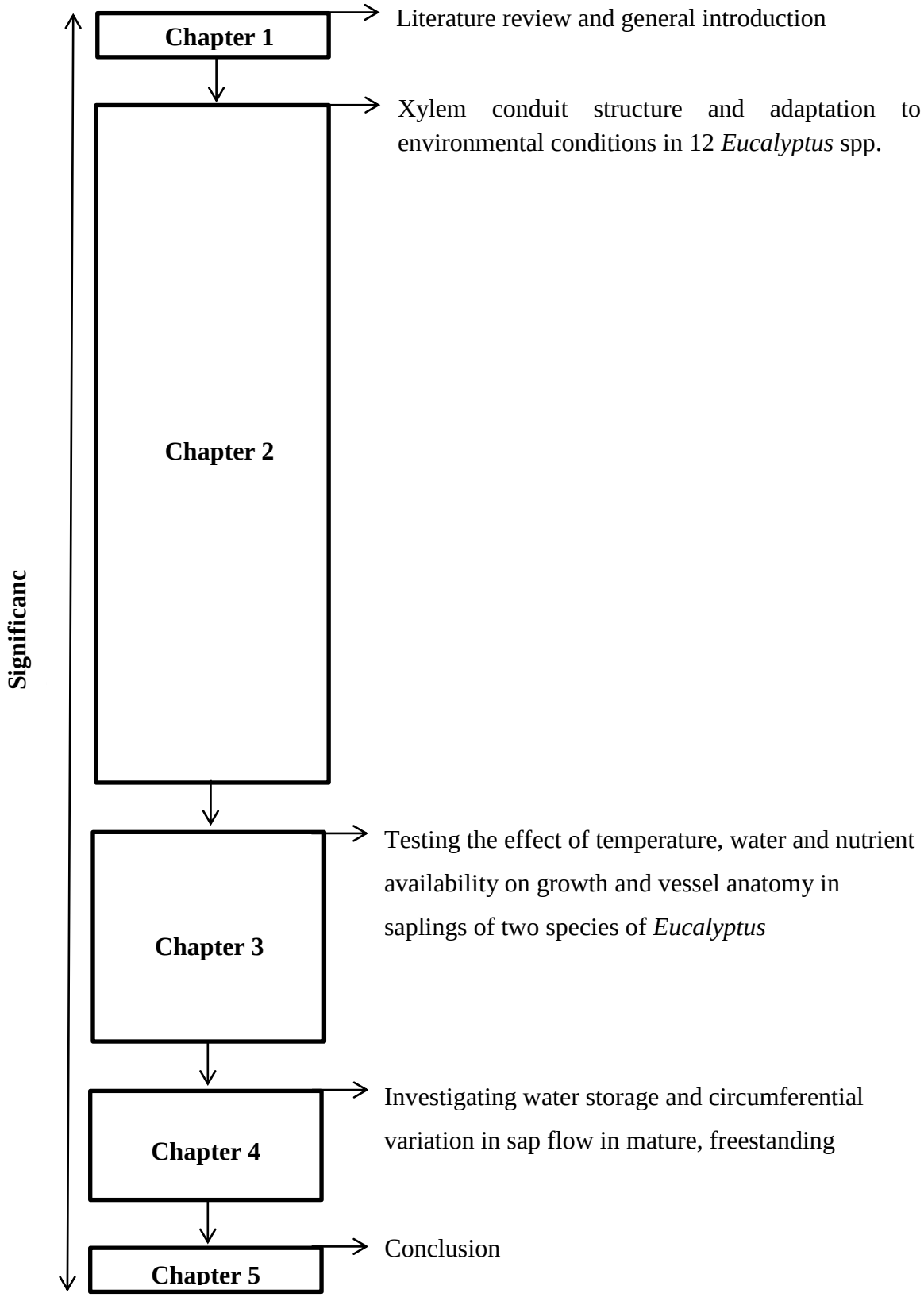

Figure 1.5: Visual representation of the relative importance of each thesis chapter, i.e. the larger the box the more important the chapter

Chapter 2 – Xylem conduit structure and adaptation to environmental conditions in 12 *Eucalyptus* spp.

2.1 Introduction

Australia encompasses an extraordinary diversity of ecosystems. This diversity is based on the continent's size and topography, stretching over six Köppen climate zones. Climate zones range latitudinally from equatorial and wet-dry tropics in the north to alpine and cool temperate areas in the mountainous regions of the south-east (Hadwen *et al.*, 2011). Independent of climate conditions, trees of the genus *Eucalyptus* dominate many terrestrial Australian ecosystems. Adaptation to, and evolution with, diverse climatic conditions over millennia has led to a wide variety of species (~800), many of them displaying strong endemism and only found within restricted geographic ranges. Approximately 50% of species have ranges spanning less than 3 °C of mean annual temperature, 40% have a range of <2 °C, and 25% a range of <1 °C (Hughes *et al.*, 1996). The genus *Eucalyptus* is one of the most widespread and diverse representatives of the angiosperms.

Highly developed hydraulic systems are a critical part of adaptation of trees to environmental conditions. In addition to structural adaptations of leaves (e.g leaf area) and roots (e.g. root diameter; Grier and Running, 1977; Norby and Jackson, 2000), the majority of recent investigations confirm a strong link between wood structure and environmental conditions. A substantial body of literature now describes vessel sizes of different species in different environments as well as vessel size adaptation of trees raised under different environmental conditions (e.g.Villar-Salvador *et al.*, 1997; Aber *et al.*, 1998; Van der Willigen and Pammenter, 1998; Carlquist, 2001; Thomas *et al.*, 2004, 2007; Chave *et al.*, 2009). The range of reported vessel diameters in different species, and at different heights within trees, is substantial, roughly from 10 – 500 µm. Generally, small trees from xeric environments have comparatively dense wood with relatively small vessels, while tall trees from mesic environments produce lighter wood and have larger vessels (e.g. Chave *et al.*, 2009; Campelo *et al.*, 2010). Furthermore, vessel density is closely linked to vessel diameter in that trees with large vessels have fewer vessels (per unit area) than trees with small vessels. All these trends have been observed on a global scale and for a wide variety of genera (e.g. Preston *et al.*, 2006; Sperry *et al.*, 2008; Chave *et al.*, 2009).

Partly triggered by possible consequences of climate change to the world's ecosystems, publications of innovative theories and models within the last two or so decades (e.g. Hydraulic Limitation Hypothesis (*HLH*); Chapter 1.4.1 and Metabolic Scaling Theory; Chapter 1.4.2) has renewed attention on wood and tree structure, and has sparked a flourishing discussion about influences of environmental factors on xylem structure, water use efficiency and biomass accumulation, i.e. wood density and maximum tree height (e.g. Ryan and Yoder, 1997; Wiemann *et al*., 1998; Wiemann and Williamson, 2002; Koch *et al*., 2004; Thomas *et al*., 2004, 2007; Preston *et al*., 2006; Swenson and Enquist, 2007; Martínez-Cabrera *et al*., 2009).

Most work, however, has been focused on species of the northern hemisphere and of the tropics, such as the rainforest species of Central- and South-America (e.g. Hacke and Sauter, 1995; Goldstein *et al.*, 1998; González and Eckstein, 2003; Hacke and Sperry, 2003; Gea-Izquierdo *et al.*, 2012) . *Eucalyptus* has received little attention in the overall dialogue. In view of the obvious potential of the genus *Eucalyptus* to adapt to prevalent environmental conditions, as well as their ecological significance within Australia and substantial economic value as a plantation tree, it is surprising that our understanding of the hydraulic architecture of this genus is limited. There are thus compelling reasons to study xylem adaptation to environmental conditions within the *Eucalyptus* genus.

One of the biggest limitations to research on whole-tree xylem structure is the workload, i.e. the microscopic examination of vessel structure, for example, is time consuming. As a result, most publications have concentrated on either the vessel structure at the base of tree trunks or a rudimentary sample extraction scheme spread over the entire height of trees (e.g. Martínez-Vilalta *et al.*, 2002; Campelo *et al.*, 2010; Poorter *et al.*, 2010). Very few studies have investigated the tapering structure of vessels throughout the entire tree (e.g. Petit *et al.*, 2010; Petit and Anfodillo, 2011). As a result, widely used models developed to explain water use efficiency of trees appear weak because modules accounting for vessel tapering structure along tree trunks remain basic and simplified.

So far, one of the key assumptions of the Metabolic Scaling Theory (Chapter 1.4.2), that vessels taper homogeneously along the entire height of trees, has been proven wrong. Investigations into tapering structures over whole path lengths have revealed different tapering intensities at different heights (e.g. Anfodillo *et al*., 2006; Petit *et al*., 2010; Petit and Anfodillo, 2011). Assuming the Hagen-Poiseuille Equation (Eq.

1.6) and the Cohesion-Tension Theory (Chapter 1.3) as underlying principles for effective transport of water, it could be expected that the tapering structure of vessels has evolved to counteract the internal rise of xylem water potentials, particularly under conditions where soil water availability is limited. At the same time water transport needs to be sufficient to support transpirational demands and the effects of increasing resistance and gravity with increasing tree height need to be overcome. All these factors are dependent on environmental conditions and influence the size of vessels. If we assume that (a) vessel size at the base of trees is adapted to climatic conditions and (b) tree size according to the *HLH* is dependent on conductivity of the vessel network (i.e. according to *MST*), it follows that whole-tree tapering structure of vessels is also the result of environmental adaptation. The few investigations that have assessed whole-tree tapering structure support this line of arguments, but no specific links to environmental conditions have been identified.

Climatic changes in Australian ecosystems are evident (e.g. Hughes, 2003; IPCC, 2007; Murphy and Timbal, 2008; Risbey *et al.*, 2009; Taschetto and England, 2009; Lavender and Abbs, 2013). Australia has warmed ~0.8 °C over the last century and annual average temperatures are, relative to 1990, predicted to increase by 0.4 – 2.0 °C until 2030 and 1.0 – 6.0 °C by 2070 (Plummer *et al.*, 1999; Hughes, 2003). High quality precipitation (P) data for Australia has only become available since the early 1900's. Those data indicate that annual distribution and total amounts of P are more variable than could be expected from similar climates elsewhere in the world (Nicholls *et al.*, 1997; Murphy and Timbal, 2008). The high complexity of influencing factors (i.e. ENSO) complicates accurate forecasting of precipitation. With the possibility of regional variations, tentative estimates predict increasing amounts of P for northern Western Australia, while P in eastern Australia is expected to decrease on average (Smith, 2004; Taschetto and England, 2009; Lavender and Abbs, 2013).

Rising temperatures and changes in annual amounts of precipitation seem likely to ensure that existing relationships between *Eucalyptus* spp. and their site may be subject to considerable evolutionary pressure over relatively short time frames. A corollary to this is that the ability of any given eucalypt species to physcially 'migrate' to sites with more favorable conditions is limited and slow (Hughes *et al.*, 1996). As a result of rapid change in the environment to warmer and possibly drier

conditions, crown dieback and/or adjustment of hydraulic architectural systems appear to be likely reactions.

Before we can forecast with any certainty adaptations of vessel and tapering structure, and related whole ecosystem impacts such as maximum tree heights, water use patterns and carbon storage capacities, broader knowledge of hydraulic architecture and vessel tapering appears crucial.

As the main component of this thesis, this chapter reports investigations of the tapering structure of vessels in different *Eucalyptus* species across a range of environments. Vessel and tapering traits of twelve different species were compared over the entire length of tree trunks. Study species were selected to represent a climatic gradient of increasing aridity from eastern to western Victoria. Additionally to the transect, one species from the arid Pilbara region, Western Australia and one species from the sub-alpine region in south-eastern New South Wales were included.

All tree- and vessel structural traits were related to climate indices calculated for long-term (100 years), mid-term (20 years) and short-term (5 years) periods, as well as for the very recent period (365 days prior to sample collection). These analyses are used to investigate the degree of plasticity of individual species to adjust their hydraulic architecture to climate of different time scales. This will help assess if *Eucalyptus* species display a similar or a different capacity to adjust their hydraulic architecture particularly to short-term variation of prevalent environmental conditions similar to what has been reported previously for ring-porous species from the northern hemisphere (e.g. Fonti *et al*., 2007; Campelo *et al*., 2010). The work conducted included development of a novel technique that allowed assessment of vessel tapering as consequence of environmental drivers.

The main research questions that are addressed are:

1. How do vessels of *Eucalyptus* spp. taper over the entire length of trees, from base to apex?
2. How do tapering structures vary in different *Eucalyptus* species?
3. How are vessel sizes and tapering structures of *Eucalyptus* spp. linked to climatic conditions?
4. What is the main factor controlling vessel tapering structure of species along the current theme of discussion on ‘height versus climate’?

2.2 Materials and methods

2.2.1 Species and field site descriptions

South-eastern mainland Australia is characterized by a pronounced altitudinal gradient from around 2000 m a.s.l. at the top of the Great Dividing Range in the east, to low-lying sand plains (approx. 50 m a.s.l.) several hundred km to the west. This altitudinal gradient corresponds with decreasing annual rainfall (P) and increasing average temperatures, from east to west. Accordingly, tall eucalypt forests dominate the mesic, mountainous region in the east. Moving west, the height of the eucalypt overstorey gradually declines, and tall, closed forests give way to open woodlands in the western semi-arid areas. High-elevation woodlands of *Eucalyptus pauciflora* are an exception along this gradient as they are of short stature but grow at the highest elevations with high amounts of annual precipitation.

Eleven species of the genus *Eucalyptus* were sampled along this environmental gradient reaching from subalpine, southern New South Wales to areas of low elevation in north-western Victoria (Fig. 2.1). To contrast the mainly temperate origins of sampled species, one eucalypt species (*E. victrix*) from a tropical, semi-arid environment in northern Western Australia was included. Location of sampling sites and species are shown in Table 2.1. Sampled forest types included semi-arid riparian woodlands, open mallee-type woodlands, box-ironbark forest, tall closed eucalypt forests, and sub-alpine woodlands. Together, these woodlands and forests cover an elevation gradient of >1500 m (Table 2.1). Although species in Fig. 2.1 and Table 2.1 are listed according to their distribution from east to west, the remaining section of the current chapter will list them according to the Aridity Index (AI, see below) of the site where species were sampled. In the State of Victoria, sample locations and species were also contingent upon access to logging activities and site permits, provided by VIC Forests and the Department of Sustainability and Environment (DSE).

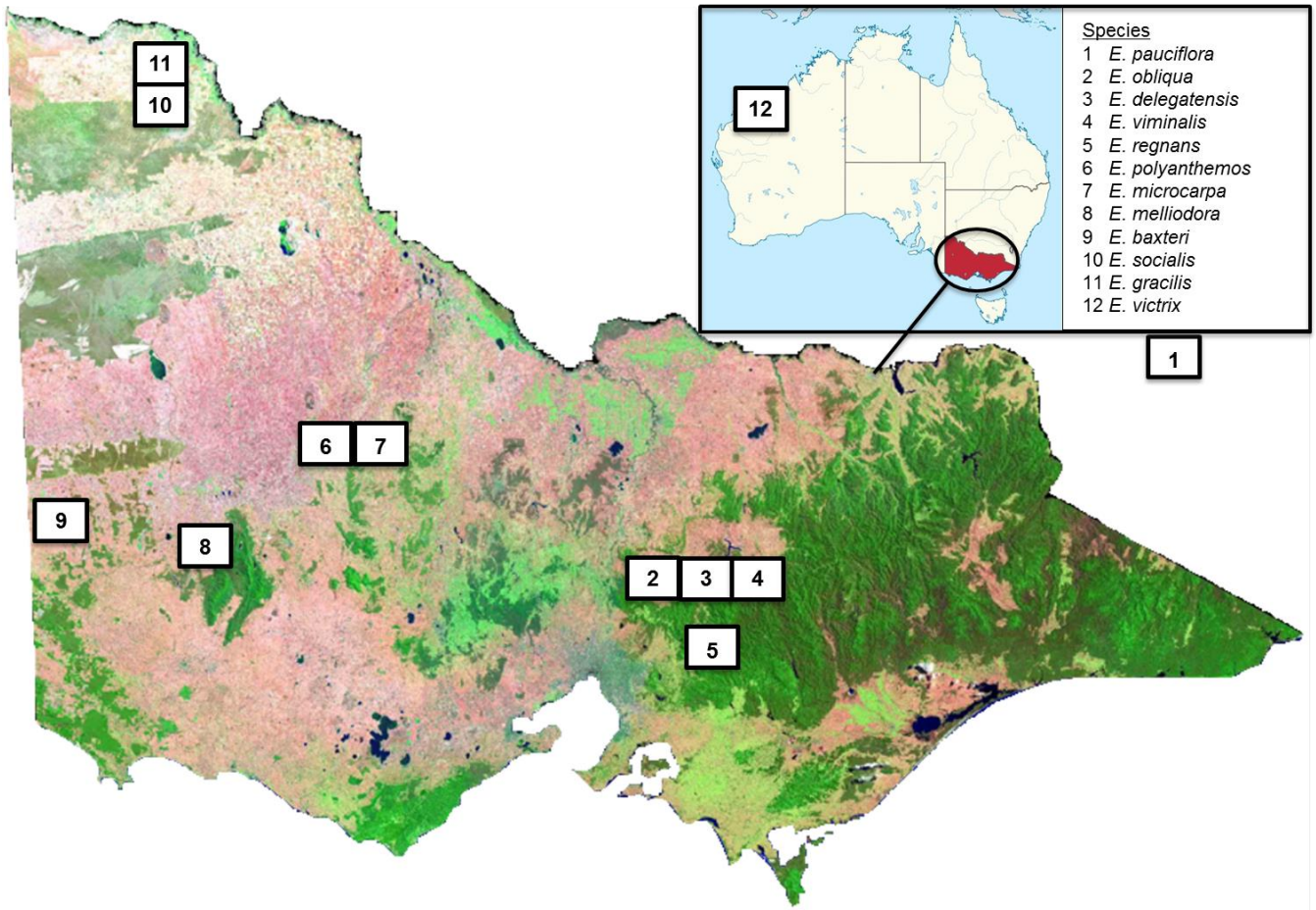

Figure 2.1 Satellite image of the state of Victoria, Australia, illustrating sample locations and species. Sample location 1 denotes the Snowy Mountain area in New South Wales, sample location 12 denotes the Pilbara (Port Hedland region) in Western Australia.

Table 2.1: Species name, eucalypt type and location of sampled *Eucalyptus* species. Information of ecosystem type were extracted from the Virdans Biological Databases (www.virdans.com, accessed 12.02.2013). Numbers before species names correspond with species locations shown in Fig. 2.1.

species	common name	sampling date	type	ecosystem	sample location	latitude (DD)	longitude (DD)	elevation (m.a.s.l.)
1 - *E. pauciflora*	Snow Gum	12.-13.12.2011	Gum	Sub-alpine open Woodland	Snowy Mountains, NSW	-36.11°	148.54°	1562
2 - *E. obliqua*	Messmate	21.-22.10.2010	Stringybark	Wet Sclerophyll Forest	Black Range State Forest, VIC	-37.34°	145.60°	753
3 - *E. delegatensis*	Alpine Ash	18.-20.10.2010	Stringybark	Wet Sclerophyll Forest	Rubicon State Forest, VIC	-37.38°	145.88°	1000
4 - *E. viminalis*	Manna Gum	22.-23.11.2010	Gum	Wet Sclerophyll Forest	Rubicon State Forest, VIC	-37.39°	145.87°	920
5 - *E. regnans*	Mountain Ash	26.-27.10.2010	Gum	Wet Sclerophyll Forest	Marysville State Forest, VIC	-37.61°	145.66°	480
6 - *E. polyanthemos*	Red Box	17.-18.06.2011	Box	Box-Ironbark Forest	Pyrenees State Forest, VIC	-36.67°	143.29°	248
7 - *E. microcarpa*	Grey Box	16.-17.06.2011	Box	Box-Ironbark Forest	Pyrenees State Forest, VIC	-36.66°	143.30°	261
8 - *E. melliodora*	Yellow Box	10.11.2011	Box	Dry Sclerophyll Forest	Grampians State Forest, VIC	-37.11°	142.17°	218
9 - *E. baxteri*	Brown Stringybark	08.-09.11.2011	Stringybark	Heathland	Kealys State Forest, VIC	-36.94°	141.25°	153
10 - *E. socialis*	Red Mallee	14.11.2011	Mallee	Mallee wood- and shrubland	Mildura State Forest, VIC	-34.33°	142.09°	52
11 - *E. gracilis*	White Mallee	13.-14.11.2011	Mallee	Mallee wood-and shrubland	Mildura State Forest, VIC	-34.33°	142.09°	52
12 - *E. victrix*	Smooth-barked coolibah	15.-16.05.2010	Box	Semi-arid woodlands	Port Hedland Area, WA	-20.54°	118.17°	19

2.2.2 Climate data

Climate descriptors for each sample location were obtained from SILO Data Drill© (State of Queensland, Department of Environment and Resource Management). Descriptors included daily maximum air temperature (T_{max}, °C), precipitation (P, mm) and evapotranspiration (FAO56, mm) recorded between 1911 and 2011. These climate data were interpolated from surrounding weather stations using an anomaly interpolation method for CLIMARC data. Interpolation procedures used in DATA DRILL are described in Jeffrey *et al.* (2001).

Using short- (5-year), mid- (20-year), and long-term (100-year) data from each sample location provided a means of assessing temporal trends in climate for each sample location. For this analysis, annual values for T, precipitation and AI were calculated and averaged for the interval of interest. Then, T, precipitation and AI were calculated for the 365-day interval prior to collection of sapwood samples. These 1-year data were compared to average climate indices for the 100-year interval, in order to evaluate if anatomy of most recently formed sapwood was influenced by the mesic conditions recorded for some, but not all, sites.

Aridity Index

The AI signifies the degree of dryness of an ecosystem and is a means of classifying regions according to their water deficit. A high index denotes a humid climate, while a low index denotes arid conditions. Potential evapotranspiration was calculated following the FAO Penman-Monteith method (i.e. FAO56; Allen *et al.*, 1998) as a more precise estimator than the simpler Thornthwaite approach (Kafle and Bruins, 2009). The index itself was calculated as:

$$AI_{UN} = \frac{P}{FAO56} \qquad \text{(Equation 2.1)}$$

where P is annual precipitation and 'FAO56' is annual potential evaptoranspiration. Following the classification provided by the United Nations, a 'Climate Class' can be assigned to an ecosystem, ranging from hyper-arid to wet (Table 2.2).

Table 2.2: Classification scheme of global aridity indices (UNEP, 1997).

Value	climate class
<0.03	Hyper-arid
0.03 – 0.2	Arid
0.2 – 0.5	Semi-arid
0.5 – 0.65	Dry sub-humid
0.65 – 0.75	Sub-humid
0.75 – 1.25	Humid
1.25 – 2.5	Very humid
>2.5	Wet

2.2.3 Collection of sapwood samples

Three mature trees per species were sampled between May 2010 and December 2011. All trees were felled shortly before sample collection. Target trees were selected according to visual assessment of the following criteria:

Each target tree:

I) was mature,

II) represented average stand diameter at breast height,

III) had a regular crown shape,

IV) had a straight basipetal stem section,

V) did not show physical damage from former logging operations.

After felling, tree length (to stem base) along the main axis was recorded, starting from the most terminal shoot (apex). Measurement tapes were attached to the tree, which allowed accurate marking of extraction points for sapwood samples, using permanent marker or spray paint. Sapwood samples were only collected from branch and stem sections that were uninfluenced by compression or tension wood (i.e. omitting branch junctions). The point of crown insertion (i.e. first green branch from base) was recorded. Diameters of extraction points along the shoot-twig-branch-trunk continuum were recorded using a vernier calliper (diameter <5 cm) or diameter tape (diameter >5 cm). A forestry calliper was used if branches or trunks (diameter >5 cm) had ground contact that prevented the use of a measuring tape. Digital images were taken of fallen and where possible, standing trees (see Appendix – Chapter 2). All samples were collected from the apex towards the base and along the axial pathway of xylem vessel on one side of the tree only. The distance between consecutive sample positions was increased with distance from the apex. With the apex as the reference point, sapwood was extracted from approximately identical

positions along all trees. This sampling strategy facilitated sample comparability independent of tree height and species. A guide to sampling frequency at varying positions along the tree is given in Table 2.3. For trees of short to medium stature (height ≤25 m; e.g. *E. microcarpa* and *E. pauciflora*), the maximum distance between sample points along the basipetal section of the bole was 200 cm. This distance increased to 500 cm along boles of tall trees (height ≥25 m; e.g. *E. delegantensis* and *E. regnans*). Sapwood samples were extracted from marked positions using secateurs and a hand- or chain saw. All samples were packed into labelled envelopes or paper bags and left to dry under ambient conditions.

Table 2. 3: Guideline to determine position of extraction points for sapwood samples.

distance from apex (cm)	distance between extraction points (cm)
0 – 30	2
30 – 50	5
50 – 100	10
100 – 200	20
200 – 500	50
500 – 1000	100
1000 – base	200 or 500

2.2.4 Sample preparation

Two different methods of sample preparation were applied. Twig samples from apical regions were often too small to be placed into the vice-like sample holder of the rotary microtome. Consequently, the strategy to prepare samples differed between small and large samples.

Preparation of samples with small diameters

Samples from the apical region with a diameter of approximately 0.1 to 0.3 cm were mounted in paraffin blocks using plastic embedding cassettes, as commonly used in histological studies. Prior to embedding, specimens of *E. delegatensis*, *E. obliqua*, *E. regnans*, *E. victrix* and *E. viminalis* were perfused with paraffin using an automated tissue processor (Shandon Excelsior Series, Thermo Scientific, USA). During initial analyses of sapwood anatomy it became obvious that this procedure was inappropriate for woody tissues as they became too fragile and paraffin wax

obstructed xylem vessel structures when viewed under a microscope. Consequently, apical sapwood samples of all remaining species were directly embedded without perfusion.

All sapwood samples were fixed into paraffin using an embedding station (Microm EC 350-1, Thermo Scientific, USA). Each sample was positioned vertically with its cut-side facing the bottom of the base mould. Samples were stabilised using a small amount of liquid paraffin. After positioning the embedding cassette over the sample, the moulds were filled with liquid paraffin. Prepared moulds were placed on a cooling surface to hasten the hardening process. After complete hardening, moulds were removed.

Prior to sectioning of apical samples with a rotary microtome (Leica RM2255, Leica Microsystems, Germany) surfaces of apical samples were trimmed and than soaked in water for two hours to soften woody tissues. Three to five sections (40 – 60 μm) were cut from each softened sample. After slicing, sections were transferred to a flotation bath (45 °C) to ease mounting onto glass slides. Paraffin was removed by placing slides into Bioclear (Bioworld, USA), for at least half an hour. All sections were stained with safranin (0.8% in H_2O). Excess stain was washed off after 1 minute using H_2O and then carefully padded dry with a paper towel. Following this procedure, sections were permanently mounted on glass slides using Eukitt (Sigma-Aldrich, Germany), protected with a glass cover slip and left to dry overnight under ambient conditions.

Preparation of samples with large diameters

Wood cubes (transverse cross section <0.5 cm^2) were prepared from the region adjacent to cambium (approximately 1 – 1.5 cm). Cubes were transferred into labelled embedding cassettes and submerged in boiling water for two hours before being soaked in water for 12 hours at room temperature. Three to five sections (35 – 45 μm) were prepared from each cube using a rotary microtome (Leica RM2255, Leica Microsystems, Germany). Staining and mounting of sapwood sections from wood blocks was identical to the procedure described for small samples.

2.2.5 Measurement of sapwood density

Following preparation of slides for microscopic analyses, sapwood cubes from tree bases were fully rehydrated by soaking them in 25 °C warm water for 72 hours. After soaking, each cube was blotted dry before recording its fresh weight to three decimal points. Volume of cubes (*V*, cm^3) was determined by Archimedes' principle of water displacement. Subsequently cubes were dried for 72 hours at 105 °C before their dry weight (*DW*, g) was recorded. Density of sapwood (*WD*, g cm^{-3}) was calculated as quotient of *DW* over *V*.

2.2.6 Measurement of sapwood anatomical traits

Prepared glass slides were placed under a transmissive light microscope (Leica DM2500M, Leica Microsystems, Germany) equipped with a high-resolution digital camera (Leica DFC 500, Leica Microsystems, Germany). Three images per glass slide (one image per sapwood section) were taken at either 5X, 10X (stem or branch samples) or 20X (apical samples).

Digital images were used to analyse characteristics of xylem vessels. A software for automated image analysis (Leica Application Suite (LAS), V3.8, Leica Microsystems, Germany) was used to identify these characteristics, which were vessel density (*VD*), n per cm^2 of sapwood) and equivalent circular diameter of vessels (*d*, µm). The relative fraction of void space to wood (*VtW*, %) was calculated for each image by summing the relative contribution of each void space to the total image area. Several manual correction procedures were used to ensure correct identification of vessel characteristics. These procedures included reconstruction of disrupted vessel walls, exclusion of large parenchymal cells and elimination of tissue fragments visible in vessels. If a section did not fill the entire image plane, as was the case for many apical and some branch sections, a manual correction procedure was implemented. This procedure included identification of the relevant area of sapwood and measurement of this area using the freeware Image J (V1.25s, National Institute of Health, USA).

Special care was taken to produce high-quality glass slides for microscopic assessment of sapwood characteristics. This included minimizing the following potential sources of error during sample preparation, image collection and also

during image analyses, including reconstruction of vessels:

I) Cutting thick slices during microtoming; this may reduce mechanical damage to vessel walls but will lead to substantial underestimation of true vessel dimensions due to strong shading effects.

II) Cutting slice from non-horizontal sapwood surface during microtoming; this can lead to overestimation of actual vessel dimensions.

III) Producing slices with non-planar surfaces during microtoming; this results in blurred images as substantial variation in the z-stage cannot be accounted for; this results in either over- or underestimation of true vessel dimensions.

IV) Leaving residues of paraffin wax within woody tissue of samples from apical branch; this results in either over- or underestimation of true vessel dimensions and can potentially affect *VD* as only a small area of sapwood is assessed.

V) Inaccuracy during reconstruction of vessel perimeter; this results in either over- or underestimation of true vessel dimensions.

2.2.7 Calculation and modelling of basic hydraulic properties

Automated measurements described above were used to calculate additional hydraulic characteristics of vessels identified in each digital image. The statistical software package R (Version 2.15.1, R Foundation for Statistical Computing, Austria) was used to program a customized script (see Supplementary Materials) for calculation of the hydraulic properties.

The mean hydraulic diameter (D*h*) was computed according to Sperry *et al.* (1994):

$$Dh = \frac{\sum_{n-1}^{N} d_n^5}{\sum_{n-1}^{N} d_n^4} \qquad \text{(Equation 2.2)}$$

where *d* is the diameter of a vessel conduit. For this calculation vessel conduits are assumed to have a perfect circular shape. The D*h* weights the importance of diameter

in proportion to the estimated hydraulic conductance of the conduits, since an increase in vessel diameter leads to a disproportionally larger increase of the vessels' hydraulic conductance (Sperry *et al.*, 1994). Hence, the larger the vessel diameter, the greater its influence on total hydraulic transport capacity.

The hydraulic resistance (*R*) of individual vessel sections (to the transport of water) was calculated using the respective D*h* of vessels. According to fluid-dynamics, *R* of a capillary tube is proportional to its length (*l*) and inversely proportional to its diameter (*d*) raised to the fourth power (i.e. Choat *et al.*, 2006):

$$R = \left(\frac{128 \eta l}{\pi D h^4} \right) \qquad \text{(Equation 2.3)}$$

where η is the dynamic viscosity of water, which is temperature-dependent and was individually calculated for 100 year average maximum temperature conditions as identified for each sample sites. In this case, length of the conduits was assumed to be 1 cm. In a second step *R* of individual 1 cm vessel sections was extrapolated to estimate *R* for an idealized conduit section (termed R_{sec}) that extends towards the mid-points of the adjacent sample positions above and below. Even though it was suggested that resistance of water moving through pit membranes may represent 80 – 87% of total hydraulic resistance, this model focusses only on the lumen resistance of tubes and assumes an ideal tube model without additional resistances of neither perforation plates nor pit membranes (Shinozaki *et al.*, 1964; Choat *et al.*, 2006). Relative hydraulic resistance (R_{rel}) was defined as quotient of R_{sec} to resistance of the entire water conducting pathway from the base towards the apex of trees (R_{tot}) according to the following formula:

$$R_{rel} = \frac{R_{sec}}{R_{tot}} \qquad \text{(Equation 2.4)}$$

Vessel density was calculated as the average of total vessel counts (*VC*) from three images per individual sapwood sample according to the formula:

$$VD = \frac{VC}{SA} * 100.000.000 \qquad \text{(Equation 2.5)}$$

where *SA* is the scanned area of sapwood in a given image. The factor of 100 Mio. is required to scale from μm^2 to cm^2.

2.2.8 Analysis of conduit taper

As tapering of vessel conduits towards the apex plays a major role in understanding hydraulic architecture and related changes of R_{tot} in trees, a novel analysis of the degree of taper was developed. For this analysis the relationship of D*h* to relative height of each tree was investigated and results of this analyses were assessed against climatic conditions of the species' habitat.
The relation between the two parameters is commonly curvilinear, and best described by a power function.

The varying degree of taper along *l* was separated into three distinct 'Phases', separating the lower stem section where taper is nearly absent (Phase 1), a section of reduced taper within the lower crown region containing the point of inflection of the curvilinear relation (Phase 2) and the final steep and linear increase of taper in the apical region (Phase 3). Accordingly, the section of the tree best characterised by Phase 1 might have the lowest slope and greatest intercept if a linear regression was applied. The opposite applies to Phase 3 where the greatest slope and least intercept would be found when relating D*h* to height of the respective sample position.

Linear regressions were used as a tool to explore how the relationship transitioned from one phase into the next. Phase 3 was defined to begin where the fitted trend line showing a steep linear slope would, in case of adding the respective next measurement to the group (downwards the stem), deviate towards a clearly lower angle. Conversely, Phase 1 was defined to end where the trend line of none or shallow incline would, in the case of adding the respective next measurement to the group (upwards the stem), deviate towards a clearly steeper slope. Finally, Phase 2 was appointed to consist of remaining measured D*h*s, which did neither belong to Phase 1 nor to Phase 3. Mean points between the last measurement belonging to Phase 1 and the first measurement identified as being Phase 2 and vice versa between the last measurement belonging to Phase 2 and the first measurement identified as being Phase 3 were calculated and defined as being both, start and end of the

respective adjacent phases.

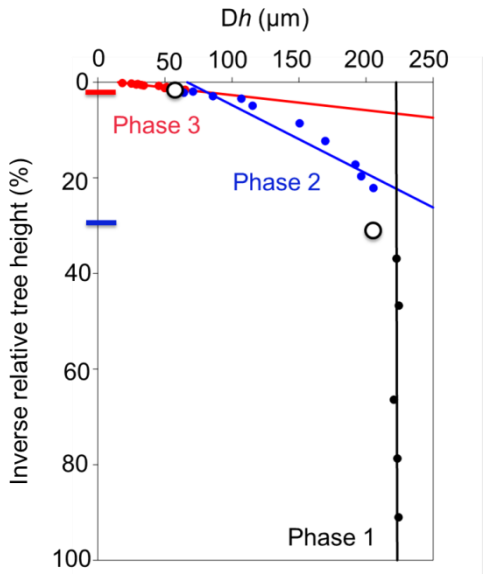

Figure 2.2: Conceptual design of "3-Phase Taper Analysis". Three trend lines indicating three different tapering intensities referred to as Phase 1, Phase 2 and Phase 3. Circles denote calculated means between the two adjacent measurements of D*h* that initiate phase change.

A tapering exponent (*b*) was calculated to examine the tapering structure of conduits as suggested by the Metabolic Scaling Theory (see Chapter 1.4.2). Based on the assumption of (i) homogeneous tapering of vessels (from base to apex) and (ii) comprehensive compensation for steadily increasing resistance, the tapering exponent expresses the slope of a linear log-log regression line of all measured D*h*s over the entire path length of a tree bole. Comparisons to former investigations will be provided by assessing changes in packing exponents (see Chapter 1.4.2; Sperry *et al.*, 2008).

2.2.9 Statistical analysis

The software "R" was used to calculate average traits for vessels, based on analyses of three digital images of sapwood per sample. Used script is shown in Appendix – Chapter 2; Fig. S2.85. To test observed trends of changing climatic conditions on sampled sites, averages of AI were calculated for each year. Groups of averages for the considered time periods (i.e. 100, 20 and 5 years) were tested against each other by using a Kruskal-Wallis ANOVA with a significance level of $p < 0.05$.

Sapwood density per species (*WD*) was calculated as an average of three measurements from DBH samples (n = 3), one from each considered individual tree. Basic vessel traits (*d*, *VD*) for samples from the most basipetal sections of trees were calculated for individual trees based on averaged values from three analysed images. Average values per species encompass therefore nine (3 x 3) measurements for a considered sample or variable. Bonferroni-Dunn test was used to evaluate if *d* differed significantly in sapwood extracted from the base of individual trees of the same species. Distribution of *d* within these samples was tested for normality and related skewness (τ) and kurtosis (κ) using the Shapiro-Wilks Test with a significance level of $p < 0.05$. To assess if size and distribution of *d* varied significantly among species, all measurements of *d* per species were pooled and differences among species were tested using Kruskal-Wallis ANOVA with a significance level of $p < 0.05$. For a pairwise comparison of means, conducted to identify differences in R_{tot} among species, a Bonferroni test with a significant level of $p < 0.05$ was used. Microsoft Excel 2010 was used for standard mathematical computations such as average values and standard deviations. Following software packages were used for statistical analysis: Sigma Plot Version 11 (SPSS Inc., Chicago, U.S.A), SPSS Version 21 (SPSS Inc., Chicago, U.S.A), JMP Version 10.0 (SAS Institute Inc., Cary, U.S.A).

2.3 Results

2.3.1 Site climate

There were large climatic differences among sites along the sample transect. . Sites at higher elevation in eastern Victoria and in southeast New South Wales are more mesic than those sampled in central- and western Victoria and in Western Australia (Table 2.4). According to classification of aridity index (AI) (see Chapter 2.2.1), climates of sample sites are based on the respective climatic zones:

Very humid sites

Sites at higher elevation in eastern VIC and in NSW received the most rainfall (P). Estimated 100-year averages were with 1804 mm $year^{-1}$ (± 36; ± 1 standard deviation) highest in the Marysville State Forest. The Black Range State Forest

received with 1246 mm year^{-1} (± 24), fully one third less precipitation. All other sites sampled within the very humid climate zone received annual amounts of P between these two extremes, but mostly well above 1400 mm year^{-1} (Table 2.4). Ecosystems of the very humid type had, compared to all other ecosystem types, the lowest long-term averages of maximum daily temperatures. The coolest site was the mountainous, open woodland site in the Snowy Plains. Here, estimated average maximum temperatures did not exceed 10.8 ºC (± 0.1). The site located in the Marysville State Forest showed comparably high average maximum temperatures of 17.2 ºC (± 0.1) and all other 'very humid' sites ranged between those two values. Overall, low actual evapotranspiration rates of 827 mm year^{-1} (± 50) to 94 mm year^{-1} (± 50) and high precipitation rates resulted in aridity indices between 1.93 (Marysville State Forest) and 1.35 (Black Range State Forest). See Table 2.4 for site-specific averages.

Dry sub-humid and semi-arid sites

In the dry sub-humid and semi-arid climate zones most sites received relatively similar amounts of precipitation. Averages varied between 581 mm year^{-1} (± 12) in the Grampians State Forest (dry sub-humid) and 490 mm year^{-1} (± 13) in Pyrenees State Forest (semi-arid). Average maximum daily temperatures differed marginally, being 20 ºC (± 0.1) for the Grampians and 21 ºC (± 0.1) for the Pyrenees. Mildura State Forest was exceptional and clearly more xeric than the other semi-arid sites. Average annual precipitation at this site was 334 mm year^{-1} (± 9) while average maximum daily temperature was 23 ºC (± 0.1)., Despite obvious similarities of both zones, potential evapotranspiration was less within the dry sub-humid sites where it ranged from 1077 mm year^{-1} (± 50) to 1080 mm year^{-1} (± 53). Consequently, the AI was slightly higher with values of 0.53 – 0.54 when compared to that of the semi-arid sites where the AI varied between 0.44 (± 0.01) Pyrenees State Forest and 0.25 (± 0.01) in the Mildura State Forest. The lower AIs were driven strongly by greater rates of potential evapotranspiration - 1164 mm year^{-1} (± 55) to 1344 mm year^{-1} (± 57). See Table 2.4 for site-specific averages.

Arid sites

According to the AI classification, the Port Hedland region in north Western Australia represented the only arid site within this study. Average precipitation was both the least 310 mm $year^{-1}$ and most variable (± 179). Mean daily maximum temperatures of 33 ºC (± 0.1) combined with fast rates of evapotranspiration (2110 mm $year^{-1}$ ± 73) resulted in the lowest AI of 0.15.

Table 2.4: Averages of annual rainfall (P), maximum daily temperatures (T_{max}), potential evapotranspirations (FAO56) and aridity indices (AI) estimated for the last 100 years and each sample site. Standard deviations for individual datasets are shown in parenthesis. Sampling sites classified into climatic zones according to the AI classification provided in Chapter 2.2.2. Data are sorted according to 100-year averages of AI.

Sample Site	Species	P (mm year^{-1})	T_{max} (°C)	FAO56 (mm year^{-1})	AI	climatic zone
Marysville State Forest, VIC	*E. regnans*	1805 (± 360)	17.2 (± 0.6)	942 (± 50)	1.93 (± 0.46)	very humid
Snowy Mountains, NSW	*E. pauciflora*	1484 (± 336)	10.8 (± 0.7)	827 (± 50)	1.82 (± 0.48)	very humid
Rubicon State Forest 1, VIC	*E. viminalis*	1484 (± 333)	13.8 (± 0.6)	868 (± 47)	1.73 (± 0.45)	very humid
Rubicon State Forest 2, VIC	*E. delegatensis*	1448 (± 323)	13.6 (± 0.6)	861 (± 47)	1.70 (± 0.44)	very humid
Black Range State Forest, VIC	*E. obliqua*	1246 (± 242)	15.9 (± 0.6)	934 (± 48)	1.35 (± 0.31)	very humid
Grampians State Forest, VIC	*E. melliodora*	581 (± 120)	19.9 (± 0.7)	1080 (± 53)	0.54 (± 0.13)	dry sub-humid
Kealys State Forest, VIC	*E. baxteri*	567 (± 116)	20.2 (± 0.6)	1077 (± 50)	0.53 (± 0.12)	dry sub-humid
Pyrenees State Forest 1, VIC	*E. microcarpa*	502 (± 134)	20.5 (± 0.7)	1164 (± 56)	0.44 (± 0.13)	semi-arid
Pyrenees State Forest 2, VIC	*E. polyanthemos*	490 (± 130)	20.6 (± 0.7)	1164 (± 55)	0.43 (± 0.13)	semi-arid
Mildura State Forest, VIC	*E. gracilis/E. socialis*	334 (± 95)	23.3 (± 0.6)	1344 (± 57)	0.25 (± 0.08)	semi-arid
Port Hedland Area, WA	*E. victrix*	310 (± 179)	33.3 (± 0.8)	2110 (± 73)	0.15 (± 0.09)	arid

2.3.2 Climate trends

For most sampling sites, average AI (on an annual basis) did not differ ($p > 0.05$) among time periods (i.e. 100-, 20- and 5-year periods). Even so, there were some obvious overall trends, especially for the very humid ecosystems (Fig. 2.3).

Precipitation (P)

There has been a clear reduction in P of 17% in the Marysville State Forest if medium-term (past 20 years) data are compared to long-term data (past 100 years). This contrast is even stronger (a 22% reduction) if data for the past 5 years were compared to long-term data. Annual P also declined by 12% (20 year / 100 year comparison) at the Rubicon State Forest and by 16% (20 / 100) at the Snowy Mountains. The medium term comparisons yielded reductions of 12% (5 / 100) for the Rubicon State Forest and 20% (5 / 100) for the Snowy Mountains. In the Black Range State Forest precipitation was relatively constant, irrespective of the basis for comparison.

Declines in precipitation were less pronounced in forests classified as dry sub-humid than those in very humid areas. Generally, annual precipitation for dry sub-humid sites declined by between 3 and 8% depending on the calculation basis. The 5-year averages for these sites were strongly influenced by above average P in 2010 and 2011, resulting in a reduction of annual precipitation at the Kealys State Forest of just 4% and an increase of 5% in the Grampians The sites classified as being semi-arid showed similar trends where due to the generally low amounts of annual precipitation, the wet years of 2010 and 2011 significantly increased the 5-year averages (by up to 11%).

Very wet years clearly induce greater bias in calculated mid- to short-term average P for arid areas than for other zones. In the Port Hedland region, for example, short-term increases in P were considerably greater than those observed in the semi-arid forests. On average, the Port Hedland region received 19% more P when the past 20 years data were compared to the 100 year data, and 13% more P if the past 5-year data were used as the basis for comparison.

Maximum air temperature (T_{max})

Average maximum air temperature has increased (e.g. past 5 years, past 20 years) at all sites compared to the long run data. At very humid sites, the last 20 years showed moderate increases ranging from 0.1 °C in the Rubicon State Forest to 0.4 °C in Marysville State forest. If the calculation is based on the latest five-year data then, again, the Marysville State Forest showed the largest increase of 1.0 °C while the smallest increase was at Rubicon State Forest with 0.5 °C.
This pattern was repeated, more or less, in dry sub-humid zone and semi-arid zone.

Aridity index (AI)

Changes in AI generally followed the patterns described for precipitation. In very humid forests of the Great Dividing Range, AI changed most according to mid- and short-term weather observations. However, none of those changes resulted in re-classification. Figure 2.3 illustrates the changes in AI for each sample site.

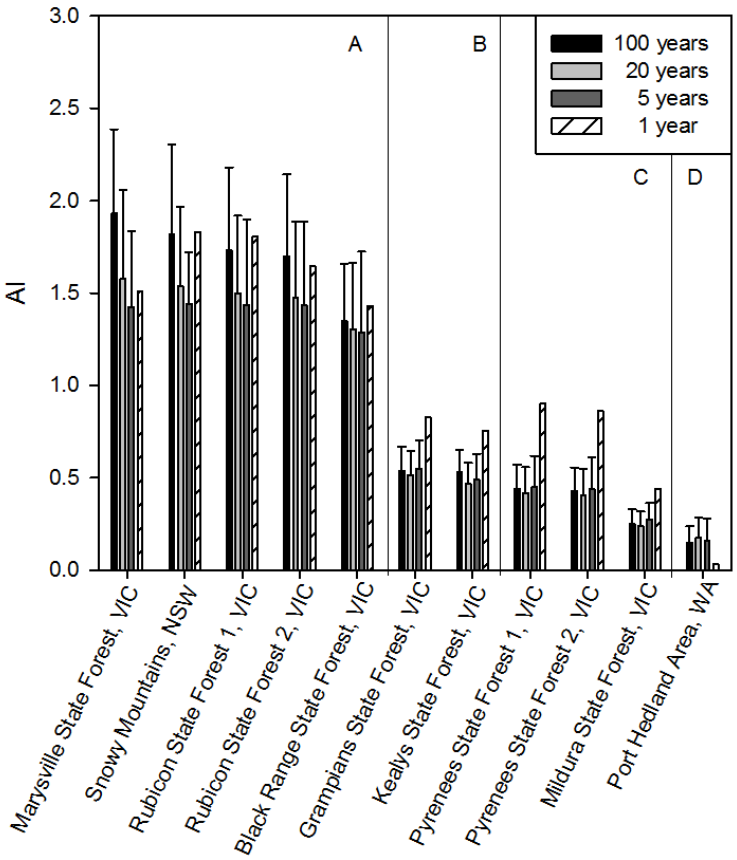

Figure 2.3: Long- (100-year), mid- (20-year), short- (5-year) term, and most recent year (1-year; 2011) averages of aridity indices (AI) estimated for all sample sites. A indicates the group of sampling sites that are in the 'very humid' climatic zone, B in the 'dry sub-humid' climatic zone, C in the 'semi-arid' climatic zone and D in the 'arid' climatic zone. Bars are mean values and error bars denote standard deviations.

2.3.3 Tree structural traits

The tallest tree sampled was a *Eucalyptus regnans* with a total height of 70.3 m, while an *E. gracilis* at 6.5 m was the shortest. Crown insertion was exponentially related to tree height ($y = 0.73x\text{-}436.23$; $R^2 = 0.96$; linear model excluded *E. victrix*). Largest diameter at breast height (DBH) of 69 cm and highest crown insertion of 50.9 m was found for *E. regnans*, while the smallest DBH of 9 cm and lowest crown insertion of 1.1 m was measured for *E. gracilis*. Table 2.5 shows basal diameter, total height and heights of crown insertion points for study trees.

Table 2.5: Basal diameter at 1.3 m above ground (DBH), total tree height and insterion point of tree crowns (measured from base) of all trees. Abbreviation used: t.n. = tree number per species. Species are sorted according to long-term (100-year) average aridity indices at sample sites. Height of crown insertion was not recorded for *Eucalyptus victrix*.

species	t.n.	DBH (cm)	height (cm)	crown insertion (cm)
E. regnans	1	61.7	6625	4705
E. regnans	2	61.5	7030	5090
E. regnans	3	69.0	6908	4558
E. pauciflora	1	27.7	1172	272
E. pauciflora	2	45.4	1090	550
E. pauciflora	3	34.5	1265	555
E. viminalis	1	56.8	5400	3690
E. viminalis	2	40.2	5000	4040
E. viminalis	3	62.2	4760	3590
E. delegatensis	1	54.3	5034	2734
E. delegatensis	2	65.3	5859	3559
E. delegatensis	3	89.8	5739	3339
E. obliqua	1	71.5	4065	1985
E. obliqua	2	54.5	3650	2020
E. obliqua	3	52.0	3720	1990
E. meliodora	1	24.5	1736	986
E. meliodora	2	42.2	1872	1072
E. meliodora	3	26.5	1795	1185
E. baxteri	1	27.2	1525	895
E. baxteri	2	17.0	1410	890
E. baxteri	3	29.3	1435	635
E. microcarpa	1	37.4	1930	750
E. microcarpa	2	38.5	1920	490
E. microcarpa	3	37.6	1910	770
E. polyanthemos	1	28.0	1420	450
E. polyanthemos	2	18.0	1200	420
E. polyanthemos	3	26.7	1370	490
E. gracilis	1	26.2	1110	360
E. gracilis	2	13.3	830	257
E. gracilis	3	9.0	645	111
E. socialis	1	17.9	917	237
E. socialis	2	13.5	695	165
E. socialis	3	18.5	915	305
E. victrix	1	25.5	1702	-
E. victrix	2	30.0	2005	-
E. victrix	3	29.5	1515	-

All main climate parameters (T, precipitation and AI) were significantly linearly related to tree structural characteristics. Tall trees, with large DBH and a high crown insertion were found on very humid sites. Table 2.6 shows the strength of linear regressions (R^2) of individual tree structural traits plotted against 100-year averages of climate parameters.

Table 2.6: Coefficients of determination (R^2) between individual tree structural traits and long-term (100-year) averages of site-specific aridity indices (AI_{100}), precipitation (P_{100}) and daily maximum temperatures (T_{max100}). All linear regression models excluded *E. pauciflora* and *E. victrix*.

	R^2	equation
AI_{100}		
Tree height	0.96	y = 3189.20x + 32.64
DBH	0.77	y = 28.19x + 13.92
Crown insertion	0.94	y = 2362.30x –433.58
P_{100} (mm year^{-1})		
Tree height	0.97	y = 3.92x – 495.02
DBH	0.76	y = 0.03x + 9.58
Crown insertion	0.95	y = 2.91x – 828.56
T_{max100} (°C)		
Tree height	0.72	y = -530.20x +12925
DBH	0.73	y = -5.25x + 138.40
Crown insertion	0.67	y = -383.10x +8935.20

On a per-species basis (n = 3), tree height and DBH were strongly correlated to AI_{100}. In both cases an increase in AI_{100} resulted in an increase of the tree-related parameter (Fig. 2.4).

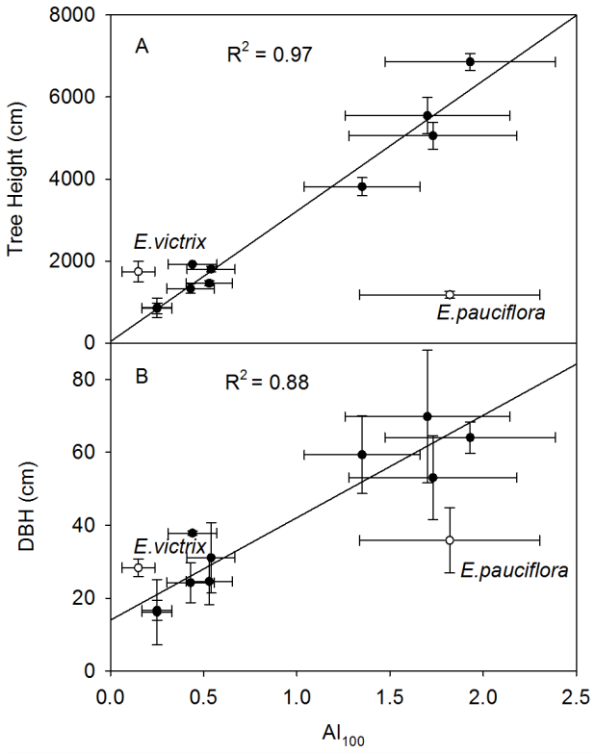

Figure 2.4: Relationships between long-term (100-year) average aridity indices (AI_{100}) of sample sites and (A) average heights (n = 3 species^{-1}) and (B) average DBHs (n = 3 species^{-1}) of sampled Eucalyptus species. Error bars represent standard deviations. Data for *E.pauciflora* and *E.victrix* are represented by circles; these data were excluded from the regression models. Coefficient of determination for the linear regression (solid lines; A) y = 3183.16x+34.91, B) y = 28.11x+13.96) are shown in figure.

2.3.4 Basic sapwood traits

The bases for all subsequent analyses were a total of 1254 collected and processed sapwood samples. Microscopic analyses of these samples produced a total of 3762 digital images. Within this set of images, the characteristics of 154368 vessels were determined.

Sapwood density (WD)

Sapwood density in samples taken from stem base varied between and within species (Table 2.8). On the species level, and excluding *Eucalyptus pauciflora* and *E. victrix*, *WD* showed clear correlation with all main long-term climate parameters such as AI_{100} ($y = -0.12x+0.74$; $R^2 = 0.58$), P_{100} ($y = 2.66x^{-0.22}$; $R^2 = 0.70$) and T_{max100} ($y = 0.02x+0.21$; $R^2 = 0.54$). *WD* was least at 0.47 g cm^{-3} (± 0.05) in *E. pauciflora*. Other

species from very humid environments ranged in density from 0.49 g cm^{-3} (± 0.05) in *E. obliqua* to 0.59 g cm^{-3} (± 0.05) in *E. delegatensis*. Of the species grown under dry sub-humid conditions *E. baxteri* had a remarkably low *WD* of 0.55 g cm^{-3} (± 0.11) compared to *E. melliodora* 0.62 g cm^{-3} (± 0.02) within the same climatic zone. Species from semi-arid and arid conditions had greater *WD* ranging between 0.67 g cm^{-3} (± 0.04) in *E. polyanthemos* and 0.79 g cm^{-3} (± 0.06) in *E. gracilis*. *E. victrix* had an unexpectedly low *WD* of 0.64 g cm^{-3} (± 0.02). Vessel size descriptors such as average vessel diameter ($y = -2.6E-03x+0.94$; $R^2 = 0.79$), average hydraulically weighted diameter ($y = -2.3E-03x+0.97$; $R^2 = 0.83$) and average vessel density ($y = 8.0E-05x+0.51$; $R^2 = 0.66$) had an obvious influence on *WD*. Tall species with large vessels had less dense wood than small species with a lot of small vessels.

Vessel diameter (d)

Vessel diameter varied greatly within single trees and among species. Basic tree structural features were strongly related to *d*. An exponential increase of tree height ($y = 285.40e^{0.02x}$; $R^2 = 0.78$) and DBH ($y = 8.11e^{0.01x}$; $R^2 = 0.62$) was observed with increasing *d*. Independent of species, the larger the average *d*, the fewer vessels were detected per square centimetre.

Figure 2.5 illustrates an exponential increase of average vessel density with decreasing average *d*. Individual tree examination supported the overall trend in vessel sizes being exponentially related to AI_{100} ($y = 0.08e^{0.02x}$; $R^2 = 0.83$) and P_{100} ($y = 129.11e^{0.01x}$; $R^2 = 0.82$) and linearly to T_{max100} ($y = -0.07x + 27.74$; $R^2 = 0.72$); *E.pauciflora* and *E. victrix* did not fit into described patterns and were excluded from models.

The widest vessel across all species was in the bole of an *E. obliqua* and was 338 µm in diameter. At the other end of the scale, the smallest vessel measured just 4 µm in diameter and was found close to the apex of an *E. melliodora*. In all trees average *d* was larger at the base of trees and declined with height. Analysis of the most basipetal sample of each individual tree was used as the foundation of inter-tree and inter-species comparisons. The largest average vessel diameter of basipetal samples of all considered trees was 317 µm in *E. viminalis*, whilst the smallest was 14 µm in *E. polyanthemos*. Across species, tall trees from the Great Dividing Range had the

largest vessel diameters, for example 171 µm (± 24) in *E. regnans* and 139 µm (± 19) in *E. obliqua*. *E. pauciflora* (110 µm, ± 13) was a clear outlier among species in the very humid zone. Less variation was detected in diameters of basipetal vessels in *E. melliodora* (126 µm, ± 4) and *E. baxteri* (125 µm, ± 8) from the dry-subhumid climate. Significantly smaller vessels were detected in species from the semi-arid ecosystems where *d* varied between 99 µm (± 9) in *E. polyanthemos* and 59 µm (± 8) in *E. gracilis*.

E. victrix, the only species sampled in an arid environment had surprisingly large vessel diameters in the lower stem (129 µm, ± 12).

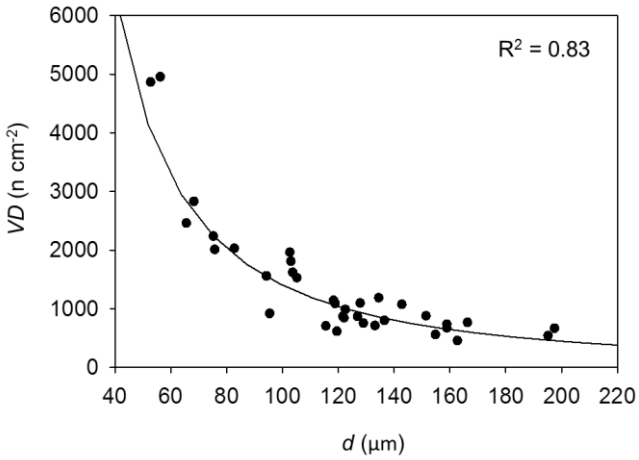

Figure 2.5: Relationship between average vessel diameter (*d*) and vessel density (*VD*) (n = 3) as measured in basipetal samples of all sampled individual trees. Coefficient of determination for the curvilinear decrease (solid line; $y = 2795968.68*x^{-1.65}$) is shown in Graph.

Vessel sizes in basipetal samples were normally distributed. Skewness of their distribution spanned values between -0.5 and 0.5 for most species, which is defined as being approximately symmetric. In *E. regnans*, *E. melliodora* and *E. baxteri* vessel distribution was moderately skewed towards a higher percentage of smaller vessels. Only *E. victrix* showed a highly skewed distribution (<-1) and proportionally had the highest proportion of small vessels among all study species. Platykurtic peakedness was found in the majority of species. Leptokurtic distributions were observed only in three species, namely *E. regnans*, *E. gracilis* and *E. victrix*. For all species, values of skewness and kurtosis of vessel size distributions are shown in Table 2.7.

Table 2.7: Skewness (τ) and kurtosis (κ) of vessel diameter distribution per species with respect to Gaussian "normal" Distributions. Reference images were taken at most basipetal samples. τ and κ are calculated values, commonly used interpretations (int.) are shown as abbreviations where 'a.s.' stands for approximately symmetric, 'm.s.' for moderately skewed, 'h.s.' for highly skewed, 'l.c.' for leptokurtic and 'p.c.' for platycurtic distributions.

Species	skewness		kurtosis	
	τ	int.	κ	int.
E. regnans	-0.54	m.s.	0.03	l.c.
E. pauciflora	-0.34	a.s.	-0.17	p.c.
E. viminalis	-0.03	a.s.	-0.33	p.c.
E. delegatensis	-0.41	a.s.	-0.55	p.c.
E. obliqua	0.04	a.s.	-0.70	p.c.
E. melliodora	-0.66	m.s.	-0.18	p.c.
E. baxteri	-0.63	m.s.	-0.16	p.c.
E. microcarpa	0.03	a.s.	-0.81	p.c.
E. polyanthemos	-0.29	a.s.	-0.71	p.c.
E. gracilis	0.17	a.s.	0.07	l.c.
E. socialis	0.08	a.s.	-0.52	p.c.
E. victrix	-1.03	h.s.	0.26	l.c.

Vessel density (VD)

Vessel density varied greatly along path length (*l*) within individual trees and among tree species. In individual trees, *VD* from basipetal sapwood samples correlated well with tree structural traits such as tree height and DBH (Fig. 2.6). Vessel densities were less in species from humid environments compared to species from semi-arid environments ($y = 911.75x^{-0.72}$; $R^2 = 0.77$; excluding *E. pauciflora* and *E. victrix*). Values for individual trees are presented in Table 2.8. The greatest *VD* (49025 vessels cm^{-2}) was recorded in sapwood 22 cm below the apex of an *E. socialis*. Sapwood from the main trunk of an *E. viminalis* had just 360 vessels cm^{-2}.

In all trees and regardless of prevailing environmental conditions, basipetal samples had low *VD*. *VD* then increased with tree height, commonly following curvilinear trajectories (see Fig. 2.9 as an example). Basipetal sapwood of trees at very humid sites had between 525 vessels cm^{-2} (± 66) (*E. delegatensis*) and 783 vessels cm^{-2} (± 107) (*E. regnans*). These densities increased towards tree apices where they reached densities of between 13680 vessels cm^{-2} (± 109) in *E. viminalis* and 20341 vessels cm^{-2} (± 723) in *E. delegatensis*. Sapwood collected from the base of trees growing under dry-subhumid conditions had almost twice as many vessels when compared to

their humid counterparts. *E. melliodora*, for example, had a *VD* of 946 vessels cm^{-2} (± 175) while *E. baxteri* showed a density of 1049 vessels cm^{-2} (± 164). Moving upwards in these trees, maximum *VD* was not greater than for taller tees in humid environments, and ranged from 17435 vessels cm^{-2} (± 2348) in *E. baxteri* to 23497 vessels cm^{-2} (± 5193) in *E. melliodora*.

Vessel density varied most in sapwood of species from semi-arid environments. For *E. microcarpa*, *VD* ranged from 1728 vessels cm^{-2} (± 268) to 29133 vessels cm^{-2} (± 3379) in *E. gracilis* the range was from 4217 vessels cm^{-2} (±1201) vessels at the base to 36289 vessels cm^{-2} (± 3569) at the apex. Sapwood of *E. victrix* had a *VD* similar to that of trees from dry-subhumid sites and did not exceed 1028 vessels cm^{-2} (±143) at the base or 19129 vessels cm^{-2} (±7908) in the apical region.

Across all sampled trees, *VD* was curvi-linearly related to tree height and DBH. As sample height declined from 70 to <10 meters and as sample DBH declined from 90 to <20 cm, *VD* increased strongly (Fig. 2.6). Table 2.8 shows all basic sapwood traits measured in individual trees.

Table 2.8: Characteristics of sapwood collected from the base of *Eucalyptus* trees that grew along an environmental gradient of increasing aridity. Abbreviated descriptors are: t.n. = tree number per species; *VC* = vessel counts, *d* = average vessel diameter, d_{min} and d_{max} = smallest and widest vessel diameters measured, n.d. = normal distribution of vessel sizes (with n for no and y for yes), *VD* = vessel density and *WD* = sapwood density. Standard deviations are shown in parenthesis. Different superscripted letters indicate significant differences of d among three individuals of one species (Bonferroni-Dunn test; p <0.05).

species	t.n.	*VC*	*d* (µm)	d_{min} (µm)	d_{max} (µm)	n.d	*VD* (n cm^{-2})	*WD* (g cm^{-3})
E. regnans	1	154	151 (± 48)^{a}	35	240	n	879 (± 60)	0.49
E. regnans	2	88	165 (± 40)^{a}	59	236	n	803 (± 104)	0.53
E. regnans	3	117	197 (± 46)^{b}	36	276	n	668 (± 149)	0.48
E. pauciflora	1	161	95 (± 27)^{a}	32	143	n	919 (± 20)	0.52
E. pauciflora	2	108	120 (± 34)^{b}	32	193	n	617 (± 17)	0.47
E. pauciflora	3	124	116 (± 25)^{b}	51	156	n	708 (± 133)	0.42
E. viminalis	1	125	133 (± 50)^{a}	36	239	n	714 (± 69)	0.60
E. viminalis	2	129	159 (± 58)^{b}	37	303	y	736 (± 51)	0.51
E. viminalis	3	95	195 (± 52)^{c}	59	317	y	542 (± 26)	0.61
E. delegatensis	1	80	163 (± 55)^{a}	44	245	n	457 (± 10)	0.59
E. delegatensis	2	103	157 (± 57)^{a}	26	257	n	588 (± 26)	0.63
E. delegatensis	3	93	151 (± 39)^{a}	48	234	n	531 (± 157)	0.54
E. obliqua	1	118	159 (± 65)^{a}	31	301	n	674 (± 97)	0.53
E. obliqua	2	37	122 (± 44)^{b}	23	195	n	845 (± 79)	0.51
E. obliqua	3	35	137 (± 59)^{ab}	30	260	y	799 (± 241)	0.44
E. melliodora	1	192	128 (± 53)^{a}	23	215	n	1096 (± 75)	0.63
E. melliodora	2	173	123 (± 34)^{a}	31	182	n	988 (± 86)	0.60
E. melliodora	3	132	129 (± 30)^{a}	31	197	n	754 (± 75)	0.63
E. baxteri	1	152	122 (± 32)^{a}	25	174	n	868 (± 77)	0.68
E. baxteri	2	208	134 (± 42)^{b}	26	217	n	1187 (± 40)	0.48
E. baxteri	3	191	119 (± 43)^{a}	25	200	n	1090 (± 60)	0.49
E. microcarpa	1	89	83 (± 26)^{a}	35	135	n	2032 (± 241)	0.72
E. microcarpa	2	71	104 (± 39)^{b}	26	181	n	1621 (± 788)	0.78
E. microcarpa	3	67	105 (± 36)^{b}	27	170	y	1530 (± 456)	0.76
E. polyanthemos	1	69	89 (± 39)^{a}	17	170	y	1576 (± 137)	0.64
E. polyanthemos	2	356	104 (± 42)^{b}	14	185	n	2032 (± 183)	0.65
E. polyanthemos	3	317	103 (± 39)^{b}	26	169	n	1810 (± 275)	0.71
E. gracilis	1	213	53 (± 16)^{a}	19	95	n	4864 (± 1140)	0.82
E. gracilis	2	124	68 (± 26)^{b}	19	118	n	2832 (± 105)	0.72
E. gracilis	3	217	56 (± 16)^{a}	16	89	n	4955 (± 933)	0.82
E. socialis	1	98	75 (± 29)^{a}	16	134	n	2238 (± 285)	0.72
E. socialis	2	405	66 (± 23)^{b}	23	133	n	2312 (± 140)	0.76
E. socialis	3	88	76 (± 29)^{a}	19	142	y	2009 (± 259)	0.78
E. victrix	1	47	143 (± 40)^{a}	34	189	n	1073 (± 79)	0.63
E. victrix	2	50	118 (± 48)^{b}	24	119	n	1142 (± 40)	0.63
E. victrix	3	38	127 (± 32)^{ab}	31	183	n	868 (± 143)	0.67

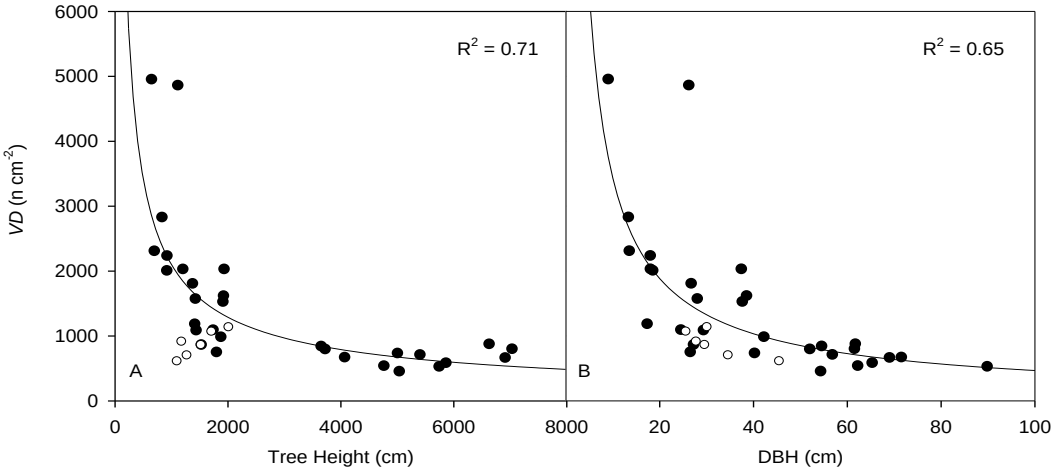

Figure 2.6: Relationships between vessel density (*VD*) of basipetal sapwood from individual trees and (A) tree height and (B) tree diameter at breast height (DBH). E. pauciflora and E. victrix are represented by circles; these data were excluded from the regression models. Coefficients of determination for the curvilinear trends (solid lines; A) $y = 1079194.78x^{-0.88}$, B) $y = 5381x^{-0.72}$) are shown.

Basic sapwood traits and climate

Long-term climate (i.e. 100 year climate data) was the better predictor of *d* or *VD* of individual trees when compared to recent (i.e. 1 year climate data, Table 2.9). This analysis revealed further that both sapwood traits were better correlated with AI_{100} (*d*: $R^2 = 0.83$; *VD*: $R^2 = 0.77$) than with either precipitation or temperature.

Table 2.9: Coefficients of determination and related quadratic and power functions that describe the relation between average basal vessel diameter (*d*) or vessel density (*VD*) of 12 Eucalyptus species (n = 3 species^{-1}) and long-term (100-year; R^2_{100}) or short-term (1 year; R^2_1) climate descriptors.

d	R^2_{100}	**equation**	R^2_1	**equation**
AI	0.83	$y = 45.94\ln(x) + 137.61$	0.79	$y = 117.99x^{0.64}$
P (mm year^{-1})	0.82	$y = 56.81\ln(x) - 253.83$	0.75	$y = 0.46x^{0.80}$
T_{max} (°C)	0.80	$y = -1.15x^2 + 32.58x - 70.80$	0.72	$y = -1.04x^2 + 28.63x - 36.94$
VD	R^2_{100}	**equation**	R^2_1	**equation**
AI	0.77	$y = 911.75x^{-0.72}$	0.75	$y = 1119.36x^{-1.11}$
P (mm year^{-1})	0.74	$y = 380002.28x^{-0.87}$	0.71	$y = 15764706.04x^{-1.38}$
T_{max} (°C)	0.77	$y = 55.16e^{0.16x}$	0.73	$y = 45.10e^{0.17x}$

2.3.5 Hydraulic sapwood traits

Hydraulically weighted diameter (Dh)

Hydraulically weighted vessel diameter (D*h*) and *VD* are widely accepted descriptors of the capacity of trees to conduct water. Both, D*h* and *VD* varied considerably among species. As expected, and similar to *d*, D*h* decreased with increasing height between base and apex.

To make full use of this unique dataset, where sapwood was analysed over the full height of trees, D*h* and *VD* at the base of trees (Dh_b and VD_b, respectively), and absolute maximum D*h* (Dh_{max}) and absolute minimum *VD* (VD_{min}), were examined in relation to environmental factors. Absolute maximum and minimum values may not necessarily be found at the base of trees, as they are strongly influenced by the size distribution of vessels in the case of Dh_{max}, and by the packing of vessels in sapwood in case of VD_{min}.

Table 2.10 illustrates this analysis. First the data show clearly that Dh_b and Dh_{max} as well as VD_b and VD_{min} do not necessarily coincide with the base of trees. Data for VD_b is equivalent to values shown in Table 2.8.
Regression models provided clear evidence that Dh_{max} and VD_{min} were more powerful descriptors for both tree structural and climate parameters than Dh_b and VD_b (Table 2.10). Based on these results Dh_{max} and VD_{min} were examined in greater detail.

Table 2.10: Coefficients of determination between vessel characteristics of sapwood from 10 Eucalyptus species (n = 3 species^{-1}) sampled across a strong gradient of aridity in south-eastern Australia and tree structural traits. Abbreviations used: AI_{100} = average aridity index of the last 100 years, DBH = Diameter at breast height, Dh_b = hydraulically weighted vessel diameter at stem base, Dh_{max} = largest indentified hydraulically weighted vessel diameter, VD_b = vessel density at stem base and VD_{min} = lowest identified vessel number. Resulting equations are shown for each of the regression models. Data for *E. pauciflora* and *E. victrix* were excluded in regression analyses.

	R^2 (AI_{100})	equation	R^2 (tree height)	equation	R^2 (DBH)	equation
Dh_b	0.83	$y = 55.92\ln(x)+176.11$	0.76	$y = 54.63\ln(x)-266.12$	0.62	$y = 63.40\ln(x)-68.03$
Dh_{max}	0.88	$y = 63.24\ln(x)+192.62$	0.80	$y = 61.61\ln(x)-306.19$	0.68	$y = 73\ln(x)-88.05$
VD_b	0.77	$911.75x^{-0.72}$	0.71	$y = 271692x^{-0.70}$	0.65	$y = 25215x^{-0.87}$
VD_{min}	0.81	$752.40x^{-0.77}$	0.76	$y = 362511x^{-0.76}$	0.68	$y = 26774x^{-0.93}$

Maximum hydraulically weighted vessel diameter (Dh_{max})

Largest Dh_{max} were recorded for the tall species from the humid foothills of the Great Dividing Range. Here, average diameters of species (n = 3) ranged from 247 µm (± 7) (*E. viminalis*) to 207 µm (± 17) (*E. regnans*). In dry-subhumid and semi-arid environments Dh_{max} were considerably smaller and varied between 167 µm (± 3) in *E. baxteri* to much smaller value for *E. socialis* and *E. gracilis*. In *E. socialis* Dh_{max} was with 106 µm (± 5) 20% wider than that of E. gracilis (84 µm, ± 16).

Across all species, Dh_{max} related well to T_{max100} as well as to AI_{100} (Fig. 2.7). *E. pauciflora* and *E. victrix* were clear outliers and their Dh_{max} did not fit model predictions.

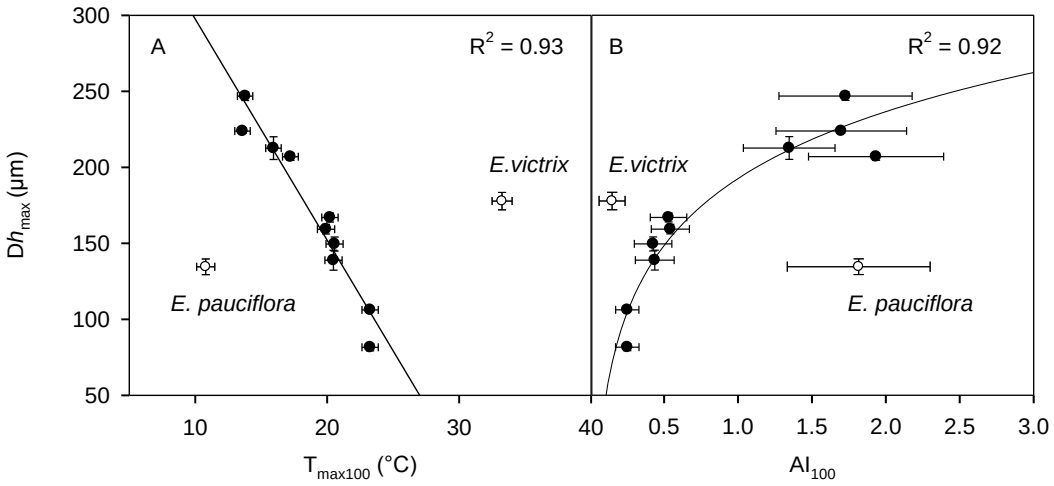

Figure 2.7: Relationships between (A) average long-term (100-year) maximum temperatures (T_{max100}), (B) average long-term (100-year) aridity indices and average maximum hydraulically weighted vessel diameters (Dh_{max}; n = 3 species^{-1}) of 12 sampled *Eucalyptus* species. Error bars depict standard deviations. Data for *E. pauciflora* and *E. victrix* is represented by circles; these data were excluded from the model. Coefficients of determination for linear regression and exponential rise (solid lines; A: y = -14.55x+443.12, B: y = 63.514ln(x) + 192.54) are shown in figures.

Minimum vessel density (VD_{min})

Sapwood from species at very humid sites had VD_{min} in the range from 431 vessels cm^{-2} (± 64) in *E. viminalis* to 681 vessels cm^{-2} (± 76) in *E. regnans*. Sapwood of E. *baxteri* (VD_{min} = 862 vessels cm^{-2}, ± 101) and *E. melliodora* (993 vessels cm^{-2}, ±

171) from dry-subhumid regions contained twice as many vessels as *E. viminalis*. Sapwood sampled from species originating from semi-arid environments showed a further increase - *E. microcarpa* had a VD_{min} of 1307 vessels cm^{-2} (±131) while *E. gracilis* had a density of 3616 vessels cm^{-2} (± 1090). These densities are approximately five times those found in sapwood of tall species from the Great Dividing Range. Once more, sapwood of *E. victrix* did not follow generally observed patterns of increasing VD_{min} with decreasing AI_{100} (VD_{min} = 875 vessels cm^{-2} (± 171). Analogus to the strong correlation between *d* and *VD* (Fig. 2.5), the smallest VD_{min} were found in species with a large Dh_{max} and vice versa. Figure 2.8 illustrates a strong correlation between VD_{min} and Dh_{max}.

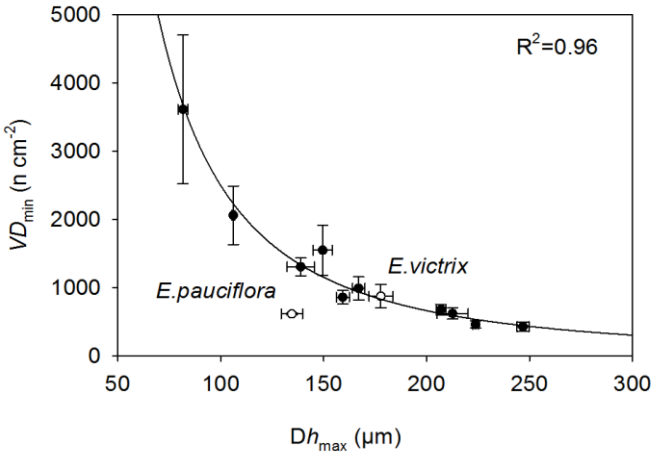

Figure 2.8: Relationship between average maximum hydraulically weighted vessel diameter (Dh_{max}; n = 3 species^{-1}) and average minimum vessel density (*VD*; n = 3 species^{-1}) of sampled 12 Eucalyptus species. Standard deviations are shown by error bars. Data for *E. pauciflora* and *E. victrix* is represented in by circles; these data were excluded from the model. Coefficient of determination for the power function (solid line; $y = 19175156.84x^{-1.94}$) is shown in figure.

In the same fashion as Dh_{max}, VD_{min} was strongly correlated to environmental and tree structural attributes such as AI_{100} (R^2 = 0.85; $758.87x^{-0.78}$), tree height (R^2 = 0.80; $427306.01x^{-0.78}$) and DBH (R^2 = 0.81; $51627.16x^{-1.11}$). All models describing the relationship of VD_{min} to environmental and tree structural parameters excluded *E. pauciflora* and *E. victrix*.

Table 2.11: Hydraulic characteristics of sapwood collected along the stems of 12 Eucalyptus species. Abbreviations: t.n. = tree number per species, Dh_b = hydraulically weighted vessel diameter at the base of stems, Dh_{max} = maximum hydraulically weighted vessel diameter and VD_{min} = minimum vessel density per square centimetre of sapwood. All locations were either Dh_b, Dh_{max} or VD_{min} were located are shown as inverse tree heights (i.e. 6000 cm indicates that the relevant parameter was detected in sapwood that was 60 m below the tree's apex).

species	t.n.	Dh_b (µm)	height Dh_b (cm)	Dh_{max} (µm)	height Dh_{max} (cm)	VD_{min} (n cm^{-2})	height VD_{min} (cm)
E. regnans	1	188	6000	196	3000	662	5000
E. regnans	2	189	6000	198	4500	765	6000
E. regnans	3	227	5000	227	5000	617	4000
E. pauciflora	1	115	1000	121	800	634	400
E. pauciflora	2	145	1000	145	1000	628	1000
E. pauciflora	3	131	1100	137	1000	605	390
E. viminalis	1	180	5000	250	3000	360	3000
E. viminalis	2	223	4500	239	3000	445	3000
E. viminalis	3	238	4500	252	3000	485	3000
E. delegatensis	1	205	4500	205	4500	457	4500
E. delegatensis	2	206	5400	238	4900	520	4900
E. delegatensis	3	180	5500	229	3490	411	4500
E. obliqua	1	224	3700	242	2200	617	900
E. obliqua	2	155	3500	191	3500	708	3000
E. obliqua	3	205	3500	205	2500	548	1000
E. melliodora	1	172	1600	172	1600	953	1400
E. melliodora	2	145	1800	156	1600	879	1600
E. melliodora	3	147	1600	151	1200	754	1600
E. baxteri	1	141	1400	170	1200	879	1400
E. baxteri	2	166	1200	168	1000	1187	1200
E. baxteri	3	154	1200	163	1000	925	1000
E. microcarpa	1	106	1800	140	1200	1176	1200
E. microcarpa	2	139	1800	139	1800	1439	900
E. microcarpa	3	138	1800	138	1800	1307	1000
E. polyanthemos	1	131	1200	141	800	1421	900
E. polyanthemos	2	144	1000	149	800	1964	1000
E. polyanthemos	3	140	1200	158	900	1267	598
E. gracilis	1	67	1000	68	800	4636	400
E. gracilis	2	93	700	100	250	2466	830
E. gracilis	3	68	500	84	600	3745	600
E. socialis	1	103	800	105	270	2238	800
E. socialis	2	89	600	102	500	2375	350
E. socialis	3	107	800	111	915	1576	915
E. victrix	1	165	1500	168	900	1073	1500
E. victrix	2	155	1900	176	1500	776	1100
E. victrix	3	147	1374	179	1273	776	1273

Vessel tapering structure

Within all trees, vessel sizes changed little for at least half the length of the bole (*l*, measured from the base). That is, there was no obvious tapering. Tapering began in the upper half of trees, and thereafter D*h* continuously declined, with the rate of tapering increasing towards the apex.

Smallest vessels identified in the apical regions were relatively similar within different species and were typically around 20 – 30 µm. Hence, the major differences in taper were between tall trees, that had initially large vessels at around half bole height, and shorter trees with that had much smaller vessels at the equivalent point. The distance from the base to the point where tapering became apparent was much greater in tall compared to shorter trees. Vessel numbers showed an identical pattern, remaining low in the lower part of stems and increasing with ongoing vessel tapering towards the tree's apex. A power function described well this increase of *VD* with height . The ratio of apical *VD* to basal *VD* varied markedly across species. For tall trees this ratio was around 20 while in short trees it was closer to 9.

Both tree height ($y = 0.52x^{0.44}$; $R^2 = 0.63$) and DBH ($y = 1.54x^{0.67}$; $R^2 = 0.66$) were moderately good predictors of *VD*. Figure 2.9 shows an example how tapering and *VD* developed in a tall (*E. regnans*) and a short (*E. gracilis*) eucalypt tree.

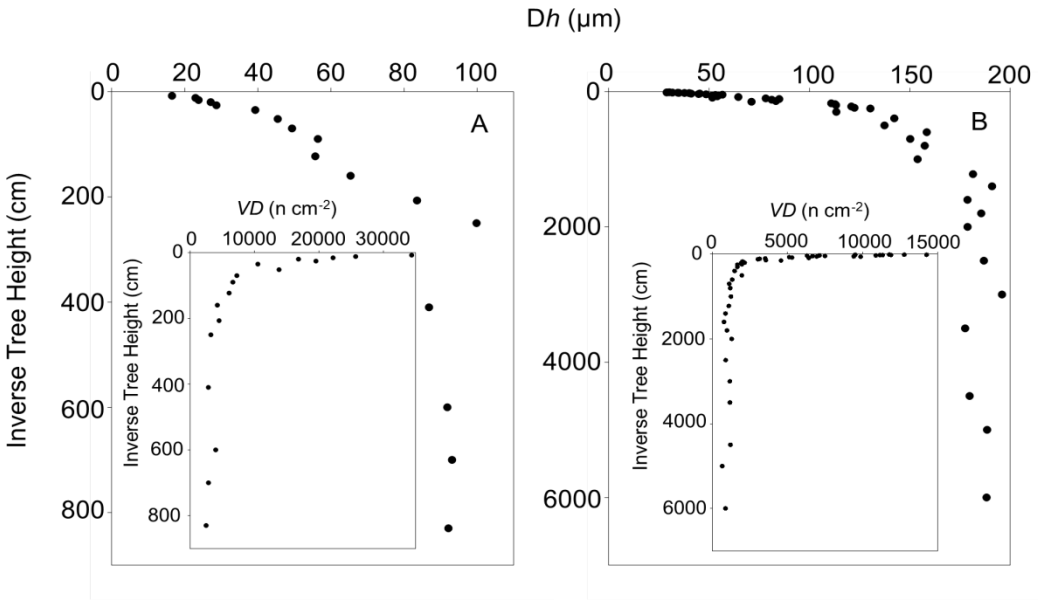

Figure 2.9: Vessel tapering structure in (A) a *Eucalyptus gracilis* and (B) a *E. regnans*. Illustrated are the relationships between hydraulically weighted vessel diameters (D*h*) and inverse tree height (from apex to base). Inserted panels show the change of vessel density (*VD*) with inverse tree heights. Figures showing changes of vessel density (*VD*) with inverse tree height for each tree considered within this thesis are illustrated in Appendix – Chapter 2.

Void to wood fraction (VtW)

Average values of *VtW* (%) (n = three per species^{-1}) calculated for samples at stem base showed neither significant correlation with climate descriptors such as AI_{100} ($y = 1.43x + 12.57$; $R^2 = 0.15$) T_{max100}($y = -0.15x + 16.66$; $R^2 = 0.04$) or P_{100} ($y = 0.01x + 12.13$; $R^2 = 0.19$) nor with basic sapwood traits such as *d* ($y = 0.03x + 10.03$; $R^2 = 0.22$) or *VD* ($y = 0.00x + 14.82$; $R^2 = 0.08$). Surprisingly, even *WD* at DBH ($y = 0.32x + 11.35$; $R^2 = 0.11$) was not correlated with *VtW*. Individual trees displayed wide variability over the majority of *l*, and *VtW* declined only slightly towards apical regions. Exemplary Figure 2.10 illustrates *VtW* structure over *l* of an *E. gracilis* from a semi-arid environment and a tall *E. regnans* from the very humid forests of south-eastern Victoria.

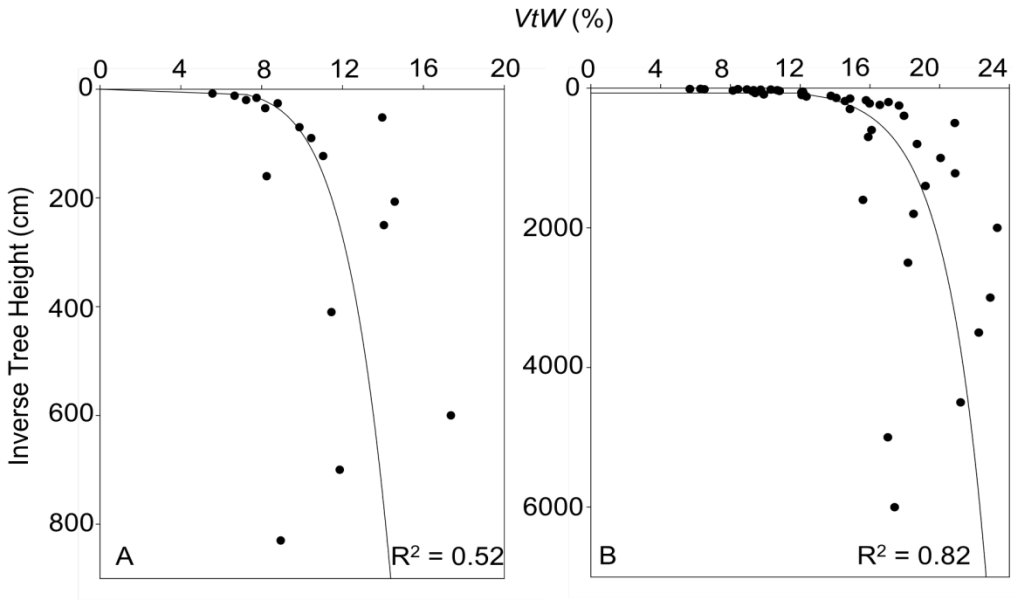

Figure 2.10: Void to Wood fraction (*VtW*) plotted against inverse tree height in (A) a *Eucalyptus gracilis* and (B) a *E. regnans* with a tapering structure as shown in Figure 2.9 and Figure 2.12 and total hydraulic resistance as shown in Figure 2.11. Coefficients of determination for (A) a power function (solid line; $y = 5.05x^{0.15}$) and (B) logarithmic decline (solid line; y = 2.34ln(x) + 1.98) are shown in pictures.

Total resistance (R_{tot})

Total resistances varied among single trees and also among species. The greatest R_{tot} was detected in an individual of *E. gracilis* with 6.48 e-3 cm^{-3} MPa s^{-1}, while the smallest R_{tot} was associated with *E. victrix* at 4.49 e-4 cm^{-3} MPa s^{-1}. The remaining species varied between these two values. Table 2.12 shows R_{tot} as calculated for individual trees and averaged for each species.

Table 2.12 (next page): Total resistance (R_{tot}) to water flow in sapwood of 12 *Eucalyptus* species. Abbreviation used: t.n. = tree number per species. Standard deviations are shown in parentheses. Different lower case letters indicate significant differences among species demonstrating results of pairwise comparisons of species means conducted with a Bonferroni t-test with a p <0.05 level of significance.

species	t.n.	R_{tot} (cm^{-3} MPa s^{-1})	average R_{tot} (cm^{-3} MPa s^{-1})
E. regnans	1	1.44e-3	2.01e-3 (± 5.03 e-4)[a]
E. regnans	2	2.41 e-3	
E. regnans	3	2.18 e-3	
E. pauciflora	1	1.63 e-3	2.17e-3 (± 9.58 e-4)[a]
E. pauciflora	2	3.27 e-3	
E. pauciflora	3	1.60 e-3	
E. viminalis	1	1.64 e-3	1.40e-3 (± 3.23 e-4)[a]
E. viminalis	2	1.53 e-3	
E. viminalis	3	1.04 e-3	
E. delegatensis	1	1.91 e-3	2.05e-3 (± 2.40 e-4)[a]
E. delegatensis	2	2.33 e-3	
E. delegatensis	3	1.92 e-3	
E. obliqua	1	3.44 e-3	2.82e-3 (± 1.23 e-3)[ab]
E. obliqua	2	3.62 e-3	
E. obliqua	3	1.40 e-3	
E. melliodora	1	1.25 e-3	1.53e-3 (± 5.78 e-4)[a]
E. melliodora	2	1.16 e-3	
E. melliodora	3	2.20 e-3	
E. baxteri	1	1.18 e-3	8.77e-4 (± 2.66 e-4)[a]
E. baxteri	2	7.13 e-4	
E. baxteri	3	7.33 e-4	
E. microcarpa	1	4.83 e-3	2.71e-3 (± 1.84 e-3)[ab]
E. microcarpa	2	1.78 e-3	
E. microcarpa	3	1.52 e-3	
E. polyanthemos	1	1.53 e-3	1.06e-3 (± 4.44 e-4)[a]
E. polyanthemos	2	6.41 e-4	
E. polyanthemos	3	1.02 e-3	
E. gracilis	1	6.48 e-3	5.22e-3 (± 1.16 e-3)[b]
E. gracilis	2	5.00 e-3	
E. gracilis	3	4.19 e-3	
E. socialis	1	2.05 e-3	2.30e-3 (± 3.30 e-4)[a]
E. socialis	2	2.17 e-3	
E. socialis	3	2.67 e-3	
E. victrix	1	1.10 e-3	7.95e-4 (± 3.28 e-4)[a]
E. victrix	2	8.35 e-4	
E. victrix	3	4.49 e-4	

Hydraulic resistance to sapflow increased with *l* in all trees. Within all trees *R* followed a similar pattern to vessel tapering structure, where based on insignificant changes in vessel sizes for ~50% of l, *R* remained uniformly low. Apical regions contributed most to R_{tot}. All pairwise comparisons of species means indicated few differences in R_{tot} among species. Only *E. gracilis* was significantly different for R_{tot} compared to other species ($p < 0.05$), although even then, R_{tot} was not different to values for *E. microcarpa* and *E. obliqua* (Table 2.12). There was no obvious relationship between total resistance, measured tree structural- or sapwood traits and/or environmental conditions. An example of how *R* developed in one tall and

one short tree along *l* is shown in Figure 2.11. The same two individuals as shown in Figures 2.9, 2.10 and 2.12 are used for this comparison. The shape of the relation between *R* and tree height was similar in all trees and species, regardless of their stature or origin.

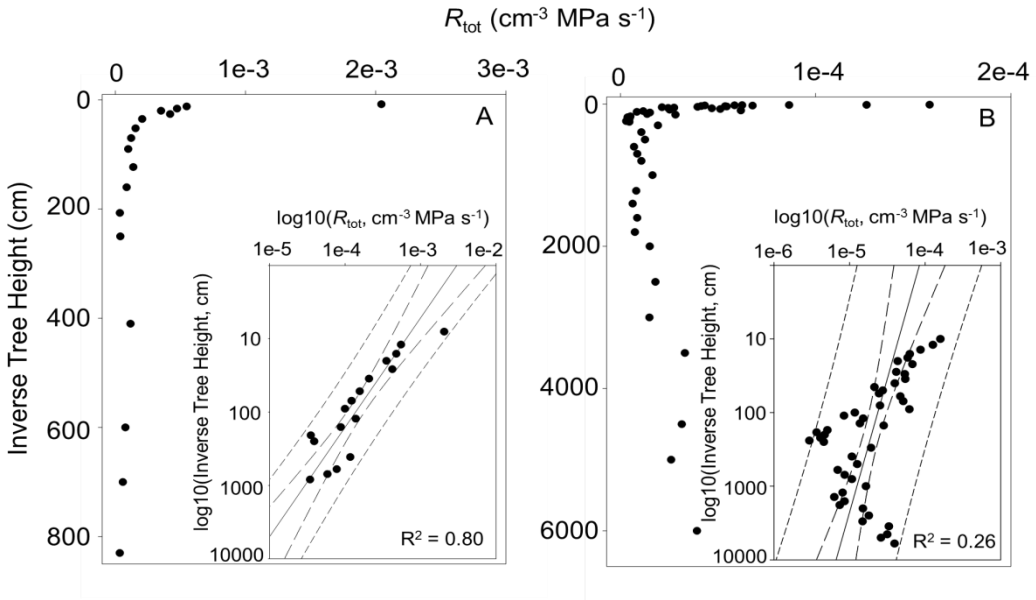

Figure 2.11: Total hydraulic resistance (R_{tot}) as a function of inverse tree height in (A) a *Eucalyptus gracilis* and (B) a *E. regnans* with a tapering structure as shown in Figure 2.9 and 2.12 and with a void to wood structure as illustrated in Figure 2.10. The inserted panels depict the identical data plotted as log–log plot, where solid lines indicate linear regressions, long dashed lines indicate 95% confidence intervals, and short dashed lines indicate 95% prediction intervals. Coefficients of determination are shown in pictures. Log-log plots of hydraulic resistance (R_{tot}) as a function of inverse tree height for all individual trees considered within this thesis are illustrated in Appendix – Chapter 2.

2.3.6 Three Phase Taper Analysis

Patterns of tapering of vessels are perhaps the most distinctive result in this thesis. A new approach to assessing these patterns was developed – and will be described as a Three Phase Taper Analysis (TPTA). This approach illustrated the similarities and differences of hydraulic architecture in *Eucalyptus* spp.

Analyses of D*h* from the base towards the apical region of all trees (n = 36) showed general trends:

1. Independent of species, tree height or environmental conditions, little or no changes in *d* could be observed within 50% to 70% (P1) of *l*.
2. Within the last 25% to 50% of *l*, the tapering structure (i.e. the relative change in D*h* or *d* to *VD*) differed strongly, especially in terms of P3 insertion point.
3. Due to its unusual tapering structure, *E. pauciflora* did not fit the general trend and was excluded from the following analyses.

Calculation of relative distance from the tree base to the point where tapering commenced (P1) shows that vessels did not taper for between 56% (±7) (*E. polyanthemos*) and 75% (±5) (*E. obliqua*) of *l*. Generally, tall trees showed by far the longest P1-section with no taper (73% ±12 of *l*).

Tapering in stems of trees from dry sub-humid to arid ecosystems thus began earlier (Table 2.13).

The relative length of the section that tapered steeply (P3) ranged from 0.4% (±0.04) in *E. regnans* to around 12% (±1.9) in *E. victrix*. Relative lengths of P3 were short in tall tree species and increased when environments became progressively more arid (Table 2.13). Hence, P3 was around to 2% (±0.5) of *l* in *E. obliqua*, 3% (±0.5) in *E. baxteri* and 5% (±0.6) in *E. melliodora*. In the two Mallee species (*E. gracilis* and *E. socialis*) sampled in Mildura State Forest, vessels tapered rapidly over the remaining 5 to 10% of *l* before the apex (Table 2.13).

Table 2.13 (next page): Relative proportion of stem sections to total path length (*l*) identified in the Three Phase Taper Analysis (TPTA) that showed no (Phase 1), moderate (Phase 2) and rapid tapering (Phase 3) of hydraulically weighted vessel diameters in sapwood of 12 *Eucalyptus* species (n = 3 species^{-1}). Standard deviations are shown in parentheses. Phase 1 represents the lower, Phase 2 the mid- and Phase 3 the apical section of trees.

species	Phase 1 *l* (%)	Phase 2 *l* (%)	Phase 3 *l* (%)
E.regnans	72.96 (±11.97)	27.04 (±11.97)	0.39 (±0.04)
E.pauciflora	44.91 (±3.98)	55.09 (±3.98)	2.97 (±0.19)
E.viminalis	74.30 (±3.21)	25.70 (±3.21)	1.08 (±0.19)
E.delegatensis	74.30 (±8.33)	25.70 (±8.33)	0.86 (±0.38)
E.obliqua	75.24 (±5.36)	24.76 (±5.36)	2.09 (±0.48)
E.melliodora	64.84 (±7.38)	35.16 (±7.38)	4.89 (±0.63)
E.baxteri	72.45 (±5.11)	27.55 (±5.11)	3.33 (±0.53)
E.microcarpa	70.07 (±8.42)	29.93 (±8.42)	4.34 (±0.89)
E.polyanthemos	55.80 (±7.11)	44.20 (±7.11)	2.96 (±0.18)
E.gracilis	62.24 (±9.12)	37.76 (±9.12)	5.18 (±0.27)
E.socialis	68.69 (±6.24)	31.31 (±6.24)	9.65 (±1.80)
E.victrix	62.44 (±4.60)	37.56 (±4.60)	11.69 (±1.94)

Figure 2.12 provides examples of three phase taper analyses produced for *E. gracilis* and *E. regnans*. Figures of TPTA for all individual trees considered within this thesis are illustrated in Appendix – Chapter 2.

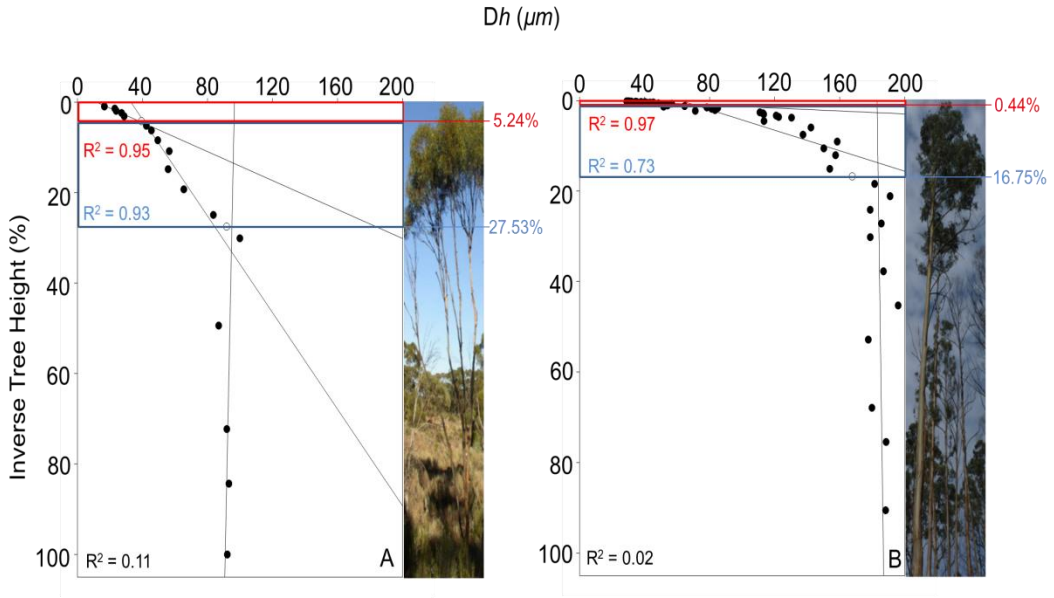

Figure 2.12: Two exemplars of Three Phase Taper Analysis (TPTA). (A) *Eucalyptus gracilis,* (B) E. *regnans*. Black dots are measured values and are averages of three analysed images. Circles are calculated medians in-between measured values. They were not part of linear regression analysis and they do express relative tree heights of phase changes. Pictures of trees are not scaled, and are inserted to provide an impression of general tree structure and intercept length of different phases. Blue boxes indicating Phase 2 (moderate tapering) blue numbers describing tapering starting point expressed as relative inverse tree height, red boxes and red numbers indicating Phase 3 (steep tapering). Coefficients of determination for linear regressions are shown in figures in the respective colours, while black Coefficients of determination are assigned to Phase 1.

Following identification of the degree of tapering in individuals, relationships of relative length of each of the three Phase-sections to environmental variables, namely T_{max100}, P_{100} and the AI_{100} were assessed. Of all variables, AI_{100} was the best predictor of the relative length of taper phases. Even though P_{100} were a marginally better predictor for P3 intervals, P1 and P2 were better related to AI_{100}. Correlation analysis, however, indicated that the relative length of the region within the stem that tapered rapidly increased with decreasing aridity and with declining amounts of annual precipitation (Fig. 2.13A). When moving downward the stem (from apex to base) the strength of the predictive character diminished (Fig. 2.13B), leaving the relative length of the P1-section with a relatively weak correlation to AI_{100} (Fig. 2.13C).

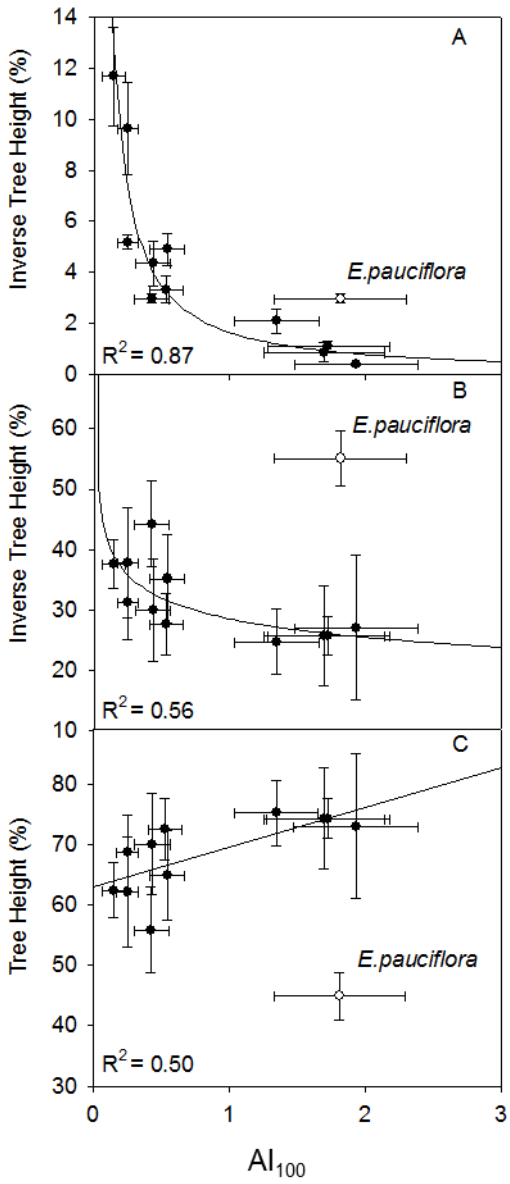

Figure 2.13: Correlation between average long-term (100-year) aridity indices (AI_{100}) and relative lengths of stem sections that showed (A) rapid tapering (or 'Phase 3'), (B) moderate tapering (or 'Phase 2') and (C) no tapering (or 'Phase 1') in 12 Eucalyptus species (n = 3 species^{-1}). Data for *E. pauciflora* is represented by circles; these data were excluded from the model. Error bars indicate standard deviations. Coefficients of determination for curvilinear and linear regressions (solid lines; A: $y = 1.39x^{-0.80}$, B: $y = 91239x^{-3.47}$, C: $y = 0.08x - 4.39$) are shown.

Table 2.14 illustrates the strength of all considered environmental descriptors.

Table 2.14: Coefficients of determination for relationships of different phases of vessel taper to long-term (100-year) averages of rainfall (P_{100}) and maximum daily temperatures (T_{max100}).

	R^2 (P_{100})	equation	R2 (T_{max100})	equation
Phase 3	0.88	$y = 1260.4x^{-0.60}$	0.68	$y = 15.79x^{0.20}$
Phase 2	0.56	$y = 5e+06x^{-2.58}$	0.49	$y = 0.7744x^{0.94}$
Phase 1	0.48	$y = 1e-06x^{4.78}$	0.41	$y = 28342x^{-1.72}$

The relative dimensions of the P3-section of individual trees also related well to structural traits of trees. These analyses showed that the length of the apical section where vessel tapering was most rapid, correlated strongly to crown insertion point ($y = 6.32e^{-6E-04x}$; $R^2 = 0.85$), *WD* ($y = 0.45e^{0.09x}$; $R^2 = 0.84$) and total tree height ($y = 10.04e^{-5E-04x}$; $R^2 = 0.82$). However the same length was only weakly related to DBH ($y = 13.34e^{-0.04x}$; $R^2 = 0.64$). As in previous analyses, values for *E. pauciflora* were excluded from all models. Due to missing data, the relationship of the relative length of the P3-section to crown insertion points could not be evaluated for *E. victrix*. Similar to the relationship of AI_{100}, the relative length of the P3-section showed a strong correlation with overall tree height, particularly for tall species from humid environments (Fig. 2.14).

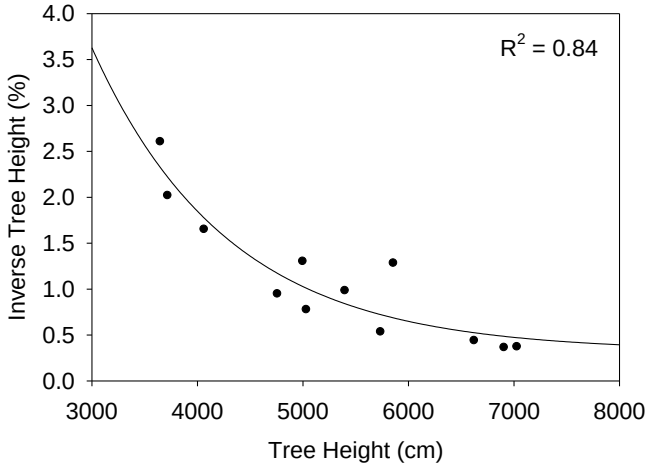

Figure 2.14: Relationship between total tree heights and relative length of stem sections that showed rapid tapering (or 'P3-section'). Data of four species was used in this analysis, namely *Eucalyptus delegatensis, E. obliqua, E. regnans and E.viminalis*. Coefficient of determination for curvi-linear trajectory (solid line; $y = 8913244206x^{-2.69}$) is shown.

Relative resistance of identified vessel taper phases

Dissection of tree stems into three regions of different degrees of tapering allowed further analysis of resistance to water flow (R_{rel}). Clearly and not surprisingly, the P3-section (i.e. rapid, steep vessel taper structure within the apical region) is the part of the stem where most of R_{rel} is concentrated. Across all species R_{rel} in P3-sections was greater than that calculated for the P2-section. The P3-section contributed at least 47% (±2.60) of R_{tot} in *E. regnans* and up to 85% (±5.07) in *E. victrix* (Table 2.15). A very strong linear relationship ($y = -0.94x+87.53$; $R^2 = 0.94$) was found between R_{rel} of the P2- and P3-section, indicating that when less R_{rel} was assigned to the P3-section, more R_{rel} was assigned to the P2-section. The P1-section contributed at most 14% R_{rel} to R_{tot} (Table 2.15).

Table 2.15: Relative contributions among stem segments (Phases 1 to 3) to resistance to water flow (R_{rel}) for 12 *Eucalyptus* trees sampled along an environmental gradient. R_{rel} is based on segment lengths of the TPTA where P1 represents the tree stem where vessels did not taper, P2 the section of the stem with moderate vessel taper and P3 the remaining, apical segment where vessels tapered rapidly. Values presented in the table are species averages (n = 3 species^{-1}); standard deviations are shown in parentheses.

species	P1-segment R_{rel} (%)	P2-segment R_{rel} (%)	P3-segment R_{rel} (%)
E.regnans	9.15 (±5.35)	43.63 (±4.70)	47.22 (±2.60)
E.pauciflora	5.98 (±3.11)	34.06 (±9.80)	59.96 (±12.84)
E.viminalis	5.22 (±0.44)	19.69 (±6.14)	75.09 (±6.40)
E.delegatensis	7.00 (±2.94)	28.71 (±12.92)	64.29 (±14.15)
E.obliqua	6.13 (±4.96)	12.20 (±7.92)	81.67 (±12.78)
E.melliodora	6.89 (±4.12)	11.58 (±4.61)	81.53 (±1.63)
E.baxteri	9.68 (±4.29)	22.22 (±6.75)	68.09 (±8.44)
E.microcarpa	13.22 (±7.11)	20.68 (±10.08)	66.10 (±17.19)
E.polyanthemos	7.52 (±2.01)	39.08 (±10.43)	53.40 (±10.88)
E.gracilis	13.93 (±8.48)	24.59 (±10.60)	61.47 (±18.56)
E.socialis	11.04 (±3.92)	12.23 (±3.46)	76.73 (±1.80)
E.victrix	7.69 (±3.07)	7.41 (±2.50)	84.90 (±5.07)

2.3.7 Remarks on Metabolic Scaling Theory (*MST*)

Tapering exponent

Tapering exponents for all species were similar and averages (n = 3) varied from 0.30 in *Eucalyptus gracilis* to 0.38 in *E. viminalis* and *E. obliqua*. The very low value calculated for *E. gracilis*, however, was strongly influenced by a single tree that had a tapering exponent of 0.22 (see Appendix Fig. S 2.104 for details).
Due to similarities of exponents, neither climate variables nor tree structural features were linked with these findings. Tapering exponents for all individual trees and species can be found in Table 2.16. Figures for each individual tree are provided in the Appendix – Chapter 2.

Packing exponent

Packing exponents differed within and among *Eucalyptus* spp. At the species level, packing exponents varied between -1.42 in *E. polyanthemos* and -1.92 in *E. pauciflora* (Table 2.16). According to information generated here, the genus *Eucalyptus* spp. have, on average, a lower packing exponent than suggested by available models, including those developed for angiosperms in general or those that are based on optimal hydraulic functioning (Chapter 2.4).

Table 2.16: Tapering exponents and packing exponents for 12 species of Eucalyptus for individual trees and for each species. Abbreviation used: t.n. = tree number per species.

species	t.n.	tapering exponent	tapering exponent per species	packing exponent	packing exponent per species
E. regnans	1	0.33	0.35	-1.49	-1.47
E. regnans	2	0.34		-1.48	
E. regnans	3	0.37		-1.45	
E. pauciflora	1	0.29	0.33	-2.08	-1.92
E. pauciflora	2	0.39		-1.87	
E. pauciflora	3	0.30		-1.83	
E. viminalis	1	0.38	0.38	-1.59	-1.58
E. viminalis	2	0.37		-1.65	
E. viminalis	3	0.37		-1.50	
E. delegatensis	1	0.34	0.35	-1.65	-1.58
E. delegatensis	2	0.35		-1.53	
E. delegatensis	3	0.35		-1.50	
E. obliqua	1	0.42	0.38	-1.39	-1.51
E. obliqua	2	0.37		-1.58	
E. obliqua	3	0.35		-1.71	
E. melliodora	1	0.36	0.35	-1.62	-1.75
E. melliodora	2	0.32		-1.96	
E. melliodora	3	0.38		-1.77	
E. baxteri	1	0.37	0.35	-1.59	-1.57
E. baxteri	2	0.35		-1.43	
E. baxteri	3	0.33		-1.72	
E. microcarpa	1	0.37	0.31	-1.56	-1.68
E. microcarpa	2	0.30		-1.89	
E. microcarpa	3	0.27		-1.82	
E. polyanthemos	1	0.35	0.33	-1.51	-1.42
E. polyanthemos	2	0.30		-1.50	
E. polyanthemos	3	0.35		-1.31	
E. gracilis	1	0.22	0.29	-1.63	-1.51
E. gracilis	2	0.38		-1.44	
E. gracilis	3	0.31		-1.53	
E. socialis	1	0.33	0.34	-1.52	-1.50
E. socialis	2	0.34		-1.46	
E. socialis	3	0.36		-1.56	
E. victrix	1	0.40	0.35	-1.77	-1.79
E. victrix	2	0.33		-1.77	
E. victrix	3	0.32		-1.78	

2.4 Discussion

According to available literature, the data presented here comprise the most comprehensive study yet of the principle water conducting systems in the stems of *Eucalyptus* ssp.. The detailed information about tree structure, sapwood and xylem vessels of 12 species of *Eucalyptus*, provide for the first time, the basis for analysis of how this genus adapts to climatic conditions. The Three Phase Taper Analysis (TPTA) developed here is a novel means of interpreting changes in vessel tapering in response to environmental cues, particularly the availability of water. By applying TPTA, I identified shared attributes as well as inter-specific differences in tree hydraulic architecture.

Climate

Climate data presented here provide evidence for changing climatic conditions over a wide range of Australian ecosystems. Temperatures (T) increased steadily at all investigated sites. The average rise of +0.77 °C over the last century is in accordance with predictions of increases in temperature on both a global and an Australian scale (Plummer *et al.*, 1999; Broecker, 2002; Hughes, 2003; Hansen *et al.*, 2006). With the exception of the Snowy Plains, the last decade was the warmest recorded across all research sites for the past 100 years. The data further confirms the widely noted warming pattern of 0.1 – 0.4 °C/ decade since the 1950s (e.g Suppiah *et al.*, 2001; Hughes, 2003). The generally lesser increases in temperature at the higher-elevation sites stand in contrast to predictions that forecast accelerated warming for Australia's mountain compared to lowland systems (Nogués-Bravo *et al.*, 2007).

Changes in annual precipitation, however, were inconclusive when climate parameters for research sites were compared with more regional- and continental-scale trends reported in the literature. Several authors have reported an increase in precipitation of 8.1 mm per decade across the Australian continent (Smith, 2004; Murphy and Timbal, 2008). For Victoria and NSW, precipitation during the last century increased by 14 – 15% (Hennessy *et al.*, 1999; Hughes, 2003; Murphy and Timbal, 2008). However, at the majority of sampled sites considered within the present study, there has been a reduction in annual rainfall rather than an increase, if compared using decadal averages. The analysis provided here suggests a decrease of

9.9 – 136.5 mm per decade. Only the Pilbara region in Western Australia showed moderate increases. It is noteworthy that in contrast to apparent long-term reductions in precipitation, the years 2010 and 2011 (when sapwood samples were collected) were unusually wet, emphasising the importance of the stronger correlation between wood traits and long-term climate, when compared to such correlations for short-term climate data.

Tree- and wood traits

Tree structural traits such as height, DBH and crown insertion point of *Eucalyptus spp.* were clearly linked to climate parameters such as precipitation (P), T and aridity index (AI). These traits also followed global patterns of tree form, where size and height increases when water availability increases (Fig. 2.4). This relation has been identified as the most important driver for maximum tree height among tree species from around the world and is in line with the widely discussed Hydraulic Limitation Hypothesis (Chapter 1.4.1) (Ryan and Yoder, 1997; Moles *et al.*, 2009). Diameter of *Eucalyptus* species sampled for the current project was strongly correlated with tree height, a relationship documented for countless other species (e.g. Curtis, 1967; Larsen and Hann, 1987; Wang and Hann, 1988; Hasenauer, 1997; Wonn and O'Hara, 2001; Soares and Tomé, 2002; Avsar, 2004; Amritphale and Sharma, 2010). Height of crown insertion points differed among species but was strongly correlated with overall tree height. This can be explained ecologically where trees in closed stands generally have a high crown insertion point relative to tree height as competition for light requires increased height growth and concentration of foliage at tree top to avoid shading by competitors. In contrast, solitary trees appear to invest available resources in a wide and low crown and an overall lower height (Iwasa *et al.*, 1985).

Sapwood density (*WD*) is a function of cell wall thickness and the summed cross-sectional area of individual vessels. Within a tree *WD* varies in both radial and axial directions (Swenson and Enquist, 2007; Pfautsch *et al.*, 2011). Sapwood, which was exclusively considered here, has been described as not as dense as heartwood, and wood at tree bases has notionally greater density compared to wood from crown regions (Swenson and Enquist, 2007; Chave *et al.*, 2009). Pioneer- and other fast

growing species normally have lighter wood with wider vessels, which in turn is associated with an increased risk of hydraulic failure. Wood density of slow growing species is usually greater, providing increased mechanical support associated with the tendency to have a greater resistance to xylem vessel implosion or rupture (Hacke *et al.*, 2001).

Wood density of species investigated here matches this general description. Tall species from very humid environments had less dense sapwood compared to trees from dry sub-humid to arid conditions (Table 2.8). The range of *WD*s reported here is within the range previously described for eucalypts (Kingston and Risdon, 1961; Attiwill, 1979; Dye, 1996; Ilic, 2001; Ilic, 2002; Pfautsch *et al*., 2011).

Sapwood density of gymnosperms and angiosperms is responsive to long-term T (e.g. Antonova and Stasova, 1993, 1997; Roderick and Berry, 2001; Thomas *et al.*, 2004, 2007). Roderick and Berry (2001) developed a model that links *WD* of gymnosperms with tree growth and environment, based on the sensitivity of water viscosity to T (Roderick and Berry, 2001). The underlying assumption of their model is that water with low viscosity (i.e. at high Ts) can be sufficiently conducted in small or few vessels compared to water of high viscosity (i.e. cool Ts). This model requires vessel diameters (*d*) to be of a sufficient size to facilitate required conductivity. In support of this hypothesis, Thomas *et al.* (2007) showed that *Eucalyptus grandis* developed thicker fibre cell walls with smaller lumen diameters when grown at greater Ts. Others have shown that *WD* is better correlated with P and aridity than with T, and to be independent of vessel traits. This might suggest that *WD* is in fact independent of vessel characteristics and rather determined by fibre traits. Overall, it would suggest that wood density, *per se*, does not impose limitations to the conduction of water (Martínez-Cabrera *et al.*, 2009).

Trends for *Eucalyptus* spp. reported here provide a means of examining these suggestions and hypotheses. Wood density was well correlated with T, P, AI and *d*. Viscosity of water at different Ts may contribute to processes of vessel formation, but both vessel size itself and water availability are more likely to be influenced by P and AI.

As proposed by Pfautsch *et al.* (2011), wood formation in *Eucalyptus* spp., and especially *WD*, is likely a result of the essential trade-off with hydraulic safety, and is therefore mostly determined by water availability. High *WD*s may reflect a large investment of structural carbon for cell wall formation, slow growth rates, and smaller vessels that have limited conductivity (Searson *et al*., 2004; Pfautsch *et al.*, 2011). Wood is mostly more dense in semi-arid to arid environments as result of reductions in the fibre lumen component accompanied by increasing axial parenchyma that have water storage capacity (Martínez-Cabrera *et al*., 2009).
The combined results of *WD* and *d*s reported here provide evidence that both parameters are negatively related. The data are also not supportive of the hypotheses of Martínez-Cabrera *et al.* (2009). More knowledge of fibre- and vessel structure in different *Eucalyptus* species grown under different environmental conditions is required for a definitive analysis.

Sapwood- and vessel traits

There are few published studies of *d* and vessel densities (*VD*) for mature eucalypts. Direct intra-specific comparison of results from existing studies is highly problematic as vessel structure continuously changes according to changes in tree height and age and crown characteristics (Bamber and Curtin, 1972; Hudson *et al*., 1998; England and Attiwill, 2007). In a study of *E. delegatensis*, Mokany *et al.* (2003) reported maximum *d* (d_{max}) of up to 270 µm, while individuals of the same species studied here showed average d_{max} of between 234 – 257 µm. England and Attiwill (2007) reported that different-aged *E. regnans* trees averaged d_{max} of 210 – 237 µm, while individuals of the same species studied here had d_{max} of 236 – 276 µm. In similar fashion, while Ilic (2002) reported that d_{max} in *E .baxteri* ranged between 140 – 210 µm, individuals of the same species studied here had d_{max} of 174 – 217 µm. These comparisons highlight that although d_{max} varies widely among individuals of the same species, the range of d_{max} reported here agrees well with the limited previously available data.

At 668 – 879 vessels cm^{-2} (Table 2.8), vessel densities for *E. regnans* were slightly greater than those reported by England and Attiwill (2007; 520 – 670 vessels cm^{-2}). Wesolowski (2010) studied sapwood structure of five species from very humid sites

of eastern Victoria (namely: *E. delegatensis*, *E. obliqua*, *E. pauciflora*, *E. regnans* and *E. viminalis*) and found similar *VD*s to those reported here for the same species (Wesolowski, 2010). In general, tall eucalypts in humid environments showed a comparatively low amount of large vessels and *d* decreased while *VD* increased towards environments with lower AI. Surprisingly, *VD*s for *E. delegatensis* are remarkably small when compared to *VD* of other eucalypt species from very humid environments (Table 2.8). This is an obvious topic for future research.

A long history of research shows that water availability influences vessel anatomy of trees. Knigge and Schulz (1961), for example, convincingly demonstrated the relationships of vessel size of *Fagus sylvatica*, *F. moesiaca*, and *Quercus robur* to water supply. Similar results were obtained by Eckstein and Frisse (1979) and by Carlquist (1975).

For eucalypts such as those species studied here, vessel size reflected the climate gradient, confirming that construction of sapwood in *Eucalyptus* spp. follows a universally applicable scheme of hydraulic architecture documented for a number of tree genera from different environments (e.g. Wiemann *et al.*, 1998; Wheeler *et al.*, 2007; Zanne *et al.*, 2010). The stronger correlation of vessel traits with long-term, rather than short-term environmental parameters suggests that hydraulic architecture is the result of long-term adaptation with limited capacity for modifications to short-term changes in prevailing weather. This stands in contrast to observations for ring- and diffuse porous species from Europe and North America that are exposed to extreme seasonal and annual variation of weather conditions, for example sub-zero conditions during winter (e.g. Knigge and Schulz, 1961; Carlquist, 1975; Eckstein and Frisse, 1979). Results of the present study provide evidence that changes in climate during the past decade have only marginally affected vessel structure.

Skewness (τ) and Kurtosis (κ) (Table 2.7) help describe curve shapes based on the concept of Gaussian "Normal Distribution" - in this case proportional occurrence of different *d* classes detected in images taken from basipetal samples. Negative values of τ imply a longer tail of Gaussian distribution curve towards left (a greater than normal fraction of small vessels), while positive τ indicates the opposite (greater than normal fraction of larger vessels). Kurtosis is a measure of the "peakedness" of the

distribution - negative values imply a platykurtic shape (‘flattened’ peak), and positive values a leptokurtic shape (a ‘pointed’ peak). Positive kurtosis suggests predominance of a particular class (or classes) of *d*s while flat curves suggest broad homogeneity of different size classes.

Images of sapwood taken adjacent to the cambium show an almost normal (symmetric) distribution of vessel sizes for the majority of species. Hence, most vessels were ‘medium sized’. Mostly distributions were platykurtic, suggesting relatively homogeneous, medium diameter vessels dominated. The skewness of distribution curves for most species were negative - more narrower and fewer wider vessels than predicted by a strictly normal distribution. Studies of vessels in semi-ring porous *Prunus serotina* have reported similar patterns, while strongly negative τ was reported for diffuse porous *Fagus sylvatica.* (Zimmermann and Jeje, 1981; Sass and Eckstein, 1995).

As diameter class allocations are relative to measured diameters, i.e. a ‘medium’ sized vessel in an *E. gracilis* is clearly smaller than a ‘medium sized vessel of e.g. *E. regnans*, τ and κ have different implications across species and ecosystems. For example, Mallee species had the smallest *d*s of all studied species. Consequently, the bulk of medium sized vessels were comparatively small. In environments like the Victorian Mallee, where rainfall events are spasmodic, a few wider vessels could allow transport of greater amounts of water for short periods, before cavitating during times where water is scarce and transport of water is facilitated by the dominant narrow vessels that are more resistant to cavitation.

Except for *E. obliqua*, all tall species from very humid environments had negative τ. Clearly, vessel diameter was skewed toward narrow vessels. That said, the majority of vessels in these tall species were relatively large and able to transport water efficiently. The slight bias to smaller vessels contributes to hydraulic safety for tall species during times of limited water availability, where the risk of cavitation is high.

Assessing the results for both τ and κ, across all species, there was no uniform pattern that could be related to either long- or short-term environmental conditions. To date very few researchers have linked the distribution of vessel sizes to

physiological functioning. Even so cambial age influences this anatomic characteristic which is mostly under genetic control (Sass and Eckstein, 1995; Leal *et al*., 2007) .

The ratio (or proportion) of total vessel area to wood area (*VtW*) measured at DBH was surprisingly unrelated to wood density. This finding contrasts with the close relationship of *WD* with *d* and *VD* (Chapter 2.3.4). Relationships between vessel area and wood density have often been reported (e.g. Thomas *et al*., 2004, 2007; Naidoo *et al*., 2006; Moya and Tomazello, 2007; Martínez-Cabrera *et al.*, 2009). On the other hand, and within a similar sized body of work, there are only marginal influences of *VtW* fraction on wood density (e.g. Preston *et al.*, 2006; Martínez-Cabrera *et al*., 2009; Poorter *et al*., 2010; Zanne *et al*., 2010). It follows that if void space within the wood matrix does not influence *WD*, then the wood matrix (e.g. thickness of cell walls) must be a major influence on *WD*. Arguably, *WD* of itself is a minor influence on water conduction.

Given similar *VtW* across species, independent of vessel size, reductions in *VtW* within apical regions of trees is deserving of comment. Declining *VtW* within apical regions, where negative tension and risks of cavitation are greatest, may have advantages for the trees. In particular, this pattern might represent a strategy to mitigate runaway embolism due to air seeding (Chapter 1.3.3). A corollary of declining *VtW* is less vessel inter-connections. Reduced numbers of vessel inter-connections might partly compensate for the reduced conductivity attributable to the sharply declining number of very small vessels. Inter-vessel pits can account for 80% of R_{tot} in *Fraxinus* and even 87% in *Ulmus* (Choat *et al*., 2006). A reduced number of vessels with thicker walls at the very apex of trees could help reduce the risk of catastrophic xylem implosion by negative pressure (e.g. Hacke *et al.*, 2001). Hence a pattern of lengthening vessels of smaller diameter, with fewer inter-connections, help compensate for reduced conductivity associated with end wall resistances (e.g. Sperry *et al.*, 2005).

Tapering structure

The 'Three Phase Taper Analysis' presented here provides impetus to further research to expand our understanding of vessel tapering - for the genus *Eucalyptus* but also for other tree genera. Negative tension within conduit systems is generated by gravity and the gradient in water potential of the soil and that of the atmosphere, and exacerbated by the many resistances within the plant.

Metabolic scaling models use scaling exponents to explain the widening of vessels towards the base of trees. These models explain the widening of vessels from the apex downwards, as being an evolutionary adaptation that optimizes conductance and at the same time compensating for resistance to the transport of water. Earlier approaches such as the Hydraulic Limitation Hypothesis, Cohesion-Tension Theory, and Ohm's and Darcy's Law explain hydraulic architecture in accordance to direction of flow (base-to-apex).

Data presented here stimulate further consideration of base-to-apex flow. The defined 'tapering initiation point' (TIP, the transition from P1 to P2), can be considered the location within the total path length where tapering must begin to ensure that the combined effects of gravity and resistance do not lead to catastrophic cavitation under prevalent environmental conditions.

At very humid sites in mountainous forests of the Great Dividing Range, sufficient availability of soil water (hence high soil water potentials) and generally low VPD allowed trees to develop a highly efficient vessel system that consisted of mostly wide vessels over the majority of path length. Vessels only began to taper in the apical 10 – 17 m of 40 – 70 m tall trees. In other words, for 75% of the path length, conduits do not change at all in diameter (Table 2.13 and Fig. 2.12, 2.13). When availability of soil water is reduced and average VPD increased, tension in the network of vessels is likely to increase. Under such environmental conditions a network that consists of narrower vessels minimises the risk of cavitation events but increases resistance to water flow. Moreover, negative pressures in such a network increase the risk of collapse of vessel walls. The lower TIP in smaller trees from drier sites can be interpreted as a trade-off of safety with efficiency. Results for a range of eucalypt species across a number of ecosystem types support this widely

discussed ‘safety-versus-efficiency concept’ (Wheeler *et al.*, 2005; Burgess *et al.*, 2006; Hacke *et al.*, 2006; Sperry *et al.*, 2008; Woodruff *et al*., 2008; Meinzer *et al*., 2010).

More importantly, the results in this thesis describe a previously undescribed adaptation of the genus *Eucalyptus* to long-term environmental conditions. With respect to Metabolic Scaling Theory (*MST*) and its derivatives, none of the sampled eucalypts showed a uniform taper from the base to the apex. Even short Mallee species from semi-arid northwest Victoria showed no obvious tapering within the first 62 – 69% of total path length (Table 2.13). Considering the importance of vessel size to conductivity and resistance of water (Eq. 1.6), this novel insight can refine our understanding of hydraulic architecture and tree water transport. It provides further detail for the tapering module within *MST* and allows a more accurate calculation of hydraulic networks of trees.

In addition to the TIP correlating well with long-term environmental conditions, the rate (per unit height) of taper changed dramatically with increasing overall tree height (expressed as decreasing relative proportion for P3 with overall tree height; see Table 2.13 and Fig. 2.13). The latter phenomenon has previously been described for eucalypts (Petit *et al.*, 2010) and other angiosperms, as well as for gymnosperms such as *Larix decidua* and *Fraxinus excelsior* (Anfodillo *et al.*, 2006; Mencuccini *et al.*, 2007; Petit *et al*., 2010). These results highlight that rapid tapering of vessels at the top of trees (from TIP to apex) could well be a function of both maximum tree height and AI and not only the result of compensating for gravitational forces and associated resistance to embolism. Other physiologically- or ecologically-driven explanations may be possible.

As previously mentioned, the widest vessels were not necessarily located in sapwood at the base of trees. Although this phenomenon seems unexpected as it contradicts continual widening of vessels with distance from the apex, it has been observed in stems of several species here and also in other studies (e.g. Fig. S.2.25, S.2.69; Petit *et al.*, 2010). Two explanations for this observation seem likely: 1) a greater number of annuli – and hence sapwood area – is actively involved in water transport at the base of tree boles; the greater area of conductive sapwood makes construction of

wider conduits redundant; 2) increased mechanical strain at the base of stems lead to conduits with smaller diameters (personal communication with T. Anfodillo).

An interesting observation is that the WBE and subsequently refined models for vessel tapering (West *et al*., 1999; Savage *et al.*, 2010; Sperry *et al.*, 2012) assume that close to the apex, *d* is size-invariant. Results presented here support this assumption. The majority of sampled eucalypt trees had a minimum D*h* of 20 to 30 µm close to the apex, with *E. gracilis* being an outlier at the low end of minimum D*h* (16 µm) and *E. victrix* at the wide end (40 µm). Similar sizes from apical- and petiole regions of between 19.3 to 30.6 µm were found in both ring-porous and diffused-porous species (Coomes *et al.*, 2008). Could therefore the minimum *d* be a mechanical consequence of connecting vessels from branches to those of leaf petioles? Future research may resolve this and other questions about hydraulic architecture of trees.

Resistance

According to TPTA the majority of resistance (*R*) to uprising sap was provided by the P3 section that incorporated a steep tapering structure over a relatively short distance (Table 2.15). In 11 of the 12 investigated eucalypt species, the P3 section contributed more than 50% *R* to total resistance (R_{tot}). In contrast, *R* within the P1-section, where tapering was negligible, contributed only 5 – 14% to R_{tot} (Table 2.15). Similar observations were made by Petit *et al.* (2010). In mature *E. regnans*, nearly all resistance was contributed by the first meter or so beneath the apical section. Consistent with overall smallest size of vessels, R_{tot} was greatest in *E. gracilis*. Patterns of *R* are in agreement with earlier observations in *E. regnans* and other angiosperm species such as *Fraxinus excelsior*, inasmuch as they support vessel size and the degree of tapering the most important hydraulic constraint to rising sap, followed by pit resistance (Anfodillo *et al.*, 2006; Domec *et al.*, 2008).

In most species, R_{tot} was independent of tree height (Table 2.12), a result that supports theories and models describing an almost complete compensation of resistance by a highly optimized vessel system and a possible contribution of changing water viscosity in different T (e.g. West *et al.*, 1999; Roderick and Berry, 2001; Anfodillo *et al.*, 2006; Petit *et al.*, 2010; Savage *et al.*, 2010). Similar R_{tot}

across species, independent of height (or path length) also supports declining conductivity of sapwood with decreasing tree height as described in the *MST* (Ryan and Yoder, 1997).

Remarks on the Metabolic Scaling Theory

To understand competition-driven and site-specific growth habits of trees, current mathematical models consider multiple interacting factors. Such factors include branching architecture, mass allometry, xylem architecture, water use allometry and metabolic isometry (Sperry *et al*., 2012). Within the WBE model, vessel tapering is described using a 'taper exponent' (for a power function) and assuming a uniform optimal tapering structure along the entire vertical axis of the tree, often referred to as 'whole path length'.

Importantly, results presented here underline the importance of developing more refined tools to accurately analyse changes in whole-tree hydraulic architecture. The current approach, using log-log transformed data appears limited as it fails to account for non-linearity of vessel widening by producing a singular value ('tapering exponent') and artificially implies a "stable behaviour" of tapering (e.g. Mencuccini *et al.*, 2007; Petit *et al.*, 2010). Despite the shortfall of using log-log transformed data and assuming linear relations of vessel widening and path length, *MST* is widely used as tool for comparing hydraulic architecture of genera and species (e.g. Mencuccini *et al.*, 2007; Enquist and Bentley, 2012; Sperry *et al.*, 2012; von Allmen *et al.*, 2012). According to the original WBE model, full compensation for R_{tot} must be reached and theoretically can be achieved when the tapering exponent equals 1/6 (0.167) (West *et al.*, 1999). Values lower than 1/6 indicate that the vascular network is not optimized and that the upper parts of the tree will experience water-stress conditions (Anfodillo *et al.*, 2006). A decade later Savage *et al.* (2010) suggested the optimum tapering exponent to be 1/3 (0.33).

As mentioned above, *MST* assumes constant basipetal widening of vessels as an adaptation to increasing tree height. This feature is presumed to be most flexible during early growth stages of trees when increments in high are proportionally far greater to those made in widening of stems (Anfodillo *et al.*, 2006; Bond, 2000). The vascular system of mature (i.e. approaching maximum height) or overmature (i.e.

reached maximum height) trees is expected to slowly turn into a non-optimal structure, as taper exponents are likely to diminish with increasing tree height (Anfodillo *et al.*, 2006; Midgley, 2003). This assumption is in overall agreement with the *HLH* (Chapter 1.4.1). Simplified, tapering exponents are expected to be small for tall trees and bigger for smaller trees (Eq. 1.11; Chapter 1.4.2). Results presented here do not support these assumptions. All trees had tapering exponents >1/6, which fits model expectations for highly adapted hydraulic architecture that compensates for R_{tot}. As described in Chapter 2.2.3 all sampled trees were mature and were part of the dominant canopy at each sampled site. It can be excluded that height growth > diameter growth. Also, tall species from humid environments showed higher taper exponents (from 0.33 to 0.38) when compared to species from more arid environments (from 0.29 to 0.35; see Table 2.16). Although not statistically significant, this finding can be seen as yet another piece of evidence that eucalypts do not fit the above described theory of decreasing taper exponents with increasing tree heights. However, all findings strongly support the revised model of Savage *et al.* (2010). The suggested universal tapering exponent of 1/3 does fit *Eucalyptus* spp., independent of species and height. According to *MST*, all sampled trees were highly adapted to their environment and maintained a hydraulically optimized network of vessels even at their mature age. Hydraulic structure models based on the principles of allometric scaling place great emphasis on the relation between vessel size and vessel density (e.g. Savage *et al.* 2010; Chapter 1.4.2) and the related concept of optimal space filling, expressed (again) as an exponent of a power function (the 'packing exponent'; see also Enquist and Bentley, 2012). Packing functions (Chapter 1.4.2, Eq. 1.12) rely on *VtW*, i.e. the fraction of the total wood area occupied by xylem conduits, and a packing exponent. In combination with square packing (one vessel per square of space; packing exponent = -2) recent suggestions for an optimal *VtW* were 10^6 mm^{-2} μm^{-2}, which in turn assumes *VtW* to be constant from twig to trunk (or pith to cambium), which is not the case for *Eucalyptus* spp. (Savage *et al.*, 2010; Sperry *et al.*, 2012).

Different genera have different packing exponents. Savage *et al.* (2010) reported the following exponents: *Quercus* = -1.44, *Acer* = -2.37, *Pinus* = -1.67 and generally angiosperms = -2.36 and conifers = -1.64 (Savage *et al.*, 2010). Identified packing exponents for eucalypts were different for both individual trees and species (Table

2.16). When all samples are considered together, there were clear deviations from model assumptions.

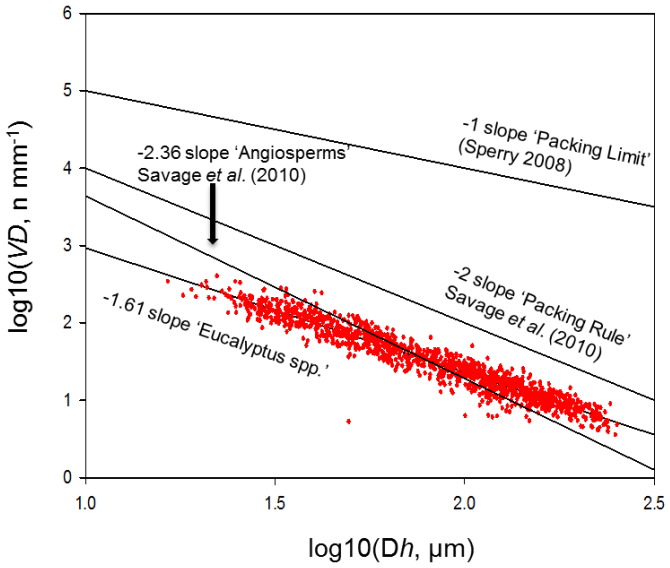

Figure 2.15: Relationship between average hydraulically weighted vessel diameters (D*h*; n = 3) and average vessel densities mm^{-2} sapwood (*VD*; n = 3) of all analysed sapwood samples plotted on a log-log scale. Three inserted reference lines illustrate hypothetical increase of *VD* for given D*h*s (original data of this study) according to metabolic scaling model predictions (packing function) with packing exponents determined in other investigations. 'Packing Limit' (packing exponent: -1) assumes all the wood to be occupied by conduit lumens of the average diameter, 'Packing Rule' (packing exponent: -2) suggests optimal vessel frequency versus vessel size for a hypothetical tree and packing structure identified in angiosperms (Savage *et al.*, 2010).

Findings in this thesis clearly show the proposed optimal multiplier (k_4; Eq. 1.12) of 10^6 mm^{-2} µm^{-2} to be incorrect. Applied to *Eucalyptus* spp. it would lead to considerable overestimations of *VD* at any given D*h*. An exponent of -2 did not apply to any species. Exponents for some individual trees were close to -2 (Table 2.16). Differences among species were pronounced and exponents ranged from -1.4 to almost -2. Differences in packing exponents across eucalypt species from a wide range of environments suggests that the arrangement of vessels in sapwood of species from very different environments do not follow a universal rule. Consequently, using a 'universal' model to estimate tree specific conductivity would, at least for *Eucalyptus* spp., likely lead to an overestimation. As the heights of

eucalypts increase, the changes in vessel diameter and density are not uniform and are largely restricted to the final ≈ 1/2 – 1/3 of tree height.

Outliers – environmental reasons

The vessel characteristics of two species, namely of *E. pauciflora* and *E. victrix*, differed significantly from all other species in as much that their characteristics did not fit climate-dependent relationships that could be developed for other species. *Eucalyptus pauciflora* dominates high elevation areas in south-eastern Australia. The AI for the respective study site in this thesis was 1.82; the second highest of all sites (Fig. 2.3). Given AI relies on annual precipitation and a large proportion of annual precipitation at the *E. pauciflora* site is deposited as snow. However much of snowmelt is generally not available to *E. pauciflora* but instead becomes runoff. In addition, these high mountain areas in south-eastern Australia often experience very dry summers. It thus appears that even though annual precipitation is large, vessel anatomy of *E. pauciflora* is adapted to withstand summer embolism and cavitation events. As pointed out by Zimmermann (1983) and also by Pockman and Sperry (1996) freezing-induced cavitation represents a significant problem particularly for evergreen trees.

Eucalyptus victrix was sampled in the Pilbara, Western Australia; the only arid ecosystem in this study. According to the predictive models developed in Chapter 2.3.3 (see Fig. 2.4A) and 2.3.5 (see Fig. 2.7B), height of *E. victrix* should have been less and D*h* smaller than observed. However *E. victrix* is largely confined to riparian zones along ephemeral rivers and creeks, where groundwater tables sit relatively close beneath the surface. Most *E. victrix* likely have permanent access to groundwater (Pfautsch *et al.*, 2011). Hence even though transpirational demands were high, water supply is independent of P and rates of evapotranspiration. The wider vessels of *E. victrix* can facilitate transport of larger quantities of water that will (a) allow to maximise growth due to leaving stomata open for a longer period and (b) more efficient transpirative cooling at the leaf level, reducing the risk of heat stress for photosynthetic tissues.

Chapter 3 – Testing the effect of temperature, water and nutrient availability on growth and vessel anatomy in saplings of two species of *Eucalyptus*

3.1 Introduction

Chapter 2 shows that the xylem structure (conduit- and wood structure) adjusted to climatic conditions across a range of mature *Eucalyptus* spp. (see Chapter 2). The patterns observed for eucalypts are broadly similar to those recorded in other angiosperm and gymnosperm species (such as *Quercus, Larix, Pinus, Ilex* and many others; Antonova and Stasova, 1993; Antonova and Stasova, 1997; Wiemann *et al.*, 1998; Corcuera *et al.*, 2004; Eilmann *et al.*, 2009), albeit the quantitative relationships are distinctly different.

The previous chapter focused on mature trees and on assessment of climatic influences on conduit structure. A natural corollary to that assessment is the study of how prevailing and future environmental conditions will affect hydraulic architecture during the early phase of seedling development. This is the focus of this chapter.

Past research suggests that early xylogenesis is highly flexible and responsive to different water, temperature and nutrient regimes (Atkinson and Taylor, 1996; Harvey and van den Driessche, 1997; Maherali and DeLucia, 2000; Thomas *et al.*, 2004; Overdieck *et al.*, 2007; Thomas *et al.*, 2007; Goldstein *et al.*, 2013). Clear effects on size and number of vessels or tracheids, as well as wood density, have been observed in early development stages of both angiosperms and gymnosperms. Tree hydraulic properties like conductivity and resistivity, together with their implications for above- and belowground growth patterns, are thus likely to be strongly influenced by one or more of the above mentioned environmental factors. There have been few studies of the conduit system for *Eucalyputs* seedlings. The available literature shows a concentrated focus on effects of temperature on early development of wood anatomy; and suggests it is highly plastic (Scurfield, 1961; February *et al.*, 1995; Searson *et al.*, 2004; Thomas *et al.*, 2004, 2007). For example, when supplied with sufficient water, seedlings of *Eucalyptus* spp. respond to increasing temperatures with increased biomass accumulation, increased wood density, increased stem diameter, and increased sapling height, but smaller diameter vessels (Scurfield, 1961; Thomas *et al.*, 2004, 2007). In a detailed study, Thomas *et*

al. (2007) subjected seedlings of *E. grandis* to five different temperature treatments (10, 20,25,30 and 35 °C) and found that wood density increased 20% with increasing growth temperature to 436 kg m^{-3} at 30 °C before it declined to 410 kg m^{-3} when seedlings were grown at 35 °C. The same trend was observed for conduit structure, where the vessel number mm^{-2} / vessel lumen fraction (%) continuously declined from 10 °C to 30 °C treatments (408 mm^{-2} – 169 mm^{-2} / 17 % – 9.6 %) before rising again within the 35 °C temperature treatment (290 mm^{-2} / 10.4 %). Seedlings in 10 °C and 35 °C treatments had low leaf areas, slow rates of carbon assimilation and thin fiber cell walls, which in turn helped explained reductions in wood density and increases in vessel number and lumen fraction in 35 °C.

Compared to seedlings raised with sufficient supply of water, increased numbers of smaller vessels, smaller stem diameters and reduced plant mass was observed in two studies of the effects of water stress on seedlings of *E. grandis*, *E. sideroxylon* and *E. occidentalis* (February *et al.*, 1995; Searson *et al.*, 2004). For example, Searson *et al.* (2004) showed that at stem base, *Eucalyptus grandis* seedlings grown under well-watered conditions had an average vessel lumen area of 778 μm^2, while under water-limited conditions lumen area declined to an average of 549 μm^2.

Our understanding of the process of adaptation of vessels to prevailing soil water availabilities is moderately good. Briefly, the rate of division of cambial cells (i.e the width of the cambial layer) dictates vessel expansion. External influences on vessel size are, obviously, restricted to the period of vessel ontogeny (Ford *et al.*, 1978; Dodd, 1984; Sass and Eckstein, 1995) – once formed, vessels retain their size and shape for many years. Future vessel cell walls do not have a stiff cellulose skeleton and contain high proportions of hemicellulose, which allows cell expansion (Catesson, 1989; Sass and Eckstein, 1995). Driving vessel widening is low tugor pressure within the vessel, that forces water external to the vessel to enter, expanding the still soft cell walls (Ray *et al.*, 1972; Boyer, 1985; Sass and Eckstein, 1995).

There is broad agreement that forecast scenarios of climate change, characterized by changed of patterns of precipitation and temperature, influence activity of soil microbes which in turn affect ecosystem function and services such as N-mineralization and nitrification, and hence the amount of nitrogen available for

plants (Murdoch *et al.*, 1998; Leirós *et al.*, 1999; IPCC, 2007; Castro *et al.*, 2010; Bradbury and Firestone, 2012; Schaeffer *et al.*, 2013). That said, the net effects of these forecast climatic conditions on activity of soil microbial communities and related N-mineralization processes, are poorly understood (Leirós *et al.*, 1999; Schaeffer *et al.*, 2013). Even small increases in soil temperature enhance biological processes including N mineralization. Similarly, increased soil moisture increases soil hydraulic connectivity and facilitates transport of transformed N to plants. A combination of both increased temperature and moisture reduced inorganic N availability in arctic soils due to net microbial immobilization of N (Schaeffer *et al.*, 2013). Gonçalves and Carlyle (1994) modeled the influence of soil moisture and temperature on N-mineralization in a forested sandy soil in South Australia and suggested a positive impact of both factors on inorganic N availability.

To date, the impact of N availability on xylem structure and water use efficiency of mature trees and seedlings is inconclusive (Ingestad and Lund, 1979; Harvey and van den Driessche, 1999; Clearwater and Meinzer, 2001). Leaf area is responsive to additional nitrogen supply, but that is the only aspect of plant anatomy where we have conclusive evdience. Ingestad and Lund (1979) described strong and rapid effects of nitrogen availability on leaf development in birch seedlings. Clearwater and Meinzer (2001) reported that leaf area of *Eucalyptus grandis* saplings increased when plants were supplied with higher concentrations of N. However, a direct link between vessel structure and N availability is missing. Harvey and van den Driessche (1999) detected in different *Populus* clones an increasing vessel size from 36.6 µm at low-N supply to 45.2 µm at high-N and both, the tendency to cavitate and water-use efficiency increased when N supply was increased. In contrast, Clearwater and Meinzer (2001) found no changes in the hydraulic architecture of *Eucalyptus grandis* supplied with different levels of N. Taken together the effects of varying levels of N on hydraulic architecture of trees are yet to be established.

The "Plant Allocation and Multiple Limitation Hypothesis" forecasts a superior influence of a single resource in lowest supply relative to demand. Therefore, one essential resource might have more influence on growth performance than a combination of multiple resources (Gleeson and Tilman, 1992). Limited indirect evidence indicates that growth of the hydraulic system of trees can adversely affected

by forecast, multi-factorial changes in environmental conditions, with consequences for ecosystem function and vitality of individuals therein (Aber *et al.*, 2001). Experiments described in the current chapter address this problem, particularly the interaction of temperature, water availability and N-supply on the development of the hydraulic architecture in young eucalypt trees. *Eucalyptus grandis* and *E. melliodora* were chosen as test species for multiple reasons, most prominently because they prefer either mesic (*E. grandis*) or xeric (*E. melliodora*) environments (for full species description see chapter 3.2). *Eucalyptus grandis* develops moderately strong wood and due to its plasticity to environmental conditions and high yield in biomass it is of high importance to plantation forestry around the world (Boland *et al.*, 2006; Trabado and Wilstermann, 2008; Hubbard *et al.*, 2010). As a result of its high growth rate, *E. grandis* is assumed to be reliant on steady water supply (February *et al.*, 1995; Dye, 1996).

Eucalyptus melliodora produces hard and durable wood. This species can cope with drier conditions than *E. grandis* and it was chosen because of its greater capacity to withstand water limitation when compared with *E. grandis* (Boland *et al.*, 2006).

The following three hypotheses will be addressed: (1) Limitation of water will lead to decreasing vessel sizes in species from mesic environments while xylem architecture in species from xeric environments remains unchanged; (2) increasing temperatures will lead to smaller xylem vessels, independent of a species' home environment; (3) changes in biomass accumulation and hydraulic architecture of tree seedlings follow a clear environmental signal (dominant effect of either water, N or temperature) and interactions can be neglected due to the "Plant Allocation and Multiple Limitation Hypothesis".

3.2 Materials and methods

3.2.1 Tree species

Eucalyptus grandis grows in moist environments (1000 – 3500 mm mean annual precipitation (MAP)) and grows well in fertile valleys and within rainforests of low to medium altitude (0 – 600 m above sea level (a.s.l.)) north of Newcastle (NSW)

and along the coastline towards Bundaberg (QLD). A second population centre can be found around Townsville (QLD). The species prefers well-drained, deep, loamy soils of alluvial or volcanic origin. While there are pure closed stands of *E. grandis*, mixed stands are more widespread. *Eucalyptus grandis* is a tall species of the gum-type eucalypts, regularly reaching heights of around 55 m, and on sites of high quality up to 75 m. As a result of site quality, wood density of this species is variable (545 – 955 kg m^{-3}), albeit the wood is of moderate durability (Boland *et al*., 2006).
In contrast to *E. grandis*, *E. melliodora* has a wider distribution. The species grows on alluvial soils, loams and sandy loams and can be found in open woodlands on moderate slopes, foothills and ephemeral floodplains, stretching inland from NW Victoria to SE Queensland. These environments typically receive between 450 and 1400 mm MAP and are mostly summer dry climates. Along the Great Dividing Range *E. melliodora* can grow at altitudes as high as 1200 m a.s.l., where frosts are frequent in winter. Trees of this species seldom exceed heights of 30 m and wood density of this species is high (910 – 1220 kg m^{-3}; Boland *et al*., 2006).

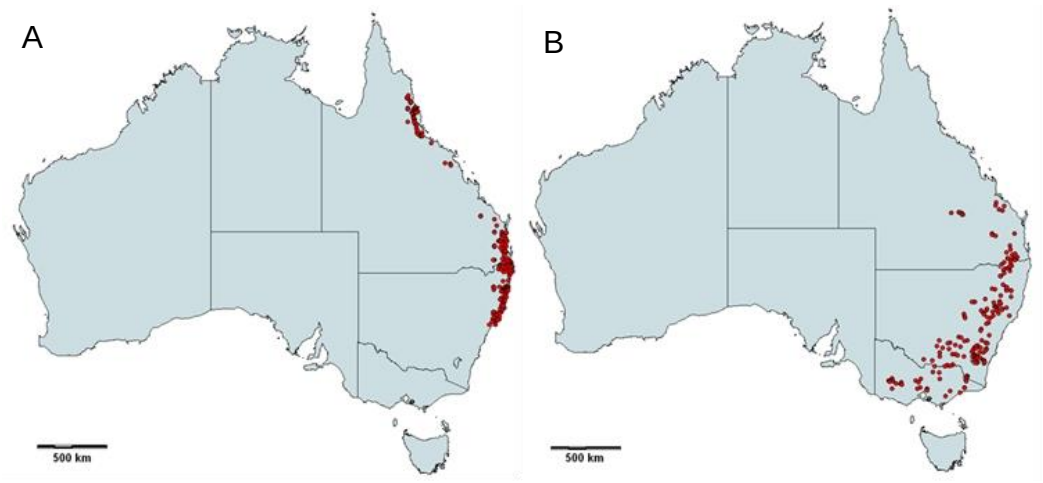

Figure 3.1: Geographical distribution of A) *Eucalyptus grandis* and B) *E. melliodora*. Source: www.florabank.org.au, accessed: 11.12.2013.

3.2.2 Experimental design

The experiment was completed in the Bosch Glasshouse at the University of Sydney between 1 July 2012 and 1 April 2013. The design was fully-factorial, incorporating the two above-described species, two growing temperatures, two rates of water supply (irrigation) and two rates of nitrogen supply. Ten commercially grown seedlings were used in each treatment combination. Seedlings were planted in

standard round plastic pots with a diameter of 250 mm and a volume of 8.1 L. Potting soil was customised as an 80 % sand/ 20 % turf mixture enriched with Canadian peat to increase the water holding capacity to 0.53 g cm^{-3}. Replicate sets of plants for both species were grown in two separate glasshouse bays (see description of bay environments below). Nutrient additions began 12 weeks after transplanting seedlings into pots and were applied fortnightly for a period of 6 months. Pots in each bay and from each treatment were positioned randomly and moved around during the experiment four times to prevent differences in tree growth due to microclimatic variation in the bays. Prior to the first application of nutrients, three seedlings per species were harvested to determine initial above- and belowground biomass, plant height and stem diameter, measured directly above soil level.

The first growth chamber was programmed to a cycle of 25 °C daytime temperature (0530-1900 hours) and 19 °C at nighttime (1901 – 0529 hours). The second growth chamber was set at 15 °C for daytime and 9 °C for nighttime temperatures at identical time intervals. A weather station (Hobo, Onset Computer Corporation, Massachusetts, USA) equipped with a data logger and a photosynthetically active radiation (PAR) sensor was installed and moved between the rooms on a regular basis, recording environmental conditions in the 25 °C bay for a total of 64 days and in the 15 °C bay for 82 days. The weather station logged data at 30 minute-intervals

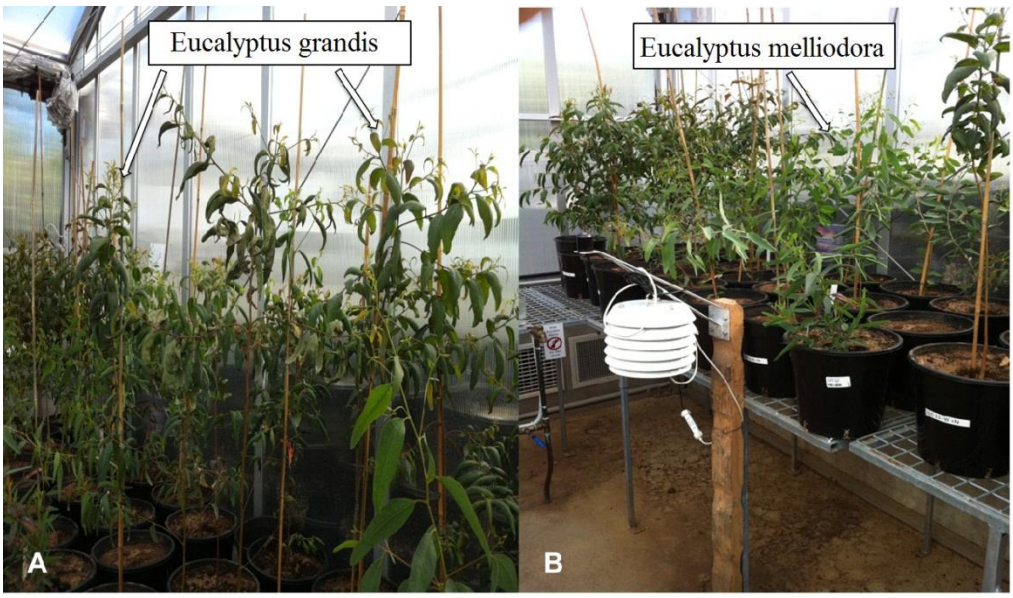

Figure 3.2: Saplings of A) *Eucalyptus grandis* and B) *E. melliodora* in the 25 °C growth chamber

3.2.3 Determination and application of irrigation and nitrogen treatments

To estimate evapotranspiration of glasshouse plants, soils of two to four average- to large-sized seedlings of each species were irrigated to water holding capacity and randomly placed in each room. At time intervals of every 15 min, 1 L of water was added until the point of oversaturation (constant dripping for 15 min) was reached. When dripping stopped, the outside surface of pots were dried and pots were weighed. Pots were reweighed every second day for 6 days. The mass loss measured was assumed to equal daily water loss (evaporation plus transpiration) of a seedling and soil under the prevailing conditions. Evaporation from soil surfaces alone was measured by applying the same method to three soil-filled pots for each temperature treatment over the same time period. Irrigation treatments were based upon initial estimates of the rate of evapotranspiration/water use. These procedures were repeated regularly and water supply was adjusted accordingly (see Table 3.1).

The amount of water that satisfied 100% of evapotranspirational demand (hereafter referred to as 'normal water', abbreviated as 'W') was added to one set of plants; the amount of water equivalent to 70% of total daily evapotransipration (hereafter referred to as 'limited water', abbreviated as '-W') was added to a replicate set of plants. Plants were watered every second day using twice the amount of water required. The amount of water required per day differed during different periods of the experiment (Table 3.1).

Table 3.1: The variable amounts of water added (ml) to pots to maintain 100% and 70% of daily evapotranspiration demands of plants growing at 15 and 25 ºC during each of four time intervals throughout the experimental period.

Species	Temperature (ºC)	Daily water requirement (100%/70%; ml)			
		18 Jul to 10 Oct 2012	10 Oct to 9 Nov 2012	9 Nov 2012 to 4 Mar 2013	4 Mar to 1 Apr 2013
E. grandis	25	260/180	260/180	300/210	300/210
E. melliodora	25	210/150	220/150	220/160	220/160
E. grandis	15	170/120	200/140	200/140	200/140
E. melliodora	15	160/110	160/110	160/110	160/110

Macro- and micronutrients were supplied using a modified Hoagland's solution (Table 3.2). A standard N supply was defined based on recommendations from research staff of The University of Western Sydney. Based on these recommendations, 45 mg of $Ca(NO_3)_2$ and 144 mg of $(NH_4)_2SO_4$ per seedling were

applied and assumed to represent a natural level of N availability (hereafter referred to as 'normal N, abbreviated as 'N'). The concentration of N was increased by 50% for plants undergoing the 'increased N' treatment, receiving 67.5 mg of $Ca(NO_3)_2$ and 216 mg of $(NH_4)_2SO_4$ (abbreviated as '+N').

Stock solutions for all macronutrients were stored in individual flasks. Micronutrients were all mixed and stored in one flask. Hoagland solutions containing all nutrients except $Ca(NO_3)_2$ and $(NH_4)_2SO_4$ were customized for different treatments, such that independent from the amount of provided water, seedlings received the same amounts of nutrients. $Ca(NO_3)_2$ and $(NH_4)_2SO_4$ were added in the glasshouse according to the respective N application scheme.

Table 3.2: Details of the macro- and micronutrients used in a modified Hoagland solution and amounts of N added to 'normal N' and 'increased N' (+50%) treatments. Asterisks mark the amount of 'increased N'

Nutrient	Molecular weight (g)	Stock solution (g l^{-1})	Amount in working solution (ml l^{-1})	Amounts provided per plant (ml l^{-1}) 100%/150%*
Macronutrients				
$Ca(NO_3)_2 \cdot 4\ H_2O$	236.16	118.08		0.7/1.1*
$(NH_4)_2SO_4$	132.13	132.13		4.0/6.0*
$MgSO_4 \cdot 7\ H_2O$	246.46	246.46	0.50	
KH_2PO_4	136.09	68.40	0.25	
K_2HPO_4	174.17	87.10	0.25	
$CaCl_2 \cdot 2H_2O$	147.02	147.02	0.50	
K_2SO_4	174.25	87.12	0.25	
Micronutrients			0.25	
Boric acid	61.83	2.86		
$MnCl_2 \cdot 4\ H_2O$	197.91	0.36		
$ZnCl_2$	136.28	0.11		
$CuCl_2 \cdot 2\ H_2O$	170.48	0.05		
Na_2MoO	205.92	0.03		
$CoCl_2 \cdot 6\ H_2O$	237.95	0.05		
Other				
Fe-Na-EDTA	367.05	34.47	0.25	

The aforementioned experimental design resulted in 16 different treatments. These treatments and their abbreviated codes are outlined in Table 3.3 below.

Table 3.3: List of treatments in two glass house bays with two different temperature treatments and two different *Eucalyptus* species, where 25 °C and 15 °C were defined as maximum daytime temperatures, W for 'normal' water supply, -W for 'limited' water supply, N for 'normal N' supply and +N for 'increased N' supply.

Eucalyptus grandis		*Eucalyptus melliodora*	
treatment 1	(25 °C W N)	treatment 9	(25 °C W N)
treatment 2	(25 °C –W N)	treatment 10	(25 °C –W N)
treatment 3	(25 °C W +N)	treatment 11	(25 °C W +N)
treatment 4	(25 °C –W +N)	treatment 12	(25 °C –W +N)
treatment 5	(15 °C W N)	treatment 13	(15 °C W N)
treatment 6	(15 °C –W N)	treatment 14	(15 °C –W N)
treatment 7	(15 °C W +N)	treatment 15	(15 °C W +N)
treatment 8	(15 °C –W +N)	treatment 16	(15 °C –W +N)

3.2.4 Sample collection and analysis

Prior to the final harvest, all plants were measured a second time to determine their final height and stem diameter. Three plants with the largest diameter were selected from each treatment and their stems were cut at the soil surface. Fresh weight of the aboveground biomass was determined. A 4 cm long basal segment of each stem was collected using secateurs. These wood samples were sealed in plastic bags before stored at 4 °C where they awaited further processing. Roots were carefully washed free of soil and their fresh weight was determined after blotting rootstocks dry. The dry weight of above- and belowground fractions were measured after drying plant biomass in an oven at 70 °C for 10 days. Wood samples were processed and their xylem vessels analysed using methods following identical procedures as previously described in Chapter 2.2.4. Wood densities of sapling base samples were measured as described in Chapter 2.2.5.

3.2.5 Statistical analyses

A script written in "R" (Version 2.15.1, R Foundation for Statistical Computing, Austria) was used to calculate average vessel traits from three digital images of sapwood collected from each sapling (i.e. 3 for each of 3 saplings from the 16 treatments = 144 images). Used script is shown in Appendix – Chapter 2; Script S2.97. This procedure was described in the Material and Methods section of Chapter 2. Microsoft Excel 2010 was used for standard mathematical computations such as

calculating averages and standard deviations of all traits investigated for trees and vessels from each treatment. Three other statistical software packages were used in subsequent analyses (Sigma Plot Version 11, SPSS Inc., Chicago, U.S.A; SPSS Version 21,SPSS Inc., Chicago, U.S.A; JMP Version 10.0, SAS Institute Inc., Cary, U.S.A).

Differences in environmental conditions between the two glasshouse bays, during day-time and night-time, were tested using a non-parametric Mann-Whitney Rank Sum Test with a significance level of $p \leq 0.001$.

Statistical analyses of tree and vessel traits followed two different approaches. First, differences of sapling- and vessel structural characteristics originating from the different water-, temperature-, or N-treatments were tested at the species-level. These individual comparisons included six saplings of two treatments were two influencing factors (water, temperature and/or N) were identical, while the factor of interest differed (e.g. same temperature and N treatment, but different water treatment). Means of traits, calculated from three saplings per treatment, were compared with either Mann-Whitney Rank Sum Test (for vessel diameter) or by one-way analysis of variance (ANOVA) (for all other tree- and vessel traits), both with a significance level of $p \leq 0.05$. Secondly, to test overall influences of single treatment factors and all conceivable combinations on sapling- and vessel formation, values for all traits of a species were pooled as either 'N', 'water' or 'temperature' effects. Average values for traits were compared against single and combined treatment factors by using either Wilcoxon signed-ranks test (for vessel diameter) or Univariate Analyses of Variances (UNIANOVA) for all other traits, both with a significance level of $p \leq 0.05$.

3.3 Results

3.3.1 Climate

Throughout the experiment, environmental conditions varied in the growth chambers due to changing solar radiation. Room internal air conditioning systems were not capable to keep temperature (T) constant. Furthermore, in case of the 15 °C growth

chamber, they were unable to cool down to 9 °C nighttime temperatures. Average daytime temperatures were 26 °C (± 1) in the growth chamber set for 25 °C (n = 1805) and 17 °C (± 3) in the growth chamber set for 15 °C (n = 2247). At nighttime, temperatures dropped to 19 °C (± 1) in the 25 °C growth chamber (n = 1307) and remained relatively constant within the 15 °C growth chamber (n = 1673; 16 ± 1 °C). However, comparing daytime and nighttime temperatures of respective treatments, even with insufficient air conditioning facilities in the 15 °C growth chamber, temperatures were significantly different (Mann-Whitney Rank Sum Test; $p \leq 0.001$).

In both rooms relative humidity was similar and generally lower during daytime compared to nighttime. Relative humidity in the 25 °C growth chamber averaged 76% (± 9) during daytime and 89% (± 6) during nighttime. In the 15 °C growth chamber these averages were slightly lower during daytime (75% ± 11) and slightly higher throughout nighttime (89% ± 3). Photosynthetically active radiation (PAR) was very similar in the two rooms. Average daytime PAR was 386 µmol $m^{-2}s^{-1}$ in the 25 °C growth chamber, and peak PAR was 1641 µmol $m^{-2}s^{-1}$. The same pattern was detected for the 15 °C growth chamber where average PAR was 394 µmol $m^{-2}s^{-1}$, but maximum PAR during midday was 1586 µmol $m^{-2}s^{-1}$. Table 3.3.1 summaries all measurements as averages for the entire duration of the experiment.

Table 3.4: Temperature (T), relative humidity (rh) and photosynthetic active radiation (PAR) average values of all daytime data recorded in the respective growth chambers with standard deviations in parentheses. Room number 1 stands for the 25 °C growth chamber and 2 for the 15 °C growth chamber.

Room	T (°C)	*rh* (%)	PAR (µmol $m^{-2}s^{-1}$)
1 daytime	26 (±1)	77 (±9)	386
1 nightime	20 (±1)	89 (±6)	
2 daytime	17 (±3)	75 (±11)	394
2 nightime	16 (±1)	89 (±3)	

3.3.2 Description of tree structural- and basic sapwood traits

Sapling height

Regardless of treatment, *E. grandis* saplings were always taller compared to those of *E. melliodora*. Differences, however, were mostly not significant (Table 3.5). Nitrogen treatment had no significant influence on height. Only in the 25 °C growth chamber, and with sufficient water supply, did application of additional N lead to

significantly taller saplings of *E. grandis* (Table 3.5). Figure 3.3 shows that across temperature treatments, both species tended to be shorter when water was withheld, but these differences were not significant. On a species level (n = 24), water had a clear impact on height of *E. grandis* but no effect on *E. melliodora*. Temperature also influenced height (Table 3.14). Saplings grown at 25 °C were in most cases significantly taller compared to those grown at 15 °C (Fig. 3.3). All considered sapwood structural properties, such as average vessel diameter (*d*; y = 2.28x + 981.29; R^2 = 0.03), hydraulically weighted diameter (D*h;* y = 0.05x + 41.53; R^2 = 0.04), vessel density (*VD*; y = 3.46x + 8271.8; R^2 = 0.004) and void to wood fraction (*VtW*; y = 0.03x + 7.13; R^2 = 0.08) showed no clear correlation with height (n = 3 species^{-1} and treatments^{-1}), neither on a species level, nor by pooling all saplings.

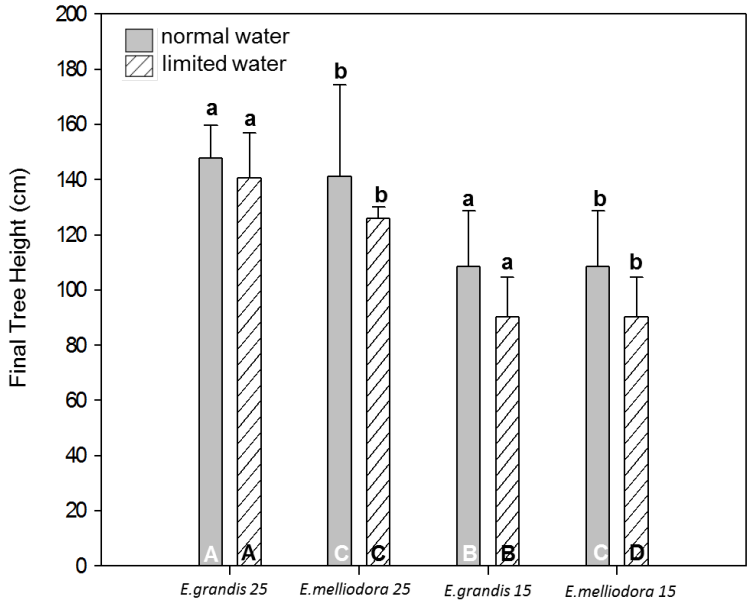

Figure 3.3: Average sapling height (cm; n = 3) of treatments (15 °C (15), 25 °C (25), normal water, limited water) and both species at normal nitrogen supply conditions. One-way ANOVAs with a p ≤0.05 level of significance were used for intra-species comparisons of temperature (T) and water effects, where lower case letters indicate significant differences in height as the result of different water treatments at the same growth temperature; capital letters indicate statistical differences of sapling height at the same water treatment but different growth temperatures where a,b (A,B) is dedicated to *Eucalyptus grandis* and c,d (C,D) to *E. melliodora*.

Eucalyptus grandis

The tallest saplings were those that grew under the normal water, additional N treatment (178 cm ± 12). These saplings were around 30 cm taller than saplings from

the limited water, increased N treatment, the second tallest (n = 3). This obvious trend of N effects was not confirmed in the 15 °C growth chamber (Table 3.5). Smallest saplings (limited W, normal N) reached only 90 cm (± 14). While saplings in the 15 °C growth chamber averaged around 100 cm of height, trees grown at 25 °C were fully one-third taller.

Eucalyptus melliodora

The tallest saplings of this species reached 141 cm (± 33; normal W, normal N) in the 25 °C chamber. All other treatments in this chamber resulted in average sapling heights of 130 cm. At 15 °C growing temperatures, saplings were considerably shorter. The shortest saplings reached only 80 cm (± 17; 15 °C, limited W, normal N). Other treatments within the cooler growth chamber produced tree heights of around 92 cm (Table 3.5). On a species level, neither water nor N had a significant effect on height of *E. melliodora* (Table 3.14).

Table 3.5: Average sapling height per species and per treatment (n = 3), standard deviations in parentheses and results of inter-species statistical comparison of sample means for the individual treatments conducted with one-way ANOVAs with a p ≤0.05 level of significance. Bold numbers indicate statistical significance. Abbreviations used: "EG" = *Eucalyptus grandis*, "EM" = *E. melliodora*, "15" = 15 °C, "25" = 25 °C, "W" = normal water, "-W" = limited water, "N" = normal N and "N+" = additional N supply.

treatment	EG height (cm)	EM height(cm)	EM*EG
15WN	109 (±20)	93 (±13)	0.31
15-WN	90 (±14)	80 (±17)	0.48
15WN+	109 (±13)	94 (±14)	0.25
15-WN+	99 (±6)	93 (±19)	0.62
25WN	148 (±12)	141 (±33)	0.76
25-WN	141 (±16)	126 (±4)	0.21
25WN+	178 (±12)	127 (±24)	**0.03**
25-WN+	149 (±13)	131 (±7)	0.11

Above- and belowground dry mass

Within all treatments *Eucalyptus grandis* saplings were, on average, larger and had more aboveground mass than *E. melliodora. E. grandis* saplings were larger in

diameter while *Eucalyptus melliodora* saplings had smaller diameters relative to height.

Final aboveground dry mass of both species grown at 25 °C was significantly less under water limited conditions compared to those grown with adequate water (Fig. 3.4). Saplings of both species grown at 25 °C had generally greater total mass compared to saplings grown at 15 °C (Table 3.6). However, this difference was only statistically significant for saplings of *E. melliodora* with normal water supply (Fig. 3.4). At a species level, water and temperature had a major influence on biomass accumulation of both species while N treatment only affected *E. grandis* (Table 3.14). Averages of above ground dry mass (n = 3 species^{-1} and treatment^{-1}) were moderately well correlated with sapwood traits such as *d* ($y = 0.05x^{0.95}$; $R^2 = 0.60$), D*h* ($y = 7E\text{-}3x^{2.23}$; $R^2 = 0.64$), *VtW* ($y = 3.33x^{1.07}$; $R^2 = 0.55$).

Table 3.6: Average aboveground dry mass per species and per treatment (n = 3), standard deviations in parentheses and results of inter-species statistical comparison of sample means for the individual treatments conducted with One-way ANOVAs with a p ≤0.05 level of significance. Bold numbers indicate statistical significance. Abbreviations used: "EG" = *Eucalyptus grandis*, "EM" = *E. melliodora*, "15" = 15 °C, "25" = 25 °C, "W" = normal water, "-W" = limited water, "N" = normal N and "N+" = additional N supply.

treatment	EG aboveground dry mass (g)	EM aboveground dry mass (g)	EM*EG
15WN	54.08 (±8.70)	30.71 (±3.86)	**0.01**
15-WN	37.23 (±6.71)	21.11 (±6.05)	**0.04**
15WN+	70.70 (±5.82)	32.99 (±8.44)	**<0.01**
15-WN+	32.82 (±3.66)	21.42 (±0.85)	**<0.01**
25WN	58.92 (±2.12)	42.17 (±3.05)	**<0.01**
25-WN	45.17 (±3.20)	26.75 (±4.88)	**<0.01**
25WN+	71.93 (±2.32)	44.61 (±2.03)	**<0.01**
25-WN+	50.90 (±8.04)	29.59 (±5.10)	**0.02**

Similar to above ground dry mass, roots of *E. grandis* were bulky and rather few, while *E. melliodora* had a mass of comparatively thin roots. With an adequate water supply, belowground biomass of *E. melliodora* was mostly greater compared to *E. grandis*, albeit the difference was not significant (Table 3.7). N treatment had no

effect on root mass. Withholding water reduced root mass, albeit not significantly (Fig. 3.4). Growth temperature had no detectable effect on root mass (Fig. 3.4, Table 3.7, 3.14).

Table 3.7: Average belowground dry weight per species and per treatment (n = 3), standard deviations in parentheses and results of inter-species statistical comparison of sample means for the individual treatments conducted with One-way ANOVAs with a p ≤0.05 level of significance. Abbreviations used: "EG" = *Eucalyptus grandis*, "EM" = *E. melliodora*, "15" = 15 °C, "25" = 25 °C, "W" = normal water, "-W" = limited water, "N" = normal N and "N+" = additional N supply.

treatment	EG belowground dry mass (g)	EM belowground dry mass (g)	EM*EG
15WN	18.60 (±1.50)	20.44 (±7.52)	0.70
15-WN	14.93 (±1.80)	12.25 (±4.89)	0.42
15WN+	20.96 (±1.75)	19.18 (±4.92)	0.59
15-WN+	11.91 (±2.88)	16.07 (±1.93)	0.11
25WN	18.96 (±2.69)	20.85 (±5.39)	0.62
25-WN	17.68 (±4.50)	13.13 (±4.29)	0.27
25WN+	16.15 (±5.13)	18.08 (±5.32)	0.67
25-WN+	17.07 (±1.97)	15.32 (±4.78)	0.59

Eucalyptus grandis

Independent of temperature, average aboveground dry weight was clearly greater in saplings raised with normal water and additional N. Aboveground biomass was least when water was withheld. The smallest aboveground biomass (32.82 g ± 3.66) was recorded for saplings that grew under water limited conditions, with increased N at 15 °C. Belowground biomass was similar among all treatments. Only the amount of water as a single factor had a significant effect on root growth (Table 3.14).

Eucalyptus melliodora

Maximum average aboveground dry mass was associated with plants grown at 25 °C, receiving normal water and increased N. In treatments with limited water supply aboveground dry mass was roughly one fourth smaller. The same pattern was observed in saplings raised at 15 °C. Compared to *E. grandis*, changes in belowground biomass with changing water availability were more obvious. In both

growth chambers, and independent of N treatment, saplings formed more root mass when supplied with sufficient water. Maximum average root mass was found in saplings raised at 25 °C, with comprehensive water and normal N supply. In contrast, minimum root biomass was associated with plants grown at 15 °C receiving limited water and normal N. Statistical analysis confirmed water was the only factor statistically influencing belowground biomass production of *E. melliodora* (Table 3.14).

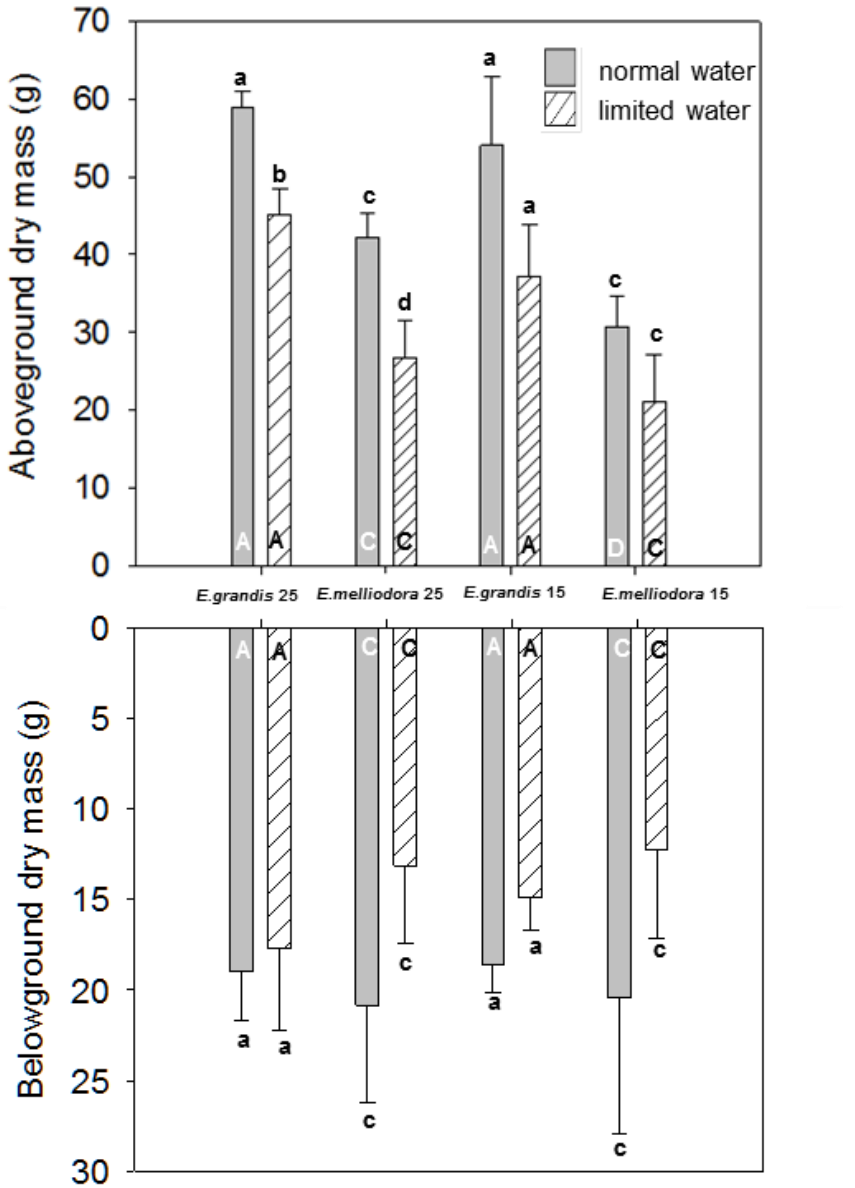

Figure 3.4 (previous page): Average aboveground and belowground dry mass (n = 3) of all treatments (15 °C (15), 25 °C (25), normal- and limited water) and both species receiving normal nitrogen supplies. One-way ANOVAs with a significance level of p ≤0.05 were used for intra-species comparisons of temperature (T) and water effects, where lower case letters indicate if above- or belowground dry mass differ due to water treatments when grown at identical temperatures; capital letters indicate differences in above- and belowground dry mass of plants grown at identical water treatments but different growth temperatures, where a,b (A,B) is dedicated to *Eucalyptus grandis* and c,d (C,D) to *E. melliodora*.

Sapwood density

Across all treatments, sapwood density (*WD*) of *E. melliodora* saplings was greater compared to *E. grandis*. Apart from the saplings grown at 15 °C under limited water conditions, these differences were statistically significant (Table 3.8). Nitrogen had no effect on *WD* (Table 3.14). When grown at 25 °C with limited water, saplings had greater wood densities than those that received adequate water. Differences were not significant (Fig. 3.5).

At a species level (n = 24), temperature had a clear effect on *WD* of E. *grandis* (Table 3.14). Sapwood densities (n = 3 species^{-1} and treatment^{-1}) were clearly influenced by xylem structural features such as *d* (y = -2E-04x + 0.76; R^2 = 0.73), D*h* (y = -9.5E-03x + 1; R^2 = 0.73) and *VtW* (y = -0.02x + 0.79; R^2 = 0.76).

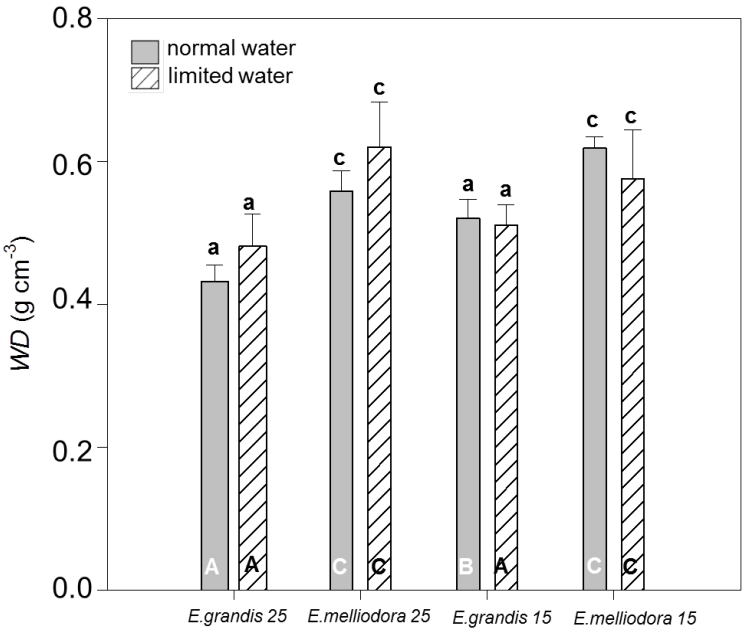

Figure 3.5 (previous page): Average sapwood density (*WD*) in sapwood of *Eucalyptus grandis* (n = 3) and *E. melliodora* (n = 3) saplings grown at 15 °C (15) and 25 °C (25), receiving normal or limited amounts of water. Nitrogen supply to these saplings was 'normal'. One-way ANOVAs with a significance level of p ≤0.05 were used to assess intra-specific differences in *WD* as a result of growth temperature or water supply. Lower case letters indicate differences in *WD* due to different water supply at identical growth temperatures; capital letters are used to indicate differences in *WD* at identical water treatments but different growth temperatures.

Eucalyptus grandis

Temperature had a significant effect on *WD* of *E. grandis* grown with sufficient water (Fig. 3.5). Independent of water and N treatments, *WD* of the majority of saplings grown at 15 °C were ≥0.5 g cm^{-3}, while the majority of saplings grown at 25 °C had WD ≤0.5 g cm^{-3}. The greatest *WD* was 0.57 g cm^{-3}. Average values of *WD* according to treatments are illustrated in Table 3.3.5. Neither water nor N had a significant effect on *WD* (Table 3.14).

Eucalyptus melliodora

Saplings of *E. melliodora* showed similar patterns of *WD* in response to treatment as observed for *E. grandis*. *WD* tended to increase when water was limited, but this difference was not significant (Table 3.14). When grown at 15 °C, water limitation had no effect on *WD*. Average values for *WD* and associated treatments are illustrated in Table 3.8. Univariate Analysis of Variance (Table 3.14) showed no significant effect of treatment on wood formation for this species.

Table 3.8 (next page): Average sapwood density (*WD)* per species and per treatment (n = 3), standard deviations in parentheses and results of inter-species statistical comparison of sample means for the individual treatments conducted with One-way ANOVAs with a significance level of p ≤0.05. Abbreviations used: "EG" = *Eucalyptus grandis*, "EM" = *E. melliodora*, "15" = 15 °C, "25" = 25 °C, "W" = normal water, "-W" = limited water, "N" = normal N and "N+" = additional N supply.

treatment	EG *WD* (g cm^{-3})	EM *WD* (g cm^{-3})	EM*EG
15WN	0.52 (± 0.03)	0.61 (± 0.02)	**<0.01**
15-WN	0.52 (± 0.03)	0.59 (± 0.07)	0.17
15WN+	0.52 (± 0.01)	0.63 (± 0.07)	**0.05**
15-WN+	0.50 (± 0.04)	0.63 (± 0.02)	**<0.01**
25WN	0.44 (± 0.02)	0.59 (± 0.03)	**<0.01**
25-WN	0.52 (± 0.05)	0.67 (± 0.06)	**0.03**
25WN+	0.46 (± 0.01)	0.59 (± 0.01)	**<0.01**
25-WN+	0.50 (± 0.05)	0.61 (± 0.01)	**0.03**

3.3.3 Basic sapwood traits

Vessel diameter

Across all treatments, average vessel diameter (*d*) of *Eucalyptus grandis* was greater compared to *E. melliodora*. These differences were significant across all treatments (Table 3.9).

Table 3.9: Total vessel counts (*VC*) per species and per treatment, average vessel diameter (*d*) per species and per treatment (n = 3), standard deviations in parentheses and results of inter-species comparison of groups median values conducted with a Mann-Whitney Rank Sum Test using a significance level of $p \leq 0.05$. Bold numbers indicate statistical significance. Abbreviations used: "EG" = *Eucalyptus grandis*, "EM" = *E. melliodora*, "15" = 15 °C, "25" = 25 °C, "W" = normal water, "-W" = limited water, "N" = normal N and "N+" = additional N supply.

treatment	EG_{VC}	EM_{VC}	EG *d* (µm)	EM *d* (µm)	EM*EG
15WN	452	451	47 (±12)	38 (±12)	**<0.01**
15-WN	267	275	42 (±13)	31 (±10)	**<0.01**
15WN+	471	405	43 (±12)	34 (±11)	**<0.01**
15-WN+	374	282	39 (±12)	33 (±12)	**<0.01**
25WN	288	469	43 (±12)	36 (±12)	**<0.01**
25-WN	449	420	39 (±11)	26 (±9)	**<0.01**
25WN+	481	260	42 (±11)	36 (±11)	**<0.01**
25-WN+	290	376	40 (±12)	30 (±10)	**<0.01**

Independent of species, average *d* was slightly smaller in saplings grown under water-limited conditions compared to those saplings that received sufficient water (Table 3.9). Furthermore, in the majority of treatments, average *d* was significantly greater (all treatment $p \leq 0.02$) in saplings grown at 15 °C compared to 25 °C. The

only exception was that *d* did not differ between growth temperatures for *E. grandis* grown under water limited and additional N conditions.

Table 3.10: Nonparametric comparisons of intra-species differences in median values of vessel diameters between WN treatments and modified treatments at identical growth temperatures using Mann-Whitney Rank Sum Test and a p ≤0.05 level of significance. Bold numbers are indicating statistical significance. Abbreviation used: "EG" = *Eucalyptus grandis*, "EM" = *E. melliodora*, "15" = 15 °C, "25" = 25 °C, "W" = normal water, "-W" = limited water, "N" = normal N and "N+" = additional N supply.

treatment*treatment	EM15	EG15	EM25	EG25
WN * -WN	**<0.01**	**<0.01**	**<0.01**	**<0.01**
WN * WN+	**<0.01**	**<0.01**	0.65	**0.03**
WN * -WN+	**<0.01**	**<0.01**	**<0.01**	**<0.01**

Vessel density

Vessel densities (*VD*) in stems of *E. grandis* and *E. melliodora* did not differ within treatments. Independent of species, *VD* increased when saplings were grown with limited water, albeit not significantly (Fig. 3.6). Saplings of both species grown at 25 °C developed more vessels per unit sapwood compared to those grown at 15 °C, but again these differences were not significant (Table 3.11; Fig. 3.6).

At a species level, water and temperature treatments had a significant effect on *VD*, whereas N-treatment had no effect (Table 3.14).

Table 3.11 (next page): Total number of vessels counted (*VC*) and vessel density per unit sapwood area (*VD*) of *Eucalyptus grandis* (EG) and *E. melliodora* (EM; n = 3 per species and treatment). Standard deviations are shown in parentheses and results of inter-species comparison of sample means for individual treatments using ANOVA (p ≤0.05) are shown. Abbreviations used: "EG" = *Eucalyptus grandis*, "EM" = *E. melliodora*, "15" = 15 °C, "25" = 25 °C, "W" = normal water, "-W" = limited water, "N" = normal N and "N+" = additional N supply.

treatment	EG_{VC}	EM_{VC}	EG *VD* (n cm^{-2})	EM *VD* (n cm^{-2})	EM*EG
15WN	452	451	6866 (±1475)	7041 (±1188)	0.88
15-WN	267	275	8129 (±1606)	8373 (±1572)	0.86
15WN+	471	405	6736 (±320)	7673 (±1198)	0.26
15-WN+	374	282	9370 (±1462)	8441 (±728)	0.38
25WN	288	469	8769 (±556)	8388 (±3753)	0.87
25-WN	449	420	10268 (±759)	12050 (±2382)	0.29
25WN+	481	260	8639 (±1361)	7916 (±2055)	0.64
25-WN+	290	376	8830 (±1101)	11448 (±2667)	0.19

Eucalyptus grandis

This species produced the largest *VD* when grown with limited water and normal N at 25 °C. In contrast, the least *VD* was calculated for sapwood from saplings grown with sufficient water supply and increased N at 15 °C. Except for limited water and increased N treatments *VD* was generally larger in sapwood of saplings grown at 25 °C. Moreover, *VD* was always larger in sapwood of saplings that received less water (Table 3.11).

Eucalyptus melliodora

In *Eucalyptus melliodora VD* differed strongly between growth temperatures, being larger when grown at 25 °C and reaching higher numbers when water was withheld (Table 3.11).

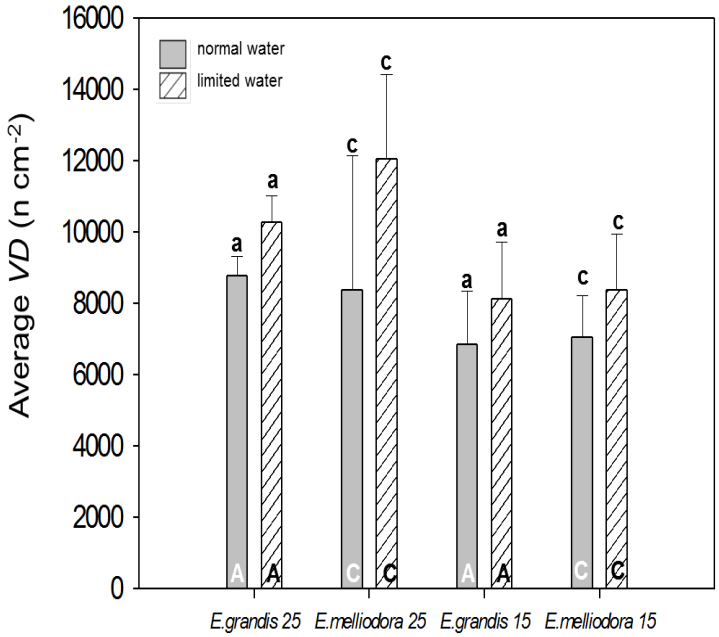

Figure 3.6: Average vessel density (*VD*; n = 3) in sapwood of *Eucalyptus grandis* (n = 3) and *E. melliodora* (n = 3) saplings grown at 15 °C (15) and 25 °C (25), receiving normal or limited amounts of water. Nitrogen supply to these saplings was 'normal'. One-way ANOVAs with a significance level of p ≤0.05 were used to assess intra-specific differences in *VD* as a result of growth temperature or water supply. Lower case letters indicate differences in *VD* due to different water supply at identical growth temperatures; capital letters are used to indicate differences in *VD* at identical water treatments but different growth temperatures.

Void to Wood fraction

In most treatments the fraction of void to wood (*VtW*) in sapwood was significantly greater in *E. grandis* compared to *E. melliodora* (Table 3.12). Independent of species, average *VtW* was marginally less in sapwood of saplings grown with limited water supplies. The observed trends were statistically not significant (Fig. 3.7). Results of Univariate Analysis of Variance (UNIANOVA) showed that *VtW* was not significantly altered by any treatment combination (Table 3.14).

Table 3.12 (next page): Average void to wood fraction (*VtW*) in sapwood of Eucalyptus grandis (EG) and E. melliodora (EM; n = 3 per species and treatment). Standard deviations are shown in parentheses. Results of inter-species comparisons (ANOVA; p ≤0.05) of *VtW* for saplings grown under identical conditions are shown. Abbreviations used: "EG" = *Eucalyptus grandis*, "EM" = *E. melliodora*, "15" = 15 °C, "25" = 25 °C, "W" = normal water, "-W" = limited water, "N" = normal N and "N+" = additional N supply.

treatment	EG *VtW* (%)	EM *VtW* (%)	EM*EG
15WN	13 (±2)	8 (±3)	0.11
15-WN	13 (±1)	7 (±1)	**<0.01**
15WN+	11 (±2)	7 (±1)	**0.01**
15-WN+	13 (±2)	7 (±2)	**0.02**
25WN	14 (±2)	8 (±1)	**0.01**
25-WN	13 (±3)	7 (±1)	**0.02**
25WN+	13 (±1)	9 (±1)	**0.01**
25-WN+	12 (±1)	9 (±2)	0.08

Eucalyptus grandis

Average *VtW* in sapwood of *E. grandis* ranged from 14% (±2) to 11% (±2). The saplings with the largest *VtW* were grown at 25 °C and received ample water and normal N, while the lowest *VtW* resulted from growing saplings at 15 °C, supplying them with ample water and additional N (Table 3.12). However, *VtW* did not differ significantly among treatments.

Eucalyptus melliodora

Although nearly a quarter less, average *VtW* in sapwood of *E. melliodora* did not vary due to different treatments. Maximum *VtW* (9% ±2) was detected in sapwood of plants grown at 25 °C, receiving limited water and additional N; minimum *VtW* (7% ±1) was detected in sapwood of plants grown at 25 °C, receiving limited water and normal N (Table 3.12). As in *E. grandis*, the *VtW* did not differ significantly among treatments.

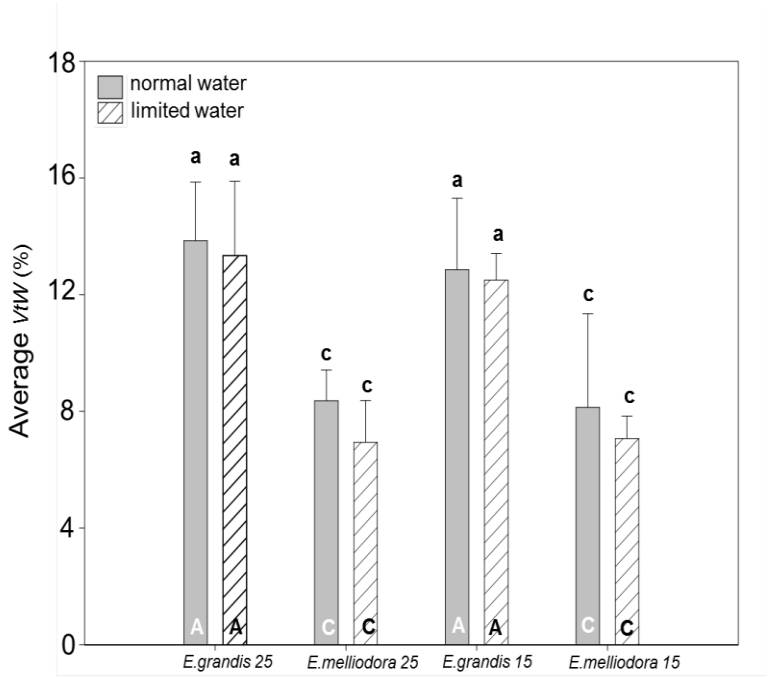

Figure 3.7: Average void to wood fraction (*VtW*) in sapwood of *Eucalyptus grandis* (n = 3) and *E. melliodora* (n = 3) saplings grown at 15 °C (15) and 25 °C (25), receiving normal or limited amounts of water. Nitrogen supply to these saplings was 'normal'. One-way ANOVAs with a significance level of p ≤0.05 were used to assess intra-specific differences in *VtW* as a result of growth temperature or water supply. Lower case letters indicate differences in *VtW* due to different water supply at identical growth temperatures; capital letters are used to indicate differences in *VtW* at identical water treatments but different growth temperatures.

3.3.4 Hydraulic architecture

Hydraulically weighted vessel diameter

The hydraulically weighted vessel diameter *(Dh)* in sapwood of *E. grandis* was, regardless of growth treatments, wider compared to the *Dh* in sapwood of *E. melliodora*. These differences were always significant, except for sapwood that was produced in both species at 25 °C, receiving normal water and additional N supply (Table 3.13). When water supply was reduced, *Dh* generally became narrower. This trend was however not significant when comparing the same species grown at the same temperature and N-supply (Fig. 3.9). On the species level water availability proved to be major influencing factor and significantly impacted the dimensions of D*h* (Table 3.14).

Table 3.13: Average hydraulically weighted vessel diameter (D*h*) in sapwood of *Eucalyptus grandis* (EG) and *E. melliodora* (EM; n = 3 per species and treatment). Standard deviations are shown in parentheses. Results of inter-species comparisons (ANOVA; p ≤0.05) of D*h* for saplings grown under identical conditions are shown. Abbreviations used: "EG" = *Eucalyptus grandis*, "EM" = *E. melliodora*, "15" = 15 °C, "25" = 25 °C, "W" = normal water, "-W" = limited water, "N" = normal N and "N+" = additional N supply.

treatment	EG D*h* (µm)	EM D*h* (µm)	EM*EG
15WN	57 (±2)	46 (±10)	0.12
15-WN	53 (±6)	40 (±5)	0.05
15WN+	55 (±3)	42 (±4)	**0.02**
15-WN+	51 (±8)	40 (±7)	0.14
25WN	52 (±3)	45 (±6)	0.14
25-WN	48 (±3)	35 (±7)	**0.04**
25WN+	53 (±4)	46 (±2)	0.63
25-WN+	50 (±5)	40 (±4)	**<0.05**

Both species exhibited a linear and negative relation between D*h* and *VD*. Sapwood of saplings with a small D*h* generally had a larger *VD* (Fig. 3.8). Similar *VD* but different *Dh* can explain differences in *VtW* among the two species where *E. grandis* > *E. melliodora*.

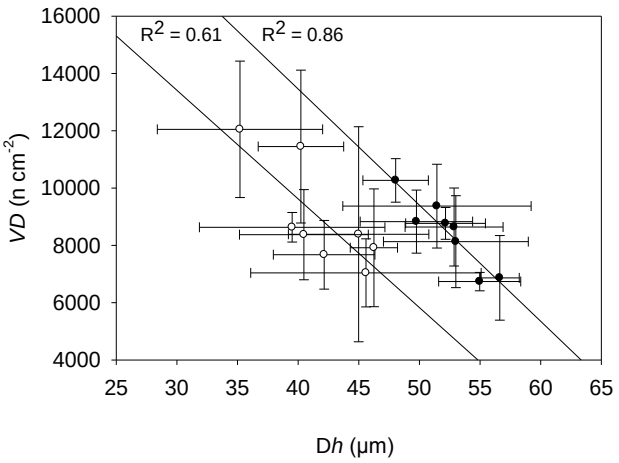

Figure 3.8 (previous page): Average vessel density (*VD*) versus average hydraulically weighted vessel diameter (D*h*) of *Eucalyptus grandis* (dots) and *E. melliodora* (circles) averaged for each of the eight growth treatments. Sapwood anatomy of three trees per treatment was analysed. Error bars represent standard deviations. Coefficients of determination are shown in the panel next to linear regression lines (*E. grandis*: f(x) = -405.37x+29675.48; *E. melliodora*: f(x) = -379.15x+24788.63)

Eucalyptus grandis

Differences in *Dh* across growth treatments were marginal in sapwood of *E. grandis*. The widest average D*h* was 57 µm (± 2) and belonged to sapwood that was produced at 15 °C where the plants received normal water and normal N supply. The smallest *Dh* (48 µm ± 3) was calculated for sapwood that was formed at 25 °C under limited water conditions and normal N supply (Table 3.13). Except for trees that were grown with limited water supply at 25 °C, D*h* was generally >50 µm. However, there was no clear statistical evidence of effects of treatments on *Dh* (Table 3.14, Fig. 3.9). Sapwood of plants grown at the lower temperature generally had wider *Dh*.

Eucalyptus melliodora

The trends of *Dh* in sapwood of *E. melliodora* were not coherent. The largest *Dh* in this species was 46 µm (± 10) and belonged to sapwood of plants grown at 15 °C, receiving normal water and additional N; the most narrow average D*h* was 35 µm (± 7) and belonged to sapwood that was formed at 25 °C, receiving reduced amounts of water and normal N supply. The amount of water provided had a significant effect on D*h* as saplings receiving comprehensive water supplies clearly developed wider vessels (Table 3.14). On an individual treatment level no effects of water, growth temperature and N-supply on *Dh* could be identified (Figure 3.9).

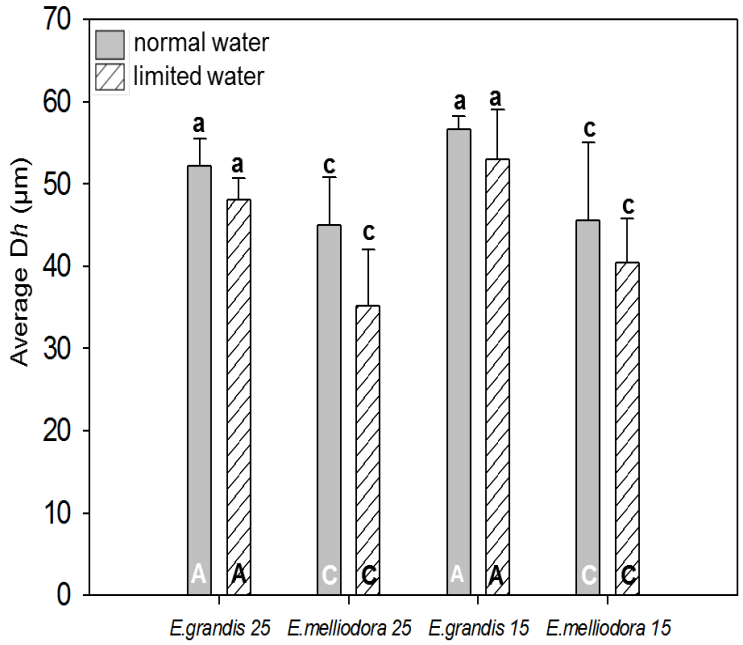

Figure 3.9: **Average hydraulically weighted vessel diameter (*Dh*) in sapwood of *Eucalyptus grandis* (n = 3) and *E. melliodora* (n = 3) saplings grown at 15 °C (15) and 25 °C (25), receiving normal or limited amounts of water. Nitrogen supply to these saplings was 'normal'. One-way ANOVAs with a significance level of p ≤0.05 were used to assess intra-specific differences in *Dh* as a result of growth temperature or water supply. Lower case letters indicate differences in *Dh* due to different water supply at identical growth temperatures; capital letters are used to indicate differences in *Dh* at identical water treatments but different growth temperatures.**

3.3.5 Statistical analyses on a species level

Differences in all investigated traits were analyzed against individual treatment factors and each conceivable combination of these factors using a univariate analyses of variance (UNIANOVA). This analysis was done for both species separately (n = 2 × 24) and the combined data of both species (n = 48) and its results are presented in Table 3.1. These statistical results were previously presented at the end of each relevant section.

Table 3.14 (next page): Results of Univariate Analysis of Variance (UNIANOVA) with a significance level of p ≤0.05. Sapling- and wood structural traits of *Eucalyptus grandis* (n = 24), *Eucalyptus melliodora* (n = 24) and the combination of both data sets (n = 48) are tested against individually against the following treatment factors: "T" = temperature (15 vs. 25 °C), "W" = water supply (normal vs. limited supply) and "N" = nitrogen supply (normal vs. elevated supply). Bold numbers indicate significant differences between treatment factors.

dependent variable	*Eucalyptus grandis*			*Eucalyptus melliodora*			All		
	T	**W**	**N**	**T**	**W**	**N**	**T**	**W**	**N**
D*h*	0.09	0.07	0.92	0.87	**<0.05**	0.81	0.40	**<0.05**	0.93
VD	**0.01**	**0.01**	0.81	**<0.05**	**<0.05**	0.92	**<0.01**	**<0.01**	0.84
WD	**0.03**	0.06	0.70	0.87	0.22	1.00	0.42	0.26	0.91
VtW	0.42	0.86	0.34	0.26	0.47	0.50	0.43	0.72	0.90
Final tree height	**<0.01**	**<0.05**	0.06	**<0.01**	0.43	0.89	**<0.01**	**<0.05**	0.25
Aboveground dry mass	**<0.05**	**<0.01**	**<0.05**	**<0.01**	**<0.01**	0.33	**<0.05**	**<0.01**	0.22
Belowground dry mass	0.50	**<0.05**	0.42	0.95	**<0.05**	0.81	0.76	**<0.01**	0.82

3.4 Discussion

The two investigated Eucalyptus species differed markedly in phenotype, reflecting their natural habitat. After growing for nine months under controlled environmental conditions, *E. grandis* was taller, had greater biomass and basal stem diameters compared to *E. melliodora* in any of the eight treatments (Fig. 3.4).

E. grandis also had fewer (Table 3.11) and wider (Table 3.9) vessels, a larger *VtW* ratio (Table 3.12) and a reduced sapwood density (Table 3.8) compared to those of *E. melliodora*. Consequently, sapwood of *E. grandis* had a greater capacity to transport water. *E. grandis* grows to considerably greater size than *E. melliodora*. Differences in sapwood anatomy between the two species and the resulting capacities to transport water can be interpreted as adaptation to prevailing environmental conditions in their natural habitats (high rainfall vs. low rainfall). Such adaptations are commonly reported across biomes and continents (e.g. Carlquist, 1975; Antonova and Stasova, 1993; Corcuera *et al.*, 2004; Campelo *et al.*, 2010). It must be noted here that most observed differences in vessel traits were not significantly different at $p \leq 0.05$.

Impact of water availability on sapling development

The amount of water supplied to tree seedlings clearly had the greatest effect on tree structure as well as on some xylem traits. At the end of the nine months of growth, well watered *E. grandis* were taller and both species had a greater above- and belowground biomass, regardless of growth temperatures (Fig. 3.4). This effect is

very well known (e.g. McAinsh, 1990; Davies and Zhang, 1991; Saliendra *et al.*, 1995; Sass and Eckstein, 1995; Aber *et al.*, 1998). Limited soil water availability and low turgor pressure in root cells can lead to an increase in synthesis of abscisic acid (ABA) that in turn is transported to guard cells in leaves. The resulting cascade of processes includes declining concentrations of osmolytes, and declining turgor of guard cells, finally leading to closing of stomata. Closing of stomata in turn limits the diffusion of CO_2 into the leaf, which in turn will reduce photosynthesis. Over a longer period, this mechanism results in decreased growth due to limits in carbohydrate synthesis (Raschke 1970).

As shown by UNIANOVA, reductions in water availability affected vessel diameters and densities in both species. Adaptation of vessel traits to soil water availability is also a well understood phenomenon (Chapter 3.1). The principle of decreasing vessel sizes with increasing vessel numbers in limited water conditions is widely accepted as being universal. It has been quantified several times in *Eucalyptus* spp. (e.g. February et al., 1995; Hudson et al., 1998; Searson et al., 2004) and other genera (e.g. Villar-Salvador et al., 1997; Lovisolo and Schubert, 1998; Preston et al., 2006). In the present study, all saplings growing with limited water showed the expected clear tendency to develop sapwood with smaller vessel diameters (Fig. 3.9) and increasing vessel densities (Fig. 3.6). *Eucalyptus grandis* generally showed weaker adaptation than *E. melliodora*.

Void to wood fraction also declined under water stress (Fig. 3.7), but the changes were slight and could not be specifically attributed to water (Table 3.14).

Beside well-documented physiological reasons for cell development (Chapter 3.1), smaller vessels must, according to the Hagen-Poiseuille Equation (Eq. 6), be accompanied by decreasing hydraulic conductivity, i.e increased resistivity (Lovisolo and Schubert, 1998). Reduced conductivity can increase negative tension within the respective vessel networks that, in environments with high VPD and low soil water availability, might lead to increased cavitation. This would in turn reduce conductivity even further (Sperry, 1986; Meinzer and Grantz, 1990; Sperry and Pockman, 1993; Lovisolo and Schubert, 1998). Other authors suggest no self-evident link between vessel size and cavitation events and instead suggest vessel pit size and

occurrence are more responsible, as the probability of air seeding seemingly increases with total pit area (Wheeler *et al.*, 2005; Hacke *et al.*, 2006; Sperry, 2008). Reduced conductivity, whether intensified by possible cavitation events or not, might result in low rates of replenishment of leaf water (Davies *et al.*, 1990; Lovisolo and Schubert, 1998). Reduced turgor in the guard cells might contribute to mitigation of the risk of cavitation (Meidner and Edwards, 1975). Clearly, small vessel sizes and high vessel numbers contribute to resistance to severe embolism events but there is still a remarkable gap between knowledge of anatomical detail and xylem function (Salleo *et al.*, 1985; Sperry, 2008). Additional investigations into xylem function are required.

Brought together, the first hypothesis, that the diameter of vessels in tree species from mesic environments would decrease when availability of water becomes limited while vessel diameters in species from xeric environments will remain unchanged, must be rejected. Results show clear flexibility of vessel structure in both species.

Impact of temperature on sapling development

After 9 months of growth, and independent of water and N treatment, the growth of the majority of saplings was increased by increased temperature (Table 3.14). Saplings in the 25 °C growth chamber were 27% – 36% taller. Increases in growth rates of plants with temperature is well described under glass house- (e.g. Thomas *et al.*, 2004, 2007) and field conditions (e.g. Rehfeldt *et al.*, 1999; Way and Oren, 2010).

Plant growth generally increases to reach a maximum at some temperature optimum. Reasons for increased growth rates at rising temperatures include enhanced biochemical processes, especially enzyme-mediated processes (Kattge and Knorr, 2007; Way and Oren, 2010). Results in this study for the two eucalypt species confirm findings by Thomas et al. (2007) of a steady increase in biomass accumulation by seedlings of *E. camaldulensis* grown at different temperatures, ranging from 10 to 25 °C. A further increase in growth temperature resulted in a curvilinear decline in seedling biomass (Thomas *et al.*, 2007).

Optimal growth temperatures differ among genera, species and habitats. For most tree species (gymnosperm and angiosperm) from the northern hemisphere this temperature ranges between 15 – 30 °C (e.g. Bonan and Sirois, 1992; Antonova and Stasova, 1997; Medlyn *et al.*, 2002). For *Eucalyptus* spp, native to different habitats in Australia, several investigations noted optimal growth temperatures of between 20 and 30 °C (Ferrar *et al.*, 1989; Battaglia *et al.*, 1996; Thomas *et al.*, 2007). In western North-America, Rehfeld *et al*. (1999) suggested growth would increase until air temperatures were 9 °C above average field temperatures for *Pinus* species. Tropical tree species often grow at temperatures in the field close to optimum, and further increases can result in declining photosynthetic activity (Doughty and Goulden, 2008).

In the current study sapwood density decreased with increasing temperature, especially in *E. grandis*. At first glance these findings run counter to those of earlier investigations of *E. grandis* and *E. camaldulensis*, where sapwood density was reported to increase in parallel with temperature (Thomas *et al.*, 2004, 2007). These studies, however, applied an overall wider temperature gradient and did not detect a significant difference in sapwood density between their 15 and 25 °C treatments. The observed trend of decreasing sapwood density may well have resulted from increased rates of growth. Available resources were seemingly invested to facilitate growth of aboveground biomass and overall plant height, rather than developing a more cavitation resistant and denser wood structure. This interpretation would support the trends observed in the present study, where height and aboveground biomass of plants were greater in the 25 °C treatment (Fig. 3.3, 3.4).

While average vessel diameters and hydraulically weighted vessel diameters showed the generally declined under warmer conditions, the effect of increasing vessel density with increasing temperature was clear. The observed increase of vessel density is contrary to observations reported in Thomas *et al.* (2004, 2007), where vessel density only differed significantly between the cold and very warm treatments, but not when plants were grown at 20 and 25 °C.

Roderick and Berry (2001) postulated that trees growing in increasingly warm environments form sapwood of declining vessel diameter, as the viscosity of water declines and similar amounts of water can be conducted through vessels of smaller

diameters. However, and in contrast to observations reported here, Roderick and Berry also suggest that vessel density would decline with increasing temperature, leading to increased sapwood density because of declining void space. The present study does not support these inferences as the void to wood ratio of both species remained relatively constant under the two temperature treatments. In contrast, however, their second hypothesis that increasing temperatures will lead to smaller xylem vessels, independent of genotype, was confirmed.

Impact of nitrogen availability on sapling development

The "Plant Allocation and Multiple Limitation Hypothesis" captures plant 'strategies' for matching growth to the least available resource (Gleeson and Tilman, 1992). In case of limited N availability, under conditions where water and light are not limiting, root growth increases facilitating exploration of larger volumes of soil for N. Conversely, reductions in root volume in environments where N is not limited can be associated with expansion of leaf and crown area (e.g. see Gleeson, 1993; Clearwater and Meinzer, 2001; Atwell *et al.*, 2009). This was not the case in the current study where root biomass did not increase with additional-N. The lack of an effect on aboveground biomass in the –WN+ compared to the –WN treatments observed in both species, suggests that N-availability was sufficient, relative to growth, in both N treatments. There were no significant effects on vessel traits of N treatment.

It has been frequently reported that the effects of N-availability on structural development on sapwood and other structural components of trees cannot be generalized. Different species and genera seem to respond differently to variation in N-availability (e.g. Clearwater and Meinzer, 2001; Bucci *et al.*, 2006; Atwell *et al.*, 2009; Goldstein *et al.*, 2013). Some reports show that additional N leads to an increase in leaf area (e.g. Brix and Mitchell, 1983; Clearwater and Meinzer, 2001) and a reduction in resource allocation to roots, resulting in a more shallow root system (e.g. Gleeson, 1993; Atwell *et al.*, 2009). In *Pinus tadea*, additional N was reported to increase growth and as a 'follow-on' to decrease wood density due to a more porous xylem tissue (Ewers *et al.*, 1999; Goldstein *et al.*, 2013).

The results of this study can only partly confirm for the above-mentioned tree- and wood structural changes. Leaf area was not investigated, and only the aboveground dry mass of *E. grandis* was clearly influenced by the variation of N supply (Table 3.14). Changes of sapwood density due to different supply of N were not detected by UNIANOVA. Previous studies found a rather weak increase in wood density when *E. grandis* seedlings were supplied with increasing amounts of N (Clearwater and Meinzer, 2001). Wood density was not affected by increased growth rates which opposes the above mentioned assumption by Goldstein (2013) and is in line with observations by Harvey and van den Driessche (1999) where increased N-supply increased growth and water-use efficiency in poplar saplings through an increased rate of photosynthesis but not wood density.

In the study by Harvey and van den Driessche (1999), xylem traits of poplar saplings were influenced by N in the way that d increased when plants were supplied with high amounts of N. Similarly, Goldstein et al. (2013) reported that hydraulic conductivity of vessels increased when N availability was increased. These results contrast with those reported in Atwell et al. (1999) for sapwood of *E. pauciflora*, where enhanced N-supply did not result in increased vessel diameters. Moreover, a decrease in vessel diameter, water transport efficiency, stomatal conductance and rate of carbon assimilation was recently reported for *Pinus taeda* that was grown in high N environments (Faustino *et al.*, 2013).

Taken together, the contribution of N to xylem ontogenesis appears controversial. Results of this study do not indicate a clear effect of changes in N-supply on vessel anatomy. *Eucalyptus grandis* and *E. melliodora* tended to develop unchanged vessel sizes when receiving additional N (Table 3.9). In both species vessel density also did not respond to differences in N-supply (Table 3.11).

Consequences under a changing climate

Although not investigated, basic tree- and sapwood structural traits investigated in the present study seem to reflect co-evolution of species with climate, as suggested in studies of other plant species (Savidge, 1996; Paux *et al.*, 2005). Furthermore, the majority of investigated traits were clearly reactive to experimental conditions as set

up in the two growth chambers. The strongest environmental signals that initiated changes in the anatomy of sapwood traits were the availability of water and the apparent growth temperature. This observation is in alignment with other studies (Aber *et al.*, 2001; Thomas *et al.*, 2004, 2007). Water availability is a key to plant function and dictates the quantity and quality of cell- and vessel development the rate of transpiration and amongst other important physiological and biochemical functions photosynthetic activity and CO_2 assimilation (Gleeson and Tilman, 1992). Increases in temperature on the other hand will promote not only plant internal enzyme activity but affect abiotic factors as VPD, rates of transpiration and evapotranspiration and also the viscosity of water. Depending on the intensity of environmental changes, the impacting combination of both, water and temperature, can therefore be assumed to have different effects on trees of respective stands.

The fact that water availability and temperature, rather than N, had major influence on xylem ontogenesis, strongly support suggestions of Clearwater and Meinzer (2001) that hydraulic architecture is partly responsible for tree structural traits such as leaf and crown physiology, rather than reverse (Clearwater and Meinzer, 2001). Results of this study indicate that young trees have a certain capacity to develop a hydraulic architecture in relation to the prevalent environmental conditions. According to Hydraulic Limitation Hypothesis (*MST*; Chapter 1.4.1) adaptation of vessel sizes are likely to affect habitus and growth performance of individual trees. However, changes in the availability of N due to climate change (see Chapter 3.1) seem not to affect hydraulic architecture and other tree structural traits in Eucalyptus. Additional research is required to disseminate if this observation is also true for other tree genera.

Overall, the third hypothesis, that changes in biomass accumulation and hydraulic architecture of tree seedlings follow a clear environmental signal (dominant effect of either water, N or temperature) and that interactions can be neglected due to the "Plant Allocation and Multiple Limitation Hypothesis", must be rejected. Tree and vessel structural traits which were significantly affected by environmental factors were often found to be simultaneously influenced by water and temperature.

Chapter 4 – Investigating water storage and circumferential variation in sap flow in mature, freestanding *Corymbia maculata*

4.1 Introduction

Trees are able to store water in woody tissues which, under conditions of increasingly negative water potentials in the xylem, can be used to support transpiration (Chapotin *et al.*, 2006). For a mature *Pseudotsuga menziesii* for instance, Phillips *et al.* (2003) estimated that use of stored water could result in an increase of up to 18% in photosynthetic activity per day. Both location of reservoirs within stems, and mechanisms responsible for mobilizing and restoring this water source, are not fully understood. So far, three different water storage mechanisms have been proposed: capillary storage, elastic storage and/or cavitation release (Holbrook, 1995; Maherali and DeLucia, 2001; Tyree and Zimmermann, 2002). Dependence on stored water is determined by a combination of environmental and species-specific (genetic) attributes, including soil water availability, leaf-specific conductivity, xylem vulnerability to cavitation and stem and leaf capacitances (Chapotin *et al.*, 2006). Capacitance (i.e. 'elastic water storage') of tress is commonly defined as the ratio of change in water content to change in water potential (Phillips *et al.* 2003). It has been reported that capacitance is strongly linked to phenology and spatial distribution, i.e. soil water availability (Borchert, 1994; Phillips *et al.*, 2003). There is increasing evidence water is stored in specialized parenchyma tissue, outside xylem vessels, where it can easily be released into the transpiration stream (e.g. Stratton *et al.*, 2000; Domec and Gartner, 2001; Domec *et al.*, 2005; Čermák *et al.*, 2007). In *Pseudotsuga menziesii* stored water accounted for 20 to 25% of total daily water use in large, and for 7% in small trees (Phillips *et al.*, 2003; Čermák *et al.*, 2007). In *Quercus garryana* stored water accounted for 10 to 23% of total daily water use in tall trees, and 9 to 13% in small trees (Phillips *et al.*, 2003). Goldstein *et al.* (1998) investigated capacitance in five broadleaf species from a tropical forest and surprisingly found a common relationship between storage capacity and sapwood area, suggesting that tree size and sapwood width, rather than genetic predisposition, determines the volume of water that can be withdrawn from sapwood.

In contrast to sapwood, capacitance of heartwood has received little attention. Low water content and occluded xylem conduits are commonly listed as major reasons to assume that heartwood is not 'designed' to contribute significant amounts of water to the transpiration stream (Holbrook, 1995; Kravka *et al.*, 1999; Maherali and DeLucia, 2001). Nevertheless, recent studies noted that the water content of heartwood in some angiosperm species, namely *Polulus*, *Eucalyptus* and *Quercus*, is similar or even greater than in sapwood (Yazawa, 2006; Pallardy, 2008). These authors named this phenomenon "wetwood" or "wet-heartwood". Possible reason for wetwood formation, however, remains poorly understood (Sano *et al.*, 1995; Yazawa, 2006). Reasons for wetwood could be bacterial infection and/or the influx of water through dead branches or mechanical injuries (Etheridge and Morin, 1962; Schink *et al.*, 1981; Murdoch *et al.*, 1983).

'Fibre Saturation Point' (FSP) is reached at approximately 30% of wood moisture content. Theoretically all water beyond 30% should be freely available for transpiration (Berry and Roderick, 2005). Pfautsch *et al.* (2012) reported that moisture content of heartwood in a range of *Eucalyptus* species can easily exceed 30%, and in some species was even twice that. Pfautsch *et al.* showed that when only healthy trees were sampled and the 'wetwood' resulting from damage or infection could be excluded, moisture content of heartwood increased from arid to mesic environments. Based on these results is reasonable to speculate that water stored in heartwood of eucalypt trees could represent a source of stored but potentially available water. Due to the novelty of the findings by Pfautsch *et al.* and the speculative nature of 'heartwood capacitance', a more thorough investigation of possible functional aspects of water stored in heartwood of trees is required.

Assuming heartwood can be used for water storage and stored water is used to support plant transpiration directly or has a refill function for embolised vessels, the cellular pathway of water movement between sap- and heartwood must be identified. Two possible pathways to move water radially in a tree have been described: 1. transport through wood rays (e.g. Zweifel *et al.*, 2000; Dickison, 2000 ; Tyree and Zimmermann, 2002) and 2. transport through pits (e.g. Jansen *et al.*, 2003; Gasco *et al.*, 2006). Wood rays are aggregations of parenchymal cells that extend from the cambium through the sapwood into the heartwood. They are the only living cells in

the xylem of woody plants and are connected to the adjacent water-conducting vessels or tracheids via pit pairs in their sidewalls (Salisbury and Ross, 1992; Dickison, 2000).

The capacity for radial conduction of water through wood rays, seem likely to be slow, because water has to transit many relatively small parenchyma cells that reduce the conductivity of rays (Dickison, 2000; Tyree and Zimmermann, 2002).

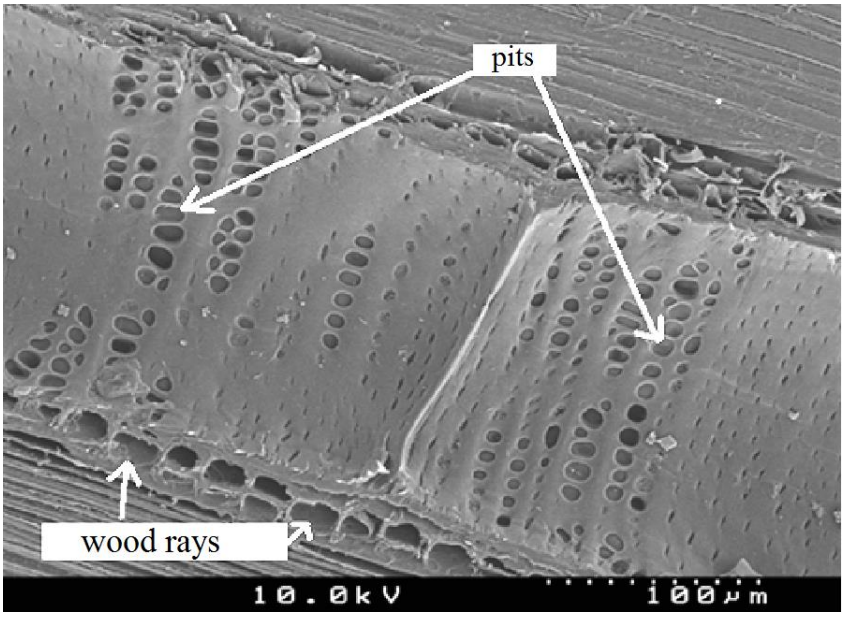

Figure 4.1: Scanning electron micrograph of a vessel sidewall of *Eucalyptus victrix* showing pit connections between vessels and wood rays. The image was generated using a S-400 SEM (Hitachi, Tokyo, Japan). Scale of the micrograph is indicated by the sequence of dashes in the right bottom corner.

Three-dimensional scanning of the vessel structure of *Fraxinus lanuginosa* and *Machilus thunbergii* revealed that vessels are interconnected in radial and tangential direction, even across year ring borders (Fujii *et al.*, 2001; Kitin *et al.*, 2004). In comparison to ray cells, water transport through inter-vessel or inter-tracheid pits is an effective way to transport water radially. However, the current lack of appropriate measurement techniques limits our ability to quantify sap interchange via pit connections (Kitin et al., 2004; Domec et al., 2006).

To characterize the movement of water through woody plants, including the study of capacitance, some researchers have injected deuteriated water (also known as ‘heavy

water', ^2H_2O or D_2O) into the transpiration stream (e.g. Meinzer *et al.*, 2006). Heavy water is also frequently used to study soil hydraulic processes (e.g. Kendall and Caldwell, 1998; Hobson and Wassenaar, 1999). The isotopic composition of water varies depending on the position of water in the natural water cycle (Gat, 1996) and also on latitude and altitude, (Dansgaard, 1964).

As an attempt to make measurements of the isotopic composition of water comparable across the globe, the International Atomic Energy Organization (IAEO) provides an internationally accepted reference standard water, termed "Vienna Standard Mean Ocean Water" (VSMOW). This reference or "ordinary water substance" contains 0.015574 atom% ^2H (IAPWS, 2001) and when measured against this standard, the isotopic ratio between ^1H and ^2H in water extracted from plants can be positive ('enriched') or negative ('depleted').

As noted above, heavy water has been used to identify water-related processes and function in trees, including the study of axial and radial water transport in sapwood as well as locating storage tissues (Kalma *et al.*, 1998; Marc and Robinson, 2004; Meinzer *et al.*, 2006). Most of these studies directly injected heavy water into the transpiration stream at the base of stems (Brooks *et al.*, 2002; James *et al.*, 2003; Meinzer *et al.*, 2003; Meinzer *et al.*, 2006). Injecting water into sapwood comes at the risk of introducing air bubbles into the xylem during both, the preparation of the injection whole and the actual injection. Once air enters the sapwood, the affected vessels embolize and loose their capacity to transport water upwards. Overall this can reduce the effective movement of the tracer, leading to underestimation of rates of water transport.

This chapter describes a trial of a new method, where heavy water is applied to trees by watering the surrounding soil, leaving the tree undisturbed and allowing for the tracer to be taken up by roots under natural conditions. The trial was conducted using a tall, mature *Corymbia maculata* tree. This study aims to shed light on the following hypotheses:

1. Enrichment of ^{2}H in the transpiration stream of trees can be achieved by irrigating trees with heavy water, and hence, irrigating with heavy water is an ideal tool to study water movement within trees.
2. If a tree accesses moisture stored in heartwood, this water needs to be restored and if heavy water is fed into the transpiration stream than enrichment of ^{2}H in water extracted from heartwood will be detected.
3. Concentrating irrigation with heavy water on one side of a tree provides the opportunity to detect patterns of radial and circumferential water transport.
4. Tracer residence time will be longer in lower compared to upper branches due to lower rates of transpiration in lower branches.

4.2 Materials and Methods

4.2.1 Pilot study

Plant material and irrigation method

As 'proof-of-concept', a pilot study tested if enrichment of ^{2}H in xylem sap of eucalypt trees could be detected after irrigation with heavy water. Five potted *Eucalyptus grandis* saplings were used for this study. Saplings were approximately 1.8 m tall (see section below; Table 4.1). All plants were of identical age and of similar crown dimensions and were planted in 8-L plastic pots. For one week prior to the irrigation with heavy water all plants were well watered each day. At the end of this period the base of each pot was sealed with a plastic bag to prevent draining of water. At 10am on day 0 all 'Treatment' plants received 300 ml heavy water. Tracer strength of ^{2}H was 1300‰, using a diluted stock solution that initially contained 70% deuterium oxide (Cambridge Isotope Laboratories, Andover, USA). A 'Control' plant received 300 ml tap water without additional tracer. On Days 2 and 4, trees that were not already destructively sampled (see section below; Table 4.1) were irrigated with 300 ml tap water.

Sample collection and analysis

After allowing trees to take up heavy water for 24 hours, one Control and one Treatment tree were harvested by cutting the stem 5 cm above its base using secateurs. One Treatment tree was then harvested each morning of Days 2, 3 and 4. Leaves of harvested trees were removed immediately after cutting the stem to prevent transpirational losses of water from the excised plants. Xylem sap was extracted from stems as described in Keitel *et al.* (2006). Silicon putty (Blu Tack, Bostic, Australia) was used to seal the basal 4 cm of the stem section and an inlet tube of a vacuum pump (PAV 2000, SDEC, Reignac sur Indre, France) in a Falcon vial (15 ml or 50 ml size, depending on sample diameter; Sarstedt, Ingle Farm, Australia). The bark and cambium of the base of the stem was removed prior to this procedure. By applying a mild vacuum (-0.8 bar), and repeatedly cutting small sections of stem, beginning at the apex and continuing towards the basal end, xylem sap was drawn into the Falcon vial. On average the extraction of xylem sap was completed within 1 – 2 minutes and the resulting sap was immediately transferred into 2 ml air-tight vials that contained a Teflon septa in their lids (Thermo Fisher Scientific, Scoresby, Australia), which was stored at 4 °C awaiting isotopic analyses. Details of analyses of ^{2}H in extracted sap are provided below.

4.2.2 Main study

Study site

The study was carried out in March 2012 at the John B. Pye Farm. The farm is located approximately 60 km southwest of Sydney in the Nepean River Catchment near the town of Cobbitty, NSW, Australia. Mature solitaire trees are scattered over the property; a mature *Corymbia maculata (Hook.) K.D. Hill & L.A. Johnson* was selected for the experiment and water from an adjacent dam was used for irrigation. The tree was 20 m tall and had a diameter at 1.3 m above ground of 61.5 cm. The crown was fully developed and had a uniform shape (Fig. 4.1). Environmental information (air temperature, relative humidity and rainfall) during the experiment was recorded by a weather station located at Mt. Annan Botanical Gardens. The

Botanical Gardens are in proximity to the experimental site. Vapour pressure deficit (VPD) was calculated from this data using the following formula:

$$\text{VPD} = \left(\frac{(0.6108 \times \exp(17.27 \times T_{air})}{(T_{air} + 237.3)}\right) \times \left(1 - \frac{rH}{100}\right) \quad \text{(Equation 4.1)}$$

Corymbia maculata grows along the entire coastal area of New South Wales, and is found in isolated stands in east Victoria and south-east Queensland. The species prefers well-drained soils where it forms pure open stands or co-occurs in mixed species forests, growing up to 45 m tall. The species grows from near sea level to up to 650 m a.s.l where annual precipitation can vary from 680 – 1700 mm; temperatures of the hottest and coldest month in the distribution range of *C. maculata* vary from 25 – 26 °C and 4 – 6 °C, respectively (Boland *et al.*, 2006).

Figure 4.2: Solitary *Corymbia maculata* at the John B. Pye Farm used in the present study.

Irrigation

Ground area around the tree was subdivided into four equally sized (approx. 4.5 m^2) triangles, representing the four cardinal directions. Their tips pointed towards the tree. Triangles were marked on the ground using spray paint. The east-facing triangle was chosen to receive all isotopically enriched irrigation water. The same stock solution of heavy water used during the pilot study was used in the main experiment, preparing 2000 L of ^2H_2O (1300‰ ^2H) using collected rainwater. Former studies provided evidence that the time required for ^2H_2O to reach the top of trees is size dependent and varies from two days in small trees to 21 days in mature trees (James *et al.*, 2003; Meinzer *et al.*, 2006). With these differences in mind, the irrigation treatment lasted for 10 days where 200 litres of ^2H_2O were watered into the soil at the eastern side of the tree every day during the early morning.

Tree water use

Sap flow was measured for 20 days (07.03.2012 – 26.03.2012). Within this period, sap flow measurements were made using the heat ratio method (HRM). Measurement principles and limitations of the method are detailed in Burgess *et al.* (2001). Briefly, HRM is a heat pulse-based method that allows estimation of water flux in stems by comparing the decline in temperature differences in wood below and above the source of the heat pulse (Burgess *et al.*, 2001; Pfautsch *et al.*, 2010).

Sap flow was measured at DBH, with 4 sets of sensor probes (HRM30, ICT International, Armidale, Australia), one at each cardinal side. Each set of sensor probes consisted of two temperature probes and a line heater probe. All probes were made from stainless steel tubing (35 mm long, 1.25 mm outer diameter) and were installed symmetrically along the axial pathway of sap. Three vertically aligned holes (1.26 mm diameter) were drilled into the sapwood after removing a 5x8 cm bark window. Temperature probes were installed into conducting sapwood, 5 mm above (downstream) and below (upstream) the heater. Each temperature probe was equipped with two type-T thermocouples located at 5 and 15 mm from tip, which allowed simultaneous measurements at two different sapwood depths. Data was recorded at 30-minute intervals using a Smart Logger (ICT International) Power was

supplied by a 12V car battery that was 'trickle-charged' using a solar panel (Fig. 4.3),

Figure 4.3: Sample tree, equipped with sap flow sensors, solar panel and logger/battery unit encased in a waterproof casing.

After installation all probes were insulated and shielded against thermal heating. The ratio of temperature increase above and below the heater was recorded for 40 seconds after a lag-time of 60 seconds from the release of the heat pulse. Heat velocity (V_h; cm h^{-1}) was calculated according to Marshall (1958):

$$V_h = \frac{k}{x}\ln\left(\frac{v1}{v2}\right)3600 \qquad \text{(Equation 4.2)}$$

where k is thermal diffusivity of fresh wood, x is the distance (cm) between the heater and either temperature probe, and v1 and v2 are increases in temperature (from initial temperatures) at equidistant points downstream and upstream, respectively, from the heater (Marshall 1958, Burgess *et al.*, 2001).

Raw heat velocity data were corrected for probe misalignment and wounding as described by Burgess *et al.*(2001) and sap velocity (V_s; cm h^{-1}) was calculated by a modified version of Marshall's (1958) equation, as described by Barrett *et al.*(1995). V_s can be calculated for a certain area of sapwood as it includes wood to void (sap) ratio considerations and accounts for their different heat permeabilities:

$$V_s = \frac{V_c \rho_b (c_w + m_c c_s)}{\rho_s c_s} \qquad \text{(Equation 4.3)}$$

Where ρ_b is the basic density of wood (dry weight/fresh volume), c_w and c_s are specific heat capacities of the wood (c_w) and the sap (c_s), m_c is the water content of sapwood and ρ_s is the density of water at 20 °C. Total volumetric water use (*Q*) was estimated by multiplying V_s with the sapwood area (cm^2) of a concentric band of sapwood. The width of this band was determined by extracting sapwood cores from each measurement position. Cores were stained with methyl orange (1% in H_2O solution) to identify the width of the entire sapwood, before assigning the width of sapwood to outer and inner measurement points of the temperature probes (Pfautsch *et al.*2010). The border between inner- and outer sapwood was defined as being the mid-point between the two points. This procedure was repeated for each of the four measurement positions. V_s of the outer and inner sapwood band were averaged for each position before calculating the total volume of *Q* as the mean of the four measurement positions. This procedure yields a representative measurement of *Q* that accounts for radial and circumferential variation of sap flow (Bleby *et al.*, 2004).

Four sapwood wedges were extracted adjacent to probe insertion holes at the end of water use measurements to determine moisture content and density of sapwood. From each wedge a cube of sapwood (approx. 3 cm^3) was the taken and its volume (immersion technique) and fresh weight were measured immediately after extraction. Samples were oven dried at 90 °C for 5 days before measuring their dry weight. Wood density was calculated as dry mass divided by fresh volume. Wood water content was determined from the ratio of the difference between wet and dry mass to the wet mass, and expressed as a percentage (Osunkoya *et al.*, 2007).

Wood collection

Prior to felling, all cardinal sides of the tree were marked at the base of the stem using spray paint. After felling, total tree length was measured with a tape measure, sample locations were marked with lumber crayon and wood sections were extracted from the stem and four branches using a chainsaw. Wood sections were split with a cleaver into quarters to facilitate collection of sap- and heartwood from each cardinal direction, keeping the time of exposure of wood to the atmosphere to a minimum. Where heartwood was wide (i.e. in the lower trunk), samples were divided into inner and outer positions (Fig. 4.4). At positions where heartwood was absent and stem or branch diameters were small (upper stem and branches) sapwood was only extracted from eastern, western and central positions (e.g. Fig. 4.4). The radius of sapwood at sample locations and diameters of heartwood at all sample heights were recorded (Appendix – Chapter 4; Table S4.1 – 4.5). Care was taken to avoid cross-contamination of samples. Each sample was extracted using a wood chisel that was triple-rinsed with deionized water after each extraction. All samples were immediately transferred into air-tight vials and stored in liquid N. A total of 91 wood samples were collected from the stem and 4 branches.

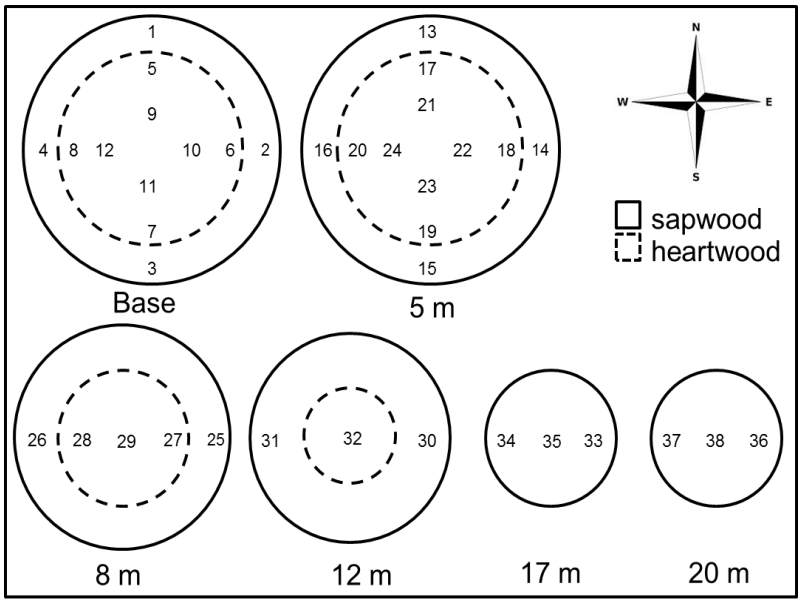

Figure 4.4: Cardinal direction and locations of wood samples extracted from main stem of a *Corymbia maculata* tree. The area inside the dashed circle indicates the proportion of heartwood. Height of the extraction point is indicated below each cross section. Numbers indicate exact location of samples in sap- and heartwood.

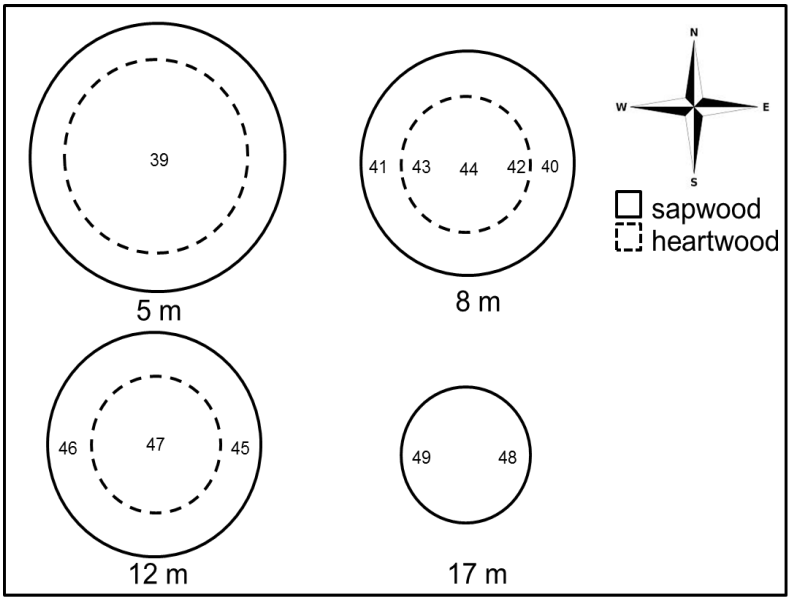

Figure 4.5: Cardinal direction and locations of wood samples extracted from a north-facing branch of a *Corymbia maculata* tree. The area inside the dashed circle indicates the proportion of heartwood. Distance from the base of the tree is indicated below each cross section. Numbers indicate exact location of samples in sap- and heartwood.

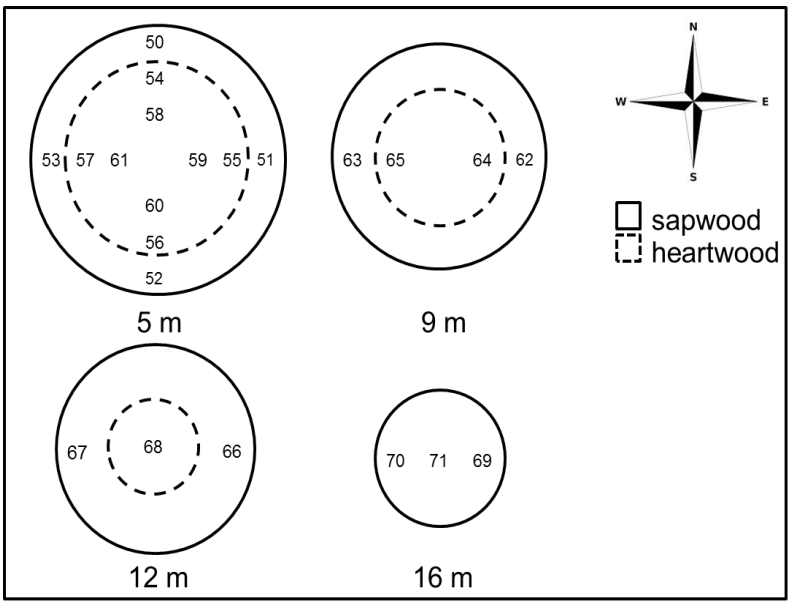

Figure 4.6: Cardinal direction and locations of wood samples extracted from an east-facing branch of a *Corymbia maculata* tree. The area inside the dashed circle indicates the proportion of heartwood. Distance from the base of the tree is indicated below each cross section. Numbers indicate exact location of samples in sap- and heartwood.

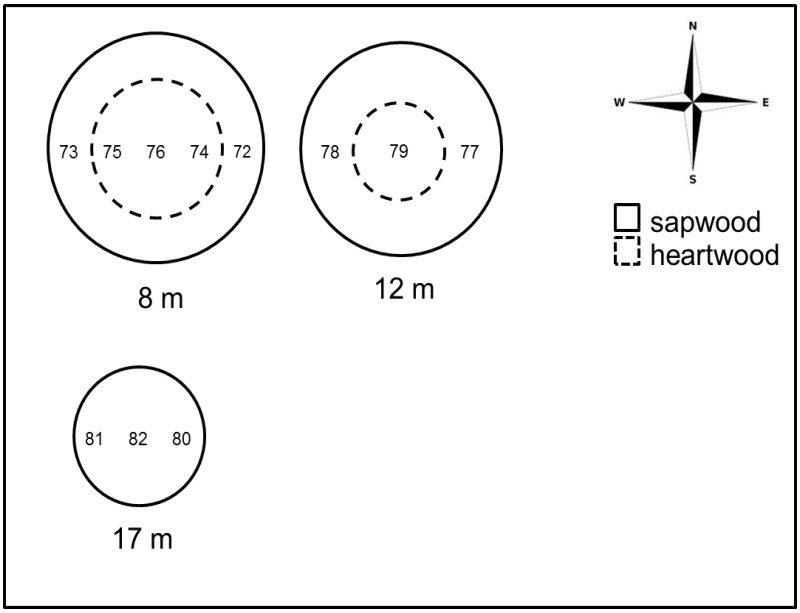

Figure 4.7: Cardinal direction and locations of wood samples extracted from a south-facing branch of a *Corymbia maculata* tree. The area inside the dashed circle indicates the proportion of heartwood. Distance from the base of the tree is indicated below each cross section. Numbers indicate exact location of samples in sap- and heartwood.

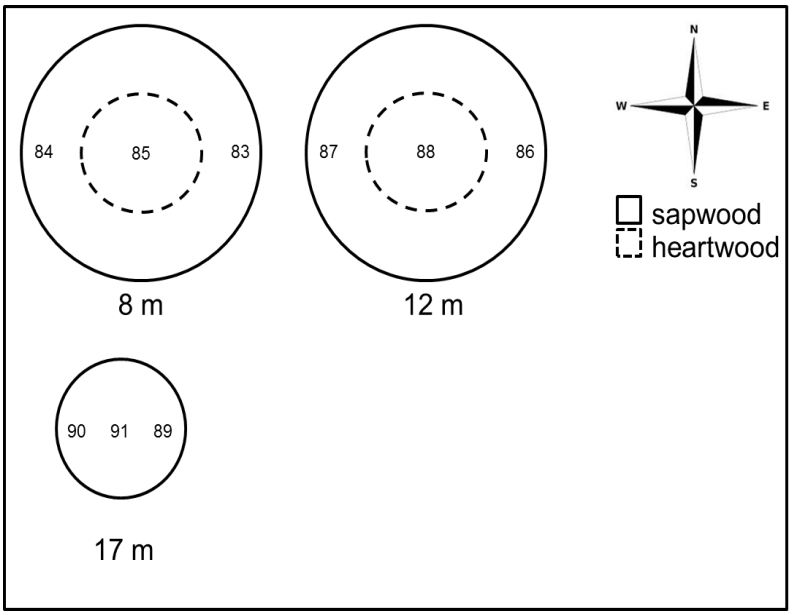

Figure 4.8: Cardinal direction and locations of wood samples extracted from a west-facing branch of a *Corymbia maculata* tree. The area inside the dashed circle indicates the proportion of heartwood. Distance from the base of the tree is indicated below each cross section. Numbers indicate exact location of samples in sap- and heartwood.

Water extraction

Water extractions as well as isotopic analysis were completed at the research facilities of the Australian Nuclear Science and Technology Organisation (ANSTO). Water was extracted from wood samples using a cryogenic vacuum distillation technique similar to that described by West *et al.* (2006). In short, a vacuum pump was connected to a tube system which ended in two extraction modules. Each module consisted of one extraction cylinder connected with a pipe to a collection tube. To start water extraction from a sample, the relevant module was evacuated and then isolated from the vacuum manifold by closing an intermediate valve. The extraction cylinder was removed and an open glass vial containing a wood sample, was placed into the cylinder. Once reconnected, the extraction cylinder was immersed in a flask that contained liquid N to refreeze the sample and any evaporated water condensed on the inner surface of the vial. After approximately two minutes, the sample was frozen, and the entire module containing the extraction and collection cylinders were evacuated by opening the intermediate valve. A vacuum pump was used to create a vacuum of around 60 mTorr (7.99 Pa).

Once the required vacuum was stable, the module was isolated to maintain the strength of the vacuum after which liquid N surrounding the extraction cylinder was replaced with a beaker filled with boiling water on a heat plate. For the duration of extraction water was kept at boiling point. At the other end of the module the collection tube was immersed in liquid N to immediately freeze incoming water vapour distilled from the sample. Time required for each extraction was around 90 minutes. West *et al.* (2006) suggested an extraction time of 60-75 minutes for wood samples. However, extractions of water out of heartwood required more time. Commonly, the extraction process should continue until at least 98% of water is extracted from the sample to receive an unfractionated sample (Araguás-Araguás *et al.*, 1995; West *et al.*, 2006). Once the extraction was complete the vacuum was released, the collection tube removed and the water allowed to thaw before being pipetted into a storage vial that was sealed with wax. Samples were stored at room temperature awaiting further analysis.

Isotopic analysis of water

Water samples were analysed using a combination of on-line combustion and a dual-inlet isotope ratio mass spectrometer (IRMS). For this procedure water samples were introduced into the septum port of the H/Device with a PAL Autosampler. 1µL of water was injected into a chromium reactor at 900ºC where H^2 is produced. The H^2 gas was then introduced into the IRMS (Delta V Advantage, Thermo Scientific, Waltham, U.S.A.), via a dual inlet system, and its isotopic composition was determined relative to pure Hydrogen gas, which is automatically loaded via reference refill into the dual inlet system. Each sample was injected in triplicate into the chromium reactor in order to prevent any memory effect. Results are reported in delta-format (δ) relative to the internationally used reference standard Vienna Standard Mean Ocean Water (VSMOW) for analyses of hydrogen. Results were normalized such that the ^2H value of Standard Light Arctic Precipitation (SLAP) is -428‰ relative to VSMOW using the following equation:

$$\delta 2H = \delta\left({}^2H/{}^1H\right)_{P/vSMOW2-SLAP} = \frac{R\left({}^2H/{}^1H\right)_p - R\left({}^2H/{}^1H\right)_{VSMOW2}}{R\left({}^2H/{}^1H\right)_{VSMOW2}} \qquad \text{(Equation 4.4)}$$

where the P represents the specimen having it's delta value(s) determined. Internal ANSTO standards used in each run were calibrated against VSMOW2 and SLAP2, which allowed for the samples to be reported relative to VSMOW. Quality control reference standard was included in each run. Results are accurate to +/- 1‰ (Nelson and Dettman, 2001).

Statistical analysis

The relationship between *Q* and VPD and also een δ^2H and tree height was tested using correlation analysis. Differences in δ^2H of water extracted from sap- and heartwood extracted from different heights within the tree were assessed using a Wilcoxon Test with a significance level of $p < 0.05$. Means and standard deviations were calculated using SPSS (V21,SPSS Inc., Chicago, U.S.A).

4.3 Results

4.3.1 Pilot study

Deuterium (^{2}H) in xylem sap of the reference tree was depleted against the international standard by 28.4‰. Xylem sap of all trees that were irrigated with heavy water showed a significant enrichment of ^{2}H. The initial concentration of ^{2}H in water supplied to tree seedlings was 1300‰ and xylem sap of the tree extracted one day after application of heavy water remained enriched, containing δ^2H of 500‰. Enrichment of xylem sap with ^{2}H gradually declined, reaching an enrichment of δ^2H of 264‰ after four days (Table 4.1).

Table 4.1: Total height, base diameter and measured δ^2H in all sapling sorted according to sampling day after key irrigation. Treatments are expressed as lower case letters where 'c' stands for control and 'd' stands for deuteriated. Standard deviations of measured ^{2}H values are parenthesized.

sampling day after irrigation	height (cm)	diameter (cm)	treatment	δ^2H $_{VSMOW}$ (‰)
1	176	1.6	c	-28.4 (±2.5)
1	162	1.7	d	492.2 (±2.5)
2	188	2.3	d	507.3 (±2.5)
3	167	2.0	d	318.1 (±2.5)
4	192	1.6	d	264.1 (±2.5)

4.3.2 Main study

Environmental conditions

During the 20 days of the field experiment, the area received 86.4 mm rainfall. Average daytime temperature was 20.8 °C (±2.4), relative humidity was 69% (±11) and VPD 0.85 kPa (±0.32). At night average temperatures were 16.31 °C (± 2.27), relative humidity increased to 87% (±9) while VPD decreased to 0.23 kPa (± 0.15). VPD throughout the day was variable and reached a maximum of around 2 kPa during the afternoon.

Tree structural traits

Sapwood area at the base of the *Corymbia maculata* tree was 844 cm^2 (±61). Width of bark and sapwood was markedly greater at the southern and eastern side of the tree, reaching 5.6 cm (Table 4.2). These differences did not affect density of sapwood that had an average density of 0.72 g cm^{-3}.

Table 4.2: Structural traits of sapwood collected from the base (1.3 m above ground) of a *Corymbia maculata* tree.

position	bark width (cm)	sapwood width (cm)	moisture content (%)	wood density (g cm^{-3})
North	1.95	4.7	38.4	0.75
West	1.75	4.8	41.2	0.70
South	2.2	5.6	42.8	0.68
East	2.5	5.5	38.2	0.75

Tree water use

Daily water use of the tree was stable during the three weeks of sap flow measurements (Figure 4.10). Across the three week period average daily water use of the tree was 425 L day^{-1} (±65), with a minimum of 258 L day^{-1} on 17.03.2012 and a maximum of 530 L day^{-1} during 24.03.2012 (Fig. 4.9).

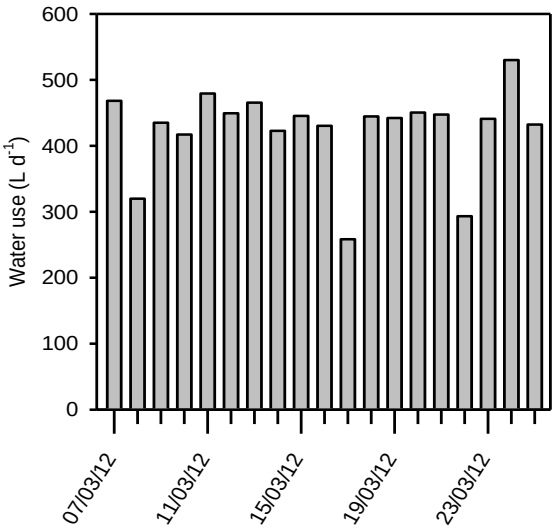

Figure 4.9: Total daily tree water use of a mature of a solitary *Corymbia maculata* tree expressed in litres per day (L d^{-1}).

Daily averages of water use were well correlated with daily sums of VPD, showing a

steep and curvilinear incline in *Q* when VPD increases from zero to 2 kPa (Fig. 4.3.2). After this inflection point, the relationship between *Q* and VPD becomes more linear but continues to rise above a daily water consumption of the tree >500 L.

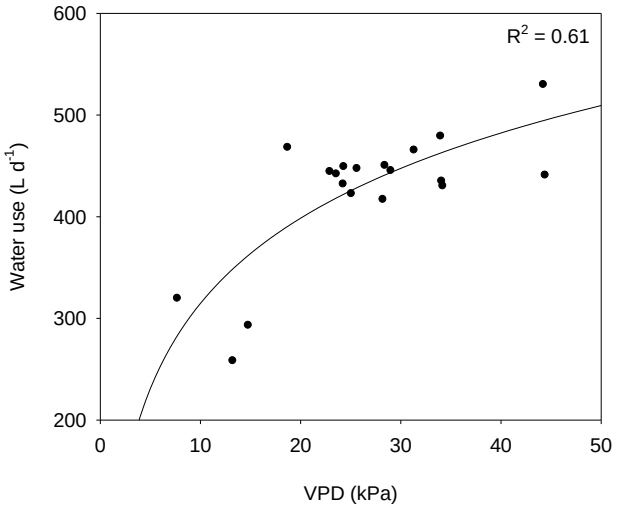

Figure 4.10: Relationship between daily water use (in litre per day; L d^{-1}) of a mature, solitary *Corymbia maculata* and the daily sum of vapour pressure deficit (VPD). Coefficients of determination for the exponential rise (solid line; y = 120.9 ln(x) + 36.38) is shown.

Whole tree water use varied during the course of a day. During March in south-eastern Australia, sunrise is around 7am and sunset around 7pm. Tree water use was generally slowest during the night before it increased rapidly around 7 – 8am, following the rising sun. During most of the day, water use of the tree remained relatively constant until the late afternoon from where it slowly declined (Fig. 4.11). During peak hours and depending on the day, water use varied between 15 and 30 litres per hour.

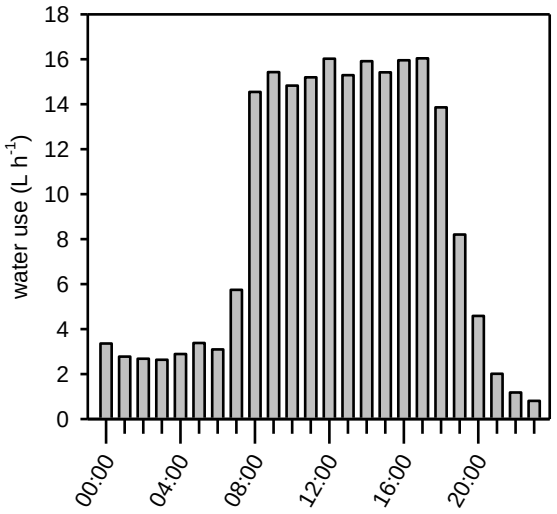

Figure 4.11: Diurnal course of water use of a mature *Corymbia maculata* tree during in early March 2012, expressed in litres per hour (L h^{-1}).

Flux density of sap (*J*s) varied consideraby with both, stem circumference and depth of sapwood. *J*s was always fastest at the eastern side of the tree (Fig. 4.12 A) in both the outer and inner sapwood (Fig. 4.12 B). Water flux was relatively constant throughout the entire sapwood width at this side of the tree. The slowest *J*s was measured at the northern side of the tree where *J*s in the outer sapwood was always significantly faster compared to *J*s of the inner sapwood. This pattern was also detected at the western side of the tree where *J*s declined nearly 50% from 45 to 25 cm h^{-1}.

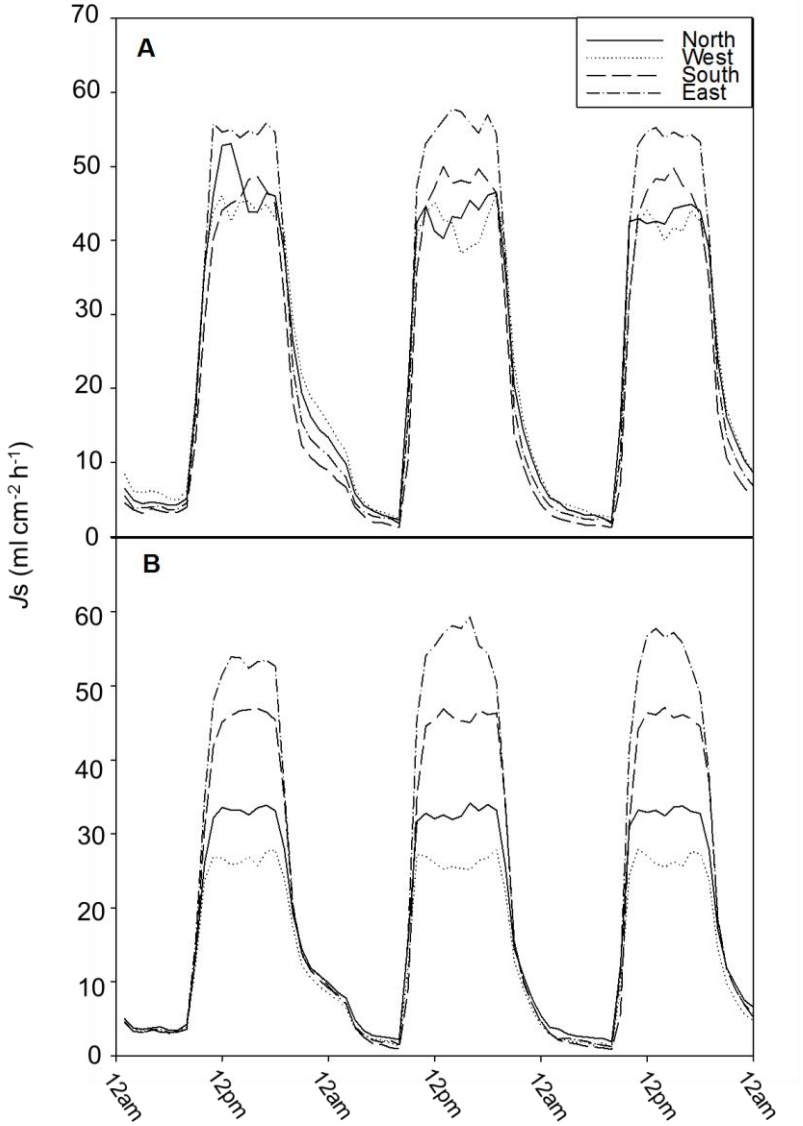

Figure 4.12: Patterns of sap flux density measured in the stem base of a solitary, mature *Corymbia maculata* tree at four cardinal directions in (A) the outer sapwood (10 mm below the cambium) and (B) the inner sapwood (25 mm below cambium). Data shown was recorded from 12.03.2012 to 14.03.2012.

Deuterium content of water in sap- and heartwood

The application of heavy water to the ground around the eastern section of the trunk did not enrich water extracted from sap- or heartwood. All 91 wood samples varied in their natural abundance of ^{2}H, and were always depleted in ^{2}H. All values for $\delta^{2}H$ tended to be similar to the 'tap water' treatment of the pilot study. To simplify results, isotopic data is only presented for sap- and heartwood of the stem, omitting data generated for sapwood from branches as outlined in the Material and Methods

section. These data can be found in Appendix – Chapter 4; Table S 4.1 – 4.5.

Depletion of ^{2}H in water extracted from both wood types ranged from -24.3 to -37.1‰. Water extracted from heartwood was increasingly less depleted when moving upwards in the tree (Fig. 4.13), having a delta value of -30‰ at the base from where ^{2}H increased linearly to -28‰ at 12 m stem height. As heartwood was absent above that height, no further samples could be extracted from the stem. Water extracted from sapwood showed a distinctly different pattern of ^{2}H along the height of the stem following a cubic function (Fig. 4.13). At the base, delta values for ^{2}H were around -34‰ before they became enriched in ^{2}H, reaching with -27‰ the highest concentration of ^{2}H at around 12 m above the base of the tree. From this point ^{2}H became increasingly depleted again and fell to -33‰ near the top of the 20 m tall tree.

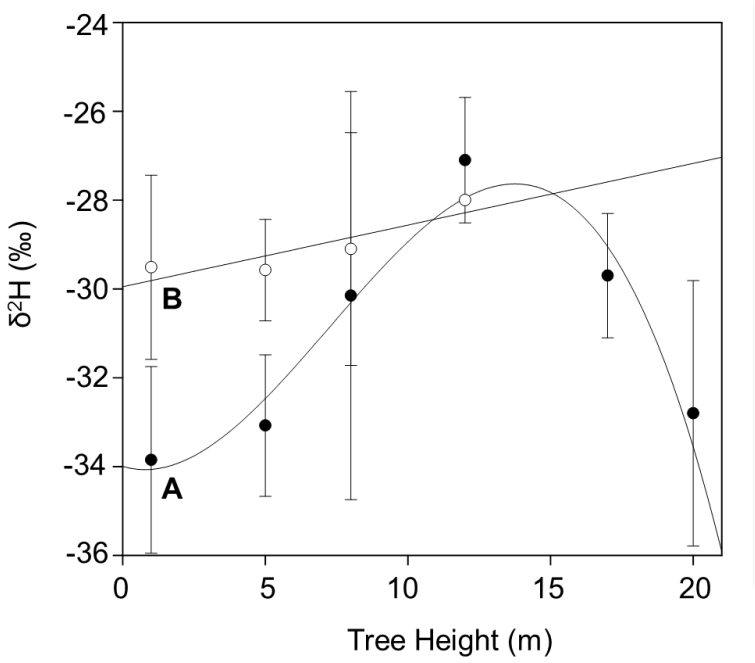

Figure 4.13: Profiles of deuterium in delta notation ($\delta^{2}H$) in water extracted from sapwood (A; dots) and heartwood (B; circles) collected along the entire stem of a mature, solitaire *Corymbia maculate*. Data are mean values of all sampled values per respective height and error bars denote standard deviations. Coefficients of determinations for cubic and linear trends (solid lines; A: $f(x) = -0.01x^3 + 0.13x^2 - 0.19x - 34$; B: $f(x) = 0.14x - 29.95$) are shown.

Across all samples, ^{2}H was significantly more depleted in water extracted from sap-, compared to that extracted from heartwood ($p = 0.03$; Table 4.3.3). The difference in depletion between water extracted from both wood types was with -4‰ particularly

pronounced at the base of the tree. This difference declined with height where at 12 m the difference in δ^2H was less than 1‰ (Table 4.3.3).

Table 4.3: Change in the average depletion of Deuterium in water extracted from sap- and heartwood of *Corymbia maculata*. Water was extracted at different heights along the main stem. Standard deviations are shown in parenthesis. Raw data can be found in Appendix – Chapter 4; S 4.1 – 4.5. A Wilcoxon test (significance level of p ≤0.05) was used to assess differences between water extracted from both wood types.

position	sapwood δ^2H (‰)	heartwood average δ^2H (‰)	p
all	-31.65 (±3.01)	-29.40 (±1.71)	**0.03**
base	-33.85 (±2.10)	-29.51 (±2.07)	**0.01**
5 m	-33.08 (±1.59)	-29.58 (±1.14)	**0.02**
8 m	-30.15 (±4.50)	-29.10 (±2.62)	0.77
12 m	-27.10 (±1.41)	-28.00	-

4.4 Discussion

The absence of any isotopic enrichment of water in sapwood- and heartwood tissue of *Corymbia maculata* was unexpected. The pilot study clearly showed that irrigated heavy water was taken up by tree roots and could be located in trees. Previous studies have also shown that roots absorb heavy water and that the applied tracer can be tracked in ascending sap and also in water extracted from various types of tissues of different genera (e.g. Smart *et al.*, 2005; Schoonmaker *et al.*, 2007; Snyder and Williams, 2007; Zarebanadkouki *et al.*, 2012). The tracer strength of 1300‰ applied in the present study has been used by other researchers and produced conclusive results (e.g. Brooks *et al.*, 2002). In a recent study, even less than half the amount of ^2H (600‰) was easily tracked (Schoonmaker *et al.*, 2007).

Tracer residence time in sapwood of mature gymnosperms and angiosperms is reported to depend on capacitance of sapwood and *Js*, and ^2H was recovered in trees, days and even months after its application (Meinzer *et al*., 2006). The pilot study showed that in young saplings of *Eucalyptus grandis* ^2H was clearly detectable four days after the irrigation with heavy water. The final irrigation treatment during the main study took place during the morning of the day prior to felling and although rates of transpiration during that day were high, which would have shortened the residence time, tracer should have been clearly identifiable in the tree.

The most parsimonious explanation for the absence of enrichment with ^2H for water extracted from sap- and heartwood, is that surface roots at the eastern side of tree did not access soil water. This is puzzling, given that this side of the tree contained the widest sapwood and recorded the fastest *J*s. A possible explanation of the absence of ^2H might be that all tree water was taken from depth and independent of surface water provided by rainfall or irrigation.

Some tall trees can meet their water requirements by taking up water from deep in the soil profile or from acquifers (e.g. Dawson and Pate, 1996; Meinzer *et al.*, 2001). Valentini *et al.* (1992) found that evergreen Mediterranean species rely largely on rainwater while deciduous species acquire most of their water almost exclusively from groundwater. Especially interesting are the results of Falkiner *et al.* (2006) that document a remarkable ability of *Corymbia maculata* roots to reach and use groundwater in ≈ 3m depth. However, even though the groundwater table at the sample site was relatively shallow (personal communication with the farm manager) and a water reservoir was in close proximity (Fig. 4.3), it is possible that the sampled tree did not take up water from these sources. Vertical 'sinker' roots are common in *Eucalyptus camaldulensis* and other Australian genera (El-Lakany and Mohamed, 1993; Dawson and Pate, 1996). Also, Acer species growing along streamsides were shown not to use stream water but water from deeper bedrock layers (Dawson and Ehleringer, 1991). Moreover, studies of Valentini et al. (1992) and Flakiner et al. (2006) both show that the dependency of trees on surface water declines with increasing age. It can therefore be speculated that the studied *C. maculata* exclusively acquired groundwater from deeper layers.

Evaporation enriches δ^2H in soil water towards the surface. Therefore δ^2H is generally more negative and more similar to precipitation in deeper strata and ground water than in upper strata (Dawson, 1996). Former research used the difference in isotopic composition of soil- and groundwater to detect sources of tree water use (e.g. Dawson and Pate 1996). In addition to enrichment due to evaporation, variation in source water may be influenced by the isotopic composition of precipitation, which varies naturally with seasons (e.g. Dawson, 1996, Dawson and Pate 1996).

At the sample site in March, average δ^2H values in precipitation range between -31 and -24‰ (http://wateriso.utah.edu/waterisotopes; accessed: 23/10/2014). Most extracted xylem water samples were within or very close to this range (Table 4.3), an indication that water was not taken from the evaporative surface or upper soil strata. Soil water analysis out of different strata would have been beneficial for this experiment to confirm this assumption. More research into root systems of mature *C. maculata* is necessary to allow characterization of water sources utilized by this species.

It remains difficult to accept that a daily dose of 200 L of highly enriched water was not sufficient to contaminate water in deeper soil layers and/or groundwater. Exclusive uptake of 100% water from groundwater appears questionable. Whatever the reason, the absence of the tracer in all water samples impeded the intended investigation of capacitance, including identification of tissues responsible for water storage.

Further research is required to test Hypotheses 2, 3 and 4.

The pilot study clearly confirmed the first hypothesis, showing that irrigation of roots with heavy water can be a useful technique to further study the movement of water within trees. This technique effectively reduces the risk of embolism in the hydraulic system that commonly accompanies other techniques.

From the study of the mature tree, the following can be said. In heartwood, the abundance of δ^2H was mostly greater compared to sapwood collected at the same height and increased with tree height. The abundance of δ^2H in sapwood increased continuously from base of the stem to 12 m, after which it rapidly declined with additional height. Similar distribution patterns of δ^2H were described after injecting ^2H into stems of *E. grandis* (Kalma *et al.*, 1998). Kalma *et al.* noted the greatest enrichment mid-canopy, and found that δ^2H decreased with path length below and above this point. They were, however, unable to offer an explanation for the observed patterns.

With increasing tree height in the *C. maculata* investigated here, δ^2H in water extracted from sapwood and heartwood continually converged until being relatively equal at 12 m height. Above 12 m the main stem and all investigated branches did not contain heartwood. The observed pattern could be interpreted as evidence of an increased exchange rate of water between sapwood and heartwood with decreasing dimension of the heartwood body – an age related function may explain the enrichment of ^2H in water stored in heartwood. Future research might address this hypothesis in greater detail.

Differences in average abundance of δ^2H in water extracted from sap- and heartwood samples of the main stem were at most ± 5‰. With respect to the relative homogeneity of values over the entire path length (see Appendix – Chapter 4; Table S4.1 – 4.5) it remains uncertain whether or not observed patterns are a systematic trend, natural variation or caused by slight inconsistencies in measurement procedures. It has been shown that minor differences in δ^2H in water extracted from *Eucalyptus* wood can originate from incomplete water extraction (Thorburn *et al.*, 1993). Once more, these questions have to be addressed by additional studies.

Not surprisingly, sap flow (*Q)* of *C. maculata* was strongly driven by VPD. During the experiment the tree used around 450 liters of water per day. This seems rather high when compared to reports of water use in other eucalypt species of similar size (e.g. Zeppel and Eamus, 2008; Pfautsch *et al.*, 2010) but have been shown to exist in very tall *E. regnans* (Vertessy *et al.*, 1997) and other genera such as for instance *Anacardium excelsum, Eperua purpurea* or *Ocotea* spp. (Wullschleger *et al.*, 1998). Overall, high *Q* of this solitaire *C. maculata* can be the result of access to sufficient water sources and the large leaf area of the fully developed large crown. Water flux varied with both, cardinal direction sapwood depth, a phenomenon that has been described for gymnosperm and angiosperm species regularly (e.g. Jimenez *et al.*, 2000; James *et al.*, 2003; Cermak *et al.*, 2004; Delzon *et al.*, 2004). Most studies attribute the reduction of *J*s towards the sapwood-heartwood boundary to increasing loss of sapwood conductivity as a result of formation of tylosis or the fact that inner sapwood is supplying the lower and older branches of trees with water. Usually these branches have low rates of transpiration due to shading and other factors like leaf age. Other influential factors can be irregularities in the wood structure, caused by branching or mechanical injury to branches, stem or roots and even variation in sap

viscosity due to different rates of bark and stem heating by the sun (e.g. Hudler and Beale, 1981; Roderick and Berry, 2001; Arbellay *et al.*, 2012).

Taken together, the study proved that irrigation of heavy water is a valuable technique to study the movement of water in intact trees. Unfortunately the efforts to use this technique to study the water movement in a tall, evergreen tree did not yield any meaningful results. The interpretation of results is therefore limited. An analysis of the isotopic composition of soil- and groundwater in combination with xylem water may be necessary to establish which water sources trees access. This approach has been successfully used in the past (e.g. Dawson and Ehleringer, 1991; Kulmatiski *et al.*, 2010) and would ideally be accomplished prior to irrigation of tree roots with heavy water.

Chapter 5 – Synthesis

The genus Eucalyptus dominates many terrestrial ecosystems in Australia. Unlike tree genera of similar latitudes in the northern hemisphere, the long uninterrupted process of speciation has seen members of the genus adapt to a wide range of climatic conditions. Today ~800 species are taxonomically described and these are botanically subdivided into 13 subgenera. Many examples species display a high degree of endemism.

The Australian continent spans six Koeppen climate zones. Clear gradients of tree height can be observed across the continent. Mature eucalypts no more than 6-10 m in height are the dominant stratum in parts of the arid center, while others that potentially reach more than 100 m can dominate humid regions in the southeast (Nevill *et al.*, 2010). Eucalypts grow in all biomes from deserts to sub-alpine and have adapted to very dry, very hot and even sub-zero conditions. *Eucalyptus* spp. are major components of, or dominate, closed or open forests, woodlands and savannas (e.g. Specht 1970). They also grow as solitary trees. They cope with floods, cyclones and fire. The enormous diversity of species makes the genus an ideal candidate to study how evolution and adaptation manifest in tree form and function, including vessel anatomy and whole-tree hydraulic architecture. The current study was designed with this background.

In recent decades, structural traits and water transport in sapwood of trees have been intensively studied. The research in this thesis provides a deeper understanding of the structural attributes of the water transport system within the genus *Eucalyptus* (*e.g.* Schiller and Cohen, 1995; Loustau *et al.*, 1996; Wullschleger *et al.*, 1998). It also illustrates the inter-connectedness of the factors that influence tree water use. The work described here sits at the intersection of studies describing the dependency of tree water use on stand structure and environmental conditions (e.g. Pfautsch *et al.*, 2010; Kozlowski, 2012), and those that have investigated relationships among xylem and traits like leaf mass, tree height and gross wood structure as guides to the safety and efficiency of water transport in trees (Ryan and Yoder, 1997; Tyree and Zimmermann, 2002).

The term 'hydraulic architecture' was coined in the late 1970's by M.H. Zimmermann and encases the theoretical and empirical assessment of plant tissues that conduct water from roots to leaves (Cruiziat *et al.*, 2002). Hydraulic architecture comprises a multitude of single components connected in series, starting at the stomatal pore, through the xylem in leaves, petioles, twigs, branches, stems and down into the roots.

Chapter 1 of this thesis summarized how the gradient in water potential between the soil and the atmosphere drives the passive conductance of water throughout this network of conduits. It is the complex interaction of individual components (i.e. vessels, pit membranes, stomata) and their characteristics (i.e. width, abundance and pore size, conductivity) that ultimately determine the 'safety and efficiency' of the entire conduit system.

Density of sapwood, as well as size and abundance of xylem vessels, respond to environmental cues (e.g. Sass and Eckstein, 1995; Wiemann and Williamson, 2002; Fonti and García-González, 2008). Commonly, small trees growing in xeric environments have more dense sapwood with relatively small vessels, when compared to trees from mesic environments that are much taller, have lower sapwood density and wider vessels (e.g. Chave *et al.*, 2009; Campelo *et al.*, 2010). Furthermore, vessel density is closely linked to vessel diameter - trees with wide

vessels have fewer vessels (per unit sapwood area) compared to trees that form more narrow vessels. These trends have been observed on a global scale and for a wide variety of genera (e.g. Preston *et al.*, 2006; Sperry *et al.*, 2008; Chave *et al.*, 2009). Data reported here suggests these global patterns also apply to *Eucalyptus* (Chapter 2 and 3). The prior absence of a significant data set for eucalypts has been at least partly corrected.

Fine adjustment of plant hydraulic architecture to site conditions is critical if conductance of water is to be optimized without compromising safety. By far the majority of *Eucalyptus* spp. must cope with drought, either seasonally or long-term. That they do so without catastrophic cavitation (Sperry *et al.*, 2008; see Chapter 1) speaks strongly to the processes of evolution and adaptation. Even so, most studies of hydraulic safety and efficiency have concentrated only on the basal section of the tree stem (e.g. Sass and Eckstein, 1995; Fonti and García-González, 2008; Campelo *et al.*, 2010). The novel data recorded here, by studying entire tree stems, highlight that the tapering of vessels (reductions in diameter) throughout trees is influenced by environmental conditions and does not follow the previously suggested universal pattern – rates of taper varied strongly over the length of the stem, from effectively zero taper over long lengths, to rapid tapering within tree crowns.

Conductivity of vessels depends largely on their diameter (Eqn. 6) and the degree of vessel tapering along the entire path length in stems contributes greatly to overcoming hydraulic resistances to water transport that compound with height. It remains surprising how few studies have investigated tapering (e.g. Anfodillo *et al.*, 2006; Petit *et al.*, 2010; Petit and Anfodillo, 2011). Reasons for this lack of data and knowledge clearly include the large workload and costs of such studies. Due to the limited availability of empirical data, tapering as integral aspect of hydraulic architecture, and systematic changes within this trait due to growth conditions, has only been described at the genus level just once – here.

When compared to the available literature, the results presented in Chapter 2 of this thesis represent the most comprehensive analysis of vessel tapering yet conducted. This analysis is based on 12 *Eucalyptus* spp. that grow along a pronounced gradient of temperature and rainfall in southern and southeastern Australia. A total of 36 trees

were felled and sapwood was systematically extracted from the apical region to the base. This resulted in 1,254 individual samples, which produced 3,762 digital images. Using these images allowed measurements of more than 154,000 individual vessels.

It is important to highlight here that analysis of these vessels provides unequivocal evidence that hydraulic architecture, and specifically the tapering of vessels in *Eucalyptus* spp. do not comply with the supposed 'universal trends' predicted by metabolic *MST*). While *MST* scaling theory (represents an intentionally simplified mathematical framework that allows modeling of highly complex patterns of water transport and tree growth, applying its predictions to *Eucalyptus* would lead to strong overestimation of vessel densities for any given vessel size. Furthermore, vessel tapering in *Eucalyptus* is not homogenous. Vessels do not taper at all over considerable lengths of stems.

The development of a new approach (*Three Phase Taper Analysis*), that helps assess how varying rates of taper in the apical region of stems relate to dominant environmental conditions, is a major step forward in understanding hydraulic architecture in the context of evolution. This approach provides straightforward quantification of tapering, and reveals that, rather than follow a universal rule, tapering varies with both environment and tree height. Xylem vessels taper almost continuously throughout the stem in short trees growing in arid environments. In contrast, in tall trees from humid environments, vessels only taper much closer to the tree apex and vary little in diameter throughout much of the stem. This allows for efficient upwards conduction of large quantities of water in tall trees. These results underscore the need for a detailed understanding of vessel tapering, including its sensitivity to environment, and its influence on water use efficiency. Without such knowledge, predicting vulnerability and resilience of forests to changes in climate, particularly increasing frequency of drought and heatwaves, will be poorly based and likely inaccurate. Candidate species of future research may include other major Australian genera such as *Acacia*, *Callitris*, and *Nothofagus* but just as importantly we lack such knowledge for genera from the northern hemisphere like *Pinus, Acer* and *Quercus*.

This important finding immediately opens the door to many interesting questions about the development of vessel networks. How does tapering develop while trees grow and age? Does this development differ among species according to environmental conditions? Does the tapering structure in widespread species change at the provenance level?

Species such as *Eucalyptus tereticornis* and *E. camaldulensis* would seem ideal candidates as they grow under vastly different climatic conditions. Answering these questions is essential for developing models that are not only of interest to evolutionary ecologists and tree physiologists, but also to forest industry and land management agencies that all seek a better understanding of how trees will grow in future, how much water will come from forested catchments, and which species will be more/less vulnerable to changing climates.

It will remain technically challenging to answer such questions if data is only collected in the field. The early stages of xylogenesis and its response to a range of environmental conditions are extraordinarily difficult to study under field conditions. Here, glasshouse experiments, where conditions can be tightly controlled, represent a good solution. In the case of eucalypts such studies have shown that early xylogenesis appears to be highly responsive to water and temperature regimes (e.g. Thomas *et al.*, 2004; 2007). The glasshouse experiment described in Chapter 3 was designed to test if interspecific differences in early xylogenesis could be attributed to prevailing environmental conditions for a given species, and also if availability of N – a critical soil resource that is predicted to increase – would affect that process.

There is broad consensus that under conditions of sufficient soil moisture and increased temperatures, soil microbial activity will increase which in turn will increase mineralization of N and nitrification, and hence the amount of N available for plants (Murdoch *et al.*, 1998; Leirós *et al.*, 1999; IPCC, 2007; Castro *et al.*, 2010; Bradbury and Firestone, 2012; Schaeffer *et al.*, 2013). To date, there are only a few studies of effects of increased N on development of vessel networks in seedlings. Even among these few, some studies suggest additional N will change conduit traits and wood density in angiosperms and gymnosperms (e.g. Harvey and van den Driessche, 1999; Beets *et al.*, 2001), while others suggest there will be no such

change (Clearwater and Meinzer, 2001). Chapter 3 supports the contention that xylem development is strongly genetically controlled. Notwithstanding this clear statement, Chapter 3 does provide some evidence that xylogenesis responds to environmental conditions. Of the tested conditions, limiting the availability of water had the strongest effect, followed by temperature. While provision of additional N slightly increased plant biomass, it did not affect vessel structure in either of the two tested species. Studies over longer periods are required to confirm if observed trends in vessel traits develop into significant differences, both within and between species. Additional measurements of stomatal conductance and photosynthetic activity would help interpret how increasing availability of N affects physiological functioning as well as the development of the water transporting system in *E. melliodora* and *E. grandis*.

In similar fashion, quantification of capacitance in mature trees, using the approach attempted here (i.e. using heavy water as a tracer), offers insights to structure and function. Numerous studies have shown that trees access stored water to support transpiration under conditions of increasingly negative water potentials in the xylem (e.g. Stratton *et al.*, 2000; Domec and Gartner, 2001; Domec *et al.*, 2005; Chapotin *et al*., 2006; Čermák *et al.*, 2007). Pfautsch *et al*. (2012) reported moisture contents greater than 30% (fiber saturation point) in heartwood of a range of *Eucalyptus* species. According to Berry and Roderick (2005), any water present in tissues above the fiber saturation point, should be available for transpiration. It seems highly likely that eucalypts utilize moisture stored in heartwood. Pfautsch *et al.* (2012) highlight questions, not only about water storage locations in stems, but also about radial and tangential transport pathways for water, and their implications for water stress and the refill of embolised vessels. While the pilot study outlined in Chapter 4 (and other studies; e.g. Meinzer *et al.*, 2006) has shown that deuterated water can successfully be used to track the pathway of water in trees, the main experiment of Chapter 4 failed. The approach of using deuterated water to trace capacitance in trees, including heartwood clearly deserves to be repeated. Repeat efforts should include detailed analysis of the isotopic composition of soil- and groundwater in combination with xylem water, in order to establish water sources used by target species (e.g. Dawson and Ehleringer, 1991; Kulmatiski *et al.*, 2010).

Finally, it is worth recording a few words about future research in hydraulic anatomy of plants. Recent technological advances provide the means for studies of wood anatomy in unprecedented detail. In contrast to classic histology, a range of alternative methods require comparably little effort for sample preparation- and analysis. Examples include X-ray computed micro-tomography (microCT) (Steppe *et al.* 2004), confocal laser scanning microscopy (Kittin *et al.* 2003) and nuclear magnetic resonance imaging (Köckenberger, 2001; Jansen *et al.*, 2008). In the present research, several new technologies were tested at the Center for Microscopy and Microanalysis at the University of Sydney, Australia. In particular, their potential for visualizing vessel architecture, interconnectivity of vessels, and reconstruction of vessel networks. Although these trials were not further used in this thesis, a selection of products is a worthwhile means of documenting the potential of these technologies when investigating hydraulic architecture in *Eucalyptus* and other tree species.

For example, microCT appears is a non-invasive method for imaging vessel structures and can be used to reconstruct scanned objects in three-dimensional space (Milien *et al.*, 2012). Originally developed as a medical diagnostic tool in the 1970s microCT was first used for plant anatomical research in the late 1990s (Pierret *et al.*, 1999; Milien *et al.*, 2012). To date this technology has been used to detect annual growth units and to locate branch knots in *Picea abies* (Longuetaud *et al.*, 2005), to measure vessel diameters and compared results with those derived using classic histological methods (Steppe *et al.*, 2004), or to create three-dimensional models of xylem vessels in *Vitis vinifera* (Brodersen *et al.*, 2011, 2013). A combination of scanning electron microscopy (SEM) and microCT can provide new insights into hydraulic architecture that cannot be achieved by histological approaches alone (see Borderson *et al.*, 2013; McElrone *et al.*, 2013). New methods, however, will not replace classical histology, because size of specimens is limited by the capacity of the tomographic chamber and hence is restricted to short branch sections or wood cubes. These restrictions may be overcome in the future and entire vessel networks within plants, ultimately including tall trees, could be studied within the living organism at high resolution.

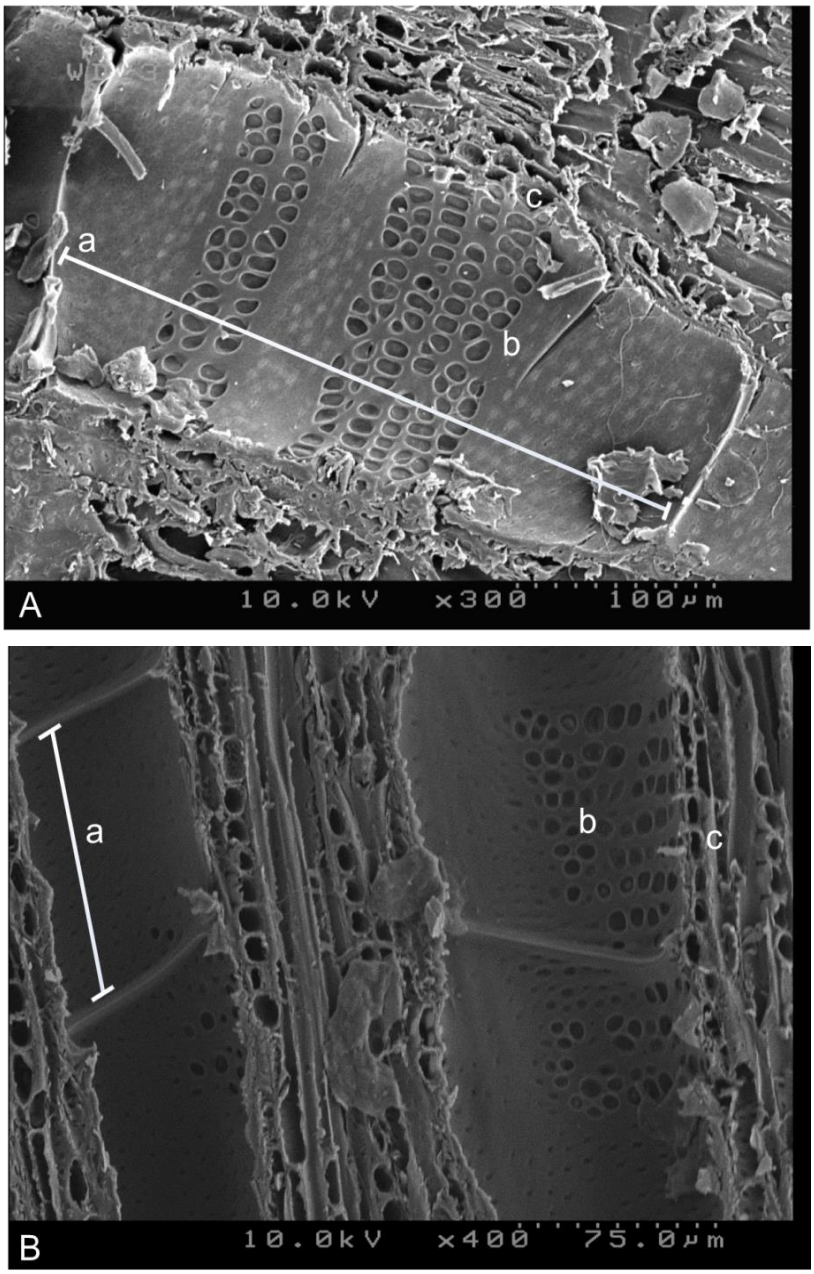

Figure 5.1: Scanning electron micrograph of sapwood in *Eucalyptus delegatensis* (A) and *E. viminalis* (B). Both images depict individual vessel elements (a) and the banded occurrence of bordered pits inside the vessel element (b) in the region of uniseriate ray parenchyma (c). Scale of each image is shown as dotted line at the lower right corner.

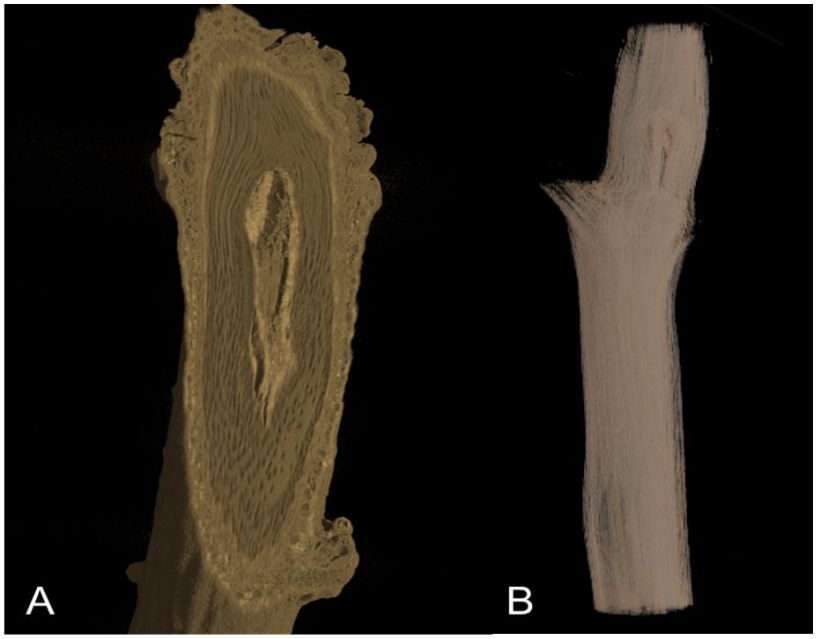

Figure 5.2: Three-dimensional reconstruction of an apical shoot (2.2 cm total length) of *Eucalyptus victrix* using microCT (Skyscan Model 1072; SkyScan, Antwerp, Belgium) at 3 µm increment resolution. The left image (A) illustrates the central pith, sapwood and bark at the cut surface. The right image (B) displays all xylem vessels with surrounding wood tissue removed by ScyScan internal tomographic reconstruction software.

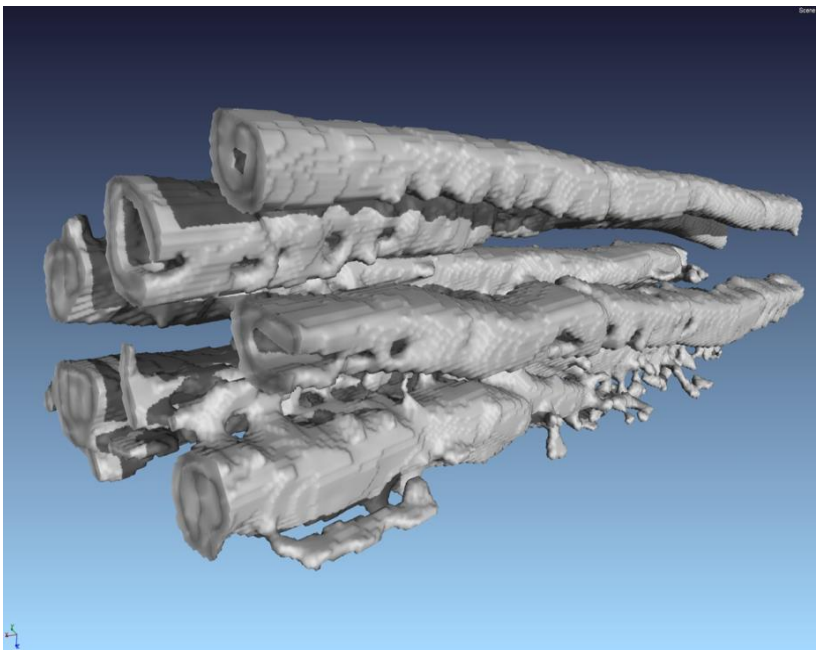

Figure 5.3: Three-dimensional reconstruction of xylem vessels in sapwood of an apical shoot in *Eucalyptus victrix*. The image was produced by 'virtual stripping' of woody tissue from the three-dimensional model produced using microCT, visualizing only void spaces. A customised, unpublished "Virtual Soil software" was used for this process.

Major conclusions:

1. Xylogenesis of *Eucalyptus ssp.* reacts on site-specific climate variables in the same way as reported for many other genera.

2. When put into the mathematical framework of metabolic scaling, *Eucalyptus ssp.* fit assumptions of optimal vessel tapering as suggested by Savage *et al.* (2010).

3. Tapering structure of vessel networks in *Eucalyptus* spp. are not linear and current modelling approaches should be refined to allow assessment of how environmental drivers impact the degree of tapering at relative path lengths of stems (i.e. zero vs. rapid narrowing of vessels).

4. A glass house experiment suggested that water availability is the most important factor influencing xylogenesis.

References

Aber, J., McDowell, W., Nadelhoffer, K., Alison, M., Berntson, G., Kamakea, M., McNulty, S., Currie, W., Rustad, L., Fernandez, I., 1998. Nitrogen Saturation in Temperate Forest Ecosystems. BioScience 48, 921-934.

Aber, J., Neilson, R.P., McNulty, S., Lenihan, J.M., Bachelet, D., Drapek, R.J., 2001. Forest Processes and Global Environmental Change: Predicting the Effects of Individual and Multiple Stressors. Bioscience 51, 735-751.

Allen, R.G., Pereira, L., Raes, D., Smith, M., 1998. FAO Irrigation and drainage paper No. 56. Rome: Food and Agriculture Organization of the United Nations, 26-40.

Aloni, R., Alexander, J.D., Tyree, M.T., 1997. Natural and experimentally altered hydraulic architecture of branch junctions in *Acer saccharum* Marsh. and *Quercus velutina* Lam. trees. Trees - Structure and Function 11, 255-264.

Ambrose, A.R., Sillett, S.C., Dawson, T.E., 2009. Effects of tree height on branch hydraulics, leaf structure and gas exchange in California redwoods. Plant, Cell & Environment 32, 743-757.

Amritphale, D., Sharma, S., 2010. Xylem hydraulics: Rising up and higher! Resonance 15, 223-231.

Anfodillo, T., Carraro, V., Carrer, M., Fior, C., Rossi, S., 2006. Convergent tapering of xylem conduits in different woody species. New Phytologist 169, 279-290.

Antonova, G.F., Stasova, V.V., 1993. Effects of environmental factors on wood formation in Scots pine stems. Trees - Structure and Function 7, 214-219.

Antonova, G.F., Stasova, V.V., 1997. Effects of environmental factors on wood formation in larch (*Larix sibirica* Ldb.) stems. Trees - Structure and Function 11, 462-468.

Aphalo, P.J., Jarvis, P.G., 1993. The boundary layer and the apparent responses of stomatal conductance to wind speed and to the mole fractions of CO2 and water vapour in the air. Plant, Cell & Environment 16, 771-783.

Araguás-Araguás, L., Rozanski, K., Gonfiantini, R., Louvat, D., 1995. Isotope effects accompanying vacuum extraction of soil water for stable isotope analyses. Journal of Hydrology 168, 159-171.

Arbellay, E., Fonti, P., Stoffel, M., 2012. Duration and extension of anatomical changes in wood structure after cambial injury. Journal of experimental botany 63, 3271-3277.

Atkinson, C.J., Taylor, J.M., 1996. Effects of elevated CO2 on stem growth, vessel area and hydraulic conductivity of oak and cherry seedlings. New Phytologist 133, 617-626.

Attiwill, P., 1979. Nutrient cycling in a *Eucalyptus obliqua* (L'Herit.) forest. III. Growth, biomass, and net primary production. Australian Journal of Botany 27, 439-458.

Atwell, B.J., Henery, M.L., Ball, M.C., 2009. Does soil nitrogen influence growth, water transport and survival of snow gum (*Eucalyptus pauciflora* Sieber ex Sprengel.) under CO_2 enrichment? Plant, Cell & Environment 32, 553-566.

Avsar, M.D., 2004. The relationships between diameter at breast height, tree height and crown diameter in Calabrian pines (*Pinus brutia* Ten.) of Baskonus Mountain, Kahramanmaras, Turkey. Journal of Biological Science 4, 437-440.

Bamber, R., Curtin, R., 1972. Some properties of wood in blackbutt trees of two ages. Australian Forestry 36, 226-234.

Barrett, D.J., Hatton, T.J., Ash, J.E., Ball, M.C., 1995. Evaluation of the heat pulse velocity technique for measurement of sap flow in rainforest and eucalypt forest species of south-eastern Australia. Plant, Cell & Environment 18, 463-469.

Barthelemy, D., Edelin, C., Halle, F., 1989. Architectural concepts for tropical trees. Academic Press, London, 89-100

Battaglia, M., Beadle, C., Loughhead, S., 1996. Photosynthetic temperature responses of Eucalyptus globulus and Eucalyptus nitens. Tree Physiology 16, 81-89.

Bauch, J., Liese, W., Schultze, R., 1972. The morphological variability of the bordered pit membranes in gymnosperms. Wood Science and Technology 6, 165-184.

Beets, P., Gilchrist, K., Jeffreys, M., 2001. Wood density of radiata pine: effect of nitrogen supply. Forest Ecology and Management 145, 173-180.

Becker, P., Gribben, R.J., Schulte, P.J., 2003. Incorporation of transfer resistance between tracheary elements into hydraulic resistance models for tapered conduits. Tree Physiology 23, 1009-1019.

Becker, P., Meinzer, F.C., Wullschleger, S.D., 2000. Hydraulic Limitation of Tree Height: A Critique. Functional Ecology 14, 4-11.

Becker, P., Tyree, M.T., Tsuda, M., 1999. Hydraulic conductances of angiosperms versus conifers: similar transport sufficiency at the whole-plant level. Tree Physiology 19, 445-452.

Berry, S.L., Roderick, M.L., 2005. Plant-water relations and the fibre saturation point. New Phytologist 168, 25-37.

Blackman, C.J., Brodribb, T.J., Jordan, G.J., 2010. Leaf hydraulic vulnerability is related to conduit dimensions and drought resistance across a diverse range of woody angiosperms. New Phytologist 188, 1113-1123.

Bleby, T.M., Burgess, S.S.O., Adams, M.A., 2004. A validation, comparison and error analysis of two heat-pulse methods for measuring sap flow in *Eucalyptus marginata* saplings. Functional Plant Biology 31, 645-658.

Bleby, T.M., Colquhoun, I.J., Adams, M.A., 2009. Architectural plasticity in young *Eucalyptus marginata* on restored bauxite mines and adjacent natural forest in south-western Australia. Tree Physiology 29, 1033-1045.

Boland, D.J., Brooker, M.I.H., Chippendale, G.M., Hall, N., Hyland, B.P.M., Johnston, R.D., Kleinig, D.A., McDonald, M.W., Turner, J.D. (eds.), 2006. Forest Trees of Australia. CSIRO Publishing.

Bonan, G.B., Sirois, L., 1992. Air temperature, tree growth, and the northern and southern range limits to *Picea mariana*. Journal of Vegetation Science 3, 495-506.

Bond, B.J., 2000. Age-related changes in photosynthesis of woody plants. Trends in Plant Science 5, 349-353.

Bond, B.J., Kavanagh, K.L., 1999. Stomatal behavior of four woody species in relation to leaf-specific hydraulic conductance and threshold water potential. Tree Physiology 19, 503-510.

Borchert, R., 1994. Soil and Stem Water Storage Determine Phenology and Distribution of Tropical Dry Forest Trees. Ecology 75, 1437-1449.

Boyer, J.S., 1985. Water transport. Annual Review of Plant Physiology 36, 473-516.

Boyer, J.S., 1995. Measuring the water status of plants and soils. Academic Press, San Diego.

Bradbury, D.C., Firestone, M.K., 2012. Responses of redwood soil microbial community structure and N transformations to climate change. In: Standiford, Richard B.; Weller, Theodore J.; Piirto, Douglas D.; Stuart, John D., tech. coords. Proceedings of coast redwood forests in a changing California: A symposium for scientists and managers.

Brix, H., Mitchell, A., 1983. Thinning and nitrogen fertilization effects on sapwood development and relationships of foliage quantity to sapwood area and basal area in Douglas-fir. Canadian Journal of Forest Research 13, 384-389.

Brodersen, C.R., Choat, B., Chatelet, D.S., Shackel, K.A., Matthews, M.A., McElrone, A.J., 2013. Xylem vessel relays contribute to radial connectivity in grapevine stems (*Vitis vinifera* and *V. arizonica*; *vitaceae*). American Journal of Botany 100, 314-321.

Brodersen, C.R., Lee, E.F., Choat, B., Jansen, S., Phillips, R.J., Shackel, K.A., McElrone, A.J., Matthews, M.A., 2011. Automated analysis of three-dimensional xylem networks using high-resolution computed tomography. New Phytologist 191, 1168-1179.

Broecker, W., 2002. Climate change: Are we on the brink of a pronounced global warming? Climate Change: Critical Concepts in the Environment 1, 135.

Brooks, J.R., Meinzer, F.C., Coulombe, R., Gregg, J., 2002. Hydraulic redistribution of soil water during summer drought in two contrasting Pacific Northwest coniferous forests. Tree Physiology 22, 1107-1117.

Brown, C., Ball, J., 2000. World view of plantation grown wood. In: Krishnapillay,B., Soepadmo, E., Arshad, N., Wong, A., Appanah, S., Chik, S., Manokaran, N., Tong, H., Choon, K. (eds.). Proceedings, XXI World Forestry Congress 1, 377-389

Brown, J.H., West, G.B., Enquist, B.J., 2005. Yes, West, Brown and Enquist"s model of allometric scaling is both mathematically correct and biologically relevant. Functional Ecology 19, 735-738.

Bucci, S.J., Goldstein, G., Meinzer, F.C., Scholz, F.G., Franco, A.C., Bustamante, M., 2004. Functional convergence in hydraulic architecture and water relations of tropical savanna trees: from leaf to whole plant. Tree Physiology 24, 891-899.

Buckley, T.N., Mott, K.A., 2013. Modelling stomatal conductance in response to environmental factors. Plant, Cell & Environment 36, 1691-1699.

Burgess, S.S.O., Adams, M.A., Turner, N.C., Beverly, C.R., Ong, C.K., Khan, A.A.H., Bleby, T.M., 2001. An improved heat pulse method to measure low and reverse rates of sap flow in woody plants. Tree Physiology 21, 589-598.

Burgess, S.S.O., Pittermann, J., Dawson, T.E., 2006. Hydraulic efficiency and safety of branch xylem increases with height in *Sequoia sempervirens* (D. Don) crowns. Plant, Cell & Environment 29, 229-239.

Calkin, H.W., Gibson, A.C., Nobel, P.S., 1986. Biophysical Model of Xylem Conductance in Tracheids of the Fern *Pteris vittata*. Journal of Experimental Botany 37, 1054-1064.

Campelo, F., Nabais, C., Gutiérrez, E., Freitas, H., García-González, I., 2010. Vessel features of *Quercus ilex* L. growing under Mediterranean climate have a better climatic signal than tree-ring width. Trees 24, 463-470.

Canny, M.J., 1991. The xylem wedge as a functional unit – speculations on the consequences of flow in leaky tubes. New Phytologist 118, 367-374.

Carlquist, S., 1975. Ecological strategies of xylem evolution. University of California Press., Berkeley

Carlquist, S., 2001. Comparative wood anatomy: systematic, ecological, and evolutionary aspects of dicotyledon wood. Springer-Verlag.

Casson, S.A., Hetherington, A.M., 2010. Environmental regulation of stomatal development. Current opinion in plant biology 13, 90-95.

Castro, H.F., Classen, A.T., Austin, E.E., Norby, R.J., Schadt, C.W., 2010. Soil microbial community responses to multiple experimental climate change drivers. Applied and Environmental Microbiology 76, 999-1007.

Catesson, A.-M., 1989. Specific characters of vessel primary walls during the early stages of wood differentiation. Biology of the Cell 67, 221-226.

Čermák, J., Jiménez, S., M.González-Rodríguez, A., Morales, D., 2002. Laurel forests in Tenerife, Canary Islands. Trees - Structure and Function 16, 538-546.

Čermák, J., Kučera, J., Bauerle, W.L., Phillips, N., Hinckley, T.M., 2007. Tree water storage and its diurnal dynamics related to sap flow and changes in stem volume in old-growth Douglas-fir trees. Tree Physiology 27, 181-198.

Čermák, J., Kučera, J., Nadezhdina, N., 2004. Sap flow measurements with some thermodynamic methods, flow integration within trees and scaling up from sample trees to entire forest stands. Trees 18, 529-546.

Chaney, W.R., Kozlowski, T.T., 1977. Patterns of Water Movement in Intact and Excised Stems of *Fraxinus americana* and *Acer saccharum* Seedlings. Annals of Botany 41, 1093-1100.

Chapotin, S.M., Razanameharizaka, J.H., Holbrook, N.M., 2006. Water relations of baobab trees (*Adansonia* spp. L.) during the rainy season: does stem water buffer daily water deficits? Plant, Cell & Environment 29, 1021-1032.

Chave, J., Coomes, D., Jansen, S., Lewis, S.L., Swenson, N.G., Zanne, A.E., 2009. Towards a worldwide wood economics spectrum. Ecology Letters 12, 351-366.

Choat, B., Brodie, T.W., Cobb, A.R., Zwieniecki, M.A., Holbrook, N.M., 2006. Direct measurements of intervessel pit membrane hydraulic resistance in two angiosperm tree species. Am. J. Bot. 93, 993-1000.

Choat, B., Jansen, S., Brodribb, T.J., Cochard, H., Delzon, S., Bhaskar, R., Bucci, S.J., Feild, T.S., Gleason, S.M., Hacke, U.G., 2012. Global convergence in the vulnerability of forests to drought. Nature 491, 752-755.

Choat, B., Pittermann, J., 2009. New insights into bordered pit structure and cavitation resistance in angiosperms and conifers. New Phytologist 182, 557-560.

Clark, J.S., Grimm, E.C., Donovan, J.J., Fritz, S.C., Engstrom, D.R., Almendinger, J.E., 2002. Drought cycles and landscape responses to past aridity on prairies of the northern great plains. Ecology 83, 595-601.

Clearwater, M., Goldstein, G., 2005. Embolism repair and long distance water transport. In N. M. Holbrook and M. A. Zwieniecki (eds.), Vascular transport in plants, 375 – 399. Academic Press, Amsterdam.

Clearwater, M.J., Meinzer, F.C., 2001. Relationships between hydraulic architecture and leaf photosynthetic capacity in nitrogen-fertilized *Eucalyptus grandis* trees. Tree Physiology 21, 683-690.

Coomes, D.A., Heathcote, S., Godfrey, E.R., Shepherd, J.J., Sack, L., 2008. Scaling of xylem vessels and veins within the leaves of oak species. Biology Letters 4, 302-306.

Corcuera, L., Camarero, J., Gil-Pelegrín, E., 2004. Effects of a severe drought on *Quercus ilex* radial growth and xylem anatomy. Trees - Structure and Function 18, 83-92.

Cruiziat, P., Cochard, H., Améglio, T., 2002. Hydraulic architecture of trees: main concepts and results. Annals of forest science 59, 723-752.

Curtis, R.O., 1967. Height-diameter and height-diameter-age equations for second-growth Douglas-fir. Forest Science 13, 365-375.

Cutter, E.G., 1978. Plant Anatomy, Part 1. Cells and Tissues (London: Edward Arnold).

Dansgaard, W., 1964. Stable isotopes in precipitation. Tellus 16, 436-468.

Darcy, H., 1856. Les fontaines publiques de la ville de Dijon: exposition et application.Paris, Dalmont.

Daudet, F.A., Le Roux, X., Sinoquet, H., Adam, B., 1999. Wind speed and leaf boundary layer conductance variation within tree crown: Consequences on leaf-to-atmosphere coupling and tree functions. Agricultural and Forest Meteorology 97, 171-185.

Davies, W.J., Zhang, J., 1991. Root signals and the regulation of growth and development of plants in drying soil. Annual review of plant biology 42, 55-76.

Dawson, T.E., Ehleringer, J.R., 1991. Streamside trees that do not use stream water. Nature 350, 335-337.

Dawson, T.E., 1996. Determining water use by trees and forests from isotopic, energy balance and transpiration analyses: the roles of tree size and hydraulic lift. Tree Physiology 16, 263-272.

Dawson, T.E., Pate, J.S., 1996. Seasonal water uptake and movement in root systems of Australian phraeatophytic plants of dimorphic root morphology: a stable isotope investigation. Oecologia 107, 13-20.

Delzon, S., Sartore, M., Granier, A., Loustau, D., 2004. Radial profiles of sap flow with increasing tree size in maritime pine. Tree Physiology 24, 1285-1293.

Dickison, W., 2000. Integrative Plant Anatomy. Academic Press, London.

Dixon, H.H., Joly, J., 1895. On the Ascent of Sap. Philosophical transactions of the royal society of London 186, 563-576.

Dodd, R.S., 1984. Radial and tangential diameter variation of wood cells within trees of *Acer pseudoplatanus*. IAWA Bulletin 5, 253-257.

Domec, J.-C., Gartner, B.L., 2001. Cavitation and water storage capacity in bole xylem segments of mature and young Douglas-fir trees. Trees - Structure and Function 15, 204-214.

Domec, J.-C., Lachenbruch, B., Meinzer, F.C., 2006. Bordered pit structure and function determine spatial patterns of air-seeding thresholds in xylem of Douglas-fir (*Pseudotsuga menziesii*; Pinaceae) trees. American Journal of Botany 93, 1588-1600.

Domec, J.-C., Lachenbruch, B., Meinzer, F.C., Woodruff, D.R., Warren, J.M., McCulloh, K.A., 2008. Maximum height in a conifer is associated with conflicting

requirements for xylem design. Proceedings of the National Academy of Sciences 105, 12069-12074.

Domec, J.-C., Meinzer, C., F., Gartner, L., B., Woodruff, D., 2006. Transpiration-induced axial and radial tension gradients in trunks of Douglas-fir trees. Tree Physiology 26, 275-284

Domec, J.C., Pruyn, M.L., Gartner, B.L., 2005. Axial and radial profiles in conductivities, water storage and native embolism in trunks of young and old-growth ponderosa pine trees. Plant, Cell & Environment 28, 1103-1113.

Doughty, C.E., Goulden, M.L., 2008. Are tropical forests near a high temperature threshold? Journal of Geophysical Research: Biogeosciences 113.

Dye, P.J., 1996. Response of *Eucalyptus grandis* trees to soil water deficits. Tree Physiology 16, 233-238.

Eckstein, D., Frisse, E., 1979. Environmental influences on the vessel size of beech and oak. IAWA Bulletin 2, 36-37.

Eilmann, B., Zweifel, R., Buchmann, N., Fonti, P., Rigling, A., 2009. Drought-induced adaptation of the xylem in scots pine and pubescent oak. Tree Physiology 29, 1011-1020.

Eisner, N.J., Gilman, E.F., Grabosky, J.C., Beeson, R.C., Jr., 2002. Branch junction characteristics affect hydraulic segmentation in red maple. Journal of Arboriculture 28, 245-251.

El-Lakany, M., Mohamed, S., 1993. Root characteristics of four tree species as affected by irrigation systems. Alexandria Journal of Agricultural Research 38, 183-210.

England, J.R., Attiwill, P.M., 2007. Changes in sapwood permeability and anatomy with tree age and height in the broad-leaved evergreen species *Eucalyptus regnans*. Tree Physiology 27, 1113-1124.

Enquist, B.J., Bentley, L.P., 2012. Land plants: new theoretical directions and empirical prospects. In: Metabolic Ecology: A Scaling Approach. Hoboken, NJ: Wiley-Blackwell, 164-187.

Etheridge, D.E., Morin, L.A., 1962. Wetwood Formation in Balsam Fir. Canadian journal of botany 40, 1335-1345.

Ewers, F., Fisher, J., Fichtner, K., 1991. Water flux and xylem structure in vines. In: Putz, F.E., Mooney, H.A. (eds.), The Biology of Vines. Cambridge University Press, New York, 127–160

Ewers, B.E., Oren, R., Albaugh, T.J., Dougherty, P.M., 1999. Carry-over effects of water and nutrient supply on water use of *Pinus taeda*. Ecological Applications 9, 513-525.

Falkiner, R.A., Nambiar, E.K.S., Polglase, P.J., Theiveyanathan, S., Stewart, L.G., 2006. Root distribution of *Eucalyptus grandis* and *Corymbia maculata* in degraded saline soils of south-eastern Australia. Agroforestry Systems 67, 279-291.

Faustino, L.I., Bulfe, N.M., Pinazo, M.A., Monteoliva, S.E., Graciano, C., 2013. Dry weight partitioning and hydraulic traits in young *Pinus taeda* trees fertilized with nitrogen and phosphorus in a subtropical area. Tree physiology 33, 241-251.

February, E.C., Stock, W., Bond, W., Le Roux, D., 1995. Relationships between water availability and selected vessel characteristics in *Eucalyptus grandis* and two hybrids. IAWA Journal 6, 269-276.

Ferrar, P., Slatyer, R., Vranjic, J., 1989. Photosynthetic temperature acclimation in *Eucalyptus* species from diverse habitats, and a comparison with *Nerium oleander*. Functional Plant Biology 16, 199-217.

Fisher, J.B., A, G.A., Ewers, F.W., López-Portillo, J., 1997. Survey of root pressure in tropical vines and woody species. International Journal of Plant Sciences 158, 44-50.

Fitter, A.H., Hay, R.K.M., 1987. Environmental Physiology of Plants. Academic Press, London.

Flynn, K.A., 1995. A review of the permeability, fluid flow, and anatomy of spruce (*Picea spp.*). Wood Fiber Science 27, 278-284.

Fonti, P., García-González, I., 2008. Earlywood vessel size of oak as a potential proxy for spring precipitation in mesic sites. Journal of Biogeography 35, 2249-2257.

Fonti, P., Solomonoff, N., García-González, I., 2007. Earlywood vessels of *Castanea sativa* record temperature before their formation. New Phytologist 173, 562-570.

Ford, E.D., Robards, A.W., Piney, M.D., 1978. Influence of environmental factors on cell production and differentiation in the early wood of *Picea sitchensis*. Annals of Botany 42, 683-692.

Fujii, T., Lee, S.J., Kuroda, N., Suzuki, Y., 2001. Conductive function of intervessel pits through a growth ring boundary of *Machilus thunbergii*. IAWA Journal 22, 1-14.

Gea-Izquierdo, G., Fonti, P., Cherubini, P., Martín-Benito, D., Chaar, H., Cañellas, I., 2012. Xylem hydraulic adjustment and growth response of *Quercus canariensis* Willd. to climatic variability. Tree Physiology 32, 401-413.

Gasco, A., Nardini, A., Gortan, E., Salleo, S., 2006. Ion-mediated increase in the hydraulic conductivity of Laurel stems: role of pits and consequences for the impact of cavitation on water transport. Plant, cell & environment 29, 1946-1955.

Gat, J.R., 1996. Oxygen and Hydrogen Isotopes in the Hydrologic Cycle. Annual Review Earth Planetary Science 24, 225–262.

Gebauer, T., Horna, V., Leuschner, C., 2008. Variability in radial sap flux density patterns and sapwood area among seven co-occurring temperate broad-leaved tree species. Tree Physiology 28, 1821-1830.

Ghannoum, O., 2009. C4 photosynthesis and water stress. Annals of Botany 103, 635-644.

Gindaba, J., Rozanov, A., Negash, L., 2004. Response of seedlings of two *Eucalyptus* and three deciduous tree species from Ethiopia to severe water stress. Forest Ecology and Management 201, 119-129.

Gitlin, A.R., Sthultz, C.M., Bowker, M.A., Stumpf, S., Paxton, K.L., Kennedy, K., Munoz, A., Bailey, J.K., Whitham, T.G., 2006. Mortality gradients within and among dominant plant populations as barometers of ecosystem change during extreme drought. Conservation Biology 20, 1477-1486.

Gleeson, S.K., 1993. Optimization of tissue nitrogen and root-shoot allocation. Annals of Botany 71, 23-31.

Gleeson, S.K., Tilman, D., 1992. Plant allocation and the multiple limitation hypothesis. American Naturalist, 1322-1343.

Goldstein, G., Andrade, J.L., Meinzer, F.C., Holbrook, N.M., Cavelier, J., Jackson, P., Celis, A., 1998. Stem water storage and diurnal patterns of water use in tropical forest canopy trees. Plant, Cell & Environment 21, 397-406.

Goldstein, G., Bucci, S.J., Scholz, F.G., 2013. Why do trees adjust water relations and hydraulic architecture in response to nutrient availability? Tree Physiology 33, 238-240.

Goncalves, J., Carlyle, J., 1994. Modelling the influence of moisture and temperature on net nitrogen mineralization in a forested sandy soil. Soil Biology and Biochemistry 26, 1557-1564.

González, I.G., Eckstein, D., 2003. Climatic signal of earlywood vessels of oak on a maritime site. Tree Physiology 23, 497-504.

Goulet, J., 2000. Effect of branch position and light availability on shoot growth of understory sugar maple and yellow birch saplings. Canadian journal of botany 8, 1077.

Grace, J., 1993. Refilling of embolized xylem. In: Borghetti, M., Grace, J., Raschi, A. (eds.) Water Transport in Plants under Climate Stress. Cambridge University Press, Cambridge.

Granier, A., Anfodillo, T., Sabatti, M., Cochard, H., Dreyer, E., Tomasi, M., Valentini, R., Bréda, N., 1994. Axial and radial water flow in the trunks of oak trees: a quantitative and qualitative analysis. Tree Physiology 14, 1383-1396.

Grantz, D.A., 1990. Plant response to atmospheric humidity. Plant, Cell & Environment 13, 667-679.

Grier, C.G., Running, S.W., 1977. Leaf area of mature northwestern coniferous forests: relation to site water balance. Ecology 58, 893-899.

Guarnaschelli, A., Lemcoff, J., Prystupa, P., Basci, S., 2003. Responses to drought preconditioning in *Eucalyptus globulus* Labill. provenances. Trees - Structure and Function 17, 501-509.

Hacke, U., Sauter, J.J., 1995. Vulnerability of xylem to embolism in relation to leaf water potential and stomatal conductance in *Fagus sylvatica*, *F. purpurea* and *Populus balsamifera*. Journal of Experimental Botany 46, 1177-1183.

Hacke, U.G., Sperry, J.S., 2003. Limits to xylem refilling under negative pressure in *Laurus nobilis* and *Acer negundo*. Plant, Cell & Environment 26, 303-311.

Hacke, U.G., Sperry, J.S., Pittermann, J., 2004. Analysis of circular bordered pit function II. Gymnosperm tracheids with torus-margo pit membranes. American Journal of Botany 91, 386-400.

Hacke, U.G., Sperry, J.S., Pockman, W.T., Davis, S.D., McCulloh, K.A., 2001. Trends in wood density and structure are linked to prevention of xylem implosion by negative pressure. Oecologia 126, 457-461.

Hacke, U.G., Sperry, J.S., Wheeler, J.K., Castro, L., 2006. Scaling of angiosperm xylem structure with safety and efficiency. Tree Physiol 26, 689-701.

Hadwen, W.L., Arthington, A.H., Boon, P.I., Taylor, B., Fellows, C.S., 2011. Do climatic or institutional factors drive seasonal patterns of tourism visitation to

protected areas across diverse climate zones in eastern Australia? Tourism Geographies 13, 187-208.

Hansen, J., Sato, M., Ruedy, R., Lo, K., Lea, D.W., Medina-Elizade, M., 2006. Global temperature change. Proceedings of the National Academy of Sciences 103, 14288-14293.

Harvey, H.P., van den Driessche, R., 1997. Nutrition, xylem cavitation and drought resistance in hybrid poplar. Tree Physiology 17, 647-654.

Harvey, H.P., van den Driessche, R., 1999. Nitrogen and potassium effects on xylem cavitation and water-use efficiency in poplars. Tree Physiology 19, 943-950.

Hasenauer, H., 1997. Dimensional relationships of open-grown trees in Austria. Forest Ecology and Management 96, 197-206.

Hennessy, K.J., Suppiah, R., Page, C.M., 1999. Australian rainfall changes, 1910-1995. Australian Meteorological Magazine 48, 1-13.

Hobson, K.A., Wassenaar, L.I., 1999. Stable isotope ecology: an introduction. Oecologia 120, 312-313.

Holbrook, N.M., 1995. Plant Stems; Physiology and Functional Morphology. Academic Press, London.

Hubbard, R.M., Stape, J., Ryan, M.G., Almeida, A.C., Rojas, J., 2010. Effects of irrigation on water use and water use efficiency in two fast growing Eucalyptus plantations. Forest Ecology and Management 259, 1714-1721.

Hudler, G., Beale, M., 1981. Anatomical features of girdling root injury. Journal of Arboriculture 7, 29-32

Hudson, I., Wilson, L., Van Beveren, K., 1998. Vessel and fibre property variation in *Eucalyptus globulus* and *Eucalyptus nitens*: some preliminary results. IAWA Journal 19, 111-130.

Huber, B., 1928. Weitere quantitative Untersuchungen ueber das Wasserleitungssystem der Pflanzen. Jahrbuch fuer wissenschaftliche Botanik 67, 877-959

Huber, B., 1956. Die Gefassleitung. In: Handbuch der Pflanzenphysiologie, Ruhland, W.(eds.), 3, 541-582. Springer Verlag, Berlin, Goettingen, Heidelberg.

Hughes, L., 2003. Climate change and Australia: trends, projections and impacts. Austral Ecology 28, 423-443.

Hughes, L., Cawsey, E., Westoby, M., 1996. Climatic range sizes of *Eucalyptus* species in relation to future climate change. Global Ecology and Biogeography Letters, 23-29.

IAPWS, 2001. Guideline on the Use of Fundamental Physical Constants and Basic Constants of Water. The International Association for the Properties of Water and Steam (eds.), Gaithersburg, Maryland, USA.

Ilic, J., 2001. Relationship among the dynamic and static elastic properties of air-dry *Eucalyptus delegatensis* R. Baker. Holz als Roh- und Werkstoff 59, 169-175.

Ilic, J., 2002. Woods of *Eucalyptus*. Part 2. Distinguishing species from the stringybark group (*E. baxteri. E. globoidea, E. muelleriana, E. macrorhyncha, E. consideniana and E. sieberi*). IAWA JOURNAL 23, 305-318.

Ingestad, T., Lund, A., 1979. Nitrogen stress in birch seedlings, 1: Growth technique and growth. Physiologia Plantarum 45, 149–157.

IPCC, 2007. Climate Change 2007: The Physical Science Basis. Contribution of Working Group I to the Fourth Assessment Report of the Intergovernmental Panel on Climate Change. Cambridge Univ. Press, Cambridge.

Iwasa, Y., Cohen, D., Leon, J.A., 1985. Tree height and crown shape, as results of competitive games. Journal of Theoretical Biology 112, 279-297.

James, S., Meinzer, F., Goldstein, G., Woodruff, D., Jones, T., Restom, T., Mejia, M., Clearwater, M., Campanello, P., 2003. Axial and radial water transport and internal water storage in tropical forest canopy trees. Oecologia 134, 37-45.

Jansen, S., Baas, P., Gasson, P., Smets, E., 2003. Vestured pits: Do they promote safer water transport? International Journal of Plant Sciences 164, 405-413.

Jansen, S., Choat, B., Pletsers, A., 2009. Morphological variation of intervessel pit membranes and implications to xylem function in angiosperms. American Journal of Botany 96, 409-419.

Jansen, S., Pletsers, A., Sano, Y., 2008. The effect of preparation techniques on SEM-imaging of pit mambranes. IAWA Journal 29 (2), 161-178.

Jeffrey, S.J., Carter, J.O., Moodie, K.B., Beswick, A.R., 2001. Using spatial interpolation to construct a comprehensive archive of Australian climate data. Environmental Modelling and Software 16, 309-330.

Jiménez, M.S., Nadezhdina, N., Čermák, J., Morales, D., 2000. Radial variation in sap flow in five laurel forest tree species in Tenerife, Canary Islands. Tree Physiology 20, 1149-1156.

Johnson, D.M., Meinzer, F.C., Woodruff, D.R., McCulloh, K.A., 2009. Leaf xylem embolism, detected acoustically and by cryo-SEM, corresponds to decreases in leaf hydraulic conductance in four evergreen species. Plant, Cell & Environment 32, 828-836.

Kafle, H.K., Bruins, H.J., 2009. Climatic trends in Israel 1970–2002: warmer and increasing aridity inland. Climatic Change 96, 63-77.

Kalma, S.J., Thorburn, P.J., Dunn, G.M., 1998. A comparison of heat pulse and deuterium tracing techniques for estimating sap flow in *Eucalyptus grandis* trees. Tree Physiology 18, 697-705.

Kattge, J., Knorr, W., 2007. Temperature acclimation in a biochemical model of photosynthesis: a reanalysis of data from 36 species. Plant, Cell & Environment 30, 1176-1190.

Keitel, C., Matzarakis, A., Rennenberg, H., Gessler, A., 2006. Carbon isotopic composition and oxygen isotopic enrichment in phloem and total leaf organic matter of European beech (*Fagus sylvatica* L.) along a climate gradient. Plant, Cell & Environment 29, 1492-1507.

Kendall, C., Caldwell, E.A., 1998. Fundamentals of Isotope Geochemistry. In: Kendall, C., McDonnell, J.J. (eds.), Isotope Tracers in Catchment Hydrology. Elsevier, 51-84.

Kingston, R.S.T., Risdon, C.J.E., 1961. Shrinkage and density of Australian and other (Southwest Pacific) woods, CSIRO (Aust.) Division of forest products technological paper 13, 1-65.

Kitin, P.B., Fujii, T., Abe, H., Funada, R., 2004. Anatomy of the vessel network within and between tree rings of *Fraxinus lanuginosa* (*Oleaceae*). American Journal of Botany 91, 779-788.

Kitin P, Sano Y, Funada R, 2003. Three-dimensional imaging and analysis of differentiating secondary xylem by confocal microscopy. IAWA Journal 24, 211-222.

Knigge, W., Schulz, H., 1961. Climatic influence of the year 1959 on distribution of cell types, fibre length and width of vessels of various wood species. Holz als Roh- und Werkstoff 19, 293-303.

Koch, G.W., Sillett, S.C., Jennings, G.M., Davis, S.D., 2004. The limits to tree height. Nature 428, 851-854

Köckenberger, W., 2001. Functional imaging of plants by magnetic resonance experiments. Trends in Plant Science 6, 286-292.

Köstner, B., Falge, E., Tenhunen, J., 2002. Age-related effects on leaf area/sapwood area relationships, canopy transpiration and carbon gain of Norway spruce stands (*Picea abies*) in the Fichtelgebirge, Germany. Tree Physiology 22, 567-574.

Kozlowski, J., Konarzewski, M., 2004. Is West, Brown and Enquist's model of allometric scaling mathematically correct and biologically relevant? Functional Ecology 18, 283-289.

Kozlowski, J., Konarzewski, M., 2005. West, Brown and Enquist's model of allometric scaling again: the same questions remain. Functional Ecology 19, 739-743.

Kozlowski, T.T., 2012. Woody Plant Communities, Vol.6. Academic Press, New York.

Kravka, M., Krejzar, T., Čermák, J., 1999. Water content in stem wood of large pine and spruce trees in natural forests in central Sweden. Agricultural and Forest Meteorology 98–99, 555-562.

Kulmatiski, A., Beard, K.H., Verweij, R.J.T., February, E.C., 2010. A depth-controlled tracer technique measures vertical, horizontal and temporal patterns of water use by trees and grasses in a subtropical savanna. New Phytologist 188, 199-209.

Larsen, D.R., Hann, D.W., 1987. Height-diameter equations for seventeen tree species in southwest Oregon. Oregon State University Forest Research Laboratory, Research Paper 4.

Larson, D.W., Doubt, J., Matthes-Sears, U., 1994. Radially sectored hydraulic pathways in the xylem of *Thuja occidentalis* as revealed by the use of dyes. International Journal of Plant Sciences 155, 569-582.

Lavender, S., Abbs, D., 2013. Trends in australian rainfall: contribution of tropical cyclones and closed lows. Clim Dyn 40, 317-326.

Leal, S., Sousa, V.B., Pereira, H., 2007. Radial variation of vessel size and distribution in cork oak wood (*Quercus suber* L.). Wood Science and Technology 41, 339-350.

Leirós, M.C., Trasar-Cepeda, C., Seoane, S., Gil-Sotres, F., 1999. Dependence of mineralization of soil organic matter on temperature and moisture. Soil Biology and Biochemistry 31, 327-335.

Lewis, A.M., Boose, E.R., 1995. Estimating volume flow rates through xylem conduits. American Journal of Botany 82, 1112-1116.

Linton, M.J., Sperry, J.S., Williams, D.G., 1998. Limits to water transport in *Juniperus osteosperma* and *Pinus edulis*: implications for drought tolerance and regulation of transpiration. Functional Ecology 12, 906-911.

Longuetaud, F., Saint-André, L., Leban, J.-M., 2005. Automatic Detection of Annual Growth Units on *Picea abies* Logs Using Optical and X-Ray Techniques. Journal of Nondestructive Evaluation 24, 29-43.

Loustau, D., Berbigier, P., Roumagnac, P., Arruda-Pacheco, C., David, J., Ferreira, M., Pereira, J., Tavares, R., 1996. Transpiration of a 64-year-old maritime pine stand in Portugal. Oecologia 107, 33-42.

Lovisolo, C., Schubert, A., 1998. Effects of water stress on vessel size and xylem hydraulic conductivity in *Vitis vinifera*. Journal of Experimental Botany 49, 693-700.

Luo, Z.-B., Polle, A., 2009. Wood composition and energy content in a poplar short rotation plantation on fertilized agricultural land in a future CO_2 atmosphere. Global Change Biology 15, 38-47.

Luzar, A., Chandler, D., 1996. Effect of environment on hydrogen bond dynamics in liquid water. Physical Review Letters 76, 928-931.

Maherali, H., DeLucia, E.H., 2000. Interactive effects of elevated CO_2 and temperature on water transport in ponderosa pine. American Journal of Botany 87, 243-249.

Maherali, H., DeLucia, E., 2001. Influence of climate-driven shifts in biomass allocation on water transport and storage in ponderosa pine. Oecologia 129, 481-491.

Marc, V., Robinson, M., 2004. Application of the deuterium tracing method for the estimation of tree sap flow and stand transpiration of a beech forest (*Fagus silvatica* L.) in a mountainous Mediterranean region. Journal of Hydrology 285, 248-259.

Marshall, D.C., 1958. Measurement of sap flow in conifers by heat transport. Plant Physiology 33, 385-396.

Martínez-Cabrera, H.I., Jones, C.S., Espino, S., Schenk, H.J., 2009. Wood anatomy and wood density in shrubs: responses to varying aridity along transcontinental transects. American Journal of Botany 96, 1388-1398.

Martínez-Vilalta, J., Prat, E., Oliveras, I., Piñol, J., 2002. Xylem hydraulic properties of roots and stems of nine Mediterranean woody species. Oecologia 133, 19-29.

Mäkelä, A., Valentine, H.T., 2006. The quarter-power scaling model does not imply size-invariant hydraulic resistance in plants. Journal of theoretical Biology 243, 283-285.

McAinsh, M.R., 1990. Abscisic acid-induced elevation of guard cell cytosolic Ca^{2+} precedes stomatal closure. Nature 343, 186–188.

McCulloh, K.A., Sperry, J.S., Adler, F.R., 2003. Water transport in plants obeys Murray's law. Nature 421, 939-942.

McDowell, N.G., Phillips, N., Lunch, C., Bond, B.J., Ryan, M.G., 2002. An investigation of hydraulic limitation and compensation in large, old Douglas-fir trees. Tree Physiology 22, 763-774.

McElrone, A.J., Grant, J.A., Kluepfel, D.A., 2010. The role of tyloses in crown hydraulic failure of mature walnut trees afflicted by apoplexy disorder. Tree Physiology 30, 761-772.

Medlyn, B., Dreyer, E., Ellsworth, D., Forstreuter, M., Harley, P., Kirschbaum, M., Le Roux, X., Montpied, P., Strassemeyer, J., Walcroft, A., 2002. Temperature response of parameters of a biochemically based model of photosynthesis II. A review of experimental data. Plant, Cell & Environment 25, 1167-1179.

Meidner, H., Edwards, M., 1975. Direct Measurements of Turgor Pressure Potentials of Guard Cells, I. Journal of experimental botany 26, 319-330.

Meinzer, F.C., Brooks, J.R., Domec, J.C., Gartner, B.L., Warren, J.M., Woodruff, D.R., Bible, K., Shaw, D.C., 2006. Dynamics of water transport and storage in conifers studied with deuterium and heat tracing techniques. Plant, Cell & Environment 29, 105-114.

Meinzer, F.C., Clearwater, M.J., Goldstein, G., 2001. Water transport in trees: current perspectives, new insights and some controversies. Environmental and Experimental Botany 45, 239-262.

Meinzer, F., Grantz, D., 1990. Stomatal and hydraulic conductance in growing sugarcane: stomatal adjustment to water transport capacity. Plant, Cell & Environment 13, 383-388.

Meinzer, F.C., James, S.A., Goldstein, G., Woodruff, D., 2003. Whole-tree water transport scales with sapwood capacitance in tropical forest canopy trees. Plant, Cell & Environment 26, 1147-1155.

Meinzer, F., McCulloh, K., Lachenbruch, B., Woodruff, D., Johnson, D., 2010. The blind men and the elephant: the impact of context and scale in evaluating conflicts between plant hydraulic safety and efficiency. Oecologia 164, 287-296.

Mencuccini, M., Grace, J., 1996. Hydraulic conductance, light interception and needle nutrient concentration in Scots pine stands and their relations with net primary productivity. Tree Physiology 16, 459-468.

Mencuccini, M., Hölttä, T., Petit, G., Magnani, F., 2007. Sanio's laws revisited. Size-dependent changes in the xylem architecture of trees. Ecology Letters 10, 1084-1093.

Mencuccini, M., Magnani, F., 2000. Comment on 'Hydraulic Limitation of Tree Height: A Critique' by Becker, Meinzer and Wullschleger. Functional Ecology 14, 135-137.

Merchant, A., Callister, A., Arndt, S., Tausz, M., Adams, M., 2007. Contrasting physiological responses of six Eucalyptus species to water deficit. Annals of Botany 100, 1507-1515.

Midgley, J.J., 2003. Is bigger better in plants? The hydraulic costs of increasing size in trees. Trends in Ecology & Evolution 18, 5-6.

Milien, M., Renault-Spilmont, A.-S., Cookson, S.J., Sarrazin, A., Verdeil, J.-L., 2012. Visualization of the 3D structure of the graft union of grapevine using X-ray tomography. Scientia Horticulturae 144, 130-140.

Mokany, K., McMurtrie, R.E., Atwell, B.J., Keith, H., 2003. Interaction between sapwood and foliage area in alpine ash (*Eucalyptus delegatensis*) trees of different heights. Tree Physiology 23, 949-958.

Moles, A.T., Warton, D.I., Warman, L., Swenson, N.G., Laffan, S.W., Zanne, A.E., Pitman, A., Hemmings, F.A., Leishman, M.R., 2009. Global patterns in plant height. Journal of Ecology 97, 923-932.

Moya, R., Tomazello, M., 2007. Relationship between anatomical features and intra-ring wood density profiles in Gmelina arborea applying x-ray densitometry. Cerne 13, 384-392.

Murdoch, P.S., Burns, D.A., Lawrence, G.B., 1998. Relation of climate change to the acidification of surface waters by nitrogen deposition. Environmental Science & Technology 32, 1642-1647.

Murdoch, W., C., Campana, J., R., 1983. Bacterial species associated with wetwood of elm. Phytopathology. 73, 1270-3.

Murphy, B.F., Timbal, B., 2008. A review of recent climate variability and climate change in southeastern Australia. International Journal of Climatology 28, 859-879.

Naidoo, S., Zboňák, A., Ahmed, F., 2006. The effect of moisture availability on wood density and vessel characteristics of *Eucalyptus grandis* in the warm temperate region of South Africa. Wood Structure and Properties' 06, 117.

Nelson, S.T., Dettman, D., 2001. Improving hydrogen isotope ratio measurements for on-line chromium reduction systems. Rapid Communications in Mass Spectrometry 15, 2301-2306.

Nevill, P.G., Bossinger, G., Ades, P.K., 2010. Phylogeography of the world's tallest angiosperm, *Eucalyptus regnans*: evidence for multiple isolated Quaternary refugia. Journal of Biogeography 37, 179-192.

Nogués-Bravo, D., Araújo, M.B., Errea, M., Martinez-Rica, J., 2007. Exposure of global mountain systems to climate warming during the 21st Century. Global Environmental Change 17, 420-428.

Nicholls, N., Drosdowsky, W., Lavery, B., 1997. Australian rainfall variability and change. Weather 52, 66-72.

Nikinmaa, E., Messier, C., Sievänen, R., Perttunen, J., Lehtonen, M., 2003. Shoot growth and crown development: effect of crown position in three-dimensional simulations. Tree Physiology 23, 129-136.

Norby, R.J., Jackson, R.B., 2000. Root dynamics and global change: seeking an ecosystem perspective. New Phytologist 147, 3-12.

Osunkoya, O.O., Sheng, T.K., Mahmud, N.-A., Damit, N., 2007. Variation in wood density, wood water content, stem growth and mortality among twenty-seven tree species in a tropical rainforest on Borneo Island. Austral Ecology 32, 191-201.

O'Grady, A., Cook, P., Eamus, D., Duguid, A., Wischusen, J., Fass, T., Worldege, D., 2009. Convergence of tree water use within an arid-zone woodland. Oecologia 160, 643-655.

Outlaw, W.H., 1983. Current concepts on the role of potassium in stomatal movements. Physiologia Plantarum 59, 302-311.

Overdieck, D., Ziche, D., Böttcher-Jungclaus, K., 2007. Temperature responses of growth and wood anatomy in European beech saplings grown in different carbon dioxide concentrations. Tree Physiology 27, 261-268.

Pallardy, S.G., 2008. Physiology of woody plants. Academic Press, Burlington.

Panshin, A.J., de Zeeuw, C., 1980. Textbook of wood technology, structure, identication, properties, and uses of the commercial woods of the United States and Canada. New York: McGraw-Hill, 1980.

Pataki, D.E., Oren, R., Phillips, N., 1998. Responses of sap flux and stomatal conductance of *Pinus taeda* L. trees to stepwise reductions in leaf area. Journal of Experimental Botany 49, 871-878.

Paux, E., Carocha, V., Marques, C., Mendes de Sousa, A., Borralho, N., Sivadon, P., Grima-Pettenati, J., 2005. Transcript profiling of *Eucalyptus* xylem genes during tension wood formation. New Phytologist 167, 89-100.

Petit, G., Anfodillo, T., 2009. Plant physiology in theory and practice: An analysis of the WBE model for vascular plants. Journal of Theoretical Biology 259, 1-4.

Petit, G., Anfodillo, T., 2011. Comment on "The blind men and the elephant: the impact of context and scale in evaluating conflicts between plant hydraulic safety and efficiency" by Meinzer et al. (2010). Oecologia 165, 271-274.

Petit, G., Pfautsch, S., Anfodillo, T., Adams, M.A., 2010. The challenge of tree height in *Eucalyptus regnans*: when xylem tapering overcomes hydraulic resistance. New Phytologist 187, 1146-1153.

Petty, J.A., 1970. Permeability and structure of the wood of Sitka spruce. Proceedings of the Royal Society of London. Series B. Biological Sciences 175, 149-166.

Pfautsch, S., Bleby, T.M., Rennenberg, H., Adams, M.A., 2010. Sap flow measurements reveal influence of temperature and stand structure on water use of Eucalyptus regnans forests. Forest Ecology and Management 259, 1190-1199.

Pfautsch, S., Keitel, C., Turnbull, T.L., Braimbridge, M.J., Wright, T.E., Simpson, R.R., O'Brien, J.A., Adams, M.A., 2011. Diurnal patterns of water use in *Eucalyptus victrix* indicate pronounced desiccation–rehydration cycles despite unlimited water supply. Tree Physiology 31, 1041-1051.

Pfautsch, S., Macfarlane, C., Ebdon, N., Meder, R., 2012. Assessing sapwood depth and wood properties in *Eucalyptus* and *Corymbia spp.* using visual methods and near infrared spectroscopy (NIR). Trees - Structure and Function 26, 963-974.

Phillips, N.G., Ryan, M.G., Bond, B.J., McDowell, N.G., Hinckley, T.M., Cermak, J., 2003. Reliance on stored water increases with tree size in three species in the Pacific Northwest. Tree Physiol 23, 237-245.

Pierret, A., Capowiez, Y., Moran, C.J., Kretzschmar, A., 1999. X-ray computed tomography to quantify tree rooting spatial distributions. Geoderma 90, 307-326.

Pittermann, J., Sperry, J., 2003. Tracheid diameter is the key trait determining the extent of freezing-induced embolism in conifers. Tree Physiology 23, 907-914.

Pittermann, J., Sperry, J.S., Hacke, U.G., Wheeler, J.K., Sikkema, E.H., 2005. Torus-Margo pits help conifers compete with angiosperms. Science 310, 1924.

Plummer, N., Salinger, M.J., Nicholls, N., Suppiah, R., Hennessy, K., Leighton, R., Trewin, B., Page, C., Lough, J., 1999. Changes in climate extremes over the Australian region and New Zealand during the twentieth century. Climatic Change 42, 183-202.

Pockman, W.T., Sperry, J.S., 1996. Freezing-induced xylem cavitation and the northern limit of *Larrea tridentata*. Oecologia 109, 19-27.

Poorter, L., McDonald, I., Alarcón, A., Fichtler, E., Licona, J.-C., Peña-Claros, M., Sterck, F., Villegas, Z., Sass-Klaassen, U., 2010. The importance of wood traits and hydraulic conductance for the performance and life history strategies of 42 rainforest tree species. New Phytologist 185, 481-492.

Preston, K.A., Cornwell, W.K., DeNoyer, J.L., 2006. Wood density and vessel traits as distinct correlates of ecological strategy in 51 California coast range angiosperms. New Phytologist 170, 807-818.

Raschke, K., 1970. Stomatal responses to pressure changes and interruptions in the water supply of detached leaves of *Zea mays* L. Plant Physiology 45, 415-423.

Ray, P.M., Green, P.B., Cleland, R., 1972. Role of turgor in plant cell growth. Nature,
239:163-164.

Rehfeldt, G.E., Ying, C.C., Spittlehouse, D.L., Hamilton, D.A., Jr., 1999. Genetic responses to climate in *Pinus contorta*: niche breadth, climate change, and reforestation. Ecological Monographs 69, 375-407.

Reid, D.E.B., Silins, U., Mendoza, C., Lieffers, V.J., 2005. A unified nomenclature for quantification and description of water conducting properties of sapwood xylem based on Darcy's law. Tree Physiology 25, 993-1000.

Risbey, J.S., Pook, M.J., McIntosh, P.C., Wheeler, M.C., Hendon, H.H., 2009. On the remote drivers of rainfall variability in Australia. Monthly Weather Review 137, 3233-3253.

Roderick, M.L., Berry, S.L., 2001. Linking wood density with tree growth and environment: a theoretical analysis based on the motion of water. New Phytologist 149, 473-485.

Rust, S., Roloff, A., 2002. Reduced photosynthesis in old oak (*Quercus robur*): the impact of crown and hydraulic architecture. Tree Physiology 22, 597-601.

Ryan, J., McAlpine, C., Ludwig, J., 2010. Integrated vegetation designs for enhancing water retention and recycling in agroecosystems. Landscape Ecology 25, 1277-1288.

Ryan, M.G., Waring, R.H., 1992. Maintenance respiration and stand development in a subalpine lodgepole pine forest. Ecology 73, 2100-2108.

Ryan, M.G., Yoder, B.J., 1997. Hydraulic limits to tree height and tree growth. Bioscience 47, 235-242.

Saliendra, N.Z., Sperry, J.S., Comstock, J.P., 1995. Influence of leaf water status on stomatal response to humidity, hydraulic conductance, and soil drought in *Betula occidentalis*. Planta 196, 357-366.

Salisbury, F.B., Ross, C.W., 1992. Plant Physiology. Wadsworth Publishing Company, Belmont, California.

Salleo, S., Gullo, M.A.L., De Paoli, D., Zippo, M., 1996. Xylem recovery from cavitation-induced embolism in young plants of *Laurus nobilis*: a possible mechanism. New Phytologist 132, 47-56.

Salleo, S., Gullo, M.L., Oliveri, F., 1985. Hydraulic parameters measured in 1-year-old twigs of some Mediterranean species with diffuse-porous wood: changes in hydraulic conductivity and their possible functional significance. Journal of Experimental Botany 36, 1-11.

Sano, Y., Fujikawa, S., Fukazawa, K., 1995. Detection and features of wetwood in *Quercus mongolica* var. *grosseserrata*. Trees - Structure and Function 9, 261-268.

Sass, U., Eckstein, D., 1995. The variability of vessel size in beech (*Fagus sylvatica* L.) and its ecophysiological interpretation. Trees 9, 247-252.

Savage, V.M., Bentley, L.P., Enquist, B.J., Sperry, J.S., Smith, D.D., Reich, P.B., von Allmen, E.I., 2010. Hydraulic trade-offs and space filling enable better

predictions of vascular structure and function in plants. Proceedings of the National Academy of Sciences 107, 22722-22727.

Savidge, R.A., 1996. Xylogenesis, genetic and environmental regulation-a review. Iawa Journal 17, 269-310.

Schaeffer, S.M., Sharp, E., Schimel, J.P., Welker, J.M., 2013. Soil–plant N processes in a High Arctic ecosystem, NW Greenland are altered by long-term experimental warming and higher rainfall. Global Change Biology 19, 3529-3539.

Schiller, G., Cohen, Y., 1995. Water regime of a pine forest under a Mediterranean climate. Agricultural and Forest Meteorology 74, 181-193.

Schink, B., Ward, J.C., Zeikus, J.G., 1981. Microbiology of wetwood: importance of pectin degradation and clostridium species in living trees. Applied and Environmental Microbiology 42, 526-532.

Scholander, P.F., 1972. Tensile water. American Scientist 60,584-590.

Schoonmaker, A.L., Teste, F.P., Simard, S.W., Guy, R.D., 2007. Tree proximity, soil pathways and common mycorrhizal networks: their influence on the utilization of redistributed water by understory seedlings. Oecologia 154, 455-466.

Scurfield, G., 1961. The effects of temperature and day length on species of *Eucalyptus*. Australian Journal of Botany 9, 37-56.

Searson, M.J., Thomas, D.S., Montagu, K.D., Conroy, J.P., 2004. Wood density and anatomy of water-limited eucalypts. Tree Physiology 24, 1295-1302.

Shao, H.-B., Chu, L.-Y., Shao, M.-A., Zhao, C.-X., 2008. Advances in functional regulation mechanisms of plant aquaporins: Their diversity, gene expression, localization, structure and roles in plant soil-water relations (Review). Molecular Membrane Biology 25, 179-191.

Sharma, G.K., Dunn, D.B., 1969. Environmental modifications of leaf surface traits in *Datura stramonium*. Canadian Journal of Botany 47, 1211-1216.

Shelburne, V., Hedden, R., Allen, R., 1993. The effect of site, stand density, and sapwood permeability on the relationship between leaf area and sapwood area in loblolly pine (*Pinus taeda* L.). Forest Ecology and Management 58, 193-209.

Shimazaki, K.-I., Doi, M., Assmann, S.M., Kinoshita, T., 2007. Light regulation of stomatal movement. Annual Review of Plant Biology 58, 219-247.

Shinozaki, K., Yoda, K., Hozumi, K., Kira, T., 1964. A quantitative analysis of plant form; the pipe model theory. Japanese Journal of Ecology 14, 97-105.

Siau, J.F., 1984. Transport Processes in Wood. Springer, Berlin.

Slatyer, R.O., Taylor, S.A., 1960. Terminology in Plant- and Soil-Water Relations. Nature 187, 922-924.

Slayter, R., 1967. Plant-water relationships. Academic Press, New York.

Smart, D., Carlisle, E., Goebel, M., Nuñez, B.A., 2005. Transverse hydraulic redistribution by a grapevine. Plant, Cell & Environment 28, 157-166.

Smith, I., 2004. An assessment of recent trends in Australian rainfall. Australian Meteorological Magazine 53, 163-173.

Snyder, K.A., Williams, D.G., 2007. Root allocation and water uptake patterns in riparian tree saplings: responses to irrigation and defoliation. Forest ecology and management 246, 222-231.

Soares, P., Tomé, M., 2002. Height–diameter equation for first rotation eucalypt plantations in Portugal. Forest Ecology and Management 166, 99-109.

Specht, R.L., 1970. Vegetation.In 'The Australian Environment', Leeper, G.W. (eds), 4th Edn.

University Press, CSIRO Melbourne.

Sperry, J.S., 1986. Relationship of xylem embolism to xylem pressure potential, stomatal closure, and shoot morphology in the palm *Rhapis excelsa*. Plant Physiology 80, 110-116.

Sperry, J.S., Hacke, U.G., Pittermann, J., 2006. Size and function in conifer tracheids and angiosperm vessels. American Journal of Botany 93, 1490-1500.

Sperry, J.S., Hacke, U.G., Wheeler, J.K., 2005. Comparative analysis of end wall resistivity in xylem conduits. Plant, Cell & Environment 28, 456-465.

Sperry, J.S., Meinzer, F.C., McCulloh, K.A., 2008. Safety and efficiency conflicts in hydraulic architecture: scaling from tissues to trees. Plant, Cell & Environment 31, 632-645.

Sperry, J.S., Nichols, K.L., Sullivan, J.E.M., Eastlack, S.E., 1994. Xylem embolism in ring-porous, diffuse-porous, and coniferous trees of northern Utah and interior Alaska. Ecology 75, 1736-1752.

Sperry, J., Pockman, W., 1993. Limitation of transpiration by hydraulic conductance and xylem cavitation in *Betula occidentalis*. Plant, Cell & Environment 16, 279-287.

Sperry, J.S., Smith, D.D., Savage, V.M., Enquist, B.J., McCulloh, K.A., Reich, P.B., Bentley, L.P., von Allmen, E.I., 2012. A species-level model for metabolic

scaling in trees I. Exploring boundaries to scaling space within and across species. Functional Ecology 26, 1054-1065.

Steppe, K., Cnudde, V., Girard, C., Lemeur, R., Cnudde, J.-P., Jacobs, P., 2004. Use of X-ray computed microtomography for non-invasive determination of wood anatomical characteristics. Journal of Structural Biology 148, 11-21.

Steudle, E., Peterson, C.A., 1998. How does water get through roots? Journal of Experimental Botany 49, 775-788.

Stratton, L., Goldstein, G., Meinzer, F.C., 2000. Stem water storage capacity and efficiency of water transport: their functional significance in a Hawaiian dry forest. Plant, Cell & Environment 23, 99-106.

Suppiah, R., Collins, D., Della-Marta, P., 2001. Observed changes in Australian climate (Internet document). CSIRO Division of Atmospheric Research, Aspendale, Victoria.

Swenson, N.G., Enquist, B.J., 2007. Ecological and evolutionary determinants of a key plant functional trait: wood density and its community-wide variation across latitude and elevation. American Journal of Botany 94, 451-459.

Taiz, L., Zeiger, E., 2002. Plant Physiology 3rd edition, Sinauer Associates, Sunderland, Massachusetts

Talbott, L.D., Zeiger, E., 1998. The role of sucrose in guard cell osmoregulation. Journal of Experimental Botany 49, 329-337.

Taschetto, A.S., England, M.H., 2009. An analysis of late twentieth century trends in Australian rainfall. International Journal of Climatology 29, 791-807.

Tausz, M., Merchant, A., Kruse, J., Samsa, G., Adams, M.A., 2008. Estimation of drought-related limitations to mid-rotation aged plantation grown *Eucalyptus globulus* by phloem sap analysis. Forest Ecology and Management 256, 844-848.

Thomas, D.S., Montagu, K.D., Conroy, J.P., 2004. Changes in wood density of *Eucalyptus camaldulensis* due to temperature--the physiological link between water viscosity and wood anatomy. Forest Ecology and Management 193, 157-165.

Thomas, D.S., Montagu, K.D., Conroy, J.P., 2007. Temperature effects on wood anatomy, wood density, photosynthesis and biomass partitioning of *Eucalyptus grandis* seedlings. Tree Physiology 27, 251-260.

Thorburn, P.J., Walker, G.R., Brunel, J.P., 1993. Extraction of water from *Eucalyptus* trees for analysis of deuterium and oxygen-18: laboratory and field techniques. Plant, Cell & Environment 16, 269-277.

Iglesias-Trabado, G., Wilstermann, D., 2008. *Eucalyptus* universalis. Global Cultivated Eucalypt Forest Map 2008. http://www.gitforestry.com /downloads/GIT_Forestry_Global_ *Eucalyptus*_Map_2009_Brochure_ENG.pdf. Accessed 23rd March 2014.

Tyerman, S.D., Niemietz, C.M., Bramley, H., 2002. Plant aquaporins: multifunctional water and solute channels with expanding roles. Plant, Cell & Environment 25, 173-194.

Tyree, M., Zimmermann, M., 2002. Xylem structure and the ascent of sap 2nd edition, Springer Verlag, Germany.

Tyree, M.T., 1997. The Cohesion-Tension theory of sap ascent: current controversies. Journal of Experimental Botany 48, 1753-1765.

Tyree, M.T., Ewers, F.W., 1991. The hydraulic architecture of trees and other woody plants. New Phytologist 119, 345-360.

Tyree, M.T., Salleo, S., Nardini, A., Assunta Lo Gullo, M., Mosca, R., 1999. Refilling of embolized vessels in young stems of laurel. Do We Need a New Paradigm? Plant Physiology 120, 11-22.

Tyree, M.T., Sperry, J.S., 1988. Do woody plants operate near the point of catastrophic xylem dysfunction caused by dynamic water stress? Answers from a model. Plant Physiology 88, 574-580.

Tyree, M.T., Sperry, J.S., 1989. Vulnerability of xylem to cavitation and embolism. Annual Review of Plant Physiology and Plant Molecular Biology 40, 19-36.

UNEP, 1997. World Atlas of Desertification, 2nd edition, Middleton, N., Thomas, D.(eds), London

Valentini, R., Mugnozza, G.S., Ehleringer, J., 1992. Hydrogen and carbon isotope ratios of selected species of a Mediterranean macchia ecosystem. Functional Ecology 6, 627-631.

van den Honert, T.H., 1948. Water transport in plants as a catenary process. Discussions of the Faraday Society 3, 146-153.

van der Willigen, C., Pammenter, N.W., 1998. Relationship between growth and xylem hydraulic characteristics of clones of Eucalyptus spp. at contrasting sites. Tree Physiology 18, 595-600.

Vertessy, R., Hatton, T., Reece, P., O'sullivan, S., Benyon, R., 1997. Estimating stand water use of large mountain ash trees and validation of the sap flow measurement technique. Tree Physiology 17, 747-756.

von Allmen, E.I., Sperry, J.S., Smith, D.D., Savage, V.M., Enquist, B.J., Reich, P.B., Bentley, L.P., 2012. A species-level model for metabolic scaling of trees II. Testing in a ring- and diffuse-porous species. Functional Ecology 26, 1066-1076.

Villar-Salvador, P., Castro-Díez, P., Pérez-Rontomé, C., Montserrat-Martí, G., 1997. Stem xylem features in three *Quercus* (Fagaceae) species along a climatic gradient in NE Spain. Trees 12, 90-96.

Villar-Salvador, P., Planelles, R., Oliet, J., Peñuelas-Rubira, J.L., Jacobs, D.F., González, M., 2004. Drought tolerance and transplanting performance of holm oak (*Quercus ilex*) seedlings after drought hardening in the nursery. Tree Physiology 24, 1147-1155.

Wang, C.-H., Hann, D.W., 1988. Height-diameter equations for sixteen tree species in the central western Willamette Valley of Oregon. Oregon State University Forest Research Laboratory, Research Paper 51.

Waring, R.H., Pitman, G.B., 1985. Modifying lodgepole pine stands to change susceptibility to mountain pine beetle attack. Ecology 66, 889-897.

Way, D.A., Oren, R., 2010. Differential responses to changes in growth temperature between trees from different functional groups and biomes: a review and synthesis of data. Tree Physiology 30, 669-688.

Weitz, J.S., Ogle, K., Horn, H.S., 2006. Ontogenetically stable hydraulic design in woody plants. Functional Ecology 20, 191-199.

Wesolowski, A., 2010. Investigating environmental effects on sapwood anatomy of *Eucalyptus* trees from Victoria and Western Australia. unpublished.

West, G.B., Brown, J.H., Enquist, B.J., 1999. A general model for the structure and allometry of plant vascular systems. Nature 400, 664-667.

West, A.G., Patrickson, S.J., Ehleringer, J.R., 2006. Water extraction times for plant and soil materials used in stable isotope analysis. Rapid Communications in Mass Spectrometry 20, 1317-1321.

Wheeler, E., Baas, P., Rodgers, S., 2007. Variations in dicot wood anatomy: a global analysis based on the insidewood database. Iawa Journal 28, 229.

Wheeler, J.K., Sperry, J.S., Hacke, U.G., Hoang, N., 2005. Inter-vessel pitting and cavitation in woody *Rosaceae* and other vesselled plants: a basis for a safety versus efficiency trade-off in xylem transport. Plant, Cell & Environment 28, 800-812.

Whitehead, D., Edwards, W.R.N., Jarvis, P.G., 1984. Conducting sapwood area, foliage area, and permeability in mature trees of Piceasitchensis and Pinuscontorta. Canadian Journal of Forest Research 14, 940-947.

Wiemann, M.C., Wheeler, E.A., Manchester, S.R., Portier, K.M., 1998. Dicotyledonous wood anatomical characters as predictors of climate. Palaeogeography 139, 83-100.

Wiemann, M., Williamson, G., 2002. Geographic Variation in Wood Specific Gravity: Effects of Latitude, Temperature, and Precipitation. Wood and Fiber Science 34, 96-107.

Williams, A.P., Allen, C.D., Millar, C.I., Swetnam, T.W., Michaelsen, J., Still, C.J., Leavitt, S.W., 2010. Forest responses to increasing aridity and warmth in the southwestern United States. Proceedings of the National Academy of Sciences 107, 21289-21294.

Woldendorp, G., Hill, M.J., Doran, R., Ball, M.C., 2008. Frost in a future climate: modelling interactive effects of warmer temperatures and rising atmospheric (CO_2) on the incidence and severity of frost damage in a temperate evergreen (*Eucalyptus pauciflora*). Global Change Biology 14, 294-308.

Wonn, H.T., O'Hara, K.L., 2001. Height: diameter ratios and stability relationships for four northern Rocky Mountain tree species. Western Journal of Applied Forestry 16, 87-94. **Woodruff, D.R., Meinzer, F.C., Lachenbruch, B., 2008.** Height-related trends in leaf xylem anatomy and shoot hydraulic characteristics in a tall conifer: safety versus efficiency in water transport. New Phytologist 180, 90-99.

Wullschleger, S.D., Meinzer, F., Vertessy, R., 1998. A review of whole-plant water use studies in tree. Tree Physiology 18, 499-512.

Yang, S., Tyree, M.T., 1992. A theoretical model of hydraulic conductivity recovery from embolism with comparison to experimental data on *Acer saccharum*. Plant, Cell & Environment 15, 633-643.

Yazawa, K., 2006. On the wet-heartwood of some broad-leaved trees grown in Japan. Journal of the Faculty of Agriculture, Hokkaido University 54.

Zaehle, S., 2005. Effect of height on tree hydraulic conductance incompletely compensated by xylem tapering. Functional Ecology 19, 359-364.

Zanne, A.E., Westoby, M., Falster, D.S., Ackerly, D.D., Loarie, S.R., Arnold, S.E.J., Coomes, D.A., 2010. Angiosperm wood structure: Global patterns in vessel

anatomy and their relation to wood density and potential conductivity. American Journal of Botany 97, 207-215.

Zarebanadkouki, M., Kim, Y., Moradi, A., Vogel, H.-J., Kaestner, A., Carminati, A., 2012. Quantification and modeling of local root water uptake using neutron radiography and deuterated water. Vadose Zone Journal 11.

Zeppel, M., Eamus, D., 2008. Coordination of leaf area, sapwood area and canopy conductance leads to species convergence of tree water use in a remnant evergreen woodland. Australian Journal of Botany 56, 97-108.

Zimmermann, M.H., 1983. Xylem sructure and the ascent of sap. SpringerVerlag, Berlin.

Zimmermann, M.H., Jeje, A.A., 1981. Vessel-length distribution in stems of some American woody plants. Canadian Journal of Botany 59, 1882-1892.

Zimmermann, M.H., Tomlinson, P.B., 1966. Analysis of complex vascular systems in plants: optical shuttle method. Science 152, 72-73.

Zweifel, R., Item, H., Häsler, R., 2000. Stem radius changes and their relation to stored water in stems of young Norway spruce trees. Trees 15, 50-57.

Appendix – Chapter 2

Eucalyptus regnans

Figure S2.1: Habitus of *Eucalyptus regnans*. Image illustrates one of three sampled trees.

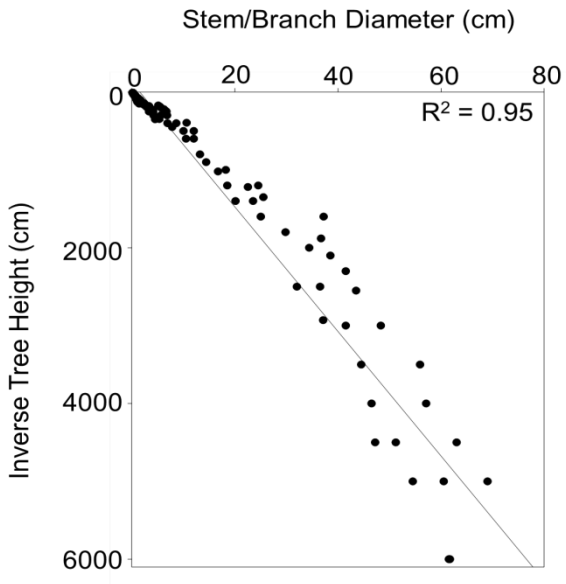

Figure S2.2: Stem and branch diameters measured at sample spots along tree main axes of all three sampled individuals. Coefficient of determination for linear regression (y = 0.01x + 1.56) is shown in figure.

Tree 1

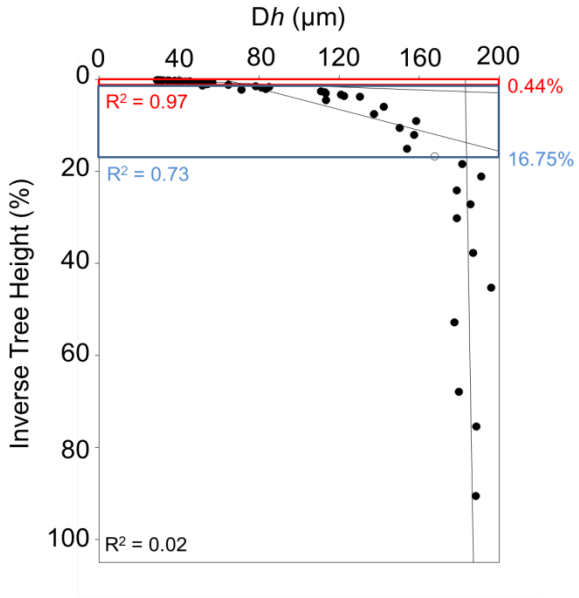

Figure S2.3: Three Phase Taper Analysis (TPTA) of changing hydraulically weighted diameters (D*h*) with inverse tree height. Black dots illustrate measured values and are averages of three analysed images. Circles are calculated medians in-between two measured values. They were not part of linear regression analyses and they do express relative tree heights of phase changes. Red box, red percentage value and red coefficient of determination (y = 61.43x + 19.17) indicate Phase 3 (steep vessel taper structure); blue box, blue percentage value and blue coefficient of determination (y = 8.82x + 62.32) indicate Phase 2 (moderate vessel taper structure); black box and black coefficient of determination (y = 0.04x + 182.99) indicate Phase 1 (no clear vessel taper structure).

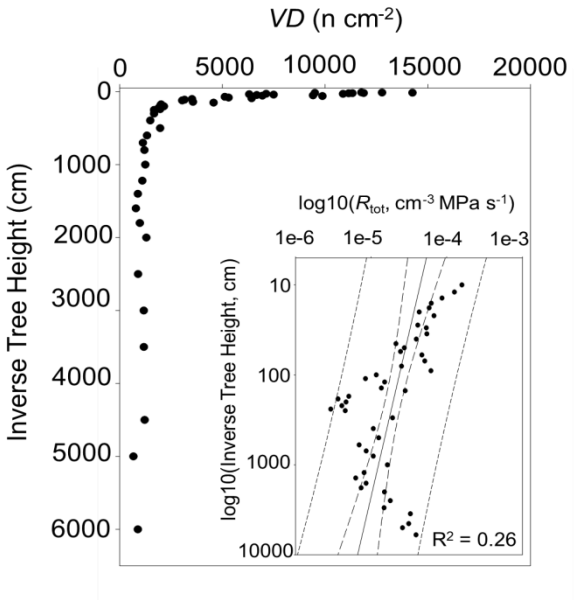

Figure S2.4: Change of vessel density (*VD*) with inverse tree height. Black dots illustrate measured values and are averages of three analyzed images. Inserted panel illustrates total hydraulic resistance (R_{tot}) plotted against inverse tree height in a log–log scaled graph, where solid line indicates linear regression (y = -0.28x - 4.08), long dashed lines indicate 95% confidence intervals, and short dashed lines indicate 95% prediction intervals. Coefficient of determination is shown in figure.

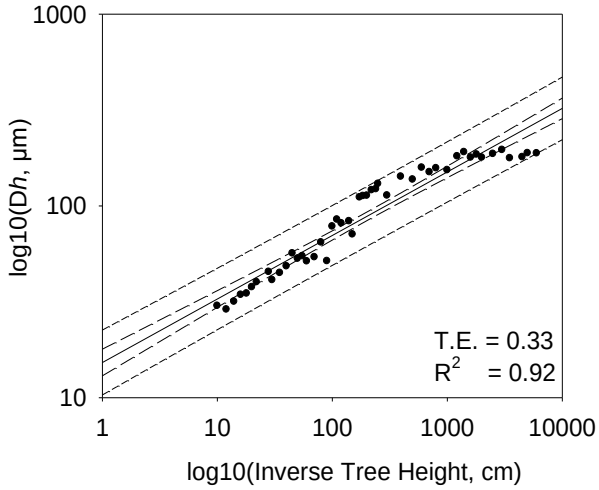

Figure S2.5: Hydraulically weighted diameters (D*h*) plotted against inverse tree height in a log–log scaled graph, where the solid line indicates the power function ($y = 15.26*x^{0.33}$), long-dashed lines indicate 95% confidence intervals and short-dashed lines indicate 95% prediction intervals. Black dots illustrate measured values and are averages of three analysed images. The degree of tapering (tapering exponent; T.E.) and coefficient of determination are shown in graph.

Tree 2

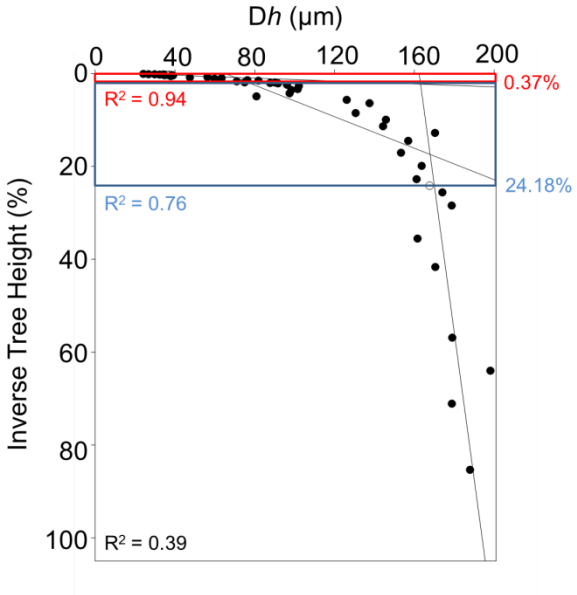

Figure S2.6: Three Phase Taper Analysis (TPTA) of changing hydraulically weighted diameters (D*h*) with inverse tree height. Black dots illustrate measured values and are averages of three analysed images. Circles are calculated medians in-between two measured values. They were not part of linear regression analyses and they do express relative tree heights of phase changes. Red box, red percentage value and red coefficient of determination (y = 63.36x + 17.05) indicate Phase 3 (steep vessel taper structure); blue box, blue percentage value and blue coefficient of determination (y = 5.89x + 65.18) indicate Phase 2 (moderate vessel taper structure); black box and black coefficient of determination (y = 0.32x + 162.40) indicate Phase 1 (no clear vessel taper structure).

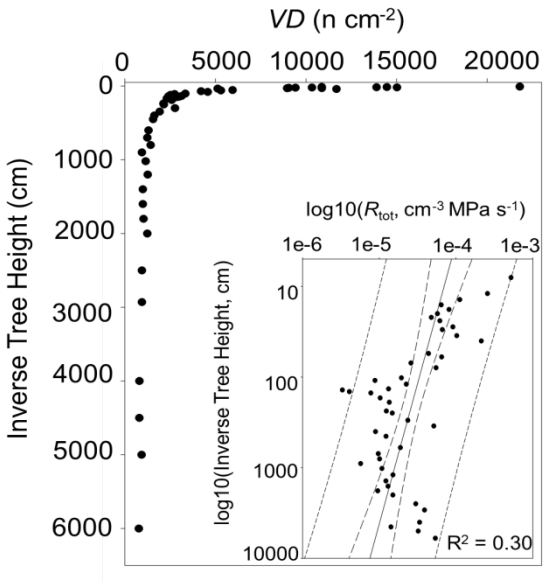

Figure S2.7: Change of vessel density (*VD*) with inverse tree height. Black dots illustrate measured values and are averages of three analyzed images. Inserted panel illustrates total hydraulic resistance (R_{tot}) plotted against inverse tree height in a log–log scaled graph, where solid line indicates linear regression (y = -0.32x - 3.83), long dashed lines indicate 95% confidence intervals, and short dashed lines indicate 95% prediction intervals. Coefficient of determination is shown in figure.

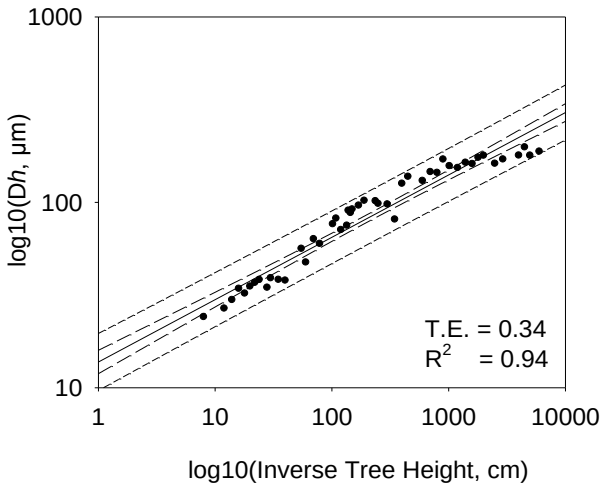

Figure S2.8: Hydraulically weighted diameters (D*h*) plotted against inverse tree height in a log–log scaled graph, where the solid line indicates the power function ($y = 13.77*x^{0.34}$), long-dashed lines indicate 95% confidence intervals and short-dashed lines indicate 95% prediction intervals. Black dots illustrate measured values and are averages of three analysed images. The degree of tapering (tapering exponent; T.E.) and coefficient of determination are shown in graph.

Tree 3

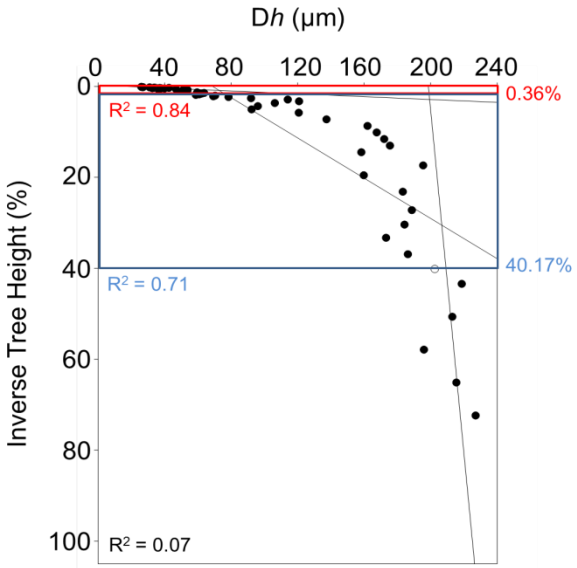

Figure S2.9: Three Phase Taper Analysis (TPTA) of changing hydraulically weighted diameters (D*h*) with inverse tree height. Black dots illustrate measured values and are averages of three analysed images. Circles are calculated medians in-between two measured values. They were not part of linear regression analyses and they do express relative tree heights of phase changes. Red box, red percentage value and red coefficient of determination (y = 63.43x + 17.43) indicate Phase 3 (steep vessel taper structure); blue box, blue percentage value and blue coefficient of determination (y = 4.52x + 68.84) indicate Phase 2 (moderate vessel taper structure); black box and black coefficient of determination (y = 0.26x + 198.63) indicate Phase 1 (no clear vessel taper structure).

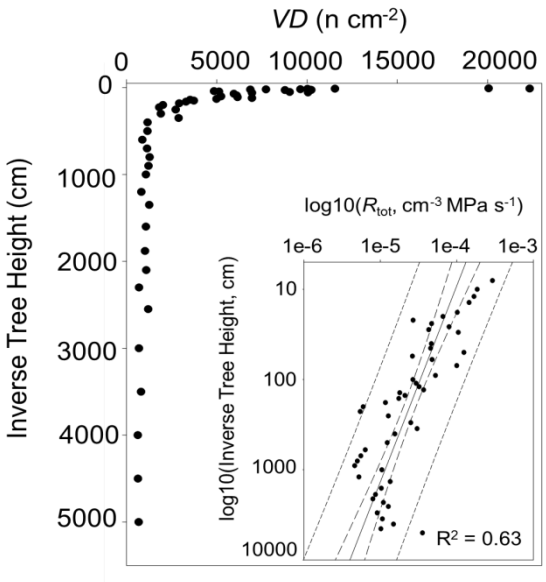

Figure S2.10: Change of vessel density (*VD*) with inverse tree height. Black dots illustrate measured values and are averages of three analyzed images. Inserted panel illustrates total hydraulic resistance (R_{tot}) plotted against inverse tree height in a log–log scaled graph, where solid line indicates linear regression (y = -0.46x - 3.56), long dashed lines indicate 95% confidence intervals, and short dashed lines indicate 95% prediction intervals. Coefficient of determination is shown in figure.

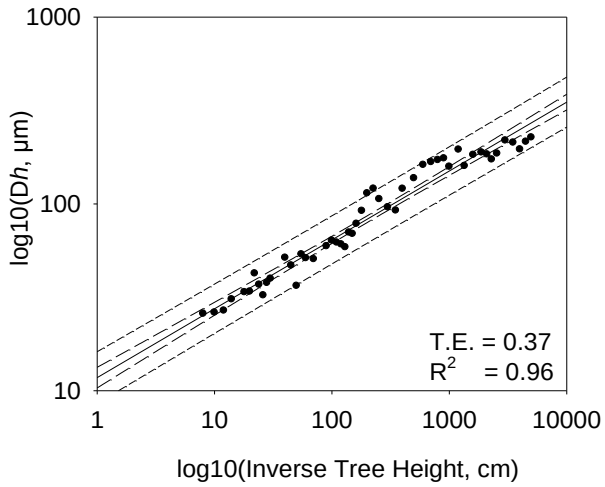

Figure S2.11: Hydraulically weighted diameters (D*h*) plotted against inverse tree height in a log–log scaled graph, where the solid line indicates the power function ($y = 11.75*x^{0.37}$), long-dashed lines indicate 95% confidence intervals and short-dashed lines indicate 95% prediction intervals. Black dots illustrate measured values and are averages of three analysed images. The degree of tapering (tapering exponent; T.E.) and coefficient of determination are shown in graph.

Eucalyptus pauciflora

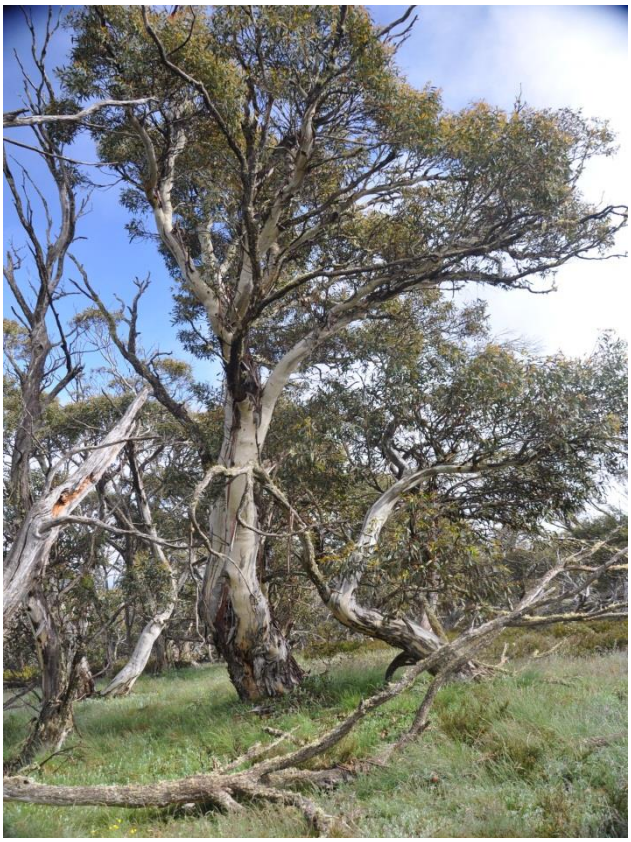

Figure S2.12: Habitus of *Eucalyptus pauciflora*. Image illustrates one of three sampled trees.

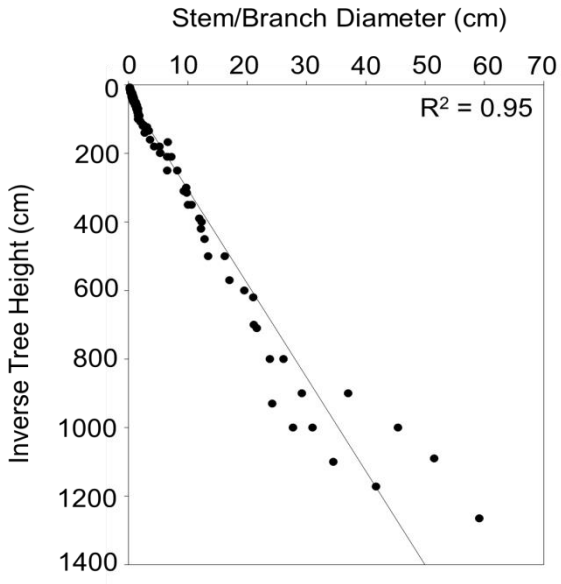

Figure S2.13: Stem and branch diameters measured at sample spots along tree main axes of all three sampled individuals. Coefficient of determination for linear regression (y = 0.04x - 1.14) is shown in figure.

Tree 1

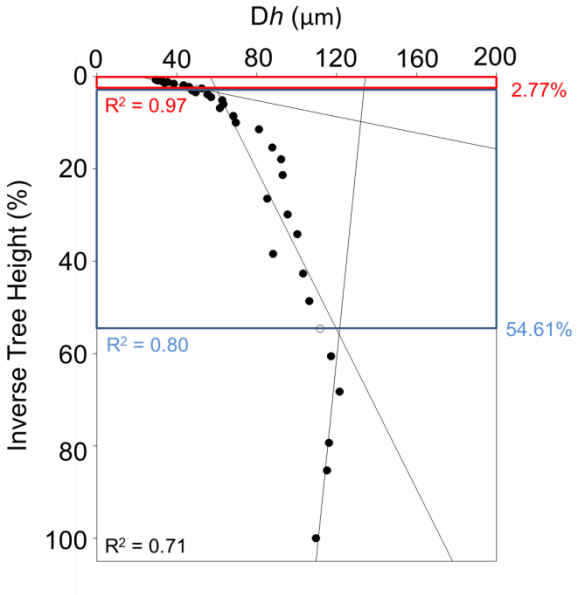

Figure S2.14: Three Phase Taper Analysis (TPTA) of changing hydraulically weighted diameters (D*h*) with inverse tree height. Black dots illustrate measured values and are averages of three analysed images. Circles are calculated medians in-between two measured values. They were not part of linear regression analyses and they do express relative tree heights of phase changes. Red box, red percentage value and red coefficient of determination (y =11.43x + 20.79) indicate Phase 3 (steep vessel taper structure); blue box, blue percentage value and blue coefficient of determination (y = 1.16x + 56.69) indicate Phase 2 (moderate vessel taper structure); black box and black coefficient of determination (y = -0.24x + 134.39) indicate Phase 1 (no clear vessel taper structure).

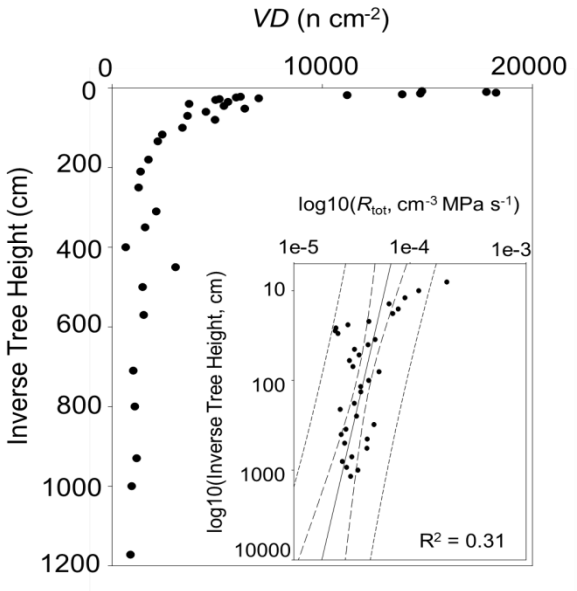

Figure S2.15: Change of vessel densities (*VD*) with inverse tree height. Black dots illustrate measured values and are averages of three analyzed images. Inserted panel illustrates total hydraulic resistance (R_{tot}) plotted against inverse tree height in a log–log scaled graph, where solid line indicates linear regression (y = -0.18x - 4.04), long dashed lines indicate 95% confidence intervals, and short dashed lines indicate 95% prediction intervals. Coefficient of determination is shown in figure.

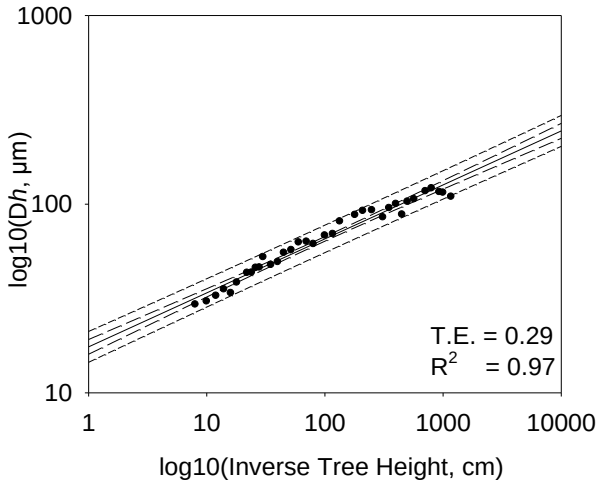

Figure S2.16: Hydraulically weighted diameters (D*h*) plotted against inverse tree height in a log–log scaled graph, where the solid line indicates the power function ($y = 17.52*x^{0.29}$), long-dashed lines indicate 95% confidence intervals and short-dashed lines indicate 95% prediction intervals. Black dots illustrate measured values and are averages of three analysed images. The degree of tapering (tapering exponent; T.E.) and coefficient of determination are shown in graph.

Tree 2

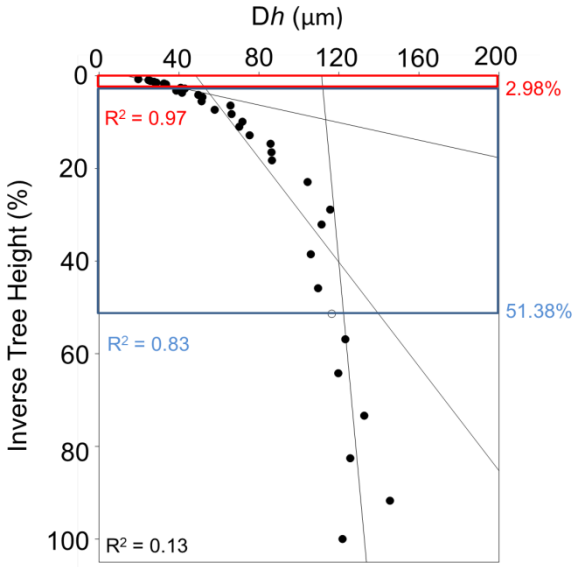

Figure S2.17: Three Phase Taper Analysis (TPTA) of changing hydraulically weighted diameters (D*h*) with inverse tree height. Black dots illustrate measured values and are averages of three analysed images. Circles are calculated medians in-between two measured values. They were not part of linear regression analyses and they do express relative tree heights of phase changes. Red box, red percentage value and red coefficient of determination (y =10.55x + 13.58) indicate Phase 3 (steep vessel taper structure); blue box, blue percentage value and blue coefficient of determination (y = 1.78x + 48.39) indicate Phase 2 (moderate vessel taper structure); black box and black coefficient of determination (y = 0.21x + 111.35) indicate Phase 1 (no clear vessel taper structure).

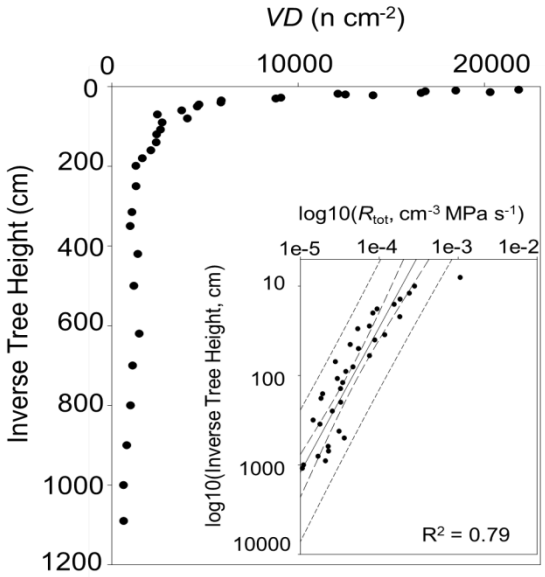

Figure S2.18: Change of vessel densities (*VD*) with inverse tree height. Black dots illustrate measured values and are averages of three analyzed images. Inserted panel illustrates total hydraulic resistance (R_{tot}) plotted against inverse tree height in a log–log scaled graph, where solid line indicates linear regression (y = -0.62x - 3.10), long dashed lines indicate 95% confidence intervals, and short dashed lines indicate 95% prediction intervals. Coefficient of determination is shown in figure.

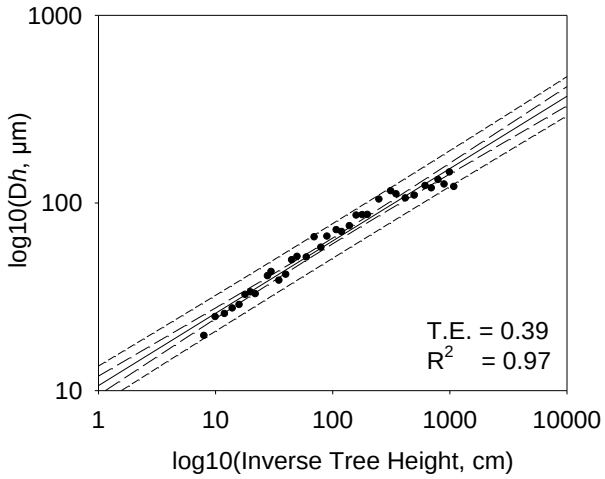

Figure S2.19: Hydraulically weighted diameters (D*h*) plotted against inverse tree height in a log–log scaled graph, where the solid line indicates the power function ($y = 10.64*x^{0.39}$), long-dashed lines indicate 95% confidence intervals and short-dashed lines indicate 95% prediction intervals. Black dots illustrate measured values and are averages of three analysed images. The degree of tapering (tapering exponent; T.E.) and coefficient of determination are shown in graph.

Tree 3

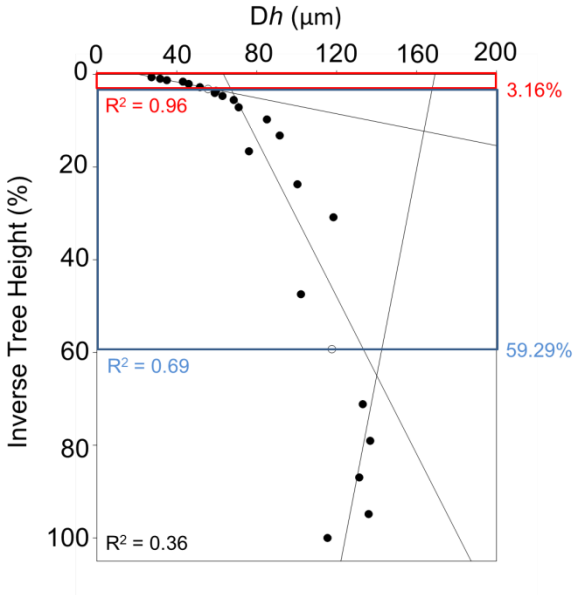

Figure S2.20: Three Phase Taper Analysis (TPTA) of changing hydraulically weighted diameters (D*h*) with inverse tree height. Black dots illustrate measured values and are averages of three analysed images. Circles are calculated medians in-between two measured values. They were not part of linear regression analyses and they do express relative tree heights of phase changes. Red box, red percentage value and red coefficient of determination (y =11.65x + 21.09) indicate Phase 3 (steep vessel taper structure); blue box, blue percentage value and blue coefficient of determination (y = 1.18x + 63.42) indicate Phase 2 (moderate vessel taper structure); black box and black coefficient of determination (y = -0.45x + 169.24) indicate Phase 1 (no clear vessel taper structure).

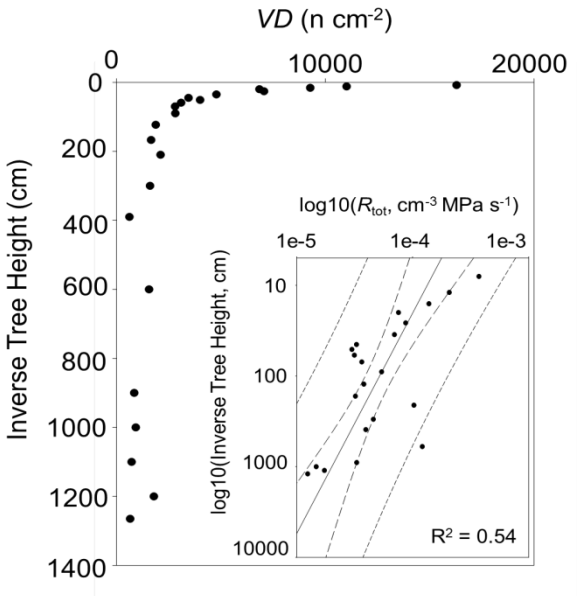

Figure S2.21: Change of vessel densities (*VD*) with inverse tree height. Black dots illustrate measured values and are averages of three analyzed images. Inserted panel illustrates total hydraulic resistance (R_{tot}) plotted against inverse tree height in a log–log scaled graph, where solid line indicates linear regression (y = -0.41x - 3.46), long dashed lines indicate 95% confidence intervals, and short dashed lines indicate 95% prediction intervals. Coefficient of determination is shown in figure.

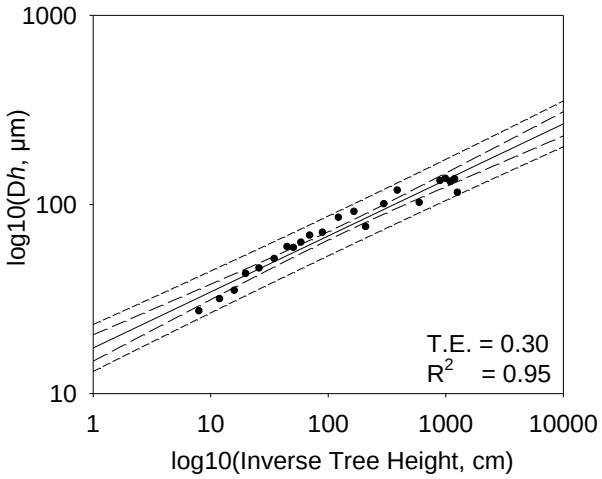

Figure S2.22: Hydraulically weighted diameters (D*h*) plotted against inverse tree height in a log–log scaled graph, where the solid line indicates the power function ($y = 17.43*x^{0.30}$), long-dashed lines indicate 95% confidence intervals and short-dashed lines indicate 95% prediction intervals. Black dots illustrate measured values and are averages of three analysed images. The degree of tapering (tapering exponent; T.E.) and coefficient of determination are shown in graph.

Eucalyptus viminalis

Figure S2.23: Habitus of *Eucalyptus viminalis*. Image illustrates one of three sampled trees.

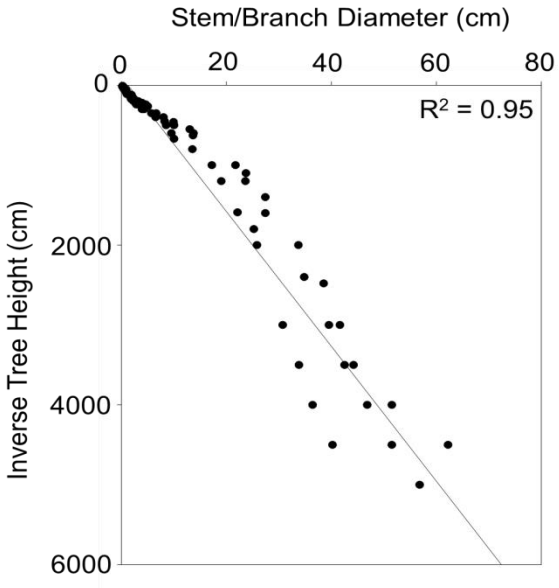

Figure S2.24: Stem and branch diameters measured at sample spots along tree main axes of all three sampled individuals. Coefficient of determination for linear regression (y = 0.01x + 1.27) is shown in figure.

Tree 1

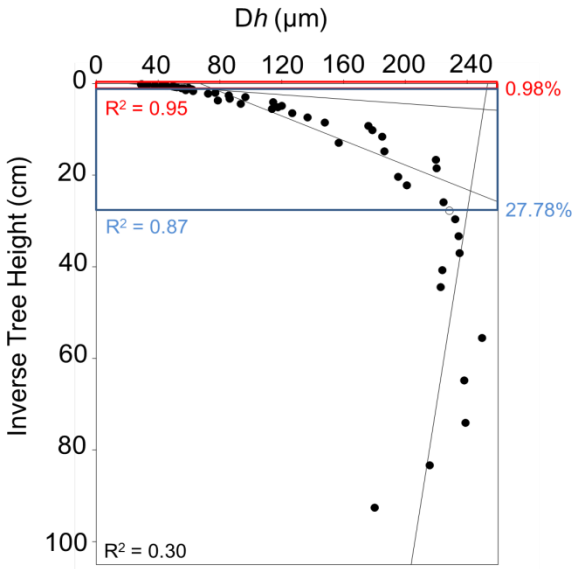

Figure S2.25: Three Phase Taper Analysis (TPTA) of changing hydraulically weighted diameters (D*h*) with inverse tree height. Black dots illustrate measured values and are averages of three analysed images. Circles are calculated medians in-between two measured values. They were not part of linear regression analyses and they do express relative tree heights of phase changes. Red box, red percentage value and red coefficient of determination (y = 40.87x + 20.69) indicate Phase 3 (steep vessel taper structure); blue box, blue percentage value and blue coefficient of determination (y = 7.46x + 67.26) indicate Phase 2 (moderate vessel taper structure); black box and black coefficient of determination (y = -0.47x + 253.22) indicate Phase 1 (no clear vessel taper structure).

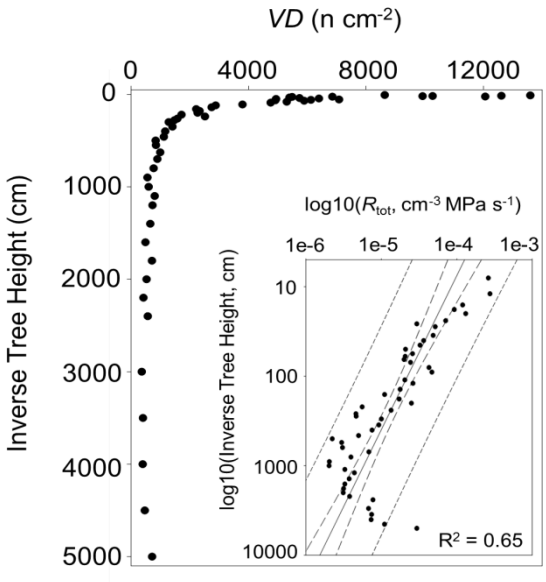

Figure S2.26: Change of vessel density (*VD*) with inverse tree height. Black dots illustrate measured values and are averages of three analyzed images. Inserted panel illustrates total hydraulic resistance (R_{tot}) plotted against inverse tree height in a log–log scaled graph, where solid line indicates linear regression (y = -0.58x - 3.49), long dashed lines indicate 95% confidence intervals, and short dashed lines indicate 95% prediction intervals. Coefficient of determination is shown in figure.

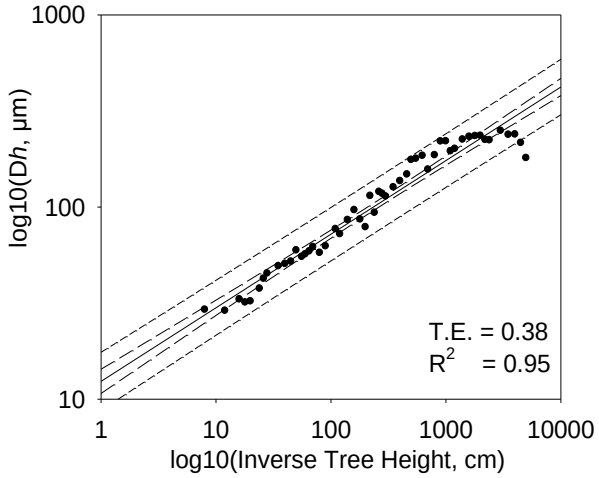

Figure S2.27: Hydraulically weighted diameters (D*h*) plotted against inverse tree height in a log–log scaled graph, where the solid line indicates the power function ($y = 12.38*x^{0.38}$), long-dashed lines indicate 95% confidence intervals and short-dashed lines indicate 95% prediction intervals. Black dots illustrate measured values and are averages of three analysed images. The degree of tapering (tapering exponent; T.E.) and coefficient of determination are shown in graph.

Tree 2

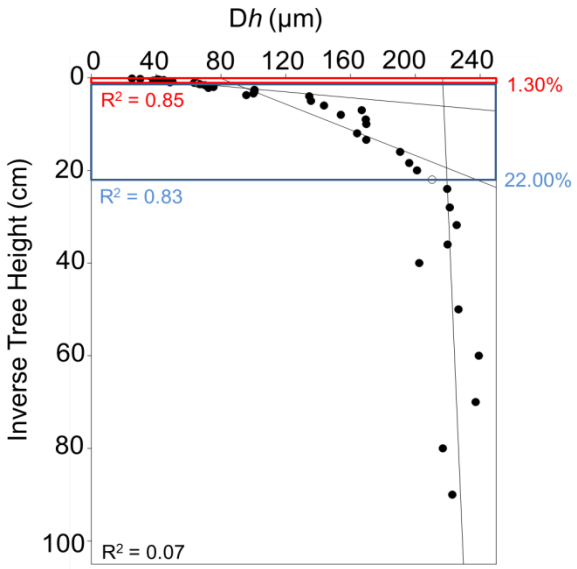

Figure S2.28: Three Phase Taper Analysis (TPTA) of changing hydraulically weighted diameters (D*h*) with inverse tree height. Black dots illustrate measured values and are averages of three analysed images. Circles are calculated medians in-between two measured values. They were not part of linear regression analyses and they do express relative tree heights of phase changes. Red box, red percentage value and red coefficient of determination (y = 31.50x + 24.59) indicate Phase 3 (steep vessel taper structure); blue box, blue percentage value and blue coefficient of determination (y = 7.22x + 79.09) indicate Phase 2 (moderate vessel taper structure); black box and black coefficient of determination (y = 0.12x + 216.83) indicate Phase 1 (no clear vessel taper structure).

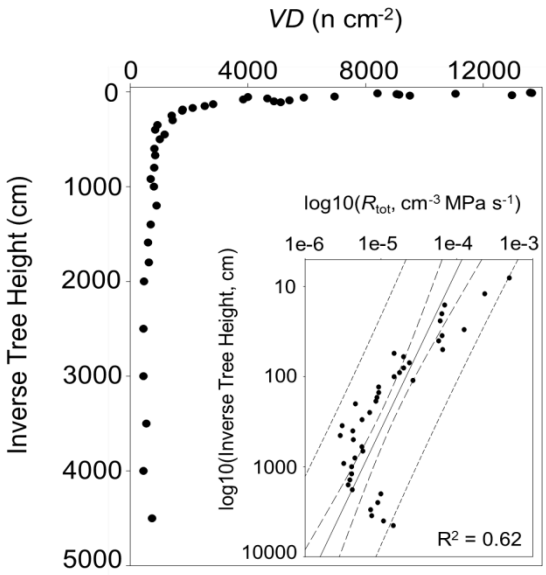

Figure S2.29: Change of vessel density (*VD*) with inverse tree height. Black dots illustrate measured values and are averages of three analyzed images. Inserted panel illustrates total hydraulic resistance (R_{tot}) plotted against inverse tree height in a log–log scaled graph, where solid line indicates linear regression (y = -0.57x - 3.54), long dashed lines indicate 95% confidence intervals, and short dashed lines indicate 95% prediction intervals. Coefficient of determination is shown in figure.

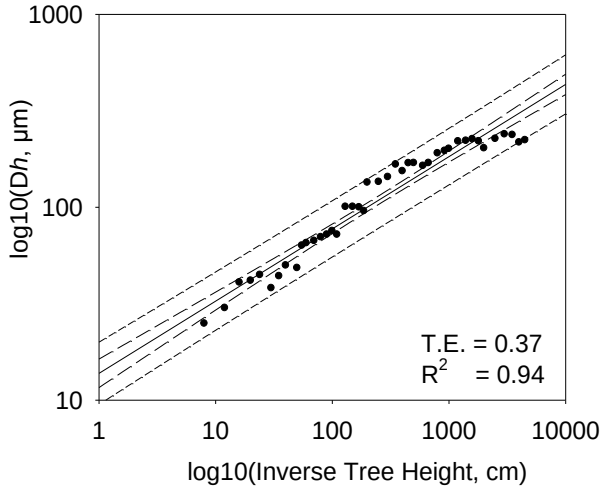

Figure S2.30: Hydraulically weighted diameters (D*h*) plotted against inverse tree height in a log–log scaled graph, where the solid line indicates the power function ($y = 13.78*x^{0.37}$), long-dashed lines indicate 95% confidence intervals and short-dashed lines indicate 95% prediction intervals. Black dots illustrate measured values and are averages of three analysed images. The degree of tapering (tapering exponent; T.E.) and coefficient of determination are shown in graph.

Tree 3

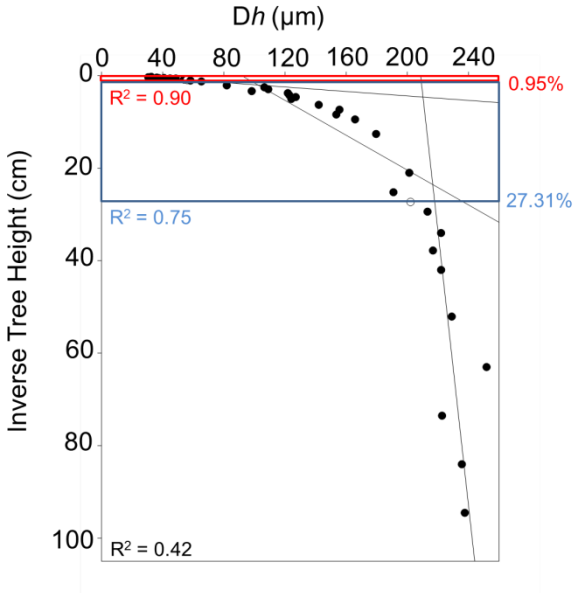

Figure S2.31: Three Phase Taper Analysis (TPTA) of changing hydraulically weighted diameters (D*h*) with inverse tree height. Black dots illustrate measured values and are averages of three analysed images. Circles are calculated medians in-between two measured values. They were not part of linear regression analyses and they do express relative tree heights of phase changes. Red box, red percentage value and red coefficient of determination (y = 41.38x + 19.16) indicate Phase 3 (steep vessel taper structure); blue box, blue percentage value and blue coefficient of determination (y = 5.31x + 92.28) indicate Phase 2 (moderate vessel taper structure); black box and black coefficient of determination (y = 0.10x + 152.29) indicate Phase 1 (no clear vessel taper structure).

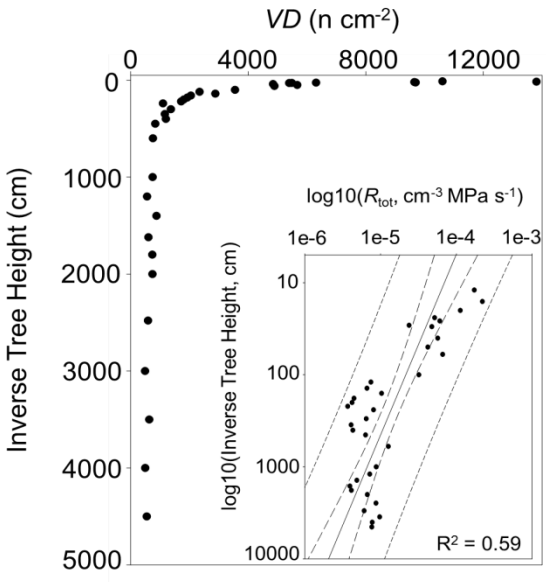

Figure S2.32: Change of vessel density (*VD*) with inverse tree height. Black dots illustrate measured values and are averages of three analyzed images. Inserted panel illustrates total hydraulic resistance (R_{tot}) plotted against inverse tree height in a log–log scaled graph, where solid line indicates linear regression (y = -3.65x - 0.51), long dashed lines indicate 95% confidence intervals, and short dashed lines indicate 95% prediction intervals. Coefficient of determination is shown in figure.

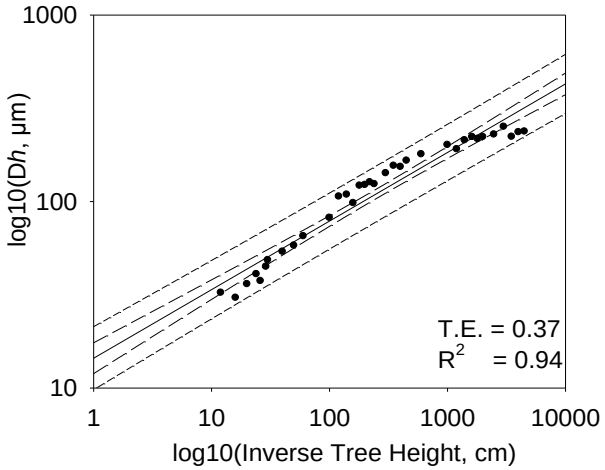

Figure S2.33: Hydraulically weighted diameters (D*h*) plotted against inverse tree height in a log–log scaled graph, where the solid line indicates the power function ($y = 14.45*x^{0.37}$), long-dashed lines indicate 95% confidence intervals and short-dashed lines indicate 95% prediction intervals. Black dots illustrate measured values and are averages of three analysed images. The degree of tapering (tapering exponent; T.E.) and coefficient of determination are shown in graph.

Eucalyptus delegatensis

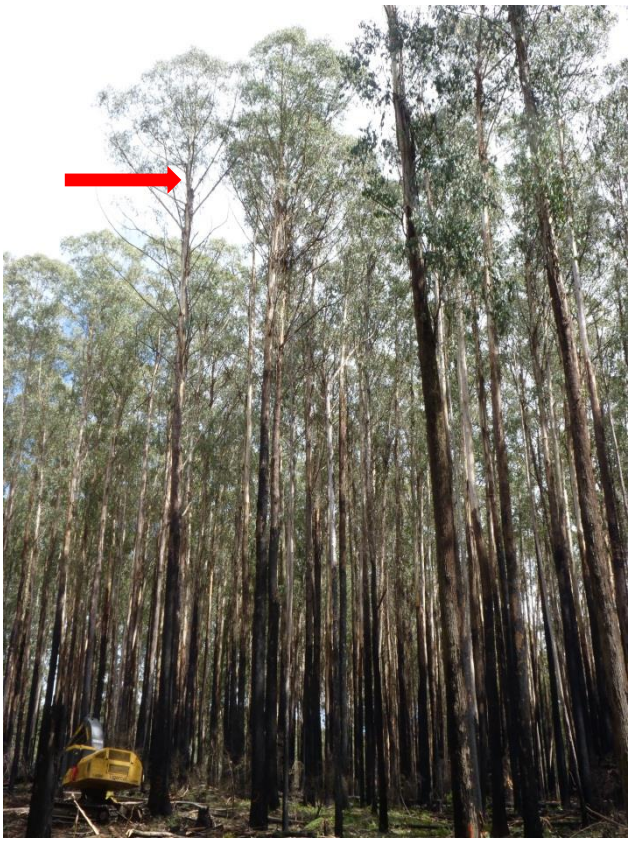

Figure S2.34: Habitus of *Eucalyptus delegatensis*. Image illustrates one of three sampled trees.

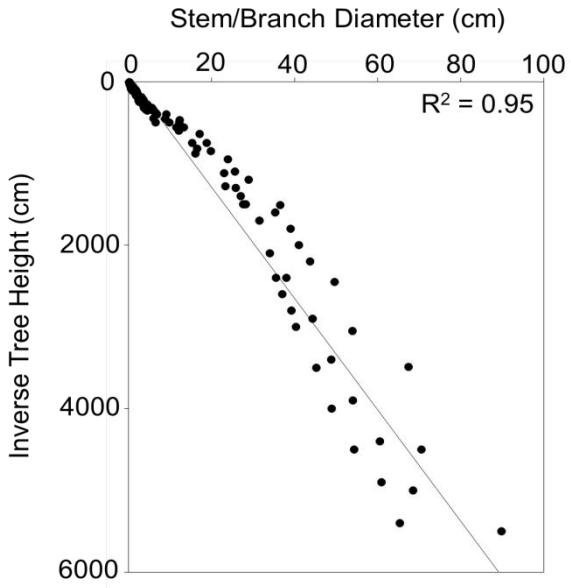

Figure S2.35: Stem and branch diameters measured at sample spots along tree main axes of all three sampled individuals. Coefficient of determination for linear regression (y = 0.01x + 1.27) is shown in figure.

Tree 1

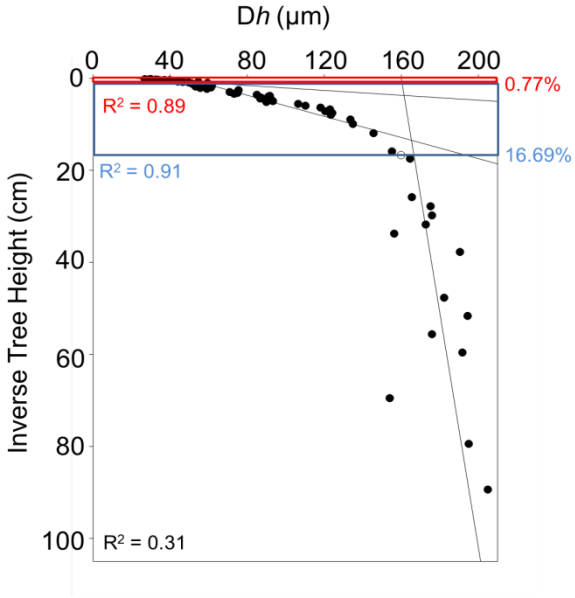

Figure S2.36: Three Phase Taper Analysis (TPTA) of changing hydraulically weighted diameters (D*h*) with inverse tree height. Black dots illustrate measured values and are averages of three analysed images. Circles are calculated medians in-between two measured values. They were not part of linear regression analyses and they do express relative tree heights of phase changes. Red box, red percentage value and red coefficient of determination (y = 37.63x + 21.60) indicate Phase 3 (steep vessel taper structure); blue box, blue percentage value and blue coefficient of determination (y = 8.71x + 48.06) indicate Phase 2 (moderate vessel taper structure); black box and black coefficient of determination (y = 0.39x + 160.00) indicate Phase 1 (no clear vessel taper structure).

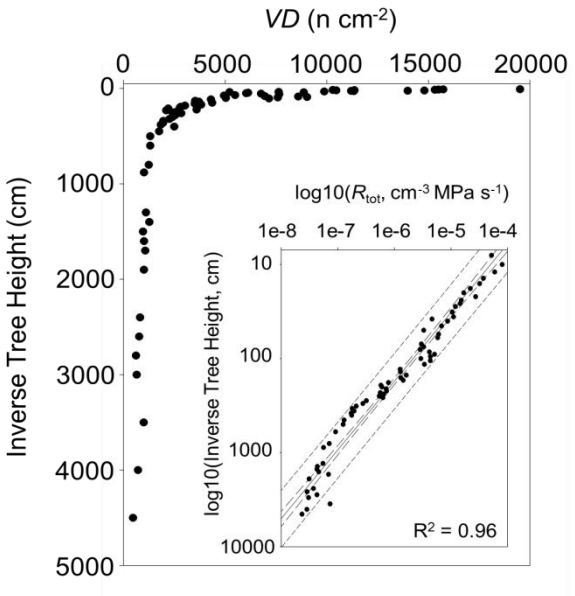

Figure S2.37: Change of vessel density (*VD*) with inverse tree height. Black dots illustrate measured values and are averages of three analyzed images. Inserted panel illustrates total hydraulic resistance (R_{tot}) plotted against inverse tree height in a log–log scaled graph, where solid line indicates linear regression (y = -1.37x - 2.93), long dashed lines indicate 95% confidence intervals, and short dashed lines indicate 95% prediction intervals. Coefficient of determination is shown in figure.

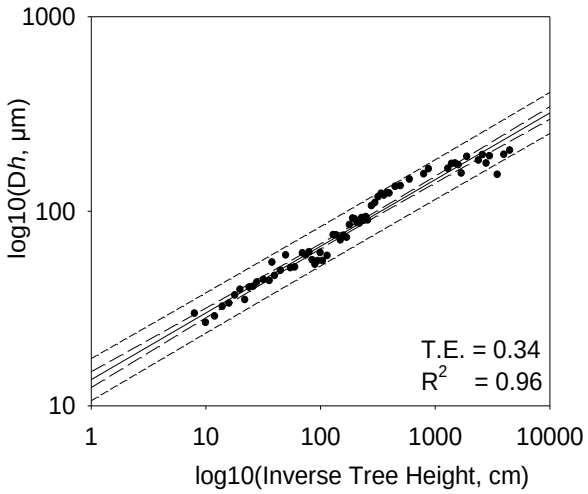

Figure S2.38: Hydraulically weighted diameters (D*h*) plotted against inverse tree height in a log–log scaled graph, where the solid line indicates the power function ($y = 13.63*x^{0.34}$), long-dashed lines indicate 95% confidence intervals and short-dashed lines indicate 95% prediction intervals. Black dots illustrate measured values and are averages of three analysed images. The degree of tapering (tapering exponent; T.E.) and coefficient of determination are shown in graph.

Tree 2

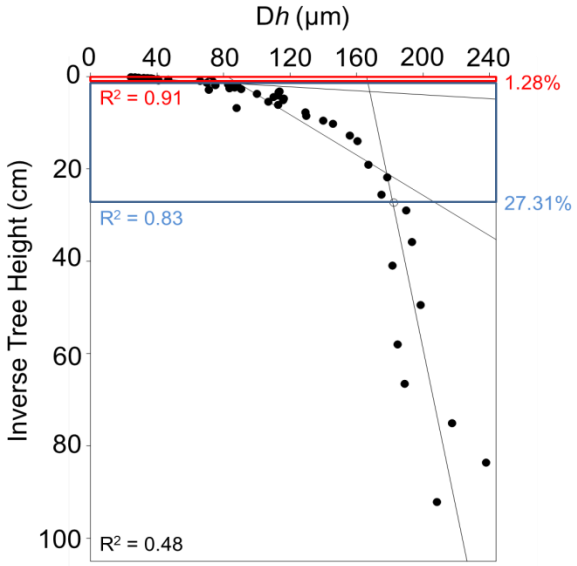

Figure S2.39: Three Phase Taper Analysis (TPTA) of changing hydraulically weighted diameters (D*h*) with inverse tree height. Black dots illustrate measured values and are averages of three analysed images. Circles are calculated medians in-between two measured values. They were not part of linear regression analyses and they do express relative tree heights of phase changes. Red box, red percentage value and red coefficient of determination (y = 46.63x + 16.41) indicate Phase 3 (steep vessel taper structure); blue box, blue percentage value and blue coefficient of determination (y = 4.58x + 82.32) indicate Phase 2 (moderate vessel taper structure); black box and black coefficient of determination (y = 0.58x + 166.13) indicate Phase 1 (no clear vessel taper structure).

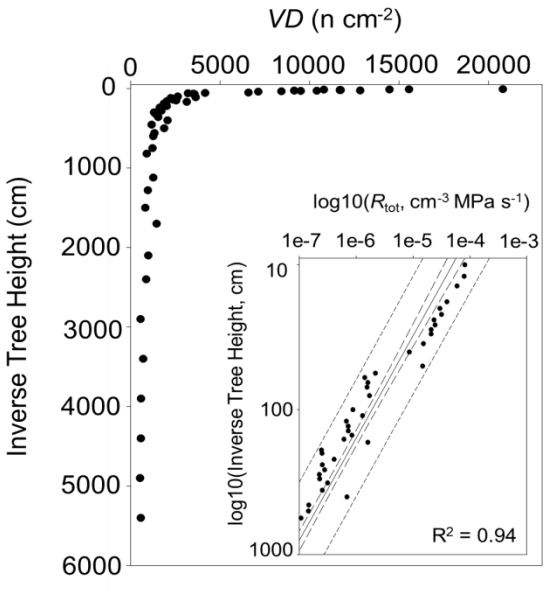

Figure S2.40: Change of vessel density (*VD*) with inverse tree height. Black dots illustrate measured values and are averages of three analyzed images. Inserted panel illustrates total hydraulic resistance (R_{tot}) plotted against inverse tree height in a log–log scaled graph, where solid line indicates linear regression (y = -1.42x - 2.89), long dashed lines indicate 95% confidence intervals, and short dashed lines indicate 95% prediction intervals. Coefficient of determination is shown in figure.

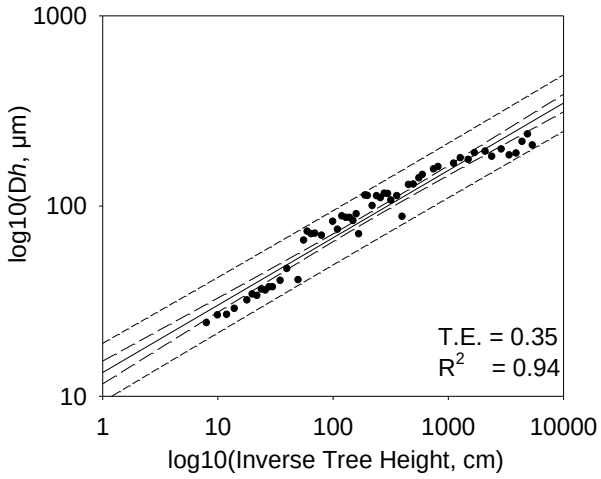

Figure S2.41: Hydraulically weighted diameters (D*h*) plotted against inverse tree height in a log–log scaled graph, where the solid line indicates the power function ($y = 13.34*x^{0.35}$), long-dashed lines indicate 95% confidence intervals and short-dashed lines indicate 95% prediction intervals. Black dots illustrate measured values and are averages of three analysed images. The degree of tapering (tapering exponent; T.E.) and coefficient of determination are shown in graph.

Tree 3

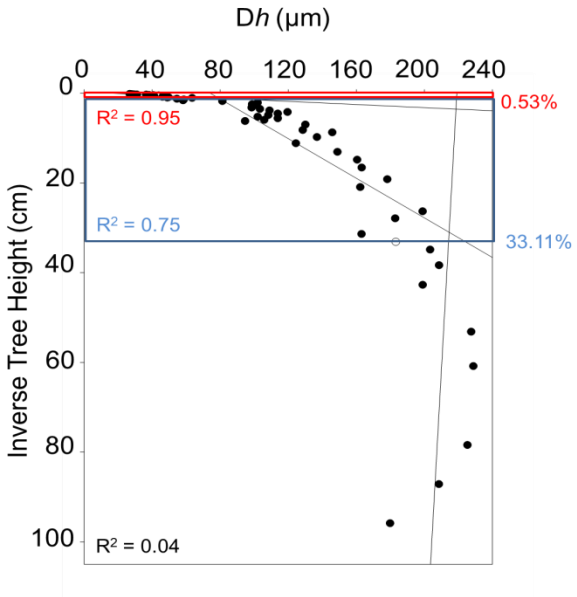

Figure S2.42: Three Phase Taper Analysis (TPTA) of changing hydraulically weighted diameters (D*h*) with inverse tree height. Black dots illustrate measured values and are averages of three analysed images. Circles are calculated medians in-between two measured values. They were not part of linear regression analyses and they do express relative tree heights of phase changes. Red box, red percentage value and red coefficient of determination (y = 57.15x + 16.74) indicate Phase 3 (steep vessel taper structure); blue box, blue percentage value and blue coefficient of determination (y = 4.53x + 74.15) indicate Phase 2 (moderate vessel taper structure); black box and black coefficient of determination (y = -0.15x + 219.12) indicate Phase 1 (no clear vessel taper structure).

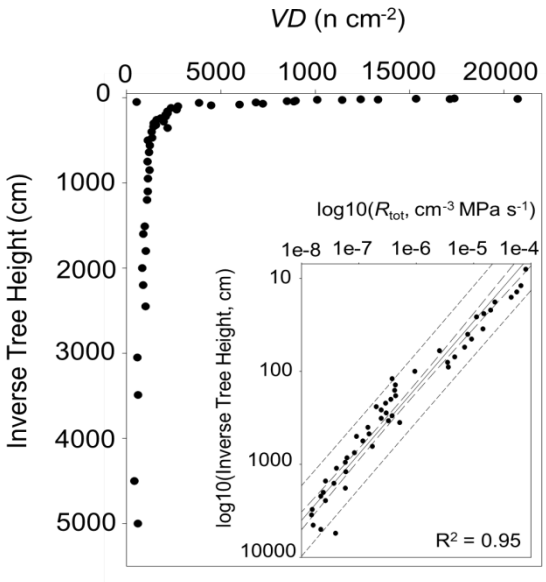

Figure S2.43: Change of vessel density (*VD*) with inverse tree height. Black dots illustrate measured values and are averages of three analyzed images. Inserted panel illustrates total hydraulic resistance (R_{tot}) plotted against inverse tree height in a log–log scaled graph, where solid line indicates linear regression (y = -1.40x - 2.95), long dashed lines indicate 95% confidence intervals, and short dashed lines indicate 95% prediction intervals. Coefficient of determination is shown in figure.

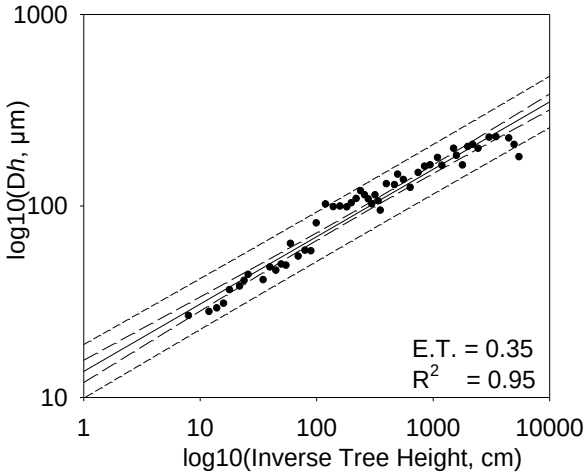

Figure S2.44: Hydraulically weighted diameters (D*h*) plotted against inverse tree height in a log–log scaled graph, where the solid line indicates the power function ($y = 13.69*x^{0.35}$), long-dashed lines indicate 95% confidence intervals and short-dashed lines indicate 95% prediction intervals. Black dots illustrate measured values and are averages of three analysed images. The degree of tapering (tapering exponent; T.E.) and coefficient of determination are shown in graph.

Eucalyptus obliqua

Figure S2.45: Habitus of *Eucalyptus obliqua*. Image illustrates one of three sampled trees.

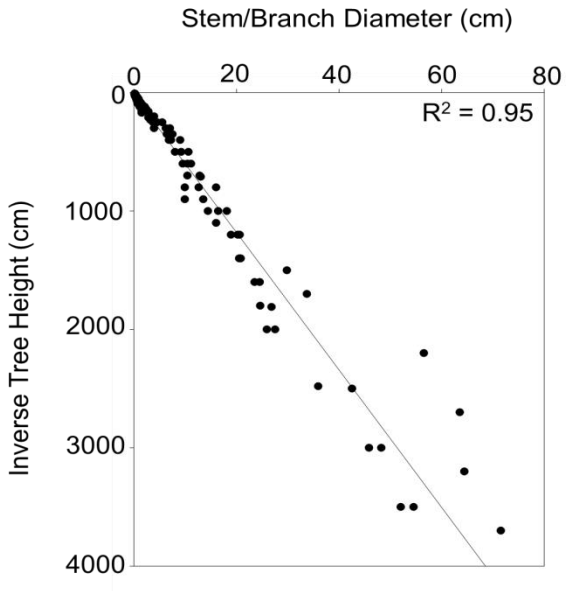

Figure S2.46: Stem and branch diameters measured at sample spots along tree main axes of all three sampled individuals. Coefficient of determination for linear regression (y = 0.02x - 0.33) is shown in figure.

Tree 1

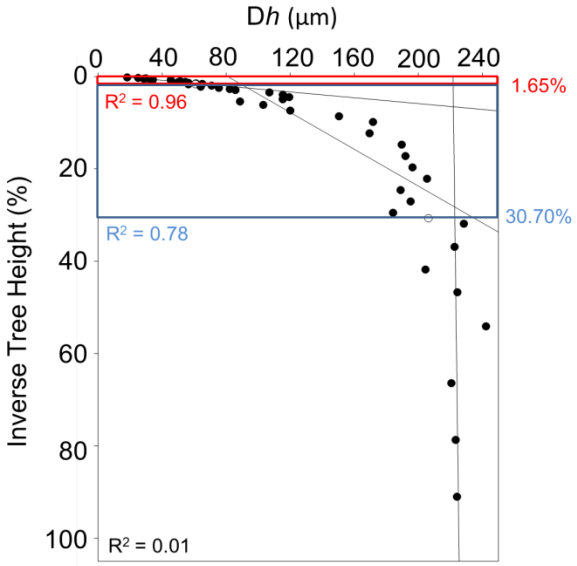

Figure S2.47: Three Phase Taper Analysis (TPTA) of changing hydraulically weighted diameters (D*h*) with inverse tree height. Black dots illustrate measured values and are averages of three analysed images. Circles are calculated medians in-between two measured values. They were not part of linear regression analyses and they do express relative tree heights of phase changes. Red box, red percentage value and red coefficient of determination (y = 0.04x + 221.69) indicate Phase 3 (steep vessel taper structure); blue box, blue percentage value and blue coefficient of determination (y = 5.01x + 81.08) indicate Phase 2 (moderate vessel taper structure); black box and black coefficient of determination (y = 31.67x + 14.97) indicate Phase 1 (no clear vessel taper structure).

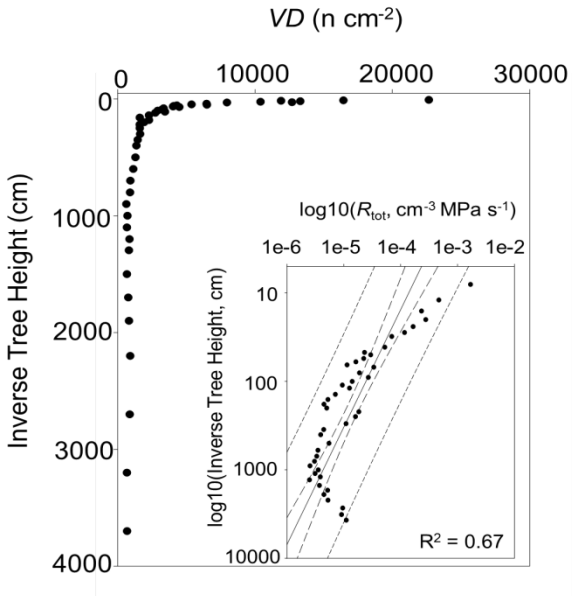

Figure S2.48: Change of vessel densities (*VD*) with inverse tree height. Black dots illustrate measured values and are averages of three analyzed images. Inserted panel illustrates total hydraulic resistance (R_{tot}) plotted against inverse tree height in a log–log scaled graph, where solid line indicates linear regression (y = -0.75x - 3.11), long dashed lines indicate 95% confidence intervals, and short dashed lines indicate 95% prediction intervals. Coefficient of determination is shown in figure.

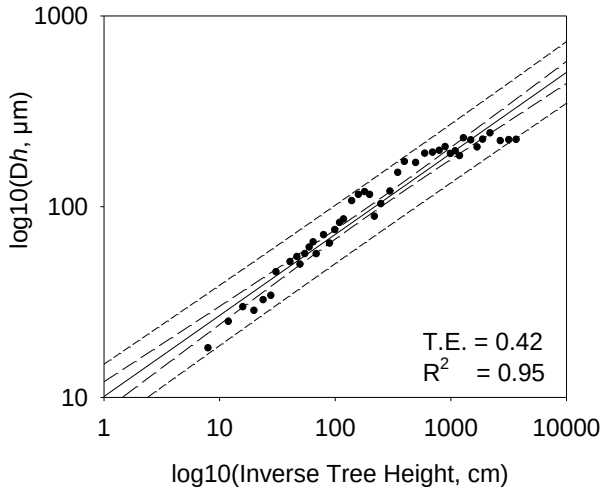

Figure S2.49: Hydraulically weighted diameters (D*h*) plotted against inverse tree height in a log–log scaled graph, where the solid line indicates the power function ($y = 10.11*x^{0.42}$), long-dashed lines indicate 95% confidence intervals and short-dashed lines indicate 95% prediction intervals. Black dots illustrate measured values and are averages of three analysed images. The degree of tapering (tapering exponent; T.E.) and coefficient of determination are shown in graph.

Tree 2

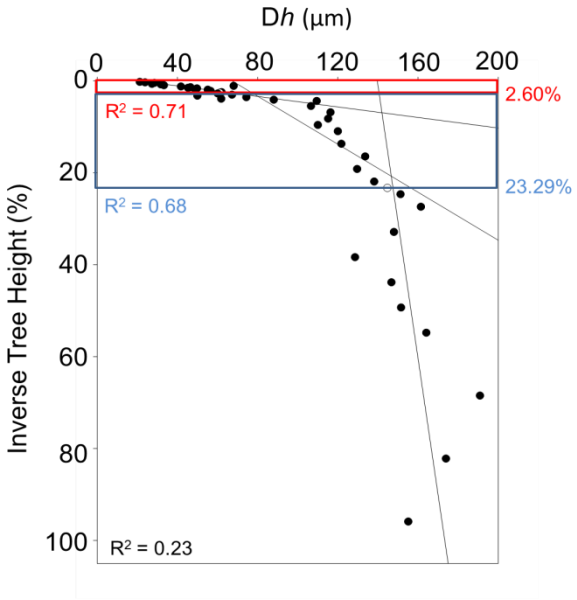

Figure S2.50: Three Phase Taper Analysis (TPTA) of changing hydraulically weighted diameters (D*h*) with inverse tree height. Black dots illustrate measured values and are averages of three analysed images. Circles are calculated medians in-between two measured values. They were not part of linear regression analyses and they do express relative tree heights of phase changes. Red box, red percentage value and red coefficient of determination (y = 17.46x + 21.02) indicate Phase 3 (steep vessel taper structure); blue box, blue percentage value and blue coefficient of determination (y = 3.83x + 67.22) indicate Phase 2 (moderate vessel taper structure); black box and black coefficient of determination (y = 0.34x + 139.67) indicate Phase 1 (no clear vessel taper structure).

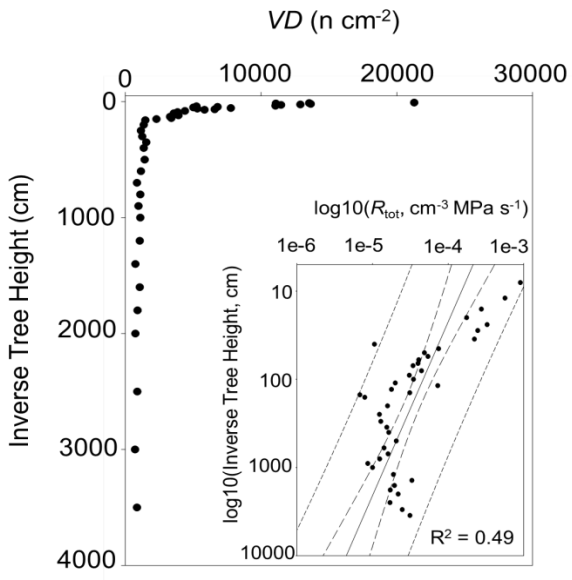

Figure S2.51: Change of vessel densities (*VD*) with inverse tree height. Black dots illustrate measured values and are averages of three analyzed images. Inserted panel illustrates total hydraulic resistance (R_{tot}) plotted against inverse tree height in a log–log scaled graph, where solid line indicates linear regression (y = -0.51x - 3.31), long dashed lines indicate 95% confidence intervals, and short dashed lines indicate 95% prediction intervals. Coefficient of determination is shown in figure.

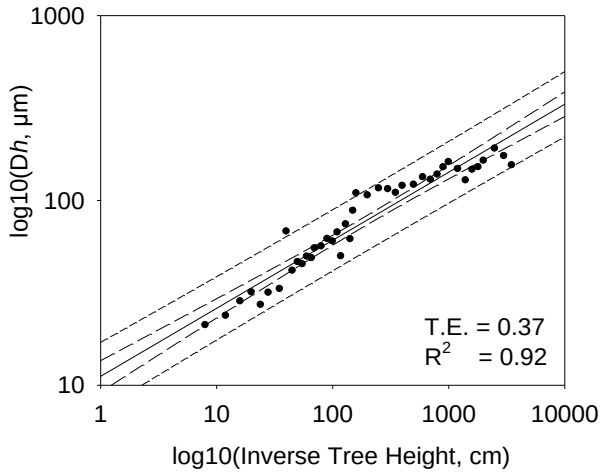

Figure S2.52: Hydraulically weighted diameters (D*h*) plotted against inverse tree height in a log–log scaled graph, where the solid line indicates the power function ($y = 11.17*x^{0.37}$), long-dashed lines indicate 95% confidence intervals and short-dashed lines indicate 95% prediction intervals. Black dots illustrate measured values and are averages of three analysed images. The degree of tapering (tapering exponent; T.E.) and Coefficient of determination are shown in graph.

Tree 3

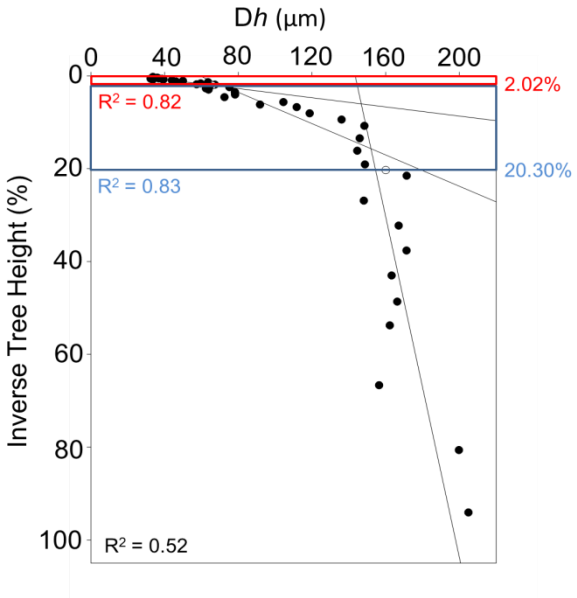

Figure S2.53: Three Phase Taper Analysis (TPTA) of changing hydraulically weighted diameters (D*h*) with inverse tree height. Black dots illustrate measured values and are averages of three analysed images. Circles are calculated medians in-between two measured values. They were not part of linear regression analyses and they do express relative tree heights of phase changes. Red box, red percentage value and red coefficient of determination (y = 20.19x + 25.15) indicate Phase 3 (steep vessel taper structure); blue box, blue percentage value and blue coefficient of determination (y = 5.93x + 59.14) indicate Phase 2 (moderate vessel taper structure); black box and black coefficient of determination (y = 0.54x + 143.47) indicate Phase 1 (no clear vessel taper structure).

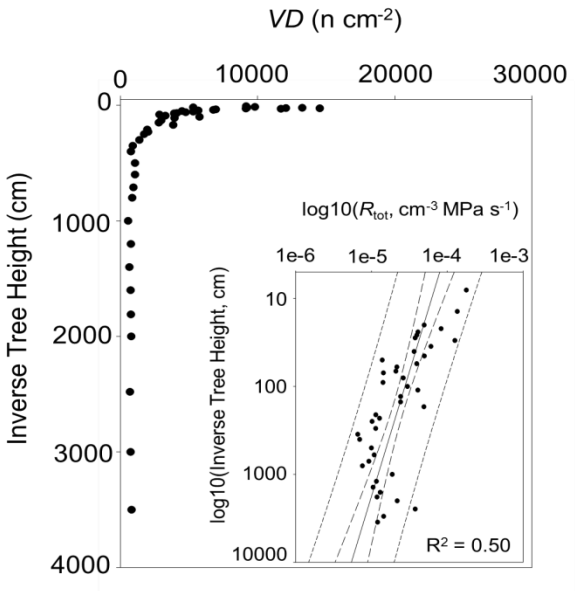

Figure S2.54: Change of vessel densities (*VD*) with inverse tree height. Black dots illustrate measured values and are averages of three analyzed images. Inserted panel illustrates total hydraulic resistance (R_{tot}) plotted against inverse tree height in a log–log scaled graph, where solid line indicates linear regression (y = -0.35x - 3.85), long dashed lines indicate 95% confidence intervals, and short dashed lines indicate 95% prediction intervals. Coefficient of determination is shown in figure.

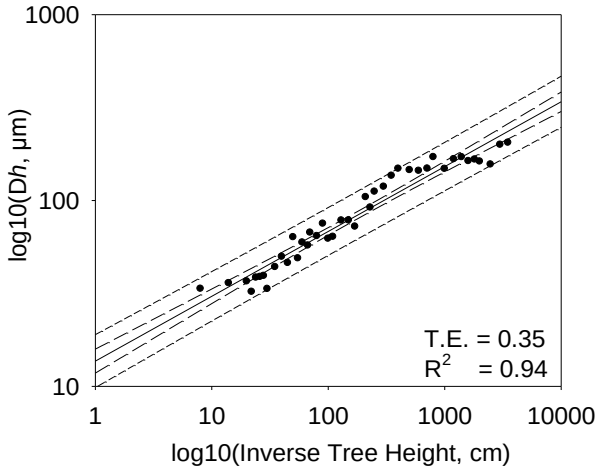

Figure S2.55: Hydraulically weighted diameters (D*h*) plotted against inverse tree height in a log–log scaled graph, where the solid line indicates the power function ($y = 13.67*x^{0.35}$), long-dashed lines indicate 95% confidence intervals and short-dashed lines indicate 95% prediction intervals. Black dots illustrate measured values and are averages of three analysed images. The degree of tapering (tapering exponent; T.E.) and coefficient of determination are shown in graph.

Eucalyptus melliodora

Figure S2.56: Habitus of *Eucalyptus melliodora*. Image illustrates one of three sampled trees.

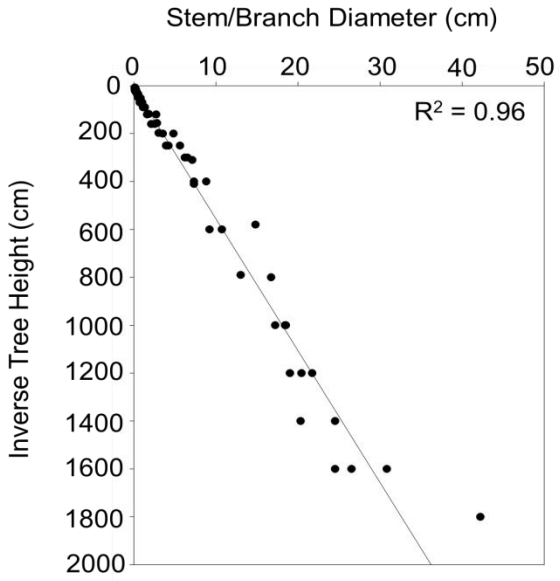

Figure S2.57: Stem and branch diameters measured at sample spots along tree main axes of all three sampled individuals. Coefficient of determination for linear regression (y = 0.02x - 0.09) is shown in figure.

Tree 1

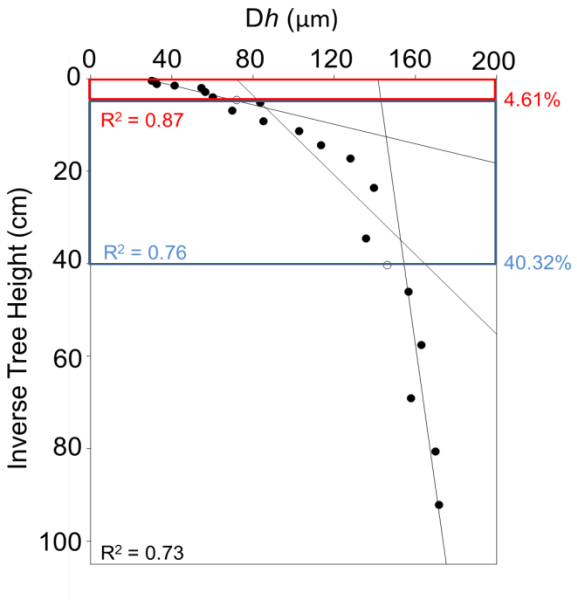

Figure S2.58: Three Phase Taper Analysis (TPTA) of changing hydraulically weighted diameters (D*h*) with inverse tree height. Black dots illustrate measured values and are averages of three analysed images. Circles are calculated medians in-between two measured values. They were not part of linear regression analyses and they do express relative tree heights of phase changes. Red box, red percentage value and red coefficient of determination (y = 9.49x + 26.55) indicate Phase 3 (steep vessel taper structure); blue box, blue percentage value and blue coefficient of determination (y = 2.32x + 71.60) indicate Phase 2 (moderate vessel taper structure); black box and black coefficient of determination (y = -0.32x + 141.57) indicate Phase 1 (no clear vessel taper structure).

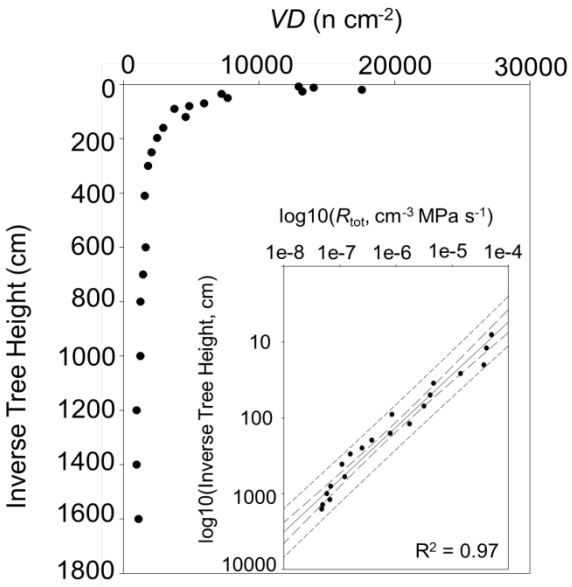

Figure S2.59: Change of vessel densities (*VD*) with inverse tree height. Black dots illustrate measured values and are averages of three analyzed images. Inserted panel illustrates total hydraulic resistance (R_{tot}) plotted against inverse tree height in a log–log scaled graph, where solid line indicates linear regression (y = -1.44x - 2.94), long dashed lines indicate 95% confidence intervals, and short dashed lines indicate 95% prediction intervals. Coefficient of determination is shown in figure.

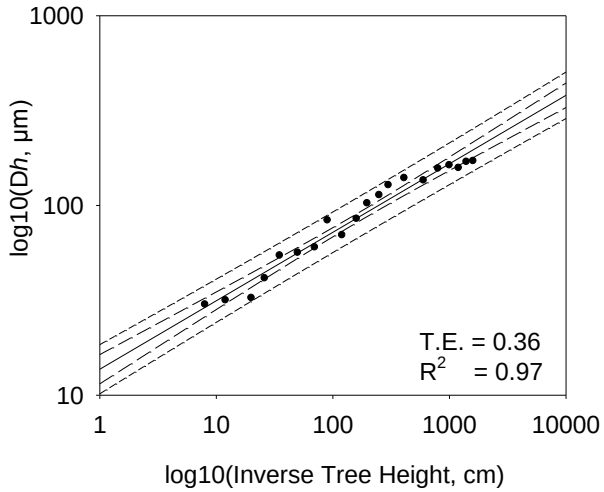

Figure S2.60: Hydraulically weighted diameters (D*h*) plotted against inverse tree height in a log–log scaled graph, where the solid line indicates the power function ($y = 13.71*x^{0.36}$), long-dashed lines indicate 95% confidence intervals and short-dashed lines indicate 95% prediction intervals. Black dots illustrate measured values and are averages of three analysed images. The degree of tapering (tapering exponent; T.E.) and coefficient of determination are shown in graph.

Tree 2

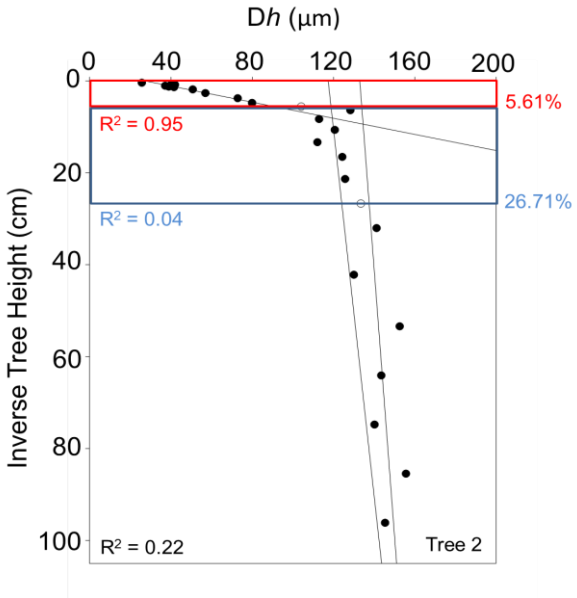

Figure S2.61: Three Phase Taper Analysis (TPTA) of changing hydraulically weighted diameters (Dh) with inverse tree height. Black dots illustrate measured values and are averages of three analysed images. Circles are calculated medians in-between two measured values. They were not part of linear regression analyses and they do express relative tree heights of phase changes. Red box, red percentage value and red coefficient of determination (y = 11.41x + 27.05) indicate Phase 3 (steep vessel taper structure); blue box, blue percentage value and blue coefficient of determination (y = 0.25x + 117.43) indicate Phase 2 (moderate vessel taper structure); black box and black coefficient of determination (y = 0.17x + 132.98) indicate Phase 1 (no clear vessel taper structure).

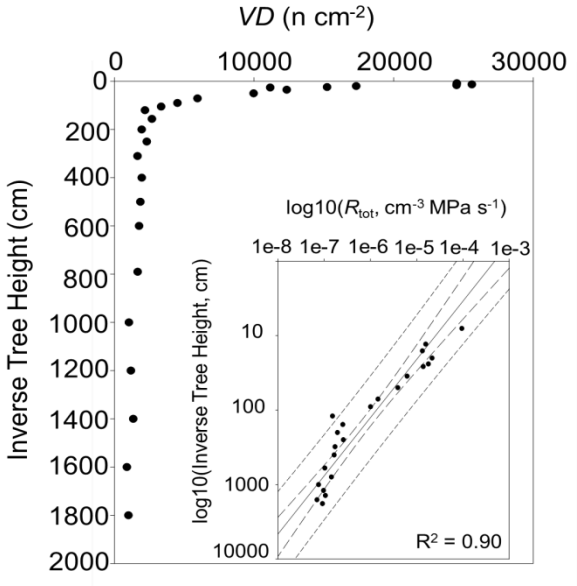

Figure S2.62: Change of vessel densities (*VD*) with inverse tree height. Black dots illustrate measured values and are averages of three analyzed images. Inserted panel illustrates total hydraulic resistance (R_{tot}) plotted against inverse tree height in a log–log scaled graph, where solid line indicates linear regression (y = -1.28x - 3.31), long dashed lines indicate 95% confidence intervals, and short dashed lines indicate 95% prediction intervals. Coefficient of determination is shown in figure.

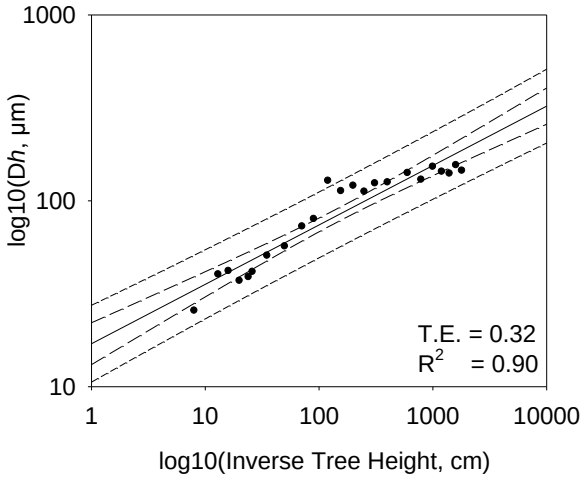

Figure S2.63: Hydraulically weighted diameters (D*h*) plotted against inverse tree height in a log–log scaled graph, where the solid line indicates the power function ($y = 17.03*x^{0.32}$), long-dashed lines indicate 95% confidence intervals and short-dashed lines indicate 95% prediction intervals. Black dots illustrate measured values and are averages of three analysed images. The degree of tapering (tapering exponent; T.E.) and coefficient of determination are shown in graph.

Tree 3

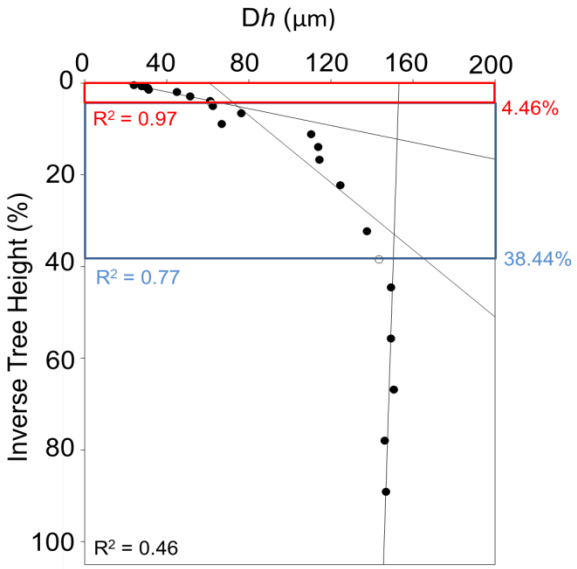

Figure S2.64: Three Phase Taper Analysis (TPTA) of changing hydraulically weighted diameters (D*h*) with inverse tree height. Black dots illustrate measured values and are averages of three analysed images. Circles are calculated medians in-between two measured values. They were not part of linear regression analyses and they do express relative tree heights of phase changes. Red box, red percentage value and red coefficient of determination (y = 10.89x + 19.48) indicate Phase 3 (steep vessel taper structure); blue box, blue percentage value and blue coefficient of determination (y = 2.73x + 60.84) indicate Phase 2 (moderate vessel taper structure); black box and black coefficient of determination (y = -0.07x + 153.18) indicate Phase 1 (no clear vessel taper structure).

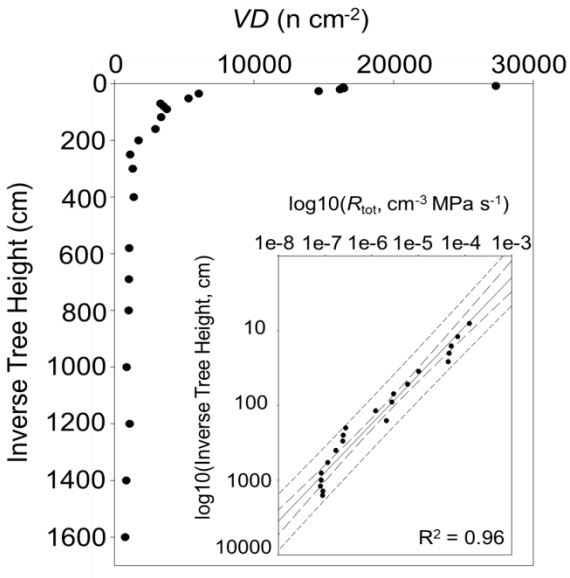

Figure S2.65: Change of vessel densities (*VD*) with inverse tree height. Black dots illustrate measured values and are averages of three analyzed images. Inserted panel illustrates total hydraulic resistance (R_{tot}) plotted against inverse tree height in a log–log scaled graph, where solid line indicates linear regression (y = -1.54x - 2.55), long dashed lines indicate 95% confidence intervals, and short dashed lines indicate 95% prediction intervals. Coefficient of determination is shown in figure.

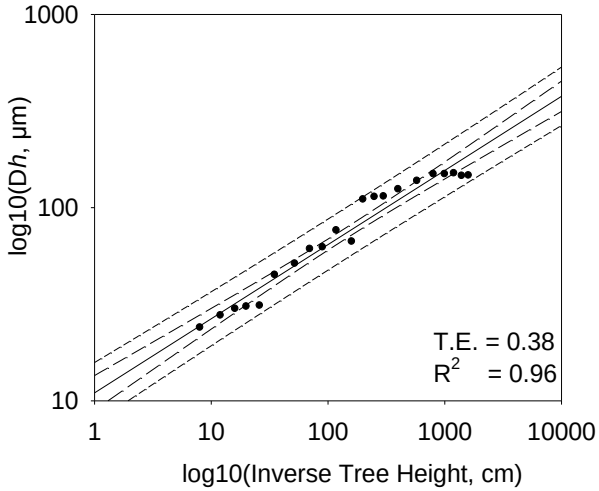

Figure S2.66: Hydraulically weighted diameters (D*h*) plotted against inverse tree height in a log–log scaled graph, where the solid line indicates the power function ($y = 10.99*x^{0.38}$), long-dashed lines indicate 95% confidence intervals and short-dashed lines indicate 95% prediction intervals. Black dots illustrate measured values and are averages of three analysed images. The degree of tapering (tapering exponent; T.E.) and coefficient of determination are shown in graph.

Eucalyptus baxteri

Figure S2.67: Habitus of *Eucalyptus baxteri*. Image illustrates one of three sampled trees.

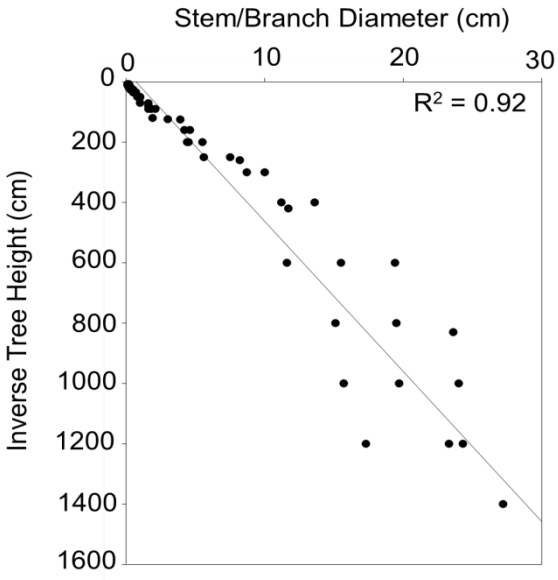

Figure S2.68: Stem and branch diameters measured at sample spots along tree main axes of all three sampled individuals. Coefficient of determination for linear regression (y = 0.03x -1) is shown in figure.

Tree 1

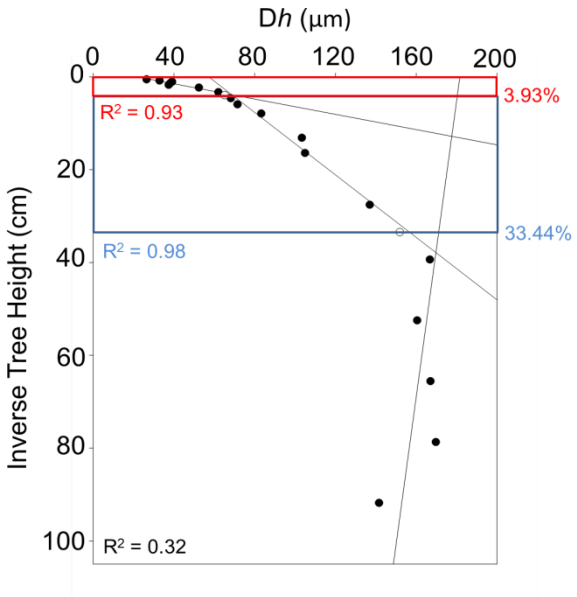

Figure S2.69: Three Phase Taper Analysis (TPTA) of changing hydraulically weighted diameters (D*h*) with inverse tree height. Black dots illustrate measured values and are averages of three analysed images. Circles are calculated medians in-between two measured values. They were not part of linear regression analyses and they do express relative tree heights of phase changes. Red box, red percentage value and red coefficient of determination (y = 12.15x + 22.08) indicate Phase 3 (steep vessel taper structure); blue box, blue percentage value and blue coefficient of determination (y = 2.97x + 57.25) indicate Phase 2 (moderate vessel taper structure); black box and black coefficient of determination (y = -0.31x + 181.56) indicate Phase 1 (no clear vessel taper structure).

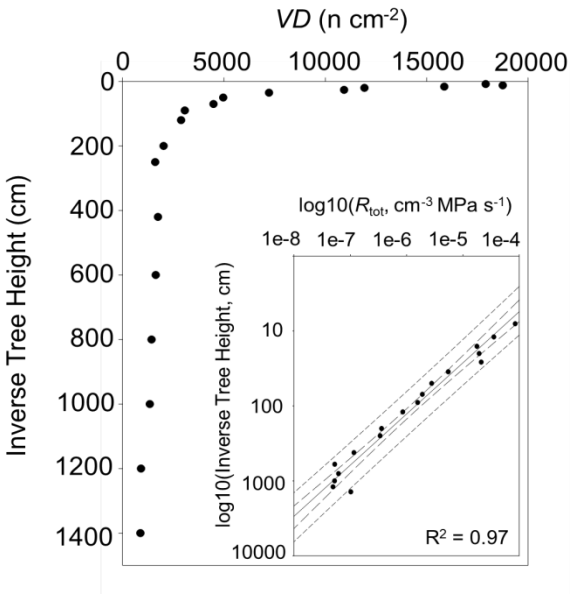

Figure S2.70: Change of vessel densities (*VD*) with inverse tree height. Black dots illustrate measured values and are averages of three analyzed images. Inserted panel illustrates total hydraulic resistance (R_{tot}) plotted against inverse tree height in a log–log scaled graph, where solid line indicates linear regression (y = -1.47x – 2.91), long dashed lines indicate 95% confidence intervals, and short dashed lines indicate 95% prediction intervals. Coefficient of determination is shown in figure.

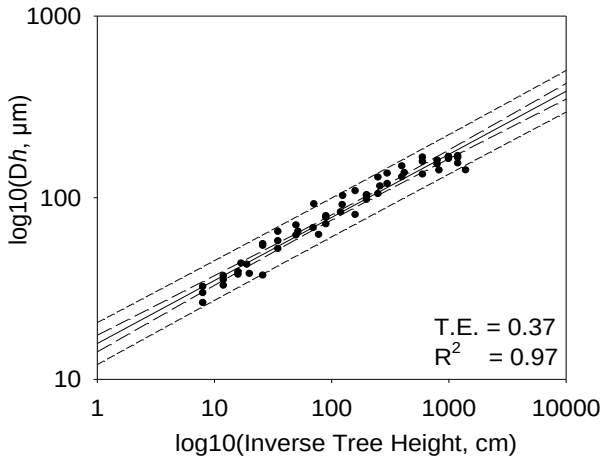

Figure S2.71: Hydraulically weighted diameters (D*h*) plotted against inverse tree height in a log–log scaled graph, where the solid line indicates the power function ($y = 13.50*x^{0.37}$), long-dashed lines indicate 95% confidence intervals and short-dashed lines indicate 95% prediction intervals. Black dots illustrate measured values and are averages of three analysed images. The degree of tapering (tapering exponent; T.E.) and coefficient of determination are shown in graph.

Tree 2

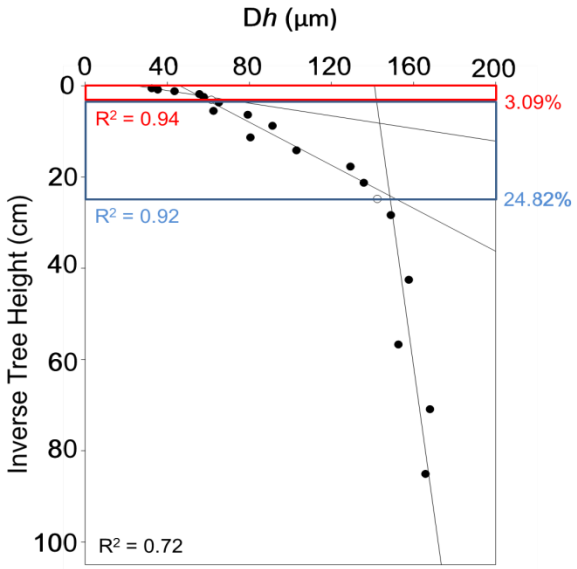

Figure S2.72: Three Phase Taper Analysis (TPTA) of changing hydraulically weighted diameters (D*h*) with inverse tree height. Black dots illustrate measured values and are averages of three analysed images. Circles are calculated medians in-between two measured values. They were not part of linear regression analyses and they do express relative tree heights of phase changes. Red box, red percentage value and red coefficient of determination (y = 14.42x + 24.80) indicate Phase 3 (steep vessel taper structure); blue box, blue percentage value and blue coefficient of determination (y = 4.24x + 46.07) indicate Phase 2 (moderate vessel taper structure); black box and black coefficient of determination (y = 0.31x + 181.56) indicate Phase 1 (no clear vessel taper structure).

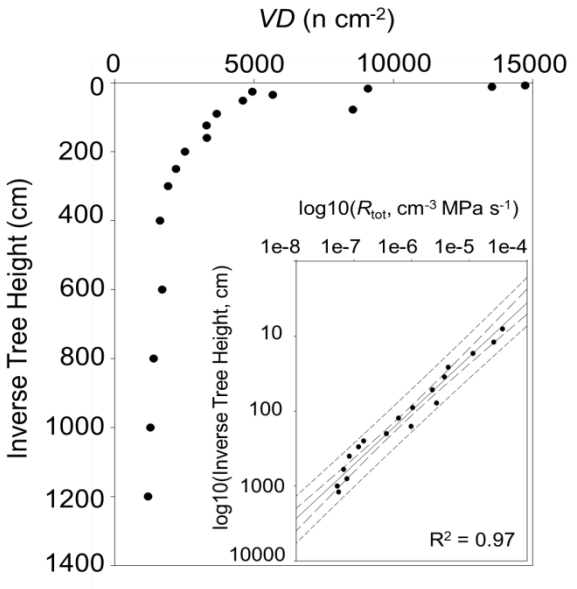

Figure S2.73: Change of vessel densities (VD) with inverse tree height. Black dots illustrate measured values and are averages of three analysed images. Inserted panel illustrates total hydraulic resistance (R_{tot}) plotted against inverse tree height in a log–log scaled graph, where solid line indicates linear regression (y = -1.39x – 3.23), long dashed lines indicate 95% confidence intervals, and short dashed lines indicate 95% prediction intervals. Coefficient of determination is shown in figure.

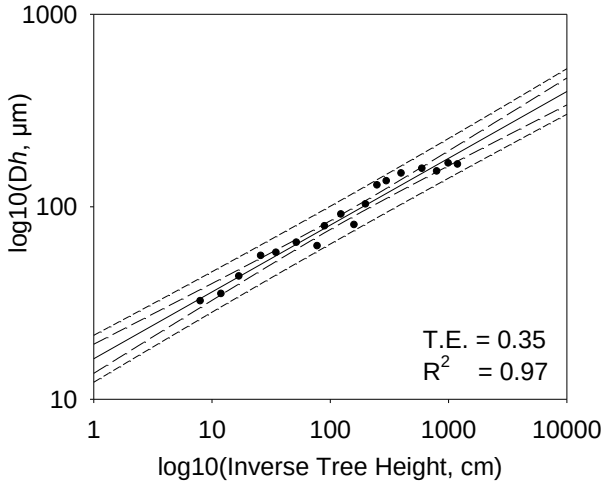

Figure S2.74: Hydraulically weighted diameters (D*h*) plotted against inverse tree height in a log–log scaled graph, where the solid line indicates the power function ($y = 16.23*x^{0.35}$), long-dashed lines indicate 95% confidence intervals and short-dashed lines indicate 95% prediction intervals. Black dots illustrate measured values and are averages of three analysed images. The degree of tapering (tapering exponent; T.E.) and coefficient of determination are shown in graph.

Tree 3

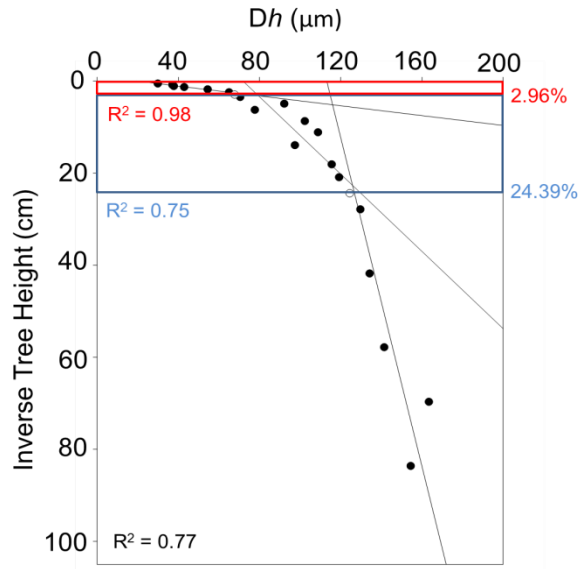

Figure S2.75: Three Phase Taper Analysis (TPTA) of changing hydraulically weighted diameters (D*h*) with inverse tree height. Black dots illustrate measured values and are averages of three analysed images. Circles are calculated medians in-between two measured values. They were not part of linear regression analyses and they do express relative tree heights of phase changes. Red box, red percentage value and red coefficient of determination (y = 18.70x + 19.25) indicate Phase 3 (steep vessel taper structure); blue box, blue percentage value and blue coefficient of determination (y = 2.38x + 71.81) indicate Phase 2 (moderate vessel taper structure); black box and black coefficient of determination (y = 0.56x + 113.10) indicate Phase 1 (no clear vessel taper structure).

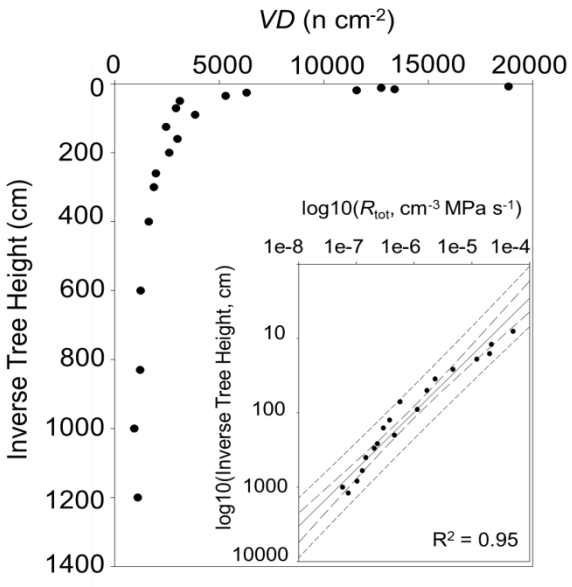

Figure S2.76: Change of vessel densities (VD) with inverse tree height. Black dots illustrate measured values and are averages of three analysed images. Inserted panel illustrates total hydraulic resistance (R_{tot}) plotted against inverse tree height in a log–log scaled graph, where solid line indicates linear regression (y = -1.31x – 3.40), long dashed lines indicate 95% confidence intervals, and short dashed lines indicate 95% prediction intervals. Coefficient of determination is shown in figure.

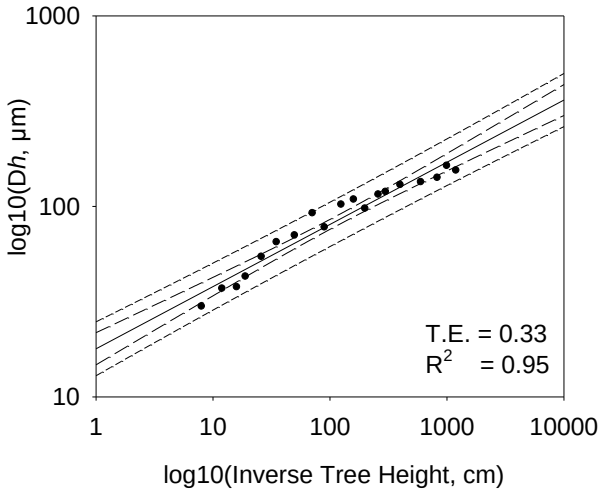

Figure S2.77: Hydraulically weighted diameters (D*h*) plotted against inverse tree height in a log–log scaled graph, where the solid line indicates the power function ($y = 17.90*x^{0.33}$), long-dashed lines indicate 95% confidence intervals and short-dashed lines indicate 95% prediction intervals. Black dots illustrate measured values and are averages of three analysed images. The degree of tapering (tapering exponent; T.E.) and coefficient of determination are shown in graph.

Eucalyptus microcarpa

Figure S2.78: Habitus of *Eucalyptus microcarpa*. Image illustrates one of three sampled trees.

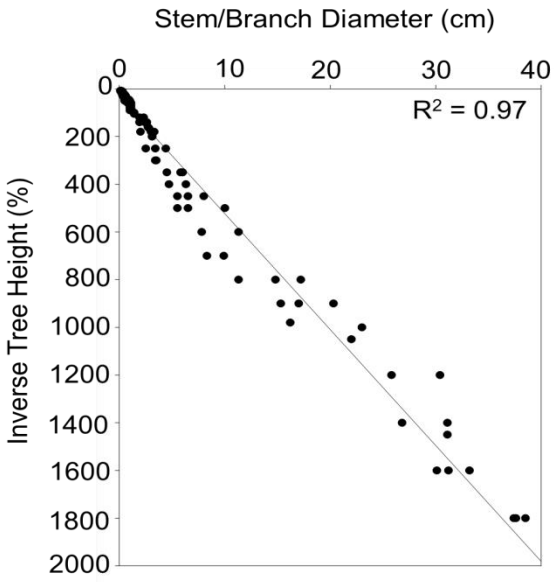

Figure S2.79: Stem and branch diameters measured at sample spots along tree main axes of all three sampled individuals. Coefficient of determination for linear regression (y = 0.02x + 0.76) is shown in figure.

Tree 1

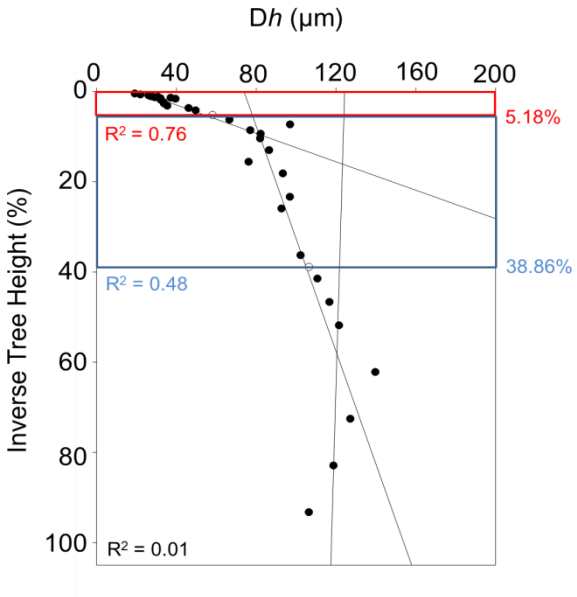

Figure S2.80: Three Phase Taper Analysis (TPTA) of changing hydraulically weighted diameters (D*h*) with inverse tree height. Black dots illustrate measured values and are averages of three analysed images. Circles are calculated medians in-between two measured values. They were not part of linear regression analyses and they do express relative tree heights of phase changes. Red box, red percentage value and red coefficient of determination (y = 6.35x + 21.29) indicate Phase 3 (steep vessel taper structure); blue box, blue percentage value and blue coefficient of determination (y = 0.80x + 73.86) indicate Phase 2 (moderate vessel taper structure); black box and black coefficient of determination (y = -0.06x + 124.33) indicate Phase 1 (no clear vessel taper structure).

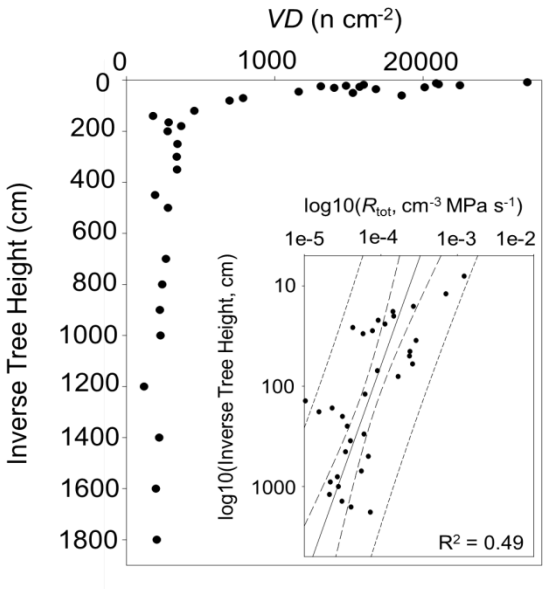

Figure S2.81: Change of vessel density (*VD*) with inverse tree height. Black dots illustrate measured values and are averages of three analyzed images. Inserted panel illustrates total hydraulic resistance (R_{tot}) plotted against inverse tree height in a log–log scaled graph, where solid line indicates linear regression (y = -0.47x - 3.16), long dashed lines indicate 95% confidence intervals, and short dashed lines indicate 95% prediction intervals. Coefficient of determination is shown in figure.

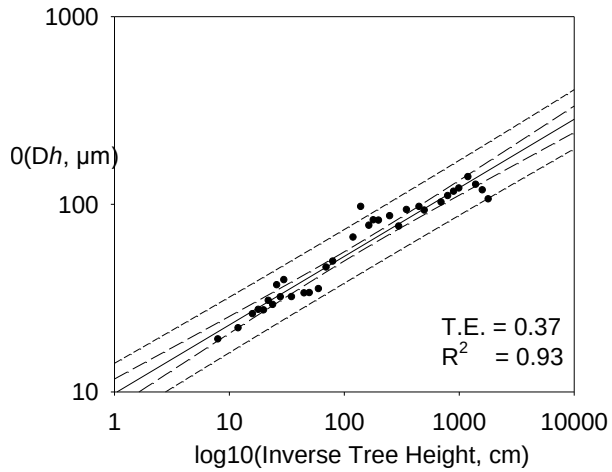

Figure S2.82: Hydraulically weighted diameters (D*h*) plotted against inverse tree height in a log–log scaled graph, where the solid line indicates the power function ($y = 9.81*x^{0.37}$), long-dashed lines indicate 95% confidence intervals and short-dashed lines indicate 95% prediction intervals. Black dots illustrate measured values and are averages of three analysed images. The degree of tapering (tapering exponent; T.E.) and coefficient of determination are shown in graph.

Tree 2

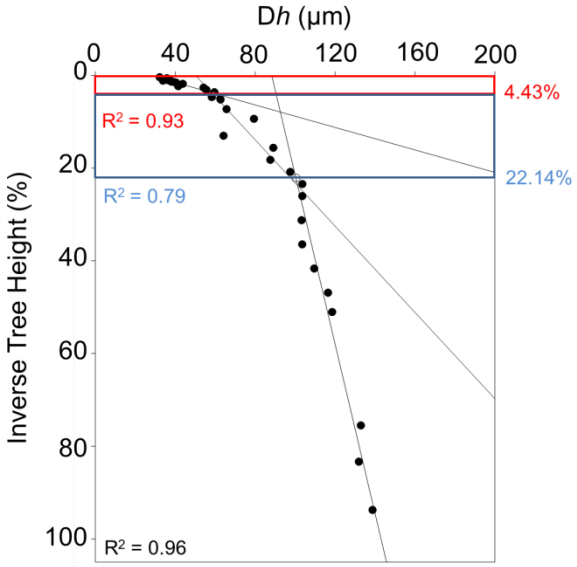

Figure S2.83: Three Phase Taper Analysis (TPTA) of changing hydraulically weighted diameters (D*h*) with inverse tree height. Black dots illustrate measured values and are averages of three analysed images. Circles are calculated medians in-between two measured values. They were not part of linear regression analyses and they do express relative tree heights of phase changes. Red box, red percentage value and red coefficient of determination (y = 8.24x + 0.93) indicate Phase 3 (steep vessel taper structure); blue box, blue percentage value and blue coefficient of determination (y = 2.15x + 50.19) indicate Phase 2 (moderate vessel taper structure); black box and black coefficient of determination (y = 0.55x + 88.29) indicate Phase 1 (no clear vessel taper structure).

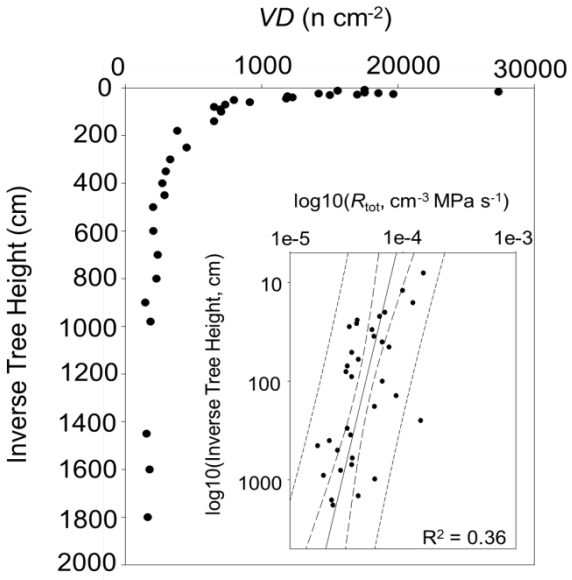

Figure S2.84: Change of vessel density (*VD*) with inverse tree height. Black dots illustrate measured values and are averages of three analyzed images. Inserted panel illustrates total hydraulic resistance (R_{tot}) plotted against inverse tree height in a log–log scaled graph, where solid line indicates linear regression (y = -0.21x - 3.91), long dashed lines indicate 95% confidence intervals, and short dashed lines indicate 95% prediction intervals. Coefficient of determination is shown in figure.

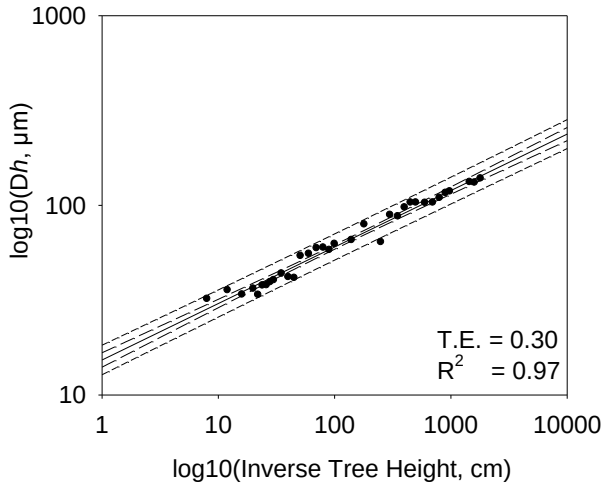

Figure S2.85: Hydraulically weighted diameters (D*h*) plotted against inverse tree height in a log–log scaled graph, where the solid line indicates the power function ($y = 15.03*x^{0.30}$), long-dashed lines indicate 95% confidence intervals and short-dashed lines indicate 95% prediction intervals. Black dots illustrate measured values and are averages of three analysed images. The degree of tapering (tapering exponent; T.E.) and coefficient of determination are shown in graph.

Tree 3

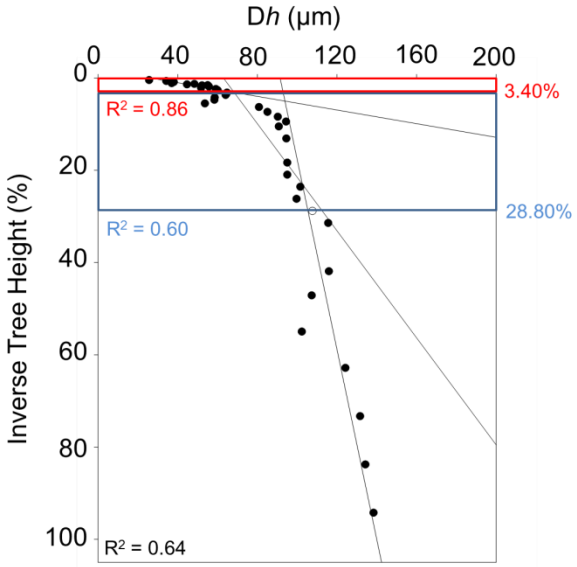

Figure S2.86: Three Phase Taper Analysis (TPTA) of changing hydraulically weighted diameters (D*h*) with inverse tree height. Black dots illustrate measured values and are averages of three analysed images. Circles are calculated medians in-between two measured values. They were not part of linear regression analyses and they do express relative tree heights of phase changes. Red box, red percentage value and red coefficient of determination (y = 13.51x + 26.60) indicate Phase 3 (steep vessel taper structure); blue box, blue percentage value and blue coefficient of determination (y = 1.72x + 63.01) indicate Phase 2 (moderate vessel taper structure); black box and black coefficient of determination (y = 0.49x + 91.47) indicate Phase 1 (no clear vessel taper structure).

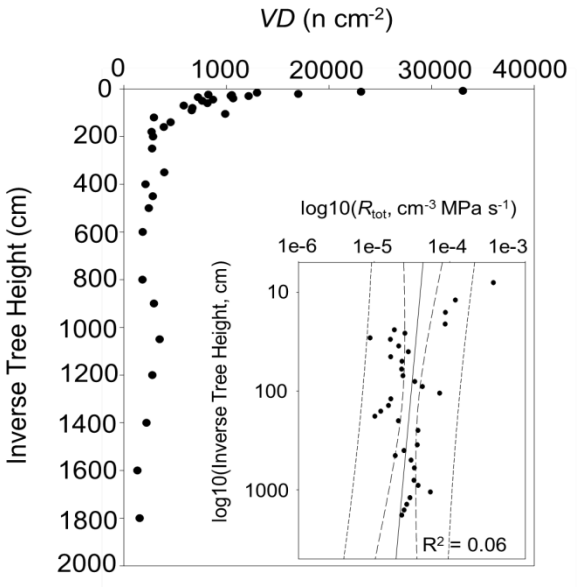

Figure S2.87: Change of vessel density (*VD*) with inverse tree height. Black dots illustrate measured values and are averages of three analyzed images. Inserted panel illustrates total hydraulic resistance (R_{tot}) plotted against inverse tree height in a log–log scaled graph, where solid line indicates linear regression (y = -0.12x - 4.27), long dashed lines indicate 95% confidence intervals, and short dashed lines indicate 95% prediction intervals. Coefficient of determination is shown in figure.

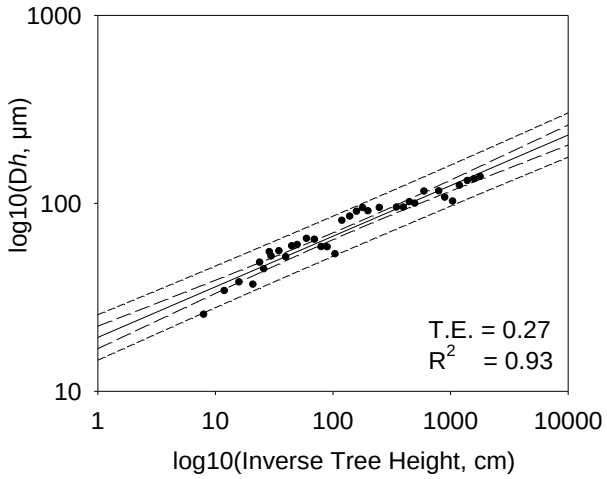

Figure S2.88: Hydraulically weighted diameters (D*h*) plotted against inverse tree height in a log–log scaled graph, where the solid line indicates the power function ($y = 19.34*x^{0.27}$), long-dashed lines indicate 95% confidence intervals and short-dashed lines indicate 95% prediction intervals. Black dots illustrate measured values and are averages of three analysed images. The degree of tapering (tapering exponent; T.E.) and coefficient of determination are shown in graph.

Eucalyptus polyanthemos

Figure S2.89: Habitus of *Eucalyptus polyanthemos*. Image illustrates one of three sampled trees.

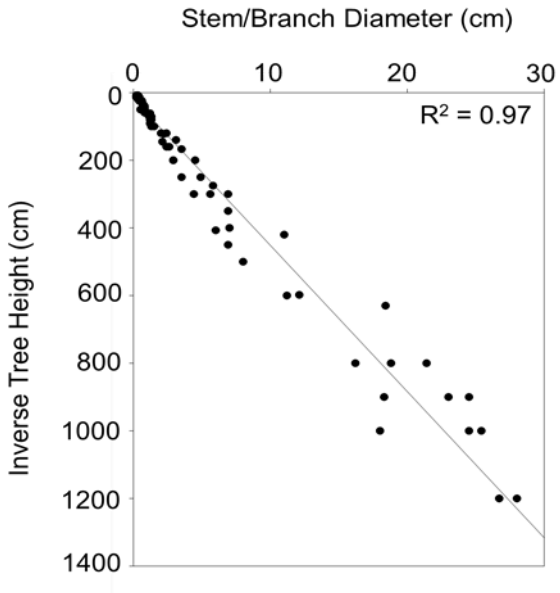

Figure S2.90: Stem and branch diameters measured at sample spots along tree main axes of all three sampled individuals. Coefficient of determination for linear regression (y = 0.02x - 0.44) is shown in figure.

Tree 1

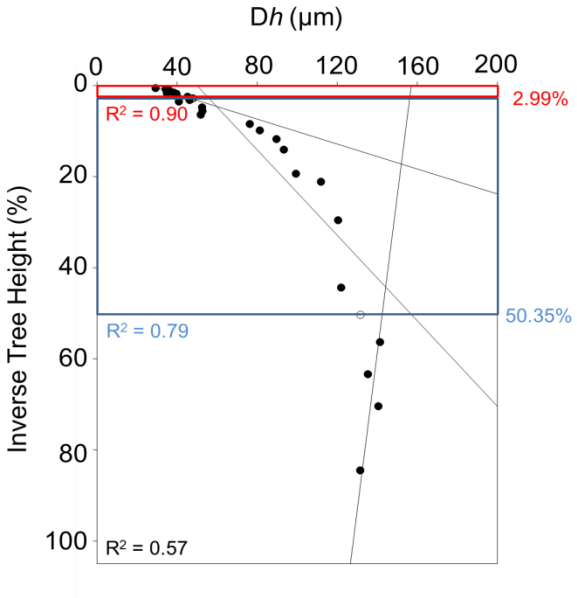

Figure S2.91: Three Phase Taper Analysis (TPTA) of changing hydraulically weighted diameters (D*h*) with inverse tree height. Black dots illustrate measured values and are averages of three analysed images. Circles are calculated medians in-between two measured values. They were not part of linear regression analyses and they do express relative tree heights of phase changes. Red box, red percentage value and red coefficient of determination (y =7.30x + 26.36) indicate Phase 3 (steep vessel taper structure); blue box, blue percentage value and blue coefficient of determination (y = 2.13x + 49.96) indicate Phase 2 (moderate vessel taper structure); black box and black coefficient of determination (y = -0.29x + 157.04) indicate Phase 1 (no clear vessel taper structure).

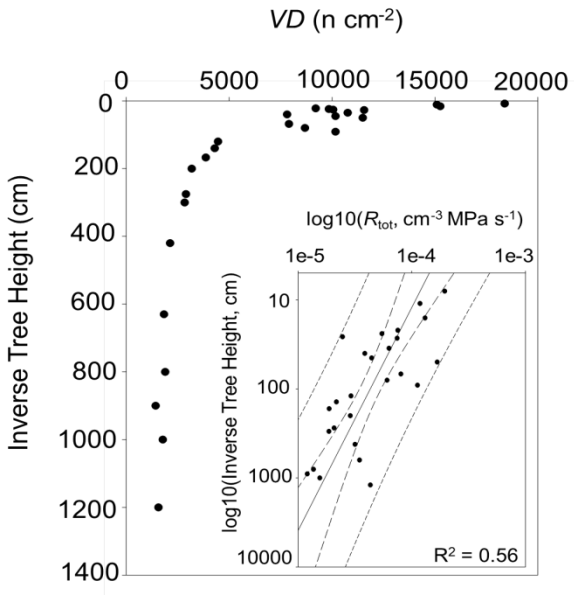

Figure S2.92: Change of vessel densities (*VD*) with inverse tree height. Black dots illustrate measured values and are averages of three analyzed images. Inserted panel illustrates total hydraulic resistance (R_{tot}) plotted against inverse tree height in a log–log scaled graph, where solid line indicates linear regression (y = -0.40x - 3.57), long dashed lines indicate 95% confidence intervals, and short dashed lines indicate 95% prediction intervals. Coefficient of determination is shown in figure.

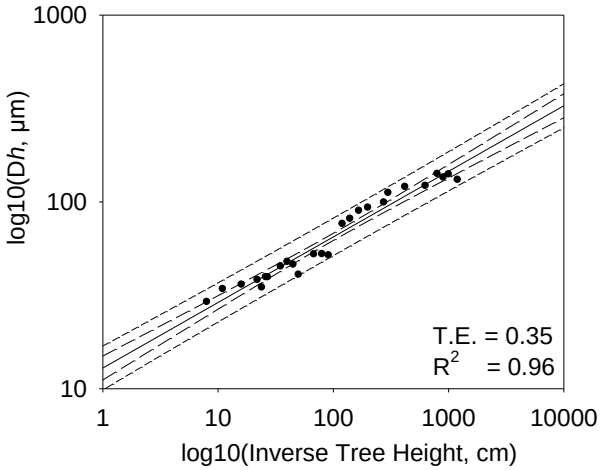

Figure S2.93: Hydraulically weighted diameters (D*h*) plotted against inverse tree height in a log–log scaled graph, where the solid line indicates the power function ($y = 12.91*x^{0.35}$), long-dashed lines indicate 95% confidence intervals and short-dashed lines indicate 95% prediction intervals. Black dots illustrate measured values and are averages of three analysed images. The degree of tapering (tapering exponent; T.E.) and coefficient of determination are shown in graph.

Tree 2

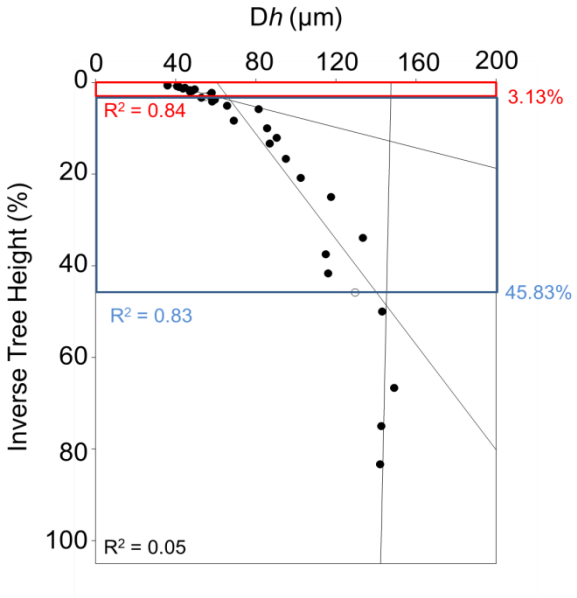

Figure S2.94: Three Phase Taper Analysis (TPTA) of changing hydraulically weighted diameters (D*h*) with inverse tree height. Black dots illustrate measured values and are averages of three analysed images. Circles are calculated medians in-between two measured values. They were not part of linear regression analyses and they do express relative tree heights of phase changes. Red box, red percentage value and red coefficient of determination (y = 8.94x + 32.61) indicate Phase 3 (steep vessel taper structure); blue box, blue percentage value and blue coefficient of determination (y = 1.74x + 60.53) indicate Phase 2 (moderate vessel taper structure); black box and black coefficient of determination (y = -0.05x + 147.54) indicate Phase 1 (no clear vessel taper structure).

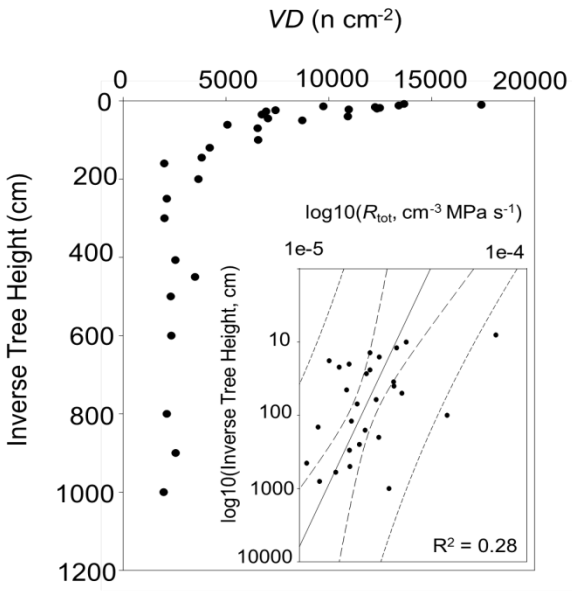

Figure S2.95: Change of vessel densities (*VD*) with inverse tree height. Black dots illustrate measured values and are averages of three analyzed images. Inserted panel illustrates total hydraulic resistance (R_{tot}) plotted against inverse tree height in a log–log scaled graph, where solid line indicates linear regression (y = -0.15x - 4.42), long dashed lines indicate 95% confidence intervals, and short dashed lines indicate 95% prediction intervals. Coefficient of determination is shown in figure.

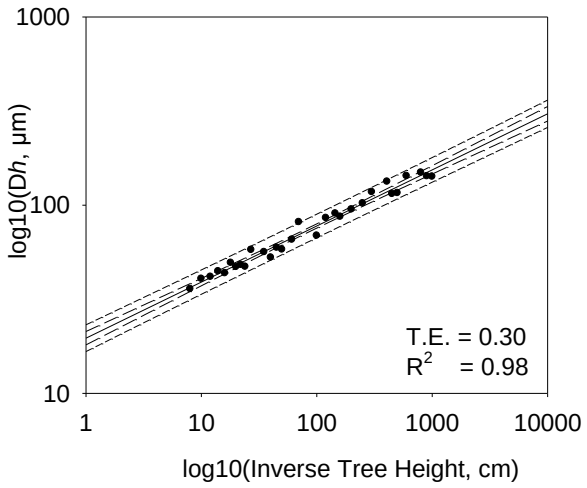

Figure S2.96: Hydraulically weighted diameters (D*h*) plotted against inverse tree height in a log–log scaled graph, where the solid line indicates the power function ($y = 19.64*x^{0.30}$), long-dashed lines indicate 95% confidence intervals and short-dashed lines indicate 95% prediction intervals. Black dots illustrate measured values and are averages of three analysed images. The degree of tapering (tapering exponent; T.E.) and coefficient of determination are shown in graph.

Tree 3

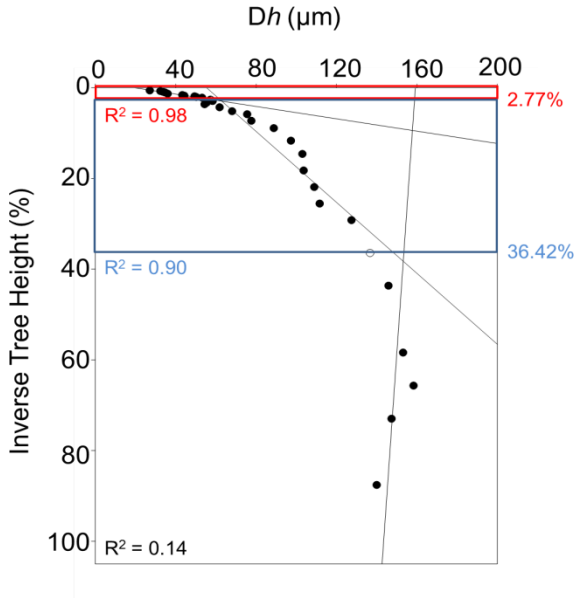

Figure S2.97: Three Phase Taper Analysis (TPTA) of changing hydraulically weighted diameters (D*h*) with inverse tree height. Black dots illustrate measured values and are averages of three analysed images. Circles are calculated medians in-between two measured values. They were not part of linear regression analyses and they do express relative tree heights of phase changes. Red box, red percentage value and red coefficient of determination (y = 14.67x + 19.65) indicate Phase 3 (steep vessel taper structure); blue box, blue percentage value and blue coefficient of determination (y = 2.56x + 55.39) indicate Phase 2 (moderate vessel taper structure); black box and black coefficient of determination (y = -0.16x + 159.24) indicate Phase 1 (no clear vessel taper structure).

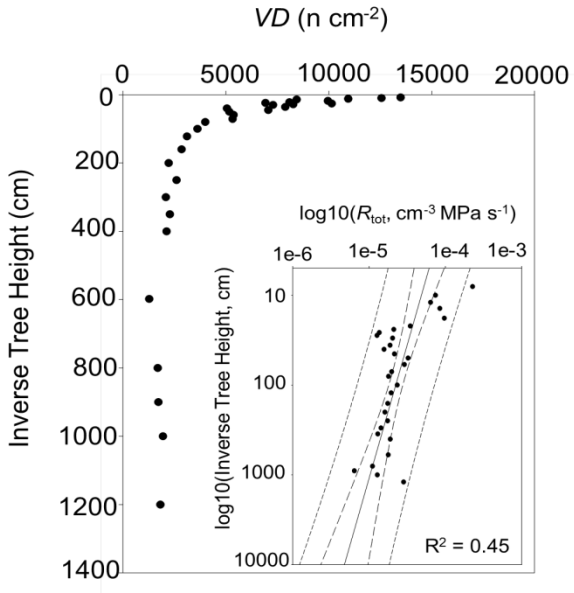

Figure S2.98: Change of vessel densities (*VD*) with inverse tree height. Black dots illustrate measured values and are averages of three analyzed images. Inserted panel illustrates total hydraulic resistance (R_{tot}) plotted against inverse tree height in a log–log scaled graph, where solid line indicates linear regression (y = -0.34x - 3.98), long dashed lines indicate 95% confidence intervals, and short dashed lines indicate 95% prediction intervals. Coefficient of determination is shown in figure.

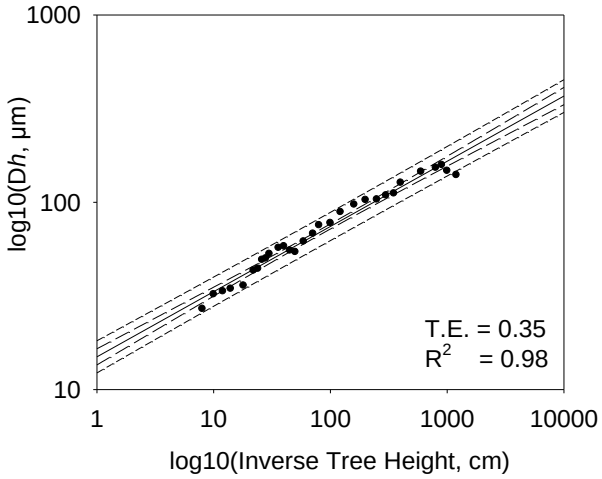

Figure S2.99: Hydraulically weighted diameters (D*h*) plotted against inverse tree height in a log–log scaled graph, where the solid line indicates the power function ($y = 14.95*x^{0.35}$), long-dashed lines indicate 95% confidence intervals and short-dashed lines indicate 95% prediction intervals. Black dots illustrate measured values and are averages of three analysed images. The degree of tapering (tapering exponent; T.E.) and coefficient of determination are shown in graph.

Eucalyptus gracilis

Figure S2.100: Habitus of *Eucalyptus gracilis*. Image illustrates one of three sampled trees.

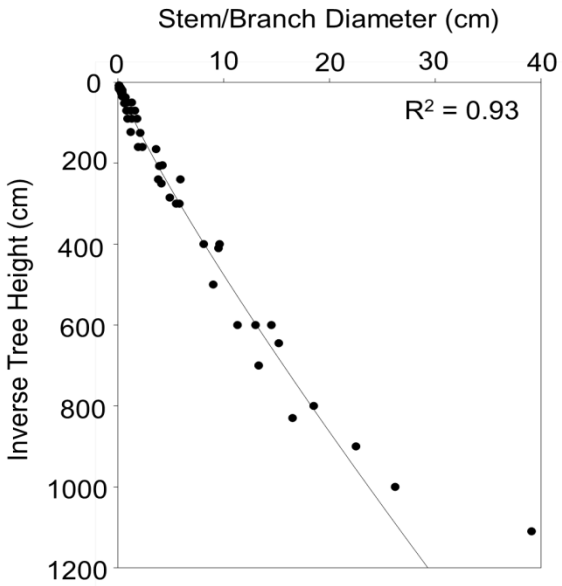

Figure S2.101: Stem and branch diameters measured at sample spots along tree main axes of all three sampled individuals. Coefficients of determination for linear regression (y = 0.03x - 1) is shown in figure.

Tree 1

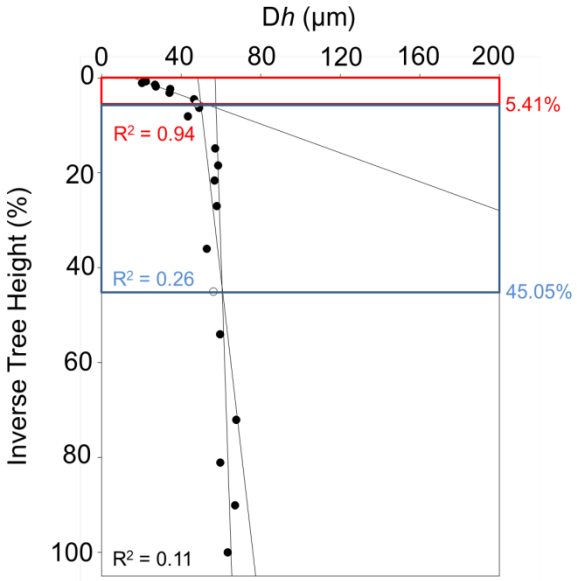

Figure S2.102: Three Phase Taper Analysis (TPTA) of changing hydraulically weighted diameters (D*h*) with inverse tree height. Black dots illustrate measured values and are averages of three analysed images. Circles are calculated medians in-between two measured values. They were not part of linear regression analyses and they do express relative tree heights of phase changes. Red box, red percentage value and red coefficient of determination (y = 6.58x + 16.06) indicate Phase 3 (steep vessel taper structure); blue box, blue percentage value and blue coefficient of determination (y = 0.28x + 48.36) indicate Phase 2 (moderate vessel taper structure); black box and black coefficient of determination (y = 0.08x + 57.04) indicate Phase 1 (no clear vessel taper structure).

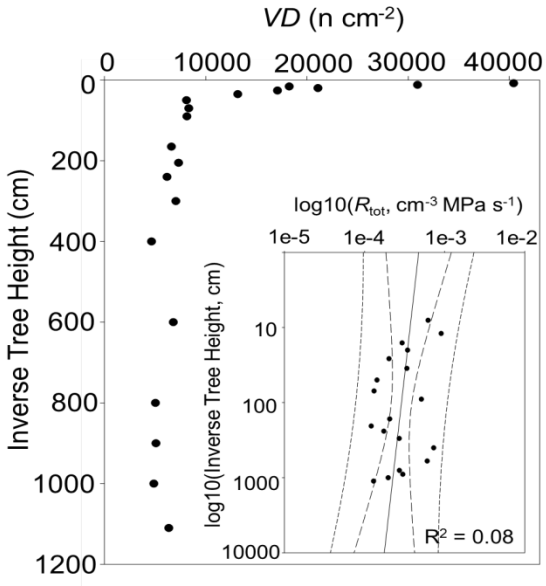

Figure S2.103: Change of vessel densities (*VD*) with inverse tree height. Black dots illustrate measured values and are averages of three analyzed images. Inserted panel illustrates total hydraulic resistance (R_{tot}) plotted against inverse tree height in a log–log scaled graph, where solid line indicates linear regression (y = -0.11x - 3.32), long dashed lines indicate 95% confidence intervals, and short dashed lines indicate 95% prediction intervals. Coefficient of determination is shown in figure.

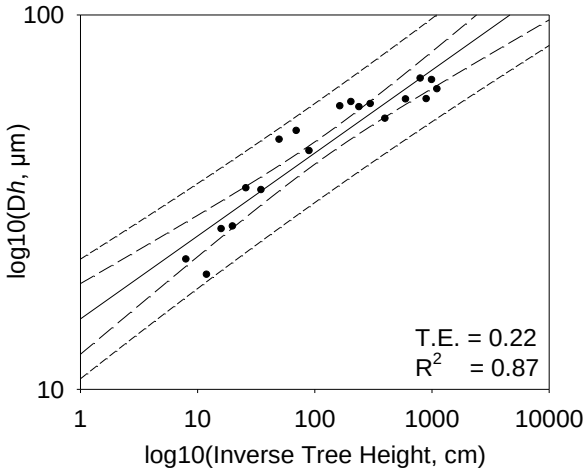

Figure S2.104: Hydraulically weighted diameters (D*h*) plotted against inverse tree height in a log–log scaled graph, where the solid line indicates the power function ($y = 15.42*x^{0.22}$), long-dashed lines indicate 95% confidence intervals and short-dashed lines indicate 95% prediction intervals. Black dots illustrate measured values and are averages of three analysed images. The degree of tapering (tapering exponent; T.E.) and coefficient of determination are shown in graph.

Tree 2

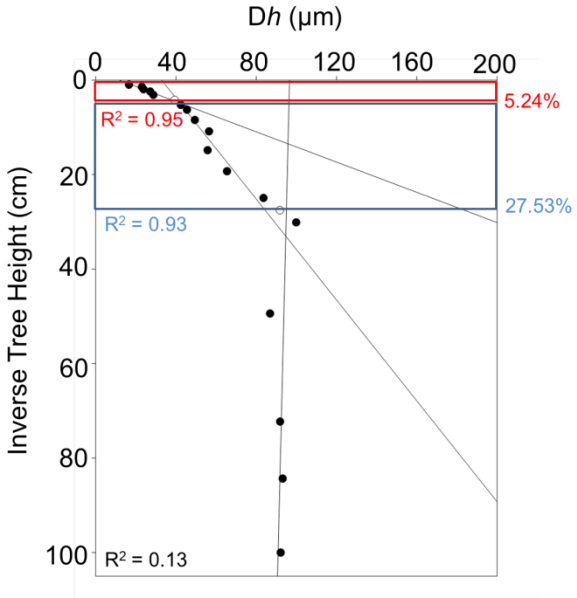

Figure S2.105: Three Phase Taper Analysis (TPTA) of changing hydraulically weighted diameters (D*h*) with inverse tree height. Black dots illustrate measured values and are averages of three analysed images. Circles are calculated medians in-between two measured values. They were not part of linear regression analyses and they do express relative tree heights of phase changes. Red box, red percentage value and red coefficient of determination (y = 6.25x + 11.69) indicate Phase 3 (steep vessel taper structure); blue box, blue percentage value and blue coefficient of determination (y = 1.87x + 32.90) indicate Phase 2 (moderate vessel taper structure); black box and black coefficient of determination (y = -0.06x + 96.57) indicate Phase 1 (no clear vessel taper structure).

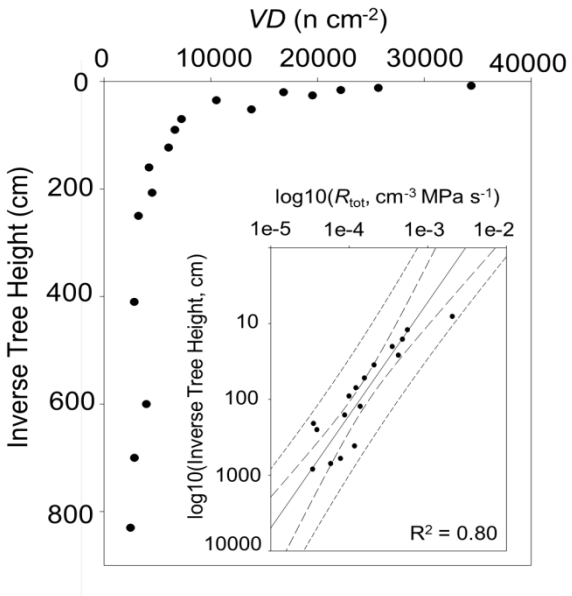

Figure S2.106: Change of vessel densities (*VD*) with inverse tree height. Black dots illustrate measured values and are averages of three analyzed images. Inserted panel illustrates total hydraulic resistance (R_{tot}) plotted against inverse tree height in a log–log scaled graph, where solid line indicates linear regression (y = -0.67x - 2.52), long dashed lines indicate 95% confidence intervals, and short dashed lines indicate 95% prediction intervals. Coefficient of determination is shown in figure.

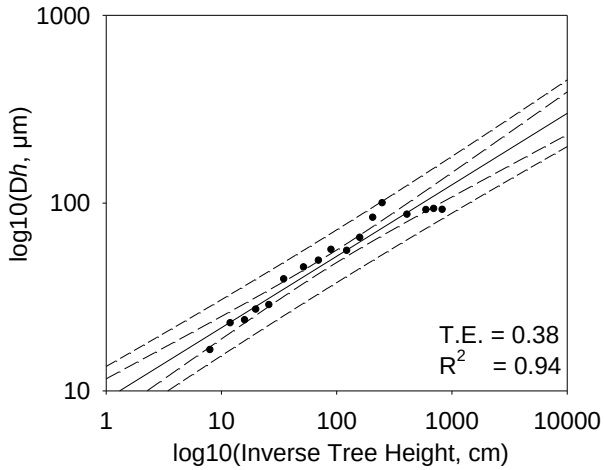

Figure S2.107: Hydraulically weighted diameters (D*h*) plotted against inverse tree height in a log–log scaled graph, where the solid line indicates the power function ($y = 9.04*x^{0.38}$), long-dashed lines indicate 95% confidence intervals and short-dashed lines indicate 95% prediction intervals. Black dots illustrate measured values and are averages of three analysed images. The degree of tapering (tapering exponent; T.E.) and coefficient of determination are shown in graph.

Tree 3

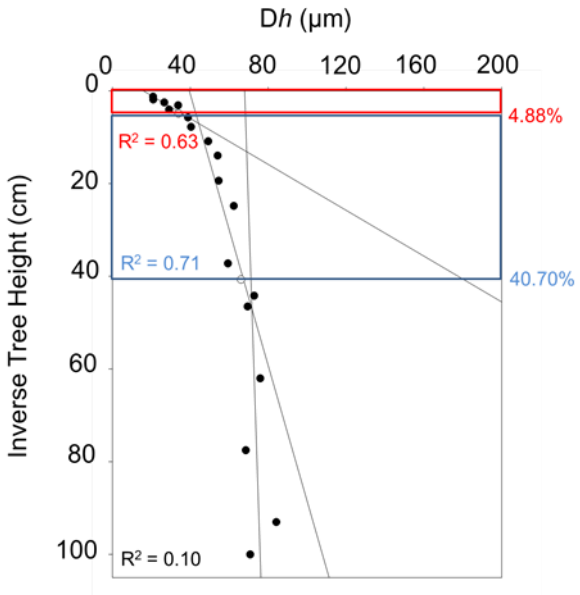

Figure S2.108: Three Phase Taper Analysis (TPTA) of changing hydraulically weighted diameters (D*h*) with inverse tree height. Black dots illustrate measured values and are averages of three analysed images. Circles are calculated medians in-between two measured values. They were not part of linear regression analyses and they do express relative tree heights of phase changes. Red box, red percentage value and red coefficient of determination (y = 4.04x + 26.55) indicate Phase 3 (steep vessel taper structure); blue box, blue percentage value and blue coefficient of determination (y = 0.68x + 39.47) indicate Phase 2 (moderate vessel taper structure); black box and black coefficient of determination (y = 0.08x + 67.96) indicate Phase 1 (no clear vessel taper structure).

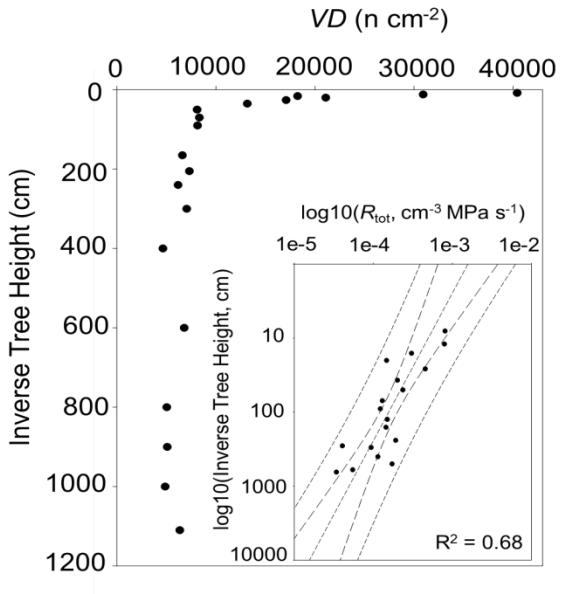

Figure S2.109: Change of vessel densities (*VD*) with inverse tree height. Black dots illustrate measured values and are averages of three analyzed images. Inserted panel illustrates total hydraulic resistance (R_{tot}) plotted against inverse tree height in a log–log scaled graph, where solid line indicates linear regression (y = -0.50x - 2.80), long dashed lines indicate 95% confidence intervals, and short dashed lines indicate 95% prediction intervals. Coefficient of determination is shown in figure.

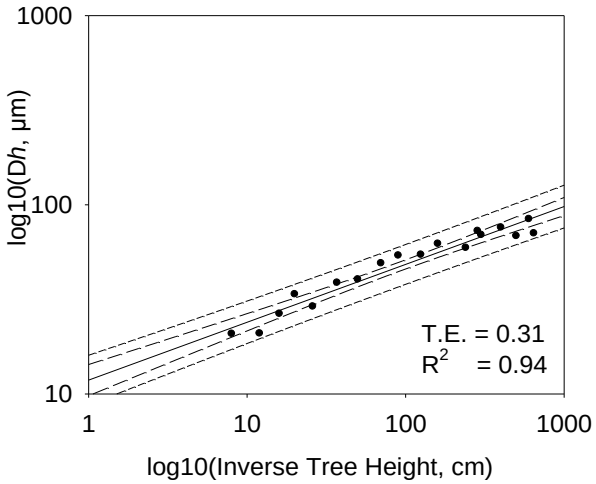

Figure S2.110*:* Hydraulically weighted diameters (D*h*) plotted against inverse tree height in a log–log scaled graph, where the solid line indicates the power function ($y = 11.83*x^{0.31}$), long-dashed lines indicate 95% confidence intervals and short-dashed lines indicate 95% prediction intervals. Black dots illustrate measured values and are averages of three analysed images. The degree of tapering (tapering exponent; T.E.) and coefficient of determination are shown in graph.

Eucalyptus socialis

S 2.111: Habitus of *Eucalyptus socialis*. Image illustrates one of three sampled trees.

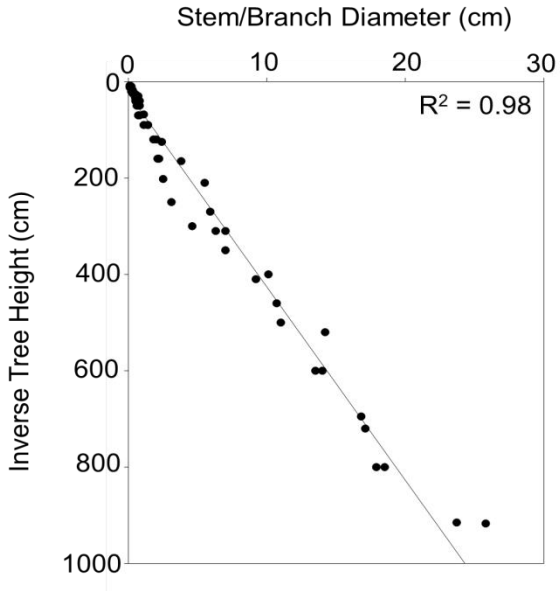

Figure S2.112: Stem and branch diameters measured at sample spots along tree main axes of all three sampled individuals. Coefficient of determination for linear regression (y = 0.02x - 0.62) is shown in figure.

Tree 1

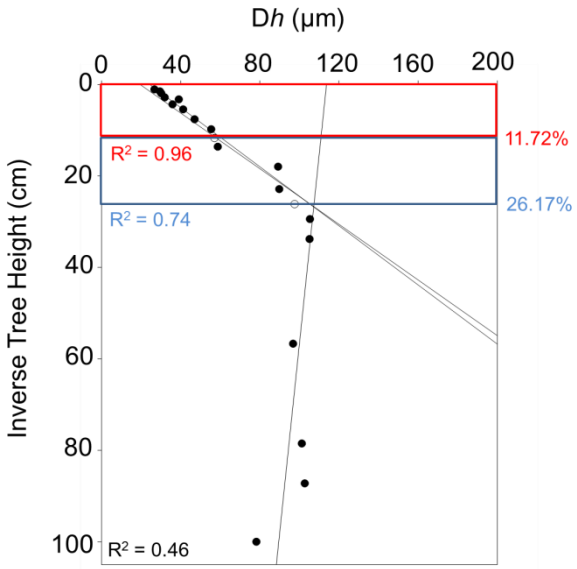

Figure S2.113: Three Phase Taper Analysis (TPTA) of changing hydraulically weighted diameters (D*h*) with inverse tree height. Black dots illustrate measured values and are averages of three analysed images. Circles are calculated medians in-between two measured values. They were not part of linear regression analyses and they do express relative tree heights of phase changes. Red box, red percentage value and red coefficient of determination (y = 3.09x + 24.33) indicate Phase 3 (steep vessel taper structure); blue box, blue percentage value and blue coefficient of determination (y = 3.29x + 19.45) indicate Phase 2 (moderate vessel taper structure); black box and black coefficient of determination (y = -0.24x + 113.70) indicate Phase 1 (no clear vessel taper structure).

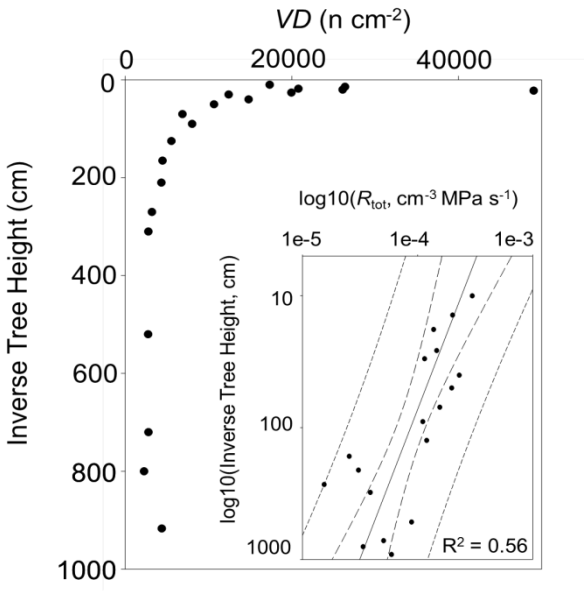

Figure S2.114: Change of vessel density (*VD*) with inverse tree height. Black dots illustrate measured values and are averages of three analyzed images. Inserted panel illustrates total hydraulic resistance (R_{tot}) plotted against inverse tree height in a log–log scaled graph, where solid line indicates linear regression (y = -0.44x - 3.18), long dashed lines indicate 95% confidence intervals, and short dashed lines indicate 95% prediction intervals. Coefficient of determination is shown in figure.

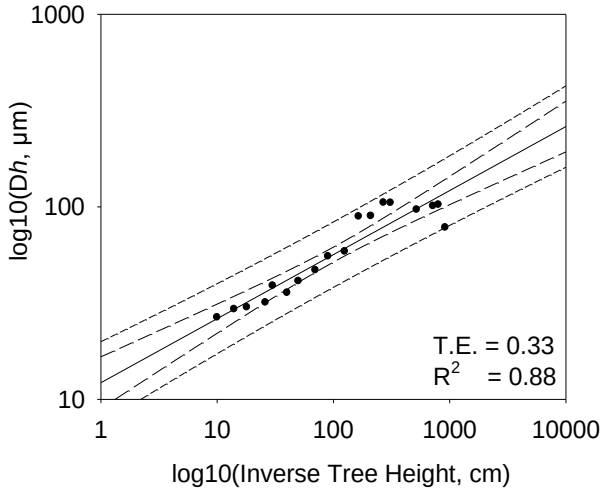

Figure S2.115: Hydraulically weighted diameters (D*h*) plotted against inverse tree height in a log–log scaled graph, where the solid line indicates the power function ($y = 12.20*x^{0.33}$), long-dashed lines indicate 95% confidence intervals and short-dashed lines indicate 95% prediction intervals. Black dots illustrate measured values and are averages of three analysed images. The degree of tapering (tapering exponent; T.E.) and coefficient of determination are shown in graph.

Tree 2

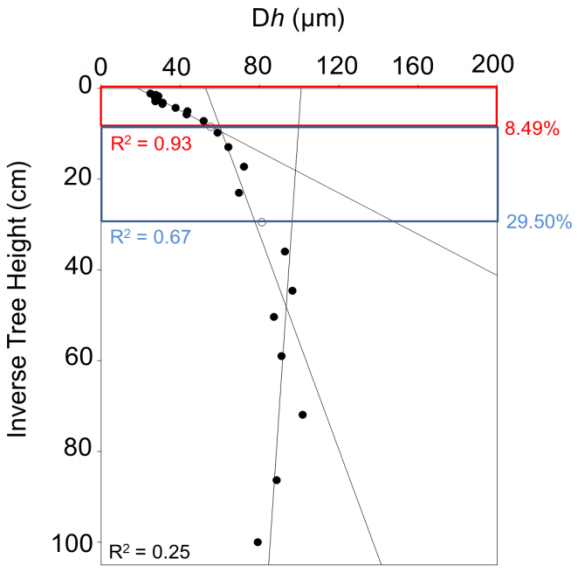

Figure S2.116: Three Phase Taper Analysis (TPTA) of changing hydraulically weighted diameters (D*h*) with inverse tree height. Black dots illustrate measured values and are averages of three analysed images. Circles are calculated medians in-between two measured values. They were not part of linear regression analyses and they do express relative tree heights of phase changes. Red box, red percentage value and red coefficient of determination (y = 4.40x + 18.56) indicate Phase 3 (steep vessel taper structure); blue box, blue percentage value and blue coefficient of determination (y = 0.84x + 52.82) indicate Phase 2 (moderate vessel taper structure); black box and black coefficient of determination (y = -0.16x + 100.99) indicate Phase 1 (no clear vessel taper structure).

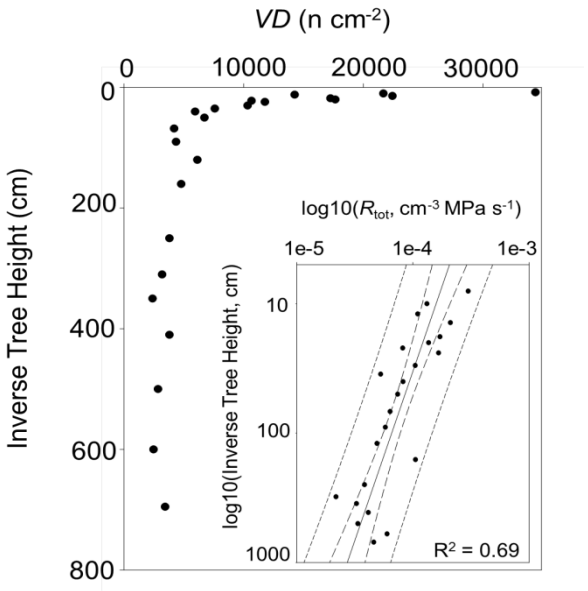

Figure S2.117: Change of vessel density (*VD*) with inverse tree height. Black dots illustrate measured values and are averages of three analyzed images. Inserted panel illustrates total hydraulic resistance (R_{tot}) plotted against inverse tree height in a log–log scaled graph, where solid line indicates linear regression (y = -0.38x - 3.42), long dashed lines indicate 95% confidence intervals, and short dashed lines indicate 95% prediction intervals. Coefficient of determination is shown in figure.

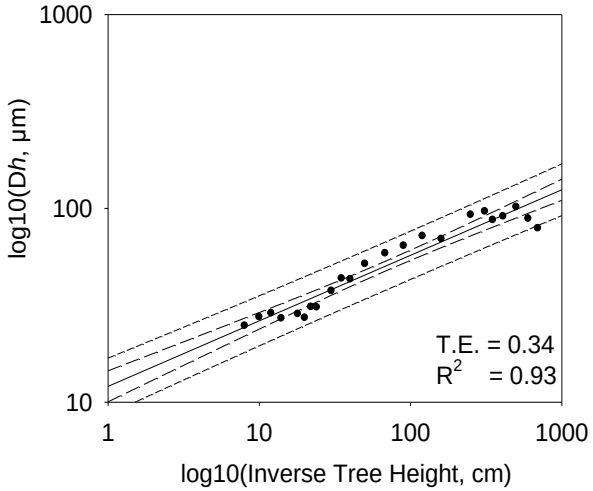

Figure S2.118: Hydraulically weighted diameters (D*h*) plotted against inverse tree height in a log–log scaled graph, where the solid line indicates the power function ($y = 12.08*x^{0.34}$), long-dashed lines indicate 95% confidence intervals and short-dashed lines indicate 95% prediction intervals. Black dots illustrate measured values and are averages of three analysed images. The degree of tapering (tapering exponent; T.E.) and coefficient of determination are shown in graph.

Tree 3

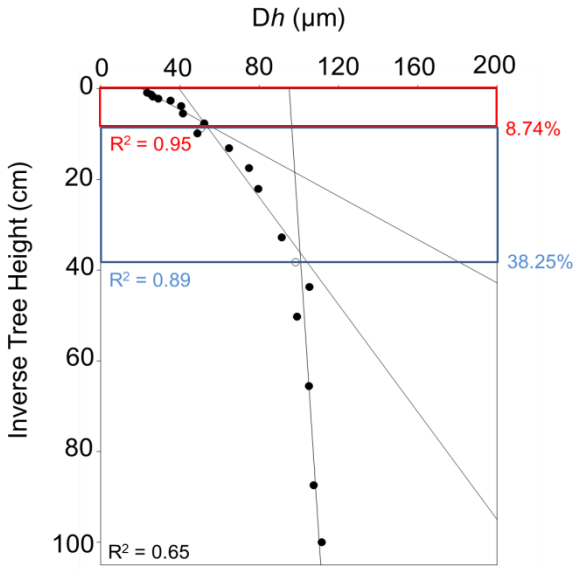

Figure S2.119: Three Phase Taper Analysis (TPTA) of changing hydraulically weighted diameters (D*h*) with inverse tree height. Black dots illustrate measured values and are averages of three analysed images. Circles are calculated medians in-between two measured values. They were not part of linear regression analyses and they do express relative tree heights of phase changes. Red box, red percentage value and red coefficient of determination (y = 4.19x + 20.75) indicate Phase 3 (steep vessel taper structure); blue box, blue percentage value and blue coefficient of determination (y = 1.69x + 39.62) indicate Phase 2 (moderate vessel taper structure); black box and black coefficient of determination (y = 0.15x + 95.12) indicate Phase 1 (no clear vessel taper structure).

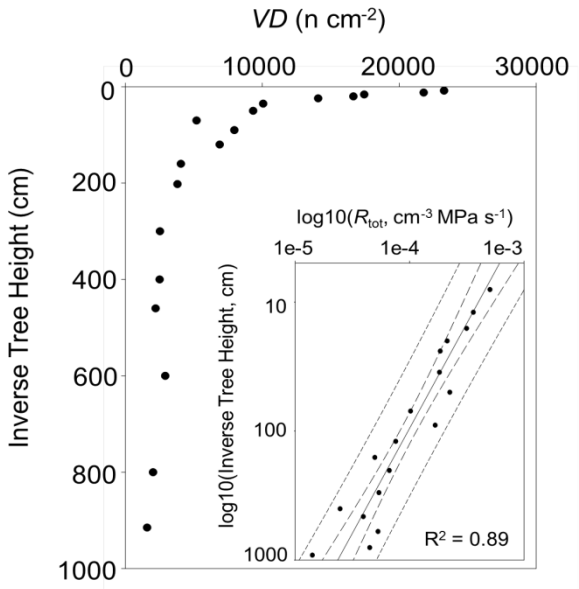

Figure S2.120: Change of vessel density (*VD*) with inverse tree height. Black dots illustrate measured values and are averages of three analyzed images. Inserted panel illustrates total hydraulic resistance (R_{tot}) plotted against inverse tree height in a log–log scaled graph, where solid line indicates linear regression (y = -0.62x - 2.78), long dashed lines indicate 95% confidence intervals, and short dashed lines indicate 95% prediction intervals. Coefficient of determination is shown in figure.

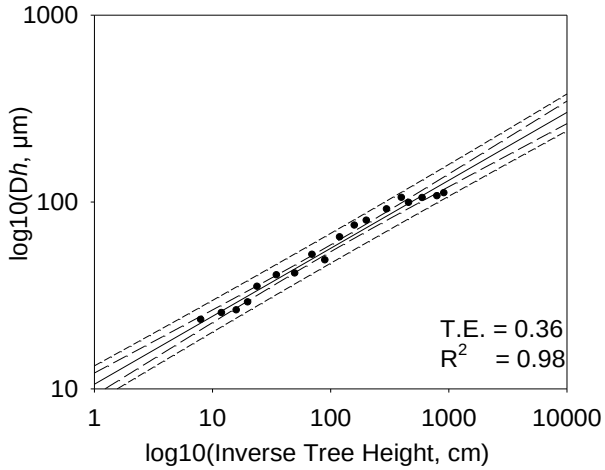

Figure S2.121: Hydraulically weighted diameters (D*h*) plotted against inverse tree height in a log–log scaled graph, where the solid line indicates the power function ($y = 10.59*x^{0.36}$), long-dashed lines indicate 95% confidence intervals and short-dashed lines indicate 95% prediction intervals. Black dots illustrate measured values and are averages of three analysed images. The degree of tapering (tapering exponent; T.E.) and coefficient of determination are shown in graph.

Eucalyptus victrix

Figure S2.122: Habitus of *Eucalyptus victrix*. Image illustrates one of three sampled trees.

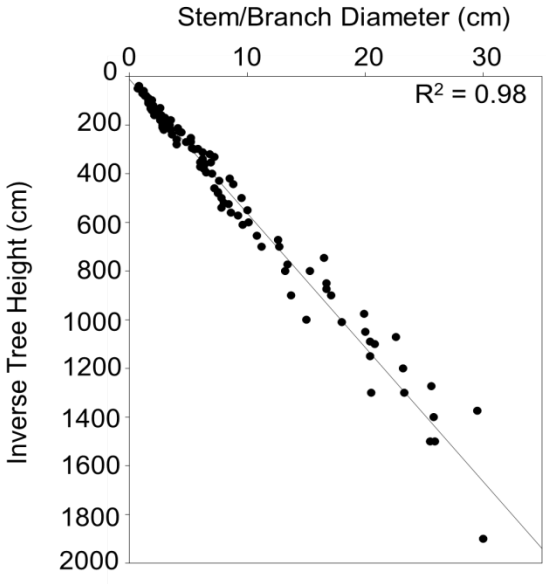

Figure S2.123: Stem and branch diameters measured at sample spots along tree main axes of all three sampled individuals. Coefficient of determination for linear regression (y = 0.02x - 0.21) is shown in figure.

Tree 1

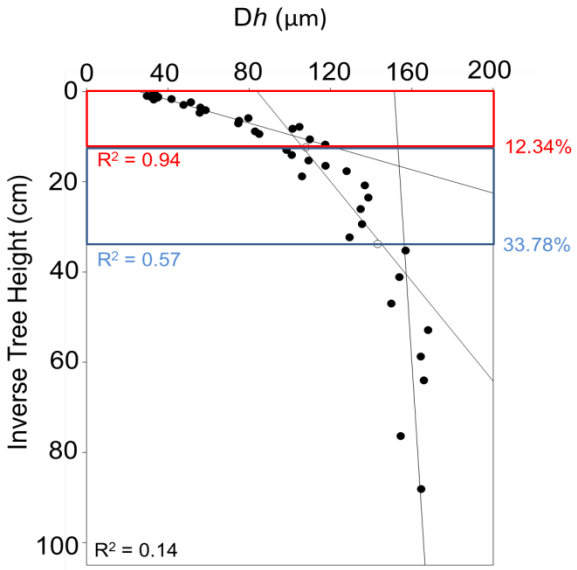

Figure S2.124: Three Phase Taper Analysis (TPTA) of changing hydraulically weighted diameters (D*h*) with inverse tree height. Black dots illustrate measured values and are averages of three analysed images. Circles are calculated medians in-between two measured values. They were not part of linear regression analyses and they do express relative tree heights of phase changes. Red box, red percentage value and red coefficient of determination (y = 7.73x + 26.16) indicate Phase 3 (steep vessel taper structure); blue box, blue percentage value and blue coefficient of determination (y = 1.81x + 83.98) indicate Phase 2 (moderate vessel taper structure); black box and black coefficient of determination (y = 0.14x + 151.35) indicate Phase 1 (no clear vessel taper structure).

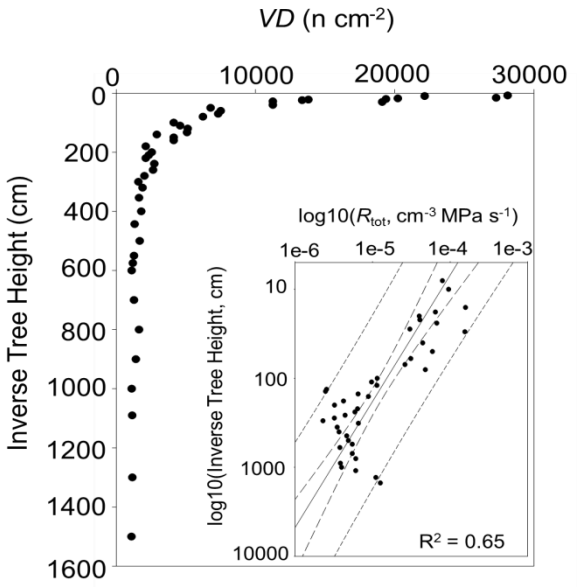

Figure S2.125: Change of vessel density (*VD*) with inverse tree height. Black dots illustrate measured values and are averages of three analyzed images. Inserted panel illustrates total hydraulic resistance (R_{tot}) plotted against inverse tree height in a log–log scaled graph, where solid line indicates linear regression (y = -0.71x - 3.41), long dashed lines indicate 95% confidence intervals, and short dashed lines indicate 95% prediction intervals. Coefficient of determination is shown in figure.

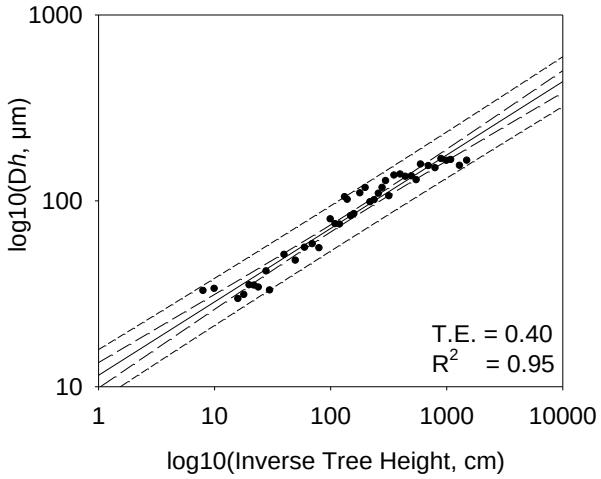

Figure S2.126: Hydraulically weighted diameters (D*h*) plotted against inverse tree height in a log–log scaled graph, where the solid line indicates the power function ($y = 11.52*x^{0.40}$), long-dashed lines indicate 95% confidence intervals and short-dashed lines indicate 95% prediction intervals. Black dots illustrate measured values and are averages of three analysed images. The degree of tapering (tapering exponent; T.E.) and coefficient of determination are shown in graph.

Tree 2

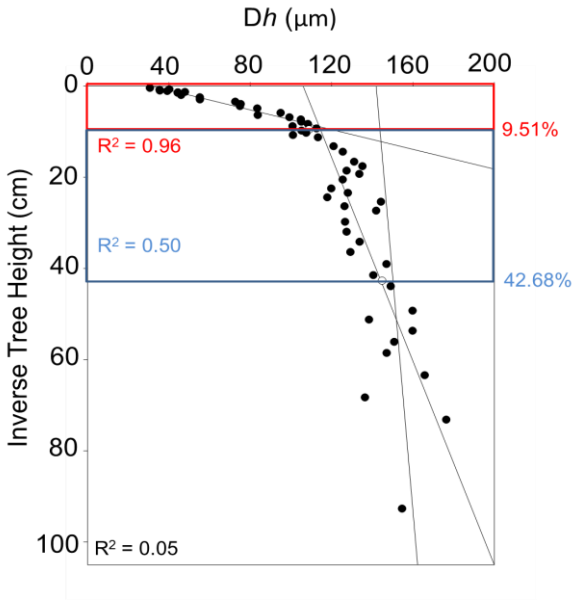

Figure S2.127: Three Phase Taper Analysis (TPTA) of changing hydraulically weighted diameters (D*h*) with inverse tree height. Black dots illustrate measured values and are averages of three analysed images. Circles are calculated medians in-between two measured values. They were not part of linear regression analyses and they do express relative tree heights of phase changes. Red box, red percentage value and red coefficient of determination (y = 9.24x + 31.94) indicate Phase 3 (steep vessel taper structure); blue box, blue percentage value and blue coefficient of determination (y = 0.89x + 106.01) indicate Phase 2 (moderate vessel taper structure); black box and black coefficient of determination (y = 0.19x + 141.90) indicate Phase 1 (no clear vessel taper structure).

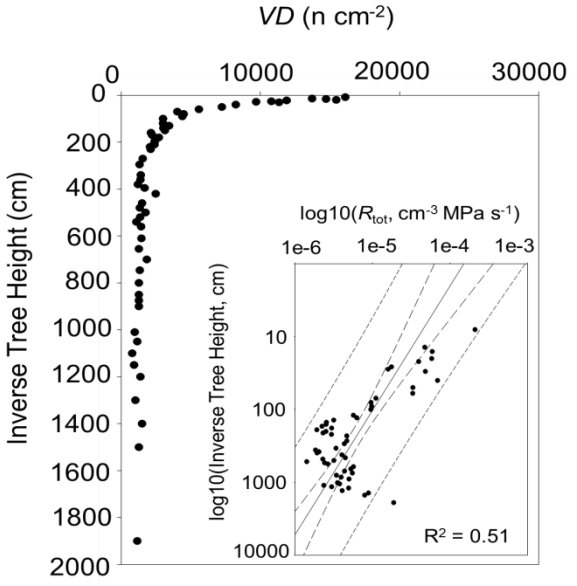

Figure S2.128: Change of vessel density (*VD*) with inverse tree height. Black dots illustrate measured values and are averages of three analyzed images. Inserted panel illustrates total hydraulic resistance (R_{tot}) plotted against inverse tree height in a log–log scaled graph, where solid line indicates linear regression (y = -0.59x - 3.82), long dashed lines indicate 95% confidence intervals, and short dashed lines indicate 95% prediction intervals. Coefficient of determination is shown in figure.

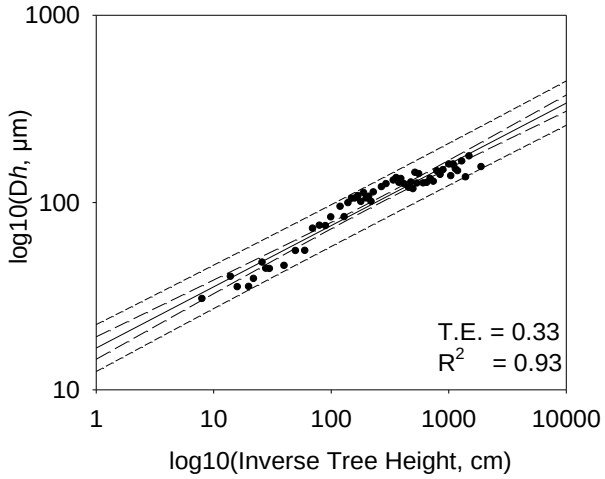

Figure S2.129: Hydraulically weighted diameters (D*h*) plotted against inverse tree height in a log–log scaled graph, where the solid line indicates the power function ($y = 16.71*x^{0.33}$), long-dashed lines indicate 95% confidence intervals and short-dashed lines indicate 95% prediction intervals. Black dots illustrate measured values and are averages of three analysed images. The degree of tapering (tapering exponent; T.E.) and coefficient of determination are shown in graph.

Tree 3

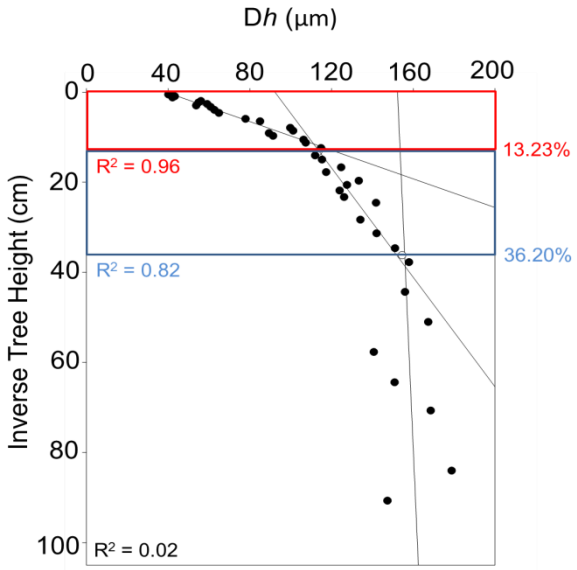

Figure S2.130: Three Phase Taper Analysis (TPTA) of changing hydraulically weighted diameters (D*h*) with inverse tree height. Black dots illustrate measured values and are averages of three analysed images. Circles are calculated medians in-between two measured values. They were not part of linear regression analyses and they do express relative tree heights of phase changes. Red box, red percentage value and red coefficient of determination (y = 6.29x + 38.90) indicate Phase 3 (steep vessel taper structure); blue box, blue percentage value and blue coefficient of determination (y = 1.65x + 92.28) indicate Phase 2 (moderate vessel taper structure); black box and black coefficient of determination (y = 0.10x + 152.29) indicate Phase 1 (no clear vessel taper structure).

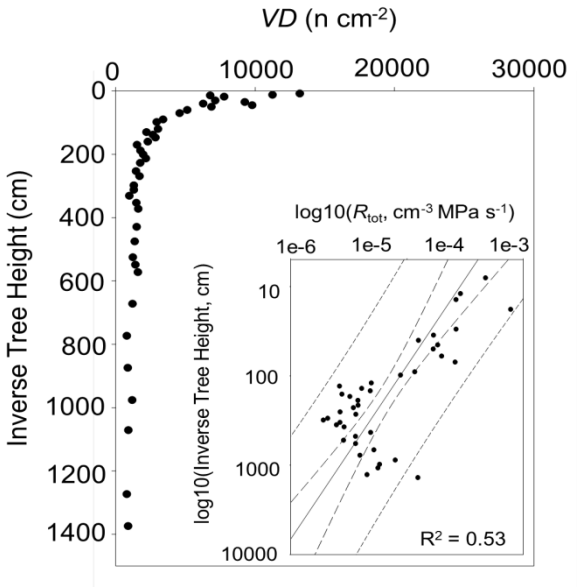

Figure S2.131: Change of vessel density (*VD*) with inverse tree height. Black dots illustrate measured values and are averages of three analyzed images. Inserted panel illustrates total hydraulic resistance (R_{tot}) plotted against inverse tree height in a log–log scaled graph, where solid line indicates linear regression (y = -0.52x - 4.03), long dashed lines indicate 95% confidence intervals, and short dashed lines indicate 95% prediction intervals. Coefficient of determination is shown in figure.

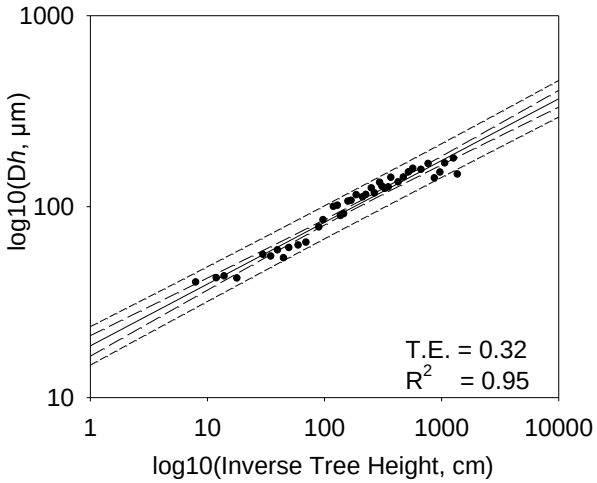

Figure S2.132: Hydraulically weighted diameters (D*h*) plotted against inverse tree height in a log–log scaled graph, where the solid line indicates the power function ($y = 18.66*x^{0.32}$), long-dashed lines indicate 95% confidence intervals and short-dashed lines indicate 95% prediction intervals. Black dots illustrate measured values and are averages of three analysed images. The degree of tapering (tapering exponent; T.E.) and coefficient of determination are shown in graph.

Customized script written with the statistical software package "R"

Script S2.97: Customized script written with the statistical software package "R" (Version 2.15.1, R Foundation for Statistical Computing, Austria) which was used for calculations of a) averages of vessel traits measured in three analyzed images per sample and b) hydraulic properties of vessel traits.

```
##### START READ AND CALCULATE PARAMETERS SCRIPT


#setwd("C:\\Users\\fvanogtrop\\Documents\\DATA\\Sebastian\\Marco\\data voor
floris\\E.delegatensis\\tree1\\reports")
#setwd("C:\\Users\\fvanogtrop\\Documents\\DATA\\Sebastian\\Marco\\data voor
floris\\E.delegatensis\\tree2\\reports")
#setwd("C:\\Users\\fvanogtrop\\Documents\\DATA\\Sebastian\\Marco\\data voor
floris\\E.delegatensis\\tree3\\reports")

#setwd("C:\\Users\\fvanogtrop\\Documents\\DATA\\Sebastian\\Marco\\data voor
floris\\E.microcarpa\\tree1\\reports")
#setwd("C:\\Users\\fvanogtrop\\Documents\\DATA\\Sebastian\\Marco\\data voor
floris\\E.microcarpa\\tree2\\reports")
#setwd("C:\\Users\\fvanogtrop\\Documents\\DATA\\Sebastian\\Marco\\data voor
floris\\E.microcarpa\\tree3\\reports")

#setwd("C:\\Users\\fvanogtrop\\Documents\\DATA\\Sebastian\\Marco\\data voor
floris\\E.regnans\\tree1\\reports")
#setwd("C:\\Users\\fvanogtrop\\Documents\\DATA\\Sebastian\\Marco\\data voor
floris\\E.regnans\\tree2\\reports")
#setwd("C:\\Users\\fvanogtrop\\Documents\\DATA\\Sebastian\\Marco\\data voor
floris\\E.regnans\\tree3\\reports")

#setwd("C:\\Users\\fvanogtrop\\Documents\\DATA\\Sebastian\\Marco\\data voor
floris\\E.socialis\\tree1\\reports")
#setwd("C:\\Users\\fvanogtrop\\Documents\\DATA\\Sebastian\\Marco\\data voor
floris\\E.socialis\\tree2\\reports")
#setwd("C:\\Users\\fvanogtrop\\Documents\\DATA\\Sebastian\\Marco\\data voor
floris\\E.socialis\\tree3\\reports")

#setwd("C:\\Users\\fvanogtrop\\Documents\\DATA\\Sebastian\\Marco\\data voor
floris\\E.baxteri\\tree1")
#setwd("C:\\Users\\fvanogtrop\\Documents\\DATA\\Sebastian\\Marco\\data voor
floris\\E.baxteri\\tree2")
#setwd("C:\\Users\\fvanogtrop\\Documents\\DATA\\Sebastian\\Marco\\data voor
floris\\E.baxteri\\tree3")

#setwd("C:\\Users\\fvanogtrop\\Documents\\DATA\\Sebastian\\Marco\\data voor
floris\\E.pauciflora\\tree1")
#setwd("C:\\Users\\fvanogtrop\\Documents\\DATA\\Sebastian\\Marco\\data voor
floris\\E.pauciflora\\tree2")
```

```
#setwd("C:\\Users\\fvanogtrop\\Documents\\DATA\\Sebastian\\Marco\\data voor floris\\E.pauciflora\\tree3")

#setwd("C:\\Users\\fvanogtrop\\Documents\\DATA\\Sebastian\\Marco\\data voor floris\\E.gracilis\\tree1")
#setwd("C:\\Users\\fvanogtrop\\Documents\\DATA\\Sebastian\\Marco\\data voor floris\\E.gracilis\\tree2")
#setwd("C:\\Users\\fvanogtrop\\Documents\\DATA\\Sebastian\\Marco\\data voor floris\\E.gracilis\\tree3")

#setwd("C:\\Users\\fvanogtrop\\Documents\\DATA\\Sebastian\\Marco\\data voor floris\\E.polyanthemos\\tree1")
#setwd("C:\\Users\\fvanogtrop\\Documents\\DATA\\Sebastian\\Marco\\data voor floris\\E.polyanthemos\\tree2")
#setwd("C:\\Users\\fvanogtrop\\Documents\\DATA\\Sebastian\\Marco\\data voor floris\\E.polyanthemos\\tree3")

#setwd("C:\\Users\\fvanogtrop\\Documents\\DATA\\Sebastian\\Marco\\data voor floris\\E.meliodora\\tree1")
#setwd("C:\\Users\\fvanogtrop\\Documents\\DATA\\Sebastian\\Marco\\data voor floris\\E.meliodora\\tree2")
#setwd("C:\\Users\\fvanogtrop\\Documents\\DATA\\Sebastian\\Marco\\data voor floris\\E.meliodora\\tree3")

#setwd("C:\\Users\\fvanogtrop\\Documents\\DATA\\Sebastian\\Marco\\data voor floris\\E.obliqua\\tree1")
#setwd("C:\\Users\\fvanogtrop\\Documents\\DATA\\Sebastian\\Marco\\data voor floris\\E.obliqua\\tree2")
#setwd("C:\\Users\\fvanogtrop\\Documents\\DATA\\Sebastian\\Marco\\data voor floris\\E.obliqua\\tree3")

#setwd("C:\\Users\\fvanogtrop\\Documents\\DATA\\Sebastian\\Marco\\data voor floris\\E.victrix\\tree1")
#setwd("C:\\Users\\fvanogtrop\\Documents\\DATA\\Sebastian\\Marco\\data voor floris\\E.victrix\\tree2")
#setwd("C:\\Users\\fvanogtrop\\Documents\\DATA\\Sebastian\\Marco\\data voor floris\\E.victrix\\tree3")

#setwd("C:\\Users\\fvanogtrop\\Documents\\DATA\\Sebastian\\Marco\\data voor floris\\E.viminalis\\tree1")
#setwd("C:\\Users\\fvanogtrop\\Documents\\DATA\\Sebastian\\Marco\\data voor floris\\E.viminalis\\tree2")
#setwd("C:\\Users\\fvanogtrop\\Documents\\DATA\\Sebastian\\Marco\\data voor floris\\E.viminalis\\tree3")

DIR <- dir()
DIR <- na.omit(gsub("Thumbs.db", NA, DIR))

library(gtools)
library(gdata)
```

```
## Extract the view area of microscope

view_area <- list()

for(i in 1:length(DIR)){
	#i=33
	sheet2 <- read.xls(DIR[i],sheet="Analysis Report", perl =
"C:\\strawberry\\perl\\bin\\perl.exe")
	view_area[[i]] <- data.frame(species_name = as.vector(sheet2[3,4]),
view_area = as.numeric(as.vector(sheet2[5,7])))
}

## Extract xylem area
Xylem_Area <- list()

for(i in 1:length(DIR)){
	#i=43
	sheet1 <- read.xls(DIR[i], pattern = "Number",sheet="Feature Details",
perl = "C:\\strawberry\\perl\\bin\\perl.exe")
	names(sheet1)
	temp <- sheet1$Area.µm². ## Extract appropriate column
	temp1 <- as.numeric(as.vector(unlist(temp)))

	foo <- function( x ){
		idx <- 1 + cumsum( is.na( x ) )
		not.na <- ! is.na( x )
		split( x[not.na], idx[not.na] )

	}

	Data <- as.vector(foo(temp1)[[1]])
	## isolate species name
	Sp1 <- sheet1$Images
	Sp2 <- gregexpr("_pic",Sp1)[[1]][1]-1
	Sp3 <- substr(Sp1, 1, Sp2)
	Species_Name <- rep(Sp3[1], times=NROW(Data))

	## Create final data frame
	Xylem_Area[[i]] <- data.frame(Species = as.character(Species_Name),
Xylem_Area = Data,
	Xylem_Diameter = sqrt(Data/pi)*2)

}

## Calculate vessel fraction
Xylem_Area2 <- Xylem_Area
for(i in 1:length(Xylem_Area2)){
	Xylem_Area2[[i]]$Vessel_fraction <-
as.vector(unlist(Xylem_Area[[i]][2])/unlist(view_area[[i]][2]))
```

```
        Xylem_Area2[[i]]$D5 <- Xylem_Area2[[i]]$Xylem_Diameter^5
        Xylem_Area2[[i]]$D4 <- Xylem_Area2[[i]]$Xylem_Diameter^4
}

vessel_number <- list()
void_to_wood <- list()
for(i in 1:length(Xylem_Area2)){
        vessel_number[[i]] <-
as.vector(nrow(Xylem_Area[[i]][2])/unlist(view_area[[i]][2]))*100000000
        void_to_wood[[i]] <-
as.vector(sum(Xylem_Area[[i]][2])/unlist(view_area[[i]][2]))*100
}

species_name2 <- do.call(rbind, view_area)[,1]
species_name4 <- vector()
for(i in 1:length(species_name2)){
        #i=43
        species_name3 <- gregexpr("_pic",species_name2[i])[[1]][1]-1
        species_name4[i] <- substr(species_name2[i], 1, species_name3)
}
species_name5 <- unique(species_name4)
## Start constructing the final data frame
Final_Data <- as.data.frame(do.call(rbind,strsplit(as.character(species_name5), "_")))
colnames(Final_Data) <- c("species", "tree_number", "sample_height") ## add or
remove "tree type" after "species" for E.victrix

## make heigh numeric
Final_Data$sample_height <-
read.table(textConnection(as.character(Final_Data$sample_height)), sep = "c")[,1]

Xylem_Area3 <- do.call(rbind, Xylem_Area2)

Final_Data$avg_diameter <- tapply(Xylem_Area3$Xylem_Diameter,
Xylem_Area3$Species, mean)
Final_Data$sd_diameter <- tapply(Xylem_Area3$Xylem_Diameter,
Xylem_Area3$Species, sd)
Final_Data$var_diameter <- tapply(Xylem_Area3$Xylem_Diameter,
Xylem_Area3$Species, var)
Final_Data$min_diameter <- tapply(Xylem_Area3$Xylem_Diameter,
Xylem_Area3$Species, min)
Final_Data$max_diameter <- tapply(Xylem_Area3$Xylem_Diameter,
Xylem_Area3$Species, max)
Final_Data$Dh <- tapply(Xylem_Area3$D5, Xylem_Area3$Species,
sum)/tapply(Xylem_Area3$D4, Xylem_Area3$Species, sum)

## Average vessel number per cm2
vessel_number2 <- data.frame(species = species_name4, vessel_cm =
unlist(vessel_number))
Final_Data$avg_vessel_number_cm2 <- tapply(vessel_number2$vessel_cm,
vessel_number2$species, mean)
```

```
## void to wood ratio
void_to_wood2 <- data.frame(species = species_name4, void_to_wood =
unlist(void_to_wood))
Final_Data$void_to_wood <- tapply(void_to_wood2$void_to_wood,
void_to_wood2$species, mean) ## need to check this calculation

Final_Data$Rk <- (128*1.002*1)/(pi*(Final_Data$Dh^4))
Final_Data$percent_Rk <- Final_Data$Rk/sum(Final_Data$Rk)*100

Final_Data1 <- Final_Data[order(Final_Data$sample_height),]

tube_length <- vector(length = nrow(Final_Data1))
tube_length[1] <- (Final_Data1$sample_height[1] +
Final_Data1$sample_height[2])/2
tube_length[nrow(Final_Data1)] <-
(Final_Data1$sample_height[nrow(Final_Data1)]
-Final_Data1$sample_height[(nrow(Final_Data1)-1)])/2

for(i in 2:(nrow(Final_Data1)-1)){
        tube_length[i] <- ((Final_Data1$sample_height[i]-
Final_Data1$sample_height[i-1])/2
        +(Final_Data1$sample_height[i+1]-Final_Data1$sample_height[i])/2)
}

##check
ifelse(sum(tube_length)==Final_Data1$sample_height[nrow(Final_Data1)], "OK",
"Not OK")

Final_Data1$tube_length <- tube_length
Final_Data1$Rk_tube_length <- Final_Data1$Rk * Final_Data1$tube_length
Final_Data1$percent_Rk_tube_length <-
Final_Data1$Rk_tube_length/sum(Final_Data1$Rk_tube_length )*100

sum(Final_Data1$percent_Rk_tube_length)


## write file
#write.csv(Final_Data1,
paste("C:\\Users\\fvanogtrop\\Documents\\DATA\\Sebastian\\Marco\\data voor
floris\\E.delegatensis\\Output\\",Final_Data1[1,1], "_" ,Final_Data1[1,2], "_out.csv",
sep = ""))

#write.csv(Final_Data1,
paste("C:\\Users\\fvanogtrop\\Documents\\DATA\\Sebastian\\Marco\\data voor
floris\\E.microcarpa\\Output\\",Final_Data1[1,1], "_" ,Final_Data1[1,2], "_out.csv",
sep = ""))

#write.csv(Final_Data1,
paste("C:\\Users\\fvanogtrop\\Documents\\DATA\\Sebastian\\Marco\\data voor
```

```
floris\\E.regnans\\Output\\",Final_Data1[1,1], "_" ,Final_Data1[1,2], "_out.csv", sep
= ""))

#write.csv(Final_Data1,
paste("C:\\Users\\fvanogtrop\\Documents\\DATA\\Sebastian\\Marco\\data voor
floris\\E.socialis\\Output\\",Final_Data1[1,1], "_" ,Final_Data1[1,2], "_out.csv", sep
= ""))

#write.csv(Final_Data1,
paste("C:\\Users\\fvanogtrop\\Documents\\DATA\\Sebastian\\Marco\\data voor
floris\\E.baxteri\\Output\\",Final_Data1[1,1], "_" ,Final_Data1[1,2], "_out.csv", sep =
""))

#write.csv(Final_Data1,
paste("C:\\Users\\fvanogtrop\\Documents\\DATA\\Sebastian\\Marco\\data voor
floris\\E.gracilis\\Output\\",Final_Data1[1,1], "_" ,Final_Data1[1,2], "_out.csv", sep
= ""))

#write.csv(Final_Data1,
paste("C:\\Users\\fvanogtrop\\Documents\\DATA\\Sebastian\\Marco\\data voor
floris\\E.pauciflora\\Output\\",Final_Data1[1,1], "_" ,Final_Data1[1,2], "_out.csv",
sep = ""))

#write.csv(Final_Data1,
paste("C:\\Users\\fvanogtrop\\Documents\\DATA\\Sebastian\\Marco\\data voor
floris\\E.polyanthemos\\Output\\",Final_Data1[1,1], "_" ,Final_Data1[1,2],
"_out.csv", sep = ""))

#write.csv(Final_Data1,
paste("C:\\Users\\fvanogtrop\\Documents\\DATA\\Sebastian\\Marco\\data voor
floris\\E.meliodora\\Output\\",Final_Data1[1,1], "_" ,Final_Data1[1,2], "_out.csv",
sep = ""))

write.csv(Final_Data1,
paste("C:\\Users\\fvanogtrop\\Documents\\DATA\\Sebastian\\Marco\\data voor
floris\\E.obliqua\\Output\\",Final_Data1[1,1], "_" ,Final_Data1[1,2], "_out.csv", sep
= ""))

#write.csv(Final_Data1,
paste("C:\\Users\\fvanogtrop\\Documents\\DATA\\Sebastian\\Marco\\data voor
floris\\E.victrix\\Output\\",Final_Data1[1,1], "_" ,Final_Data1[1,3], "_out.csv", sep =
""))

#write.csv(Final_Data1,
paste("C:\\Users\\fvanogtrop\\Documents\\DATA\\Sebastian\\Marco\\data voor
floris\\E.viminalis\\Output\\",Final_Data1[1,1], "_" ,Final_Data1[1,2], "_out.csv",
sep = ""))

###### END SCRIPT
```

```
## START RMA SCRIPT

setwd("C:\\Users\\fvanogtrop\\Documents\\DATA\\Sebastian\\Marco\\data voor
floris\\Combined")
dir()
combined_species <- read.csv("2013_Combined_species3.csv")
head(combined_species)

## log values
combined_species$log_Dh <- log(combined_species$Dh, 10)
combined_species$log_sample_height <- log(combined_species$sample_height, 10)

require(lmodel2)

modfun <- function(X) lmodel2(log_Dh ~ log_sample_height, data=X,
"relative","relative",99)

combined_list <- aggregate(cbind(combined_species$log_Dh,
combined_species$log_sample_height), list(combined_species$species,
combined_species$tree_number), as.list)

model_out <- list()
for(i in 1:nrow(combined_list)){
        logDh <- as.vector(unlist(combined_list[i,3]))
        logSh <- as.vector(unlist(combined_list[i,4]))
        DF <- data.frame(logDh, logSh)
        model_out[[i]] <- lmodel2(logDh ~ logSh,data = DF,
"relative","relative",99)
}

names_model_out <- paste(as.vector(unlist(combined_list[1])), "tree",
as.vector(unlist(combined_list[2])))
names(model_out[[1]])

model_out2 <- list()
for(i in 1:nrow(combined_list)){
        model_out2[[i]] <- data.frame(species=names_model_out[i],
a=model_out[[i]]$regression.results[4,2], b=model_out[[i]]$regression.results[4,3]
        , "a_2.5"=model_out[[i]]$confidence.intervals[4,2],
"a_97.5"=model_out[[i]]$confidence.intervals[4,3],
"b_2.5"=model_out[[i]]$confidence.intervals[4,4]
        , "b_97.5"=model_out[[i]]$confidence.intervals[4,5],
r_square=model_out[[i]]$rsquare)
}


final_data <- do.call(rbind, model_out2)

##### END SCRIPT
```

Appendix – Chapter 4

Table S4.1: Deuterium contents (δ^2H) measured in extracted water from wood tissue samples of specified locations in the main stem of a mature *Corymbia maculata*; heartwood diameter (hwd) and sapwood width (sww) for considered sample heights.

n	sample height (m)	sample location	sample orientation	δ^2H	hwd (cm)	sww (cm)
1	base	sapwood	north	-35.60	-	4.7
2	base	sapwood	east	-32.80	-	5.5
3	base	sapwood	south	-31.40	-	5.6
4	base	sapwood	West	-35.60	-	4.8
5	base	outer heartwood	north	-28.90	47	-
6	base	outer heartwood	east	-29.70	-	-
7	base	outer heartwood	south	-31.20	-	-
8	base	outer heartwood	west	-31.60	-	-
9	base	inner heartwood	north	-30.70	-	-
10	base	inner heartwood	east	-29.70	-	-
11	base	inner heartwood	south	-30.10	-	-
12	base	inner heartwood	west	-25.00	-	-
13	5	sapwood	north	-30.70	-	4
14	5	sapwood	east	-34.10	-	5.5
15	5	sapwood	south	-33.70	-	5.5
16	5	sapwood	west	-33.80	-	4.5
17	5	outer heartwood	north	-28.20	24	-
18	5	outer heartwood	east	-28.60	-	-
19	5	outer heartwood	south	-29.00	-	-
20	5	outer heartwood	west	-29.40	-	-
21	5	inner heartwood	north	-30.20	-	-
22	5	inner heartwood	east	-31.40	-	-
23	5	inner heartwood	south	-28.90	-	-
24	5	inner heartwood	west	-30.90	-	-
25	8	sapwood	east	-26.90	-	3.5
26	8	sapwood	west	-33.40	-	3.5
27	8	outer heartwood	east	-28.40	13	-
28	8	outer heartwood	west	-26.90	-	-
29	8	inner heartwood	center	-32.00	-	-
30	12	sapwood	east	-28.10	-	4.5
31	12	sapwood	west	-26.10	-	3
32	12	heartwood	center	-28.00	8.5	-
33	17	sapwood	east	-30.30	-	-
34	17	sapwood	west	-28.10	-	-
35	17	sapwood	center	-30.70	-	-
36	20	sapwood	east	-30.60	-	-
37	20	sapwood	west	-31.60	-	-
38	20	sapwood	center	-36.20	-	-

Table S4.2: Deuterium contents (δ^2H) measured in extracted water from wood tissue samples of specified locations in a northwards oriented branch of a mature *Corymbia maculata*; heartwood diameter (hwd) and sapwood width (sww) for considered sample heights.

n	sample height (m)	sample location	sample orientation	δ^2H	hwd	sww
39	5	inner heartwood	center	-	-	-
40	8	sapwood	east	-32.90	-	4
41	8	sapwood	west	-31.00	-	4.5
42	8	outer heartwood	east	-28.00	13	-
43	8	outer heartwood	west	-27.50	-	-
44	8	inner heartwood	center	-31.70	-	-
45	12	sapwood	east	-30.30	-	3
46	12	sapwood	west	-31.10	-	3
47	12	heartwood	center	-30.00	7	-
48	17	sapwood	east	-35.20	-	-
49	17	sapwood	west	-31.30	-	-

Table S4.3: Deuterium contents (δ^2H) measured in extracted water from wood tissue samples of specified locations in an eastwards oriented branch of a mature *Corymbia maculata*; heartwood diameter (hwd) and sapwood width (sww) for considered sample heights.

n	sample height (m)	sample location	sample orientation	δ^2H	hwd	sww
50	5	sapwood	north	-32.50	-	5.5
51	5	sapwood	east	-35.00	-	5
52	5	sapwood	south	-32.40	-	4
53	5	sapwood	west	-30.10	-	5
54	5	outer heartwood	north	-26.80	30.1	-
55	5	outer heartwood	east	-28.40	-	-
56	5	outer heartwood	south	-33.90	-	-
57	5	outer heartwood	west	-28.30	-	-
58	5	inner heartwood	north	-27.70	-	-
59	5	inner heartwood	east	-37.10	-	-
60	5	inner heartwood	south	-27.20	-	-
61	5	inner heartwood	west	-28.70	-	-
62	9	sapwood	east	-30.10	-	3.5
63	9	sapwood	west	-30.20	-	5.5
64	9	heartwood	east	-30.70	11	-
65	9	heartwood	west	-28.20	-	-
66	12	sapwood	east	-33.10	-	5
67	12	sapwood	west	-31.80	-	5
68	12	heartwood	center	-30.10	6	-
69	16	sapwood	east	-32.20	-	-
70	16	sapwood	west	-32.30	-	-
71	16	sapwood	center	-32.20	-	-

Table S4.4: Deuterium contents (δ^2H) measured in extracted water from wood tissue samples of specified locations in a southwards oriented branch of a mature *Corymbia maculata*; heartwood diameter (hwd) and sapwood width (sww) for considered sample heights.

n	sample height (m)	sample location	sample orientation	δ^2H	hwd	sww
72	8	sapwood	east	-28.50	-	4.5
73	8	sapwood	west	-31.40	-	4
74	8	outer heartwood	east	-29.20	13	-
75	8	outer heartwood	west	-28.30	-	-
76	8	inner heartwood	center	-33.80	-	-
77	12	sapwood	east	-27.90	-	3
78	12	sapwood	west	-32.40	-	3
79	12	heartwood	center	-29.40	7	-
80	17	sapwood	east	-24.30	-	-
81	17	sapwood	west	-23.90	-	-
82	17	sapwood	center	-	-	-

Table S4.5: Deuterium contents (δ^2H) measured in extracted water from wood tissue samples of specified locations in a westwards oriented branch of a mature *Corymbia maculata*; heartwood diameter (hwd) and sapwood width (sww) for considered sample heights.

n	sample height (m)	sample location	sample orientation	δ^2H	hwd	sww
83	8	sapwood	east	-31.30	-	3
84	8	sapwood	west	-33.3	-	5
85	8	heartwood	center	-31.60	10.5	-
86	12	sapwood	east	-	-	4.5
87	12	sapwood	west	-31.20	-	4
88	12	heartwood	center	-31.90	4	-
89	17	sapwood	east	-30.60	-	-
90	17	sapwood	west	-31.10	-	-
91	17	sapwood	canter	-28.00	-	-